# Deciphering the vascular functions of Bone Morphogenetic Protein 9 and 10 using knock-out mouse models

Martina Rossi

THÈSE

Pour obtenir le grade de

**DOCTEUR DE L'UNIVERSITÉ GRENOBLE ALPES**

École doctorale : CSV- Chimie et Sciences du Vivant
Spécialité : Biologie cellulaire
Unité de recherche : Biologie et Biotechnologie pour la Santé

# Etude des fonctions vasculaires des Bone Morphognetic Proteins 9 et 10 à laide de modèles murins transgéniques

# Deciphering the vascular functions of Bone Morphogenetic Protein 9 and 10 using knock-out mouse models

Présentée par :


## Martina ROSSI


Direction de thèse :

| | |
|---|---|
| **Emmanuelle TILLET**<br>UGA | de thèse |
| **Claire BOUVARD** | Co-encadrante de thèse |

Rapporteurs :

**Delphine MEYNARD**
CHARGE DE RECHERCHE HDR, NSERM DELEGATION OCCITANIE PYRENEES
**Ebba BRAKENHIELM**
DIRECTEUR DE RECHERCHE, INSERM DELEGATION NORD OUEST

Thèse soutenue publiquement le **9 novembre 2022**, devant le jury composé de :

| | |
|---|---|
| **Emmanuelle TILLET**<br>MAITRE DE CONFERENCES HDR, UNIVERSITE GRENOBLE ALPES | Directrice de thèse |
| **Delphine MEYNARD**<br>CHARGE DE RECHERCHE HDR, NSERM DELEGATION OCCITANIE PYRENEES | Rapporteure |
| **Ebba BRAKENHIELM**<br>DIRECTEUR DE RECHERCHE, INSERM DELEGATION NORD OUEST | Rapporteure |
| **Philippe HUBER**<br>INGENIEUR HDR, CEA CENTRE DE DAM ILE-DE-FRANCE | Examinateur |
| **François BOUCHER**<br>PROFESSEUR DES UNIVERSITES, UNIVERSITE GRENOBLE ALPES | Président |
| **Ulrich VALCOURT**<br>PROFESSEUR DES UNIVERSITES, UNIVERSITE LYON 1 - CLAUDE BERNARD | Examinateur |

Invités :

**Claire Bouvard**
PROFESSEUR ASSISTANT, Université Grenoble Alpes

# Acknowledgements

I want to express my gratitude to Dr. Ebba Brakenhielm and Dr. Delphine Meynard as well as Dr. Philippe Huber, Prof. Francois Boucher and Prof. Ulrich Valcourt for having agreed in evaluating my thesis project.

I also want to thank, again, Dr. Philippe Huber, Dr. Serge Candeias and Dr. Laurence Aubry for having participated to my comité de suivi de these. Your support and expertise allowed me to move forward in my work and broaden my point of view on the subject.

I wish to express my gratitude to my thesis director, Dr. Emmanuelle Tillet and my thesis co-supervisor Dr. Claire Bouvard, for their support, their invaluable advice, their patience and for always keeping their door open throughout my PhD studies. Their vast knowledge and experience have inspired me throughout my academic research. Emma, to you goes my great professional respect. It has been a hard path, and supported me through thick and thin. Thank you, for showing me that is indeed possible. Claire, I thank you for your kindness, your fairness, and your thoroughness. For your great scientific input, and your support over these years. You were not only a great supervisor but great a mentor too.

I extend my great appreciation to Dr. Jean-Jacques Feige for welcoming me to his laboratory at the beginning of my PhD and to Dr. Sabine Bailly, who took his place few months after I started my project. Sabine, I am grateful for the time you took to provide me with advice during the course of my thesis. Your rigour, your tireless scientific curiosity, your determination and your ethics are, for me, a font of inspiration.

Also, I wish to thank all the other members of the BAL team. In particular, Nicolas C., Caroline, and Lisa for doing all the genotyping. Lisa, you have truly been a friend in and out of the lab. I am truly grateful for your help and to have had the chance to get to know you. Nicolas R., thank you for your advice and help with the retina dissection during the last year of my thesis. Aude, thank you for your help with the animal work during my last mile. I also wanted to thank Agnes,

for her support, in particular for her qPCR expertise, which has been of help many times. Tala and Mohammad, working next to you made me feel not alone on this path. Thank you for the moments we shared. I wish you all the best guys, you truly deserve it. I wish to extend my appreciation to the rest of the team and the Biosanté group.

To all the others that helped me during my project: thank you to the master students Elisa for your work with Lrat mice, Laura that helped me with some bone immunofluorescence, Iza and Charlene for your help with the animal handling, Veronique for your help with flow cytometry experiments, Jenny for the help with the blood analyser at Clinatec and Thierry and Laurence for your support and scientific discussions.

I would like to acknowledge the VA Cure consortium, and the constant involvement of the PIs in my project. In particular, I wish to thank Dr. Taija Mäkinen for having welcomed me into her lab, and Hans for being there during my secondment.

I would like to thank my family and close friends for the support you have given me during these years of study. The family is large and spread out and I have many people to thank. Giulia, thank you for always being there, for listening to me, and for rooting for me. Mom, Dad, Michi and Nico, thank you for your love and support. Vale, despite the length that separates us, I feel you close. To my parents in Brazil, especially to tio Julio. To the family from Naples, Paola, my aunt and uncle. My crazy fun aunts and uncles Mariella, Paolo, Giancarla, Italo and Tonino a constant presence in my life. To Gianfranco, for everything you have done for me. To Letizia and Steve for their affection.
To the present and the missing ones.

Thank you to all my friends spread all over the world among whom, I would like to mention a few:

Giulia, we went through a PhD together and I am coming out of this experience with a friend. Thank you for these years, for the moments we spent, for the ugly coffees and the many laughter.

Dom, thank you for your many years of friendship and support. To our countless hours of music and words on roofs. You are living proof of resilience. The best is yet to come, my friend.

Maggie, thank you, for your gifting me with your beautiful alliance since our first day of university, when you sat next to me during the Chemistry seminar, and for being my friend ever since. You have always been there for me over these years, and surely you brought many colours to this wonderful experience.

Gabriele, Chiara, Giovanni and Arianna, we've come a long way since the day when we first met. If I got here, it is also thanks to you guys.

Matilde and Philippe, thank you for the kindness you showed me these years, for your welcoming and sense of family.

Paola, what you need to know I have told you. I dedicate this one to us, to our future. Thank you for your huge support over these years, for your creative input, and for believing in me when even I did not believe in myself. One-step at a time, one can really come a long way. Finally, I wish to thank Cairo and Popi, I am everyday grateful to you, you gave me much more than I would ever imagine.

# Table of contents

List of Figures ..... 4
List of Tables ..... 6
Abbreviations ..... 7
Summary ..... 11
Résumé ..... 12
Introduction ..... 13
1. Vascular system (circulatory system) ..... 13
1.1 Blood vasculature development ..... 15
1.1.1 Endothelial cells differentiations and vasculogenesis ..... 16
1.1.2 Angiogenesis and endothelial cell specification ..... 17
1.1.2.1 Intussusceptive angiogenesis ..... 18
1.1.2.2 Sprouting angiogenesis ..... 19
1.1.2.2.1 Mechanochemical drivers of sprouting angiogenesis ..... 20
1.1.2.3 Factors involved in vessel maturation, quiescence and maintenance ..... 22
1.1.3. Arteriovenous identity ..... 23
1.2 Lymphatic system development ..... 27
1.2.1 Mechanochemical drivers of lymphangiogenesis ..... 28
1.2.2 Methods to study the lymphatic system development ..... 30
1.3 Other routes of endothelial cell differentiations ..... 31
1.3.1 The process of haematopoiesis ..... 31
1.3.1.1 Endothelial-to-Haematopoietic Transition (EHT) ..... 35
1.3.2 Endothelial to Mesenchymal Transition (EndMT) ..... 36
2. Transforming Growth Factor β (TGF-β) superfamily proteins ..... 39
2.1 Ligand-receptor interactions ..... 40
2.1.1 Classification of the BMPs ..... 44
2.1.2 BMPs regulatory proteins and targets ..... 45
2.1.3 BMPs sites of expression ..... 47
2.2 BMP9 and BMP10 ..... 47

2.2.1 Ligands and regulation of their activity ..... 48
2.2.2 BMP9 and BMP10 receptor specificity targeted gene expression ..... 49
2.2.3 BMP9 and BMP10 during embryogenesis ..... 50
2.2.3.1 Cardiac implications – BMP10 specific role ..... 51
2.2.3.2 Lymphatics implication – BMP9 "specific" role ..... 53
2.2.4 BMP9 and BMP10 role in angiogenesis - *In vitro* functions ..... 53
2.2.5 BMP9 and BMP10 role in angiogenesis - *In vivo* functions ..... 54
2.2.6 The heterodimer BMP9-BMP10 ..... 55
2.2.7 Diseases associated to BMP9-BMP10 signalling pathways ..... 57
2.2.7.1 Hereditary Haemorrhagic Telangiectasia (HHT) ..... 58
2.2.7.2 Pulmonary Arterial Hypertension (PAH) ..... 59
3. Mouse models to study in vivo gene function ..... 62
3.1. The Cre/loxP mediated recombination ..... 63
3.2 Models to study vascular development and diseases ..... 65
3.2.1 Mouse retina as a model to study postnatal angiogenesis ..... 66
3.2.1.1 Retina arterio-venous differentiation ..... 68
3.2.1.2 Mouse models of vascular malformations (VM) in the context of BMP9/BMP10 ALK1-induced signalling ..... 69
Aims ..... 75
Results ..... 78
Part I - Introduction to 1st article (contribution as 3rd author) ..... 78
Part II – Consequences of BMP10 deletion in young mice using Rosa26 CreERT2 line ..... 118
1. Rosa CreERT2 BMP10 iKO displayed haematopoiesis defect ..... 118
2. Bone marrow vasculature defect observed in Rosa Cre BMP10 iKO ..... 121
3. Rosa Cre BMP10 iKO phenotype does not coincide with loss of activity and cannot be reproduced by blocking ALK1 receptor ..... 124
Part III – Deciphering the function of cardiac versus liver BMP10 ..... 153
1. Combined loss of BMP9 and BMP10 leads to severe vascular defects during active angiogenesis ..... 155
2. Validation of generated mice models and characterisation of circulating BMP10 homodimer and BMP9/BMP10 heterodimer ..... 159

3. Deletion of cardiac BMP10 in parallel with BMP9 did not reveal aberrant postnatal angiogenesis ..... 160
4. BMP10 seems to hold a function in postnatal lymphatic vessels remodelling and maintenance ..... 162
Methodology ..... 169
Transgenic mice generation ..... 169
Enzyme-linked immunosorbent assay (ELISA) ..... 170
Cell culture, transfection, and dual luciferase activity assay ..... 170
Retina preparation and immunofluorescence ..... 171
Organs preparation for lymphatic vessel immunofluorescence ..... 171
Ear preparation for 2-photon confocal ..... 171
Discussion ..... 173
Perspectives ..... 181
Bibliography ..... 185

# List of Figures

**Figure 1:** Schematic illustration of circulatory system composed of blood vascular system and lymphatic system. ..... 14

**Figure 2:** Structure of different types of blood vessels. ..... 15

**Figure 3:** Schematic illustration of vasculogenesis. ..... 17

**Figure 4:** Schematic illustration of intussusceptive angiogenesis. ..... 18

**Figure 5:** Schematic illustration of a vessel sprout. ..... 20

**Figure 6:** Mechanochemical drivers of sprouting angiogenesis. ..... 22

**Figure 7:** Schematic illustration of arterio-venous differentiation. ..... 26

**Figure 9:** Schematic overview of lymphatic network hierarchical structure. ..... 29

**Figure 10:** Schematic overview of the haematopoietic system in adults. ..... 32

**Figure 11:** Diagram representing an overview of the timing and main events of haematopoiesis in mouse embryo. ..... 34

**Figure 12:** Diagram showing factors involved in the process of haemogenic endothelium (HE) formation and rise of HSPC. ..... 36

**Figure 13:** Schematic diagram representing the endothelial to mesenchymal transition (EndMT). ..... 37

**Figure 14:** Phylogenetic tree of the 33 TGF-β family polypeptides in human. ..... 39

**Figure 15:** Schematic representation of TGF-β and BMP signalling. ..... 41

**Figure 16:** Diagram representing sub-group differentiation of BMP/GDFs based on their structural homology. ..... 44

**Figure 17:** Schematic representation of BMP biosynthesis and processing. ..... 45

**Figure 18:** Schematic illustration of mouse heart development. ..... 52

**Figure 19:** Schematic summary of BMP9 and BMP9-10 functions in vascular homeostasis. ..... 57

**Figure 20:** Mutation in the BMP9/BMP10-ALK1 pathway cause cardiovascular diseases. ..... 61

**Figure 21:** Different possibilities of Cre-mediated DNA recombination. ..... 63

**Figure 22:** Schematic diagram representing Cre/loxP-mediated recombination. ..... 64

**Figure 23:** Schematic illustration of inducible Cre-loxP recombination system. ..... 65

**Figure 24:** Representation of vascular retina development in 3C57Bl/6 strain. ..... 67

**Figure 25:** Representation of fully formed retina at P25 C57Bl/6 strain at P25. ..... 68

**Figure 26:** Schematic illustration of EC migration during active angiogenesis. ..... 69

**Figure 27:** Rosa CreERT2 BMP10 iKO displayed strong defects in haematopoietic organs.....117

**Figure 28:** Lineage precursors cells in bone marrow are affected in Rosa Cre BMP10 iKO. ...118

**Figure 29:** Rosa Cre BMP10 iKO models revealed a slight increase in percentage of lineage non-committed cells and HPC-2 $CD150^{+}CD48^{+}$. .....120

**Figure 30:** Diagram showing the blood vessel arrangement in the bone. .....121

**Figure 31:** Increase and dilation of diaphyseal sinusoidal vessels in Rosa Cre BMP10 iKO. ....122

**Figure 32:** Increase of bone marrow $Emcn^{+}CD31^{+}$ endothelial cells in Rosa Cre BMP10 iKO. 122

**Figure 33:** Rosa Cre BMP10 iKO mice revealed the bone marrow vascular phenotype at P12 when there is still circulating BMP10 activity. .....123

**Figure 34:** Injecting neutralising antibodies against either BMP9, BMP10 or ALK1 did not phenocopied hematopoietic defect observed in Rosa Cre iKO BMP10. .....124

**Figure 35:** Concomitant deletion of Bmp9 and Bmp10 increases retina vascularisation. .....151

**Figure 36**:Concomitant deletion of BMP9 and BMP10 results in increase vasculature in the capillaries front, EC hyperplasia and veins enlargement. .....153

**Figure 37:** Rosa Cre BMP10 iKO show abnormal veins smooth muscle coverage in postnatal angiogenic retina. .....154

**Figure 38:** qPCR of liver BMP10 and BMP9 and liver and right atria of P9 pups. .....155

**Figure 39:** BMP10 secreted from the liver, but not the heart, is responsible for activity detected in the plasma. .....156

**Figure 40:** Circulating measured BMP10 comes from the liver. .....158

**Figure 41:** BMP9-BMP10 heterodimer comes from the liver. .....159

**Figure 42:** BMP10 from the right atria is not critical for postnatal retinal development. .....161

**Figure 43:** BMP9 and BMP10 single KO present capillaries lymphatics vessels enlargement. 163

**Figure 44:** Rosa Cre ERT2 activation does not influence lymphatic maintenance in postnatal pups. .....164

**Figure 45:** Early deletion of cardiac BMP10 does not affect lymphatic capillaries in young mouse models. .....165

**Figure 46:** Deletion of hepatic BMP10 does not affect lymphatic capillaries in adult mouse models. .....166

**Figure 47:** Whole ear staining of VEGFR3+ lymphatic vessels in WT BMP10 lox/lox at P9. ....167

**Figure 48:** Deletion of BMP10 results in in slight increase in diameter of total lymphatic vessels in trachea of postnatal mice. .....168

**Figure 49:** Final result for P9 ear mounting for 2-photon microscopy. .....172

# List of Tables

**Table 1:** Interactions between ligands and receptors in the TGF-β family .....43

**Table 2:** Non-exhaustive list of principle constitutive and inducible transgenic mouse models to study vascular malformations induced by defects in BMP9-10/ALK1/ENG/SMAD4 signalling pathway. .....71

**Table 3:** Summary of most commonly used mice and rat models for PAH.....73

**Table 4:** Transgenic mice models used during PhD thesis.....77

# Abbreviations

4-OHT: 4-HydoxyTamoxifen
αMHC: α-Myosin Heavy Chain
αSMA: α Smooth Muscle Actin
Acvlr1: Activin A Receptor Like Type 1
ADAM17: A Disintegrin And Metalloprotease 17
ADM: Adrenomedullin
AGM: Aorta-Gonad-Mesonephros
ALK: Activin receptor-Like Kinase
ANGPT: Angiopoietin
APJ: Apelin receptor
A/V: Arterio-Venous
AVM: Arteriovenous Malformation
BAC: Bacterial Artificial Chromosomes
BAEC: Bovine Aorta Endothelial Cells
BAMBI: BMP and Activin Membrane-Bound Inhibitor
BMP: Bone Morphogenetic Protein
BMPER: Bone Morphogenetic Protein-binding Endothelial Regulator
bp: Base pairs
BRAM: Bone morphogenetic protein-Receptor-Associated Molecule
CAV-1: Caveolin-1
CBC: Complete Blood Count
Cbfβ: Core Binding Factor-β
Chd5: Cadherin 5
CKGF: Cysteine Knot Growth Factor
cKO: Conditional Knock-out
CLP: Common-Lymphoid Progenitor
CMP: Common-Myeloid Progenitors
CO: Cardiac Output
Co-SMAD: Common partner SMAD
COUP-TFII: Chicken Ovalbumin Upstream Promoter-Transcription Factor II
CRACC: CD2-like Receptor Activating Cytotoxic Cells
Cre: Cyclization Recombinase
CreERT: Cre Estrogen Receptor Tamoxifen
CRISPR: Clustered Regularly Interspaced Short Palindromic Repeats
CV: Crossveinless
DKO: Double knock-out
DLL4: Delta-Like Ligand 4

ds: Double Strand
E: Embryonic day
ECM: Extracellular Matrix
EDA: Extra Domain A
EGFL: Epidermal Growth Factor-Like Domain
EHT: Endothelial to Haematopoietic Transition
EIF2AK: Eukaryotic translation Initiation Factor 2 Alpha Kinase
EMP: Erythro-Myeloid Progenitor
Emcn: Endomucin
EndMT: Endothelial to Mesenchymal Transition
ENG: Endoglin
ERK: Extracellular Signal–Regulated Kinase
Eph: Ephrin
ES: Embryonic Stem
ERG: ETS-related gene
FAP: Fibroblast Activating Protein
FGF: Fibroblast Growth Factor
FHF: First Heart Field
FSP: Fibroblast Special Protein
FOXC2: Forkhead Box Protein C2
FRT: Flippase Recognition Target
GOF: Gain-Of-Function
GS: Glycine/Serine
HE: Haemogenic Endothelium
HECs: Haemogenic Endothelial Cells
HES: Hairy and Enhancer of Split
HHT: Hereditary Haemorrhagic Telangiectasia
HMVEC-D: Human Microvascular Endothelial Cells Dermal
HOHF: High Output Heart Failure
HPAEC: Human Pulmonary Artery Endothelial Cells
HPSC: Haematopoietic Stem and Progenitor Cells
HPC: Hematopoietic Progenitors Cell
HSCs: Haematopoietic Stem Cells
HSP90: Heat Shock Protein 90
HUVEC: Human Umbilical Vein Endothelial Cells
IAR: Intussusceptive Arborisation
IB4: Isolectin B4
IBR: Intussusceptive Branching Remodelling
ID: Inhibitor of Differentiation or Inhibitor of DNA binding
iKO: Inducible Knock-out

IKK: IκB kinase
IL: Interleukin
IMG: Intussusceptive Microvascular Growth
IR: Insulin Receptor
JAG1: Jagged1
JAM: Junctional Adhesion Molecule
JNK: c-Jun amino terminal Kinase
JP: Juvenile Polyposis
KCNK: K Subfamily Potassium Channel Member
KO: Knock-Out
LDL: Low-Density Lipoprotein
LECs: Lymphatic Endothelial Cells
L1: Line1 Transposon
LMPP: Lymphoid Multipotent Progenitor
LOF: Loss-Of-Function
LoxP: Locus Of X-over, P1
LPS: Lipopolysaccharide
LYVE-1: Lymphatic Vessel Endothelial Hyaluronic Acid Receptor-1
MAPK: Mitogen-Activated Protein Kinase
MEF: Mouse Embryo Fibroblasts
mPAP: Mean Pulmonary Arterial Pressure
MPP: Multipotent Progenitors
N: Neural
NFkB: Nuclear Factor Kappa Beta
NRP1: Neuropilin 1
NTB-A: Natural Killer T- and B-cell Antigen
OASIS: Old Astrocyte Specifically Induced Substance
P: Postnatal
PAH: Pulmonary Arterial Hypertension
PAVMs: Pulmonary Arteriovenous Malformation
PDGFB: Platelet-Derived Growth Factor Beta Polypeptide
PDPN: Podoplanin
PH: Pulmonary Hypertension
PI3K: Phosphoinositide-3 Kinase
PLVAP: Plasmalemma Vesicle Associated Protein
P-SP: Para-aortic Splanchnopleura
PTPN14: Protein Tyrosine Phosphatase Non-Receptor Type 14
Prox-1: Prospero-Homeobox-1
Prx2: Paired-related homeobox
PVR: Pulmonary Vascular Resistance

R26: Rosa26
RBC: Red Blood Cell
RGM: Repulsive Guidance Molecule
R-SMAD: Receptor-Regulated SMAD
RVSP: Right Ventricle Systolic Pressure
Runx: Runt-related transcription factor 1
SCF: Stem Cell Factor
SCL: Stem Cell Leukemia
SHF: Second Heart Field
SHH: Sonic Hedgehog
SLAM: Signalling Lymphocytic Activation Molecule
SMAD: Suppressor of Mothers against Decapentaplegic
SMMHC: Smooth Muscle Myosin Heavy Chain
SNAI: Snail Family Transcriptional Repressor
Sox: SRY-Box Transcription Factor
SPEM: Spasmolytic Polypeptide-Expressing Metaplasia
S1PR1: Sphingosine-1-Phosphate Receptor;
TBX: T-box
TIE2: Tyrosine Kinase with Immunoglobulin-like and EGF-like domains 2
TIEG: TGFβ -Inducible Early Gene
TGF-β: Transforming Growth Factor β
TNFα: Tumour Necrosis Factor alpha
VA: Vascular Anomalies
VE: Vascular Endothelial
VEGF: Vascular Endothelial Growth Factor
VEGFR: Vascular Endothelial Growth Factor Receptor
VM: Vascular Malformations
vSMC: Vascular Smooth Muscle Cell
vWF: Von Willebrand Factor
Wnt: Wingless/Integrated
WT: Wild-Type
XIAP: X-linked inhibitor of apoptosis protein
ZEB: Zinc Finger E-Box Binding Homeobox

# Summary

BMP9 and BMP10 are two specific ligands of the receptor ALK1, a type I BMP receptor mainly expressed on vascular endothelial cells. Mutations in the BMP9/BMP10/ALK1/ENG signalling pathway are linked to vascular diseases including hereditary hemorrhagic telangiectasia (HHT) and pulmonary arterial hypertension (PAH). BMP9 is expressed by the liver, whereas the primary source of BMP10 is the heart. However, BMP10 is also found to some extent in the liver, where it could form a BMP9/10 heterodimer, that has been described as circulating form responsible for ALK1 activity on endothelial cells. The aim of my thesis project was to unveil BMP9 and BMP10 functions in cardiovascular homeostasis in both postnatal and adult mouse models deficient for BMP9 and/or BMP10 and to discriminate between cardiac and hepatic BMP10 roles. While BMP9 was constitutively deleted, BMP10 deletion had to be achieved using the ubiquitous Rosa26 CreERT2 tamoxifen-inducible promoter, to bypass embryonic lethality.

Our results show that BMP10 iKO adults did not develop any obvious age-dependent cardiovascular defects, however, concomitant deletion of the two ligands (double-KO *Bmp9*$^{-/-}$ R26CreERT2 *Bmp10*$^{lox/lox}$) results in strong vascular defects, showing that both ligands participate to vascular homeostasis. In younger animals, we initially identified that tamoxifen-injected Rosa26 CreERT2 BMP10 iKO mice showed strong hematopoiesis defects. Unfortunately, we demonstrated that the observed phenotype was an artefact induced by CreERT2 toxicity. Indeed, upon tamoxifen administration to Rosa 26 CreERT2 pups lacking a targeted floxed allele, we observed a similar phenotype to that of the Rosa Cre BMP10 iKO. In the bone marrow of these animals, highly proliferative haematopoietic cells were strongly depleted, and the sinusoidal vessels were completely disorganised. Our work shed light on the importance of using the right controls when working with inducible Cre dependent mice models. Conversely, in the context of newborn lymphangiogenesis, we confirmed a functional role of BMP10 in the lymphatic vasculature which is not due to the Rosa 26 CreERT2.

In addition, we proved the importance of BMP9 and BMP10 in vascular development and angiogenesis using the postnatal retina angiogenesis model. In particular, combined loss of BMP9 and BMP10 resulted in a significant decrease of the vascular radial extension, veins enlargement, arterial loss of αSMA coverage and a strong increase in capillaries density. In order to discriminate between cardiac and liver BMP10 function, we generated BMP10 KO models using either the cardiac-specific α-myosin heavy chain (αMHC)-MerCreMer inducible promoter or lecithin-retinol acyltransferase (Lrat)-Cre constitutive promoter, expressed in hepatic stellate cells. We could confirm tissue-specific BMP10 invalidation in both mice models. Moreover, analysis of the plasma obtained from these animals allowed us to confirm the hepatic origin of the circulating active heterodimer composed by BMP9 and BMP10, yet their functional role remains to be determined.

# Résumé

BMP9 et BMP10 sont deux ligands spécifiques du récepteur ALK1 exprimé principalement sur les cellules endothéliales. Des mutations dans la voie de signalisation BMP9/BMP10/ALK1/ENG sont liées à des pathologies vasculaires, notamment la maladie de Rendu-Osler et l'hypertension artérielle pulmonaire (HTAP). BMP9 est exprimé par le foie, tandis que la source principale de la BMP10 est le cœur. Cependant, BMP10 est aussi exprimé par le foie, où il pourrait former un hétérodimère BMP9/10 circulant responsable de l'activité d'ALK1 activité sur les cellules endothéliales. L'objectif de ma thèse était de caractériser les rôles de BMP9 et BMP10 dans l'homéostasie cardiovasculaire à l'aide de modèles de souris déficients pour BMP9 et/ou BMP10 et de discriminer les fonctions cardiaques et hépatiques de BMP10. Alors que l'expression de BMP9 a été invalidée de manière constitutive, la délétion de BMP10 a dû être générée à l'aide du promoteur inductible ubiquitaire Rosa26-CreERT2, afin de contourner la létalité embryonnaire.

Nos résultats montrent que, alors que les souris adultes iKO Bmp10 n'ont pas développé de défauts cardiovasculaires majeurs, la délétion concomitante des deux ligands (double-KO *Bmp9*$^{-/-}$ R26CreERT2 *Bmp10*$^{lox/lox}$) entraîne d'importants défauts vasculaires, montrant que les deux ligands participent à l'homéostasie vasculaire. Chez les animaux plus jeunes, nous avons initialement identifié que les souris Rosa26 CreERT2 BMP10 iKO injectées par tamoxifène présentaient des défauts d'hématopoïèse. Malheureusement, nous avons démontré que le phénotype observé était un artefact induit par la toxicité de CreERT2. En effet, des souris CreERT2 dépourvus d'un allèle floxé developpent un phénotype similaire à celui des Rosa Cre BMP10 iKO. Dans la moelle osseuse de ces animaux, le réseau vasculaire est fortement désorganisé associés à une réduction des cellules hématopoïétiques. Notre travail a mis en lumière l'importance d'utiliser les bons contrôles lorsque l'on travaille avec des modèles de souris dépendantes de la Cre inductible. Par ailleurs, dans le contexte de la lymphangiogenèse postnatale, nous avons confirmé un rôle de BMP10 montrant une augmentation et dilatation des vaisseaux LYVE1$^{+}$ en l'absence de BMP10, défaut qui n'est pas dû à la toxicité de la CreERT2.

Enfin, nous avons prouvé l'importance de BMP9 et BMP10 dans le développement vasculaire en utilisant le modèle d'angiogenèse de la rétine postnatale. La perte combinée de BMP9 et BMP10 a entraîné une diminution de l'extension radiale vasculaire, l'élargissement des veines, et densification du réseau capillaire. Afin de distinguer la fonction cardiaque et hépatique de la BMP10, nous avons généré des modèles BMP10 KO en utilisant le promoteur inductible α-myosin heavy chain (αMHC)-MerCreMer ou le promoteur constitutif lecithin-retinol acyltransferase (Lrat)-Cre, exprimé dans les cellules stellaires hépatiques. Nous avons pu confirmer l'invalidation tissulaire spécifique de BMP10. De plus, l'analyse du plasma a révélé l'origine hépatique de l'hétérodimère BMP9/BMP10, dont le rôle reste à déterminer.

# Introduction

## 1. Vascular system (circulatory system)

The vascular system is defined as the network of blood vessels in which nutritional fluids circulate and it comprises the blood (blood circulatory system) and lymph (lymphatic circulatory system). In vertebrates, the circulatory system consists of a central pumping organ, the heart, which pushes blood to all the tissues in the body (1). The heart consists of four chambers in which blood flows: the right and left atria (upper chambers) receiving incoming blood and the right and left ventricles (lower chambers) pumping blood away from the heart. The right ventricle is responsible to send low-oxygenated blood coming from tissues to the lungs where it travels through the pulmonary artery, gets oxygenated and returns into the heart's left atrium via the pulmonary veins (pulmonary circulation). The left atrium then pushes the oxygenated blood into the left ventricle that is responsible of pumping blood out to the body through the arteries (systemic circulation) **(Figure 1)**. Based on their structure and function, blood vessels are classified as either arteries, arterioles, capillaries, veins and venules. Arteries are generally responsible for transporting oxygenated blood to the tissues with the exception of the pulmonary artery which role is to carry de-oxygenated away from the heart back into the pulmonary circulation for oxygen. On the other hand, the function of systemic veins is to transport de-oxygenated blood from the rest of the body to the heart, where it enters the pulmonary circulation. Once the blood has been oxygenated it returns it to the heart via the pulmonary veins, which are unique in that they carry oxygenated blood (2,3).

Overall, arteries branch into smaller arterioles carrying oxygenated blood into the smallest blood vessels, the capillaries. The capillaries represent the connection between arteries and veins and they are responsible for the exchange of oxygen and nutrients to carbon dioxide and waste between blood and tissue cells. Deoxygenated blood is collected from the capillary beds to the venules, from there it will travel through the veins and flow back to the heart to get oxygenated in the lungs **(Figure 1)** (2).

On the other hand, the lymphatic system is a one-way fluid drainage and transport system, that also acts as an immune response and disease resistance system. During physiological circulation, fluid is pushed out of the bloodstream and filtered by the lymph nodes that will remove bacteria, abnormal cells, and other unwanted substances. The "cleaned" fluid is then returned to the bloodstream via lymph vessels **(Figure 1)** (4).

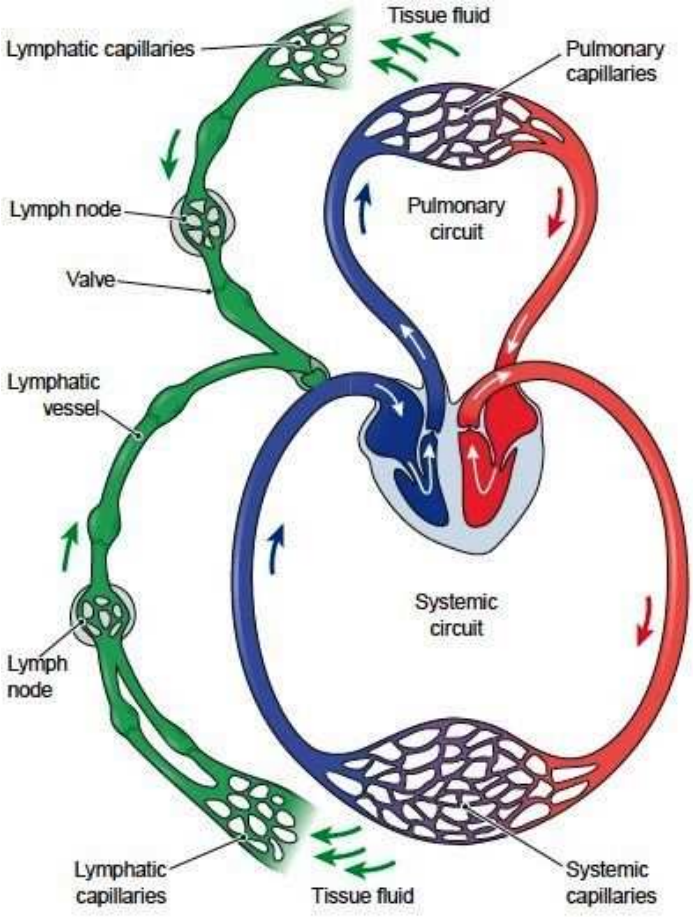


***Figure 1: Schematic illustration of circulatory system composed of blood vascular system and lymphatic system.***
*The heart is the main pumping organs responsible for delivering oxygenated blood to all the tissues. It consist of four chambers: the right and left atria (upper chambers) receiving incoming blood and the right and left ventricles (lower chambers) pumping blood away from the heart. The right ventricle sends low-oxygenated blood coming from tissues to the lungs where it travels through the pulmonary artery, gets oxygenated and returns into the heart's left atrium via the pulmonary veins (pulmonary circulation). The left atrium then pushes the oxygenated blood into the left ventricle that will pump blood to the body via the arteries (pulmonary circulation). The lymphatic system is a one-way fluid drainage and transport system that also act as an immune response and disease resistance system. During blood circulation, fluid is pushed out of the bloodstream and filtered by the lymph nodes to remove unwanted substances. The "cleaned" fluid is then returned to the bloodstream via lymph vessels. Image adapted from https://sphweb.bumc.bu.edu/otlt/mph-modules/ph/ph709_heart/ph709_heart2.html*

The structure of the different types of vessels varies depending on their identity. On one side, capillaries are made up of a layer of endothelial cells (EC) making up the inner lining of the wall with a surrounding basal lamina and pericytes **(Figure 2)**. The other blood vessels are made up of three layers:

- The tunica adventitia: which makes up the outer layer and provides the vessels with the structural supports needed;
- The tunica media: which makes up the middle layer and is composed of both elastic and muscular tissue;
- The tunica intima: which makes up the inner layer and consists of endothelial lining in direct contact with flowing blood.

The main role of the arteries is to deliver blood and nutrients to the body to accommodate all the pressure coming from the pumping heart. Arteries closer to the heart are surrounded by elastin allowing them for maintaining a relatively constant pressure gradient by stretching, as needed, in response to the blood coming from the heart and have low levels of smooth muscle cells (Figure 2). When an artery reaches a particular organ, it branches into smaller arterioles characterised by more smooth muscle and less elastic tissue: this feature will allow them to receive high flow blood from larger arteries into smaller diameter vessels. Veins, differently from the arteries, are characterised by a thinner tunica media and are less elastic as they are exposed to lower levels of pressure (Figure 2).

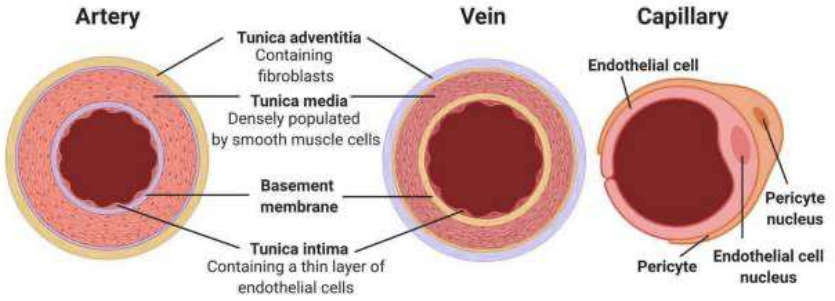


***Figure 2: Structure of different types of blood vessels.***
*Diagram showing the composition of the different layers making up arteries, veins and capillaries in the blood circulatory system. Image taken from "Current Progress in Vascular Engineering and Its Clinical Applications" by Jouda* et al., *Cells, 2022 (3).*

This first introductory chapter is aimed to give a thorough description of the blood vascular and lymphatic systems.

## 1.1 Blood vasculature development

The development of the vasculature, one of the first organ forming during embryogenesis, is crucial for the expansion, maintenance, and function of all other subsequently developing organs. Endothelial cells (ECs) make up the inner luminal layer of blood vessels, while smooth muscle cells (SMC) constitute the surrounding vessel wall. Endothelial cells arise during the development of blood vessels, and they quickly expand and merge into capillary plexi, which later develop into a circulatory network. Smooth muscle cell recruitment, coordinated migration, growth control, and selection of arterial and venous endothelial subtypes are all aspects of vascular remodelling and maturation. The endothelium within the vasculature of different organs is further phenotypically specialised to fit the needs of the tissue. For instance, tight connections are established in the brain and retina to build a barrier against the infiltration of circulating cells and molecules. In contrast, the endothelium can be discontinuous and grow fenestrae in organs with filtering activities, including the kidney and liver, to aid in the infiltration and extravasation of circulating components (5).

Blood vessel formation occurs via two main mechanisms namely vasculogenesis and angiogenesis. Vasculogenesis occurs during embryogenesis and consists of the emergence of

primordial (non-specialised) endothelial cells ultimately resulting into the establishment of a primitive blood vessels plexus, while angiogenesis is defined as the formation of new vessels from pre-existing ones (6,7). During embryonic development, blood vessels are formed via both vasculogenesis and angiogenesis. On the other hand, in the adult, the temporary formation of new blood vessels occurs mainly via angiogenesis and under certain circumstances such as during menstruation cycle, placenta development, myocardium or skeletal muscle adapting process, or wound healing. Nonetheless, it has been shown that also vasculogenesis can occur in adults under certain circumstances such as during tumour development (8,9).

In the following sub-chapters, these two mechanisms will be further explored, with a particular focus to the process of angiogenesis. In particular, as the experiments carried out during the course of the project have been performed using transgenic mouse models, mechanisms of vasculature formation relative to this specie will be mainly described. In some instances, they will be compared to that of other species.

### 1.1.1 Endothelial cells differentiations and vasculogenesis

Vasculogenesis is a process that allows for the formation of endothelial cells from precursor cells (angioblasts), eventually leading to the establishment of a primitive vascular network (10). This process occurs during embryogenesis in parallel to haematopoiesis, as well as in adults under specific circumstances (10,11). The progression of vasculogenesis starts from the migration of mesodermal cells to the yolk sac where they differentiate into hematopoietic cell precursor (haemangioblast) and endothelial cell precursor (angioblast) in response to fibroblast growth factor (FGF)-2 (12). *In vivo* studies revealed that together with FGF2, bone morphogenetic protein (BMP)-4 is implicated in the differentiation of ECs from pluripotent embryonic stem cells (ESCs) (13). To this account, in mouse embryo explants lacking endoderm, Indian hedgehog (IHH) signalling, which is a BMP4 mediator, is sufficient to promote endothelial cell differentiation (14). Moreover, transcriptional regulators of the ETS family are also known to be crucial for the ECs differentiation and virtually all endothelial genes include ETS binding sites in their regulatory domains (15). In particular, ETS (&&variant 2 (Etv2) is a crucial master regulator mediating the differentiation of mesodermal progenitors into ECs (16). Another essential regulator of vasculogenesis is vascular endothelial growth factor (VEGF)-A. VEGF-A primarily binds to two vascular endothelial growth factor receptors (VEGFR) those being VEGFR2, which is the main receptor and is required for the development of the primary vascular plexus, and VEGFR1 which serves as a sink to trap excessive bioactive VEGF-A (5). Mouse embryonic stem cells lacking VEGFR2 are still able to generate ECs, although they fail to proliferate *in vitro*. This could mean that signalling of VEGF-A via VEGFR2 may regulate the survival and/or proliferation of EC, but do not have a function in their fate specification (17). Once precursors are established, they can then fuse to form blood islands from which, shortly

thereafter, endothelial lumens appear transforming these whole-less tubes into functional tubes making up a primitive vascular network via a process known as tubulogenesis that is mediated by VEGF **(Figure 3)** (11,18). The endothelial cell matrix created during the process of vasculogenesis will then serve as a scaffold for angiogenesis.

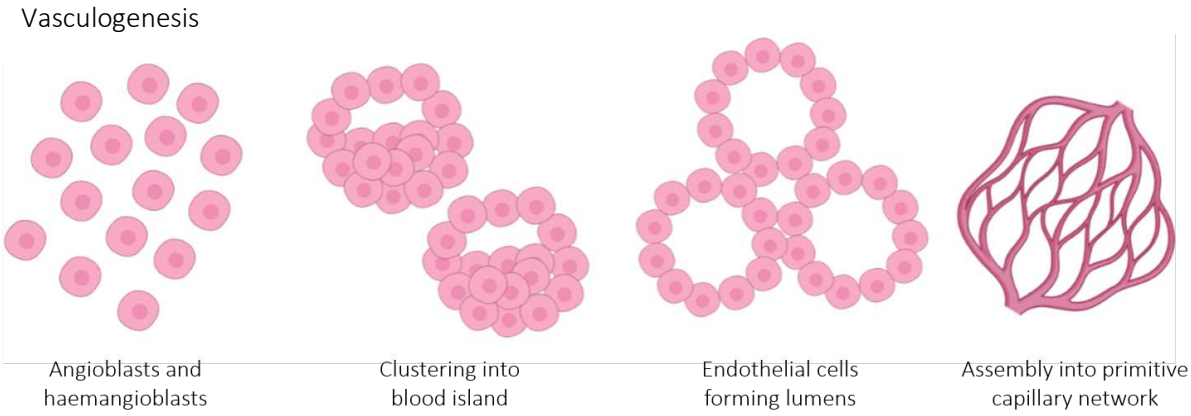


***Figure 3: Schematic illustration of vasculogenesis.***
*Neovessel formation during vasculogenesis: angioblasts and haemangioblast precursors cluster together forming blood islands, resulting in the appearance of lumens and assembly into a primitive vascular network. Image created with BioRender.com.*

### 1.1.2 Angiogenesis and endothelial cell specification

Once established, primitive vascular plexus undergoes further differentiation and specialisation, which will ultimately result in the development of distinct arterial, venous and lymphatic vasculature. The developmental process leading to a fully formed mature endothelium from a vasculogenesis-derived plexus is known as angiogenesis. This process consists of the sprouting and branching of new vessels from the pre-existing ones. Equally to vasculogenesis, angiogenesis occurs during embryonic development when both circulatory system's and organs specific vasculature's are established (8–10). Angiogenesis is an intricate process that relies on the coordination of a wide variety of factors in different cell types. In particular, endothelial cells, pericytes, fibroblasts, and immune cells express many cytokines and growth factors that affect cellular migration, proliferation, tube formation, and vessel establishment. Besides, biomechanical forces such as blood flow and shear stress are also essential during the process of angiogenesis (8).

During tissue development, two different mechanisms of angiogenesis have been described: (i) intussusceptive (also known as splitting) and (ii) sprouting angiogenesis. Sprouting angiogenesis is the main mechanism leading to vascular growth, whereas intussusceptive angiogenesis is a complementary process to sprouting angiogenesis resulting in the formation of trans-capillary tissue pillars from the remodelling and pruning of the vascular plexus. The mechanisms of

intussusceptive and sprouting angiogenesis will be further explained in the following sub-chapters.

### *1.1.2.1 Intussusceptive angiogenesis*

Intussusceptive angiogenesis (or splitting angiogenesis) consist of a non-sprouting mechanics leading to vessel growth and it was firstly described by Burry *et al.* as "the alternative to capillary sprouting" (19,20). Contrary to the well-characterised sprouting angiogenesis, this process was firstly described at the end of the 20$^{th}$ century however, today, it still remains poorly understood (21). Nonetheless, it seems to hold an important function in both physiological growth and remodelling of most vascular beds, as well as in tumorigenic conditions (22).

Intussusceptive angiogenesis occurs via the engulfment of capillary walls into the lumen of established vessels resulting into a segregation and remodelling of the pre-existing vascular network (6,19,22). This process leads to the formation of the so-called intraluminal tissue pillars, which occurs following three main steps hereafter described. Firstly, facing endothelial cell walls start migrating toward each other, inducing a reorganisation of the endothelial junction and the formation of a gap in the centre of the pillar. Secondly, these pillars are colonised by pericytes and myofibroblasts, which will deposit extracellular matrix (ECM) providing the needed structure to the newly forming vessels. Lastly, pillars increase in size, fuse with each other and split up the original vessel into two new vessels leading to expansion of the capillary network and establishing the organ-specific architecture (
Figure **4**) (20). Generation of new blood vessels following this mechanism has also been termed intussusceptive microvascular growth (IMG).

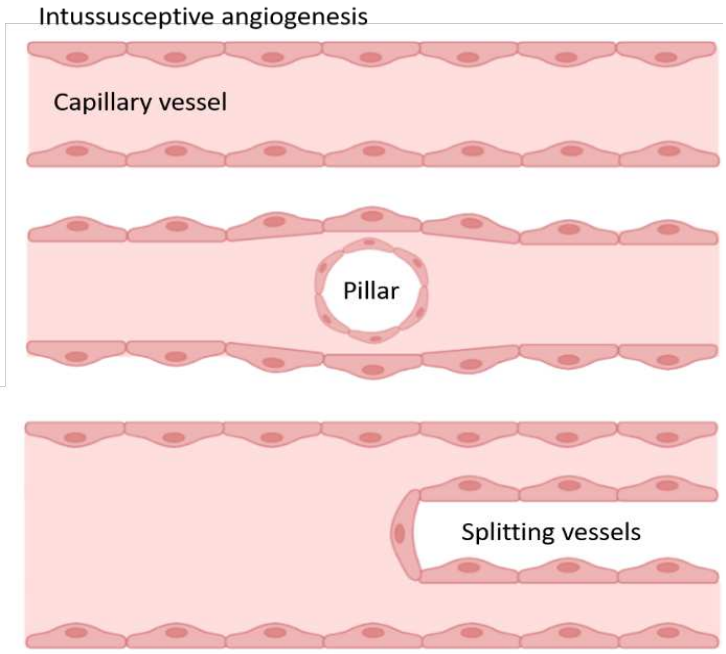


***Figure 4: Schematic illustration of intussusceptive angiogenesis.***
*Intussusceptive angiogenesis occurs via the engulfment of capillary walls into the lumen of established vessels resulting into the formation of intraluminal tissue pillars. Pillars are then colonised by pericytes and myofibroblasts that will deposit extracellular matrix, they will then increase in size, fuse with each other and split up the original vessel into two new vessels. Image created with BioRender.com*

Apart from IMG, two other different forms of intussusceptive angiogenesis have been described: intussusceptive arborisation (IAR), and intussusceptive branching remodelling (IBR) (20). IAR contributes to the hierarchical remodelling of a vascular plexus where major arterioles, venules, and capillaries can be distinguished. In contrast, IBR allows for the optimisation of the vessel number to allow for an orderly supply of blood throughout the whole tissue (20,23). In particular, IBR occurs usually close to the divergence of two blood vessels. Furthermore, the remodelling of existing capillary beds occurs either via expansion or pruning of the vessels to optimise the haemodynamics in the existent vascular trees (24–26). Under physiological conditions, all three intussusceptive angiogenesis routes can take place in parallel to meet the requirements of the forming vascular bed.

### *1.1.2.2 Sprouting angiogenesis*

Sprouting angiogenesis is mostly regulated by paracrine signalling from angiogenic growth factors expressed in hypoxic tissues (27,28). The process is characterised by two separate phases, those being neovessel growth and vessel stabilisation. During the first step, vessels dilate and permeabilise. This allows for extravasation of proteins necessary for the dissolution of endothelial basement membrane into a temporary scaffold for migration towards an angiogenic gradient and eventual proliferation at the vascular forming active front (7). As proliferation follows, the vessels continue to grow, followed by formation of loops via anastomosis which will ultimately lumenise (29,30). The growth of the neovessels is then trailed by a stabilisation phase that consist of proliferation arrest, remodelling of the vessels and recruitment of mural cells that will cover the vessels (29,30). The composition of angiogenic sprouts have been extensively studied over the years. The growing vascular sprout is characterised by three different cell types: tip cells, stalk cells, and phalanx cells (Figure 5). An angiogenic sprout contains a single tip cell at the peak of the growth, which relies on its copious filopodia to scan the surrounding environment and reach toward the angiogenic gradient. Vessels growth in further secured by fusion of tip cells so that new circuits can be added to the existing plexus. Just behind the tip cells, follows the stalk cells, devoid of filopodia, which function is to trail behind the tip cells and proliferate at high rate.

These cells are responsible for the process of vessel lumenization and formation of the vascular basement membrane contributing to the integrity of the capillaries. During the maturation step, stalk cells switch into phalanx cells, which constitute the well-arranged monolayer of endothelial cells that are in direct contact with blood flow. Phalanx cells are characterised by being less proliferative compared to stalk cells and their main function is to line the established blood vessels and form a tight barrier between flowing blood and surrounding tissue, ensuring a quiescent state (31).

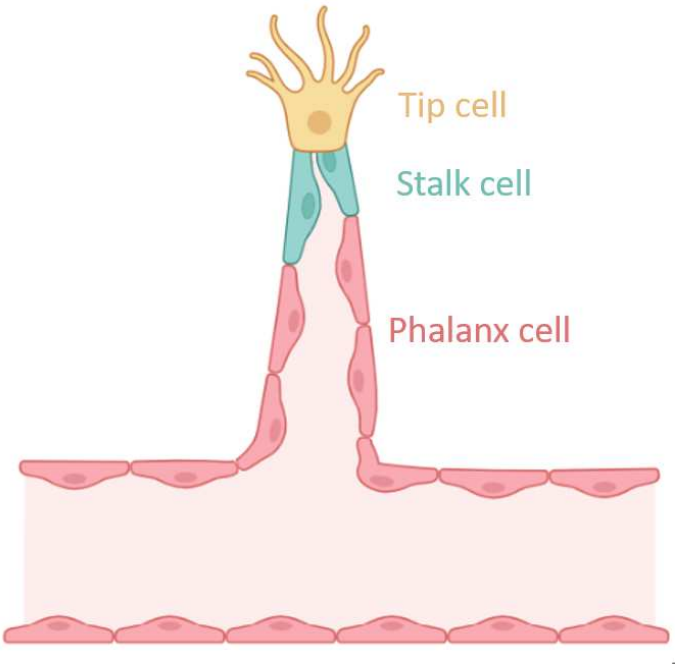


***Figure 5: Schematic illustration of a vessel sprout.***

*The growing vascular sprout is characterised by three different cell types: a single tip cells at the apex of the sprout that relies on its copious filopodia to scan the surrounding environment and reach toward the angiogenic gradient, highly proliferative stalk cells trailing behind the tip cell, and phalanx cells forming basement membrane and enhancing tight junctions. Image created with BioRender.com*

### *1.1.2.2.1 Mechanochemical drivers of sprouting angiogenesis*

Sprouting angiogenesis happens mostly in state of low-perfusion and hypoxia such as tissue development during embryogenesis or wound healing, and it is mainly driven by signals related to local hypoxia (32). A tight mechanism limits the number of tip cells to one-per-sprout, impeding their excessive formation by relying on the competition between adjacent endothelial cells. In particular, formation of tip cells is induced by the expression of VEGF receptors (VEGFR) on the surface of the cells **(Figure 6)** (31). Higher expression levels of VEGFR2 and lower VEGFR1 ensures better chances to gain and maintain the status of tip cell. This happens because the selection of tip cell relies on delta-like ligand 4 (DLL4)/Notch induced pathway, which controls the lateral inhibition and competitive interactions between tip and stalk cells **(Figure 6)**. DLL4 synthesis is induced by VEGFR2 and its expression on tip cells suppresses tip cell fate in neighbouring stalk cells induced via VEGFR1/Notch signalling pathway (33). Notch activation induces an intercellular feedback loop in which VEGFR1 expression is favoured to the expenses of VEGFR2 and VEGFR3 thus impeding the adjacent cells from becoming tip cells (34). In the absence of Notch, this equilibrium is disrupted and stalk cells become tip cells (35). Besides VEGF-A gradients, the direction of sprout protrusion depends also on other ligand/receptor interaction that control tip cell guidance mainly by repulsion. These as axon guidance molecules such as Ephrin/Eph, Semaphorin/Plexin, Slit/Robo and Netrin/UNC5B have been implicated in the control of angiogenic sprouting **(Figure 6)** (32,36).

Tip cells, in addition to VEGFR2 and VEGFR3, express platelet-derived growth factor beta polypeptide (PDGFB), which is important for the recruitment of pericytes to newly formed

vessels (Figure 6) (37,38). Also, macrophages expressing neuropilin 1 (NRP1) and tyrosine kinase with immunoglobulin-like and EGF-like domains 2 (TIE2) have been shown to be important for the anastomosis of tip cells by inducing signalling downstream of VEGF allowing for development of new circuits to the existing plexus (39). In stalk cells, an important ligand is Jagged1 (JAG1), which antagonises the DLL4/Notch interaction (angiogenesis inhibitor), therefore allowing these cells to maintain responsiveness to VEGF and proliferate, but impeding them from transforming into endothelial cells (40). Stalk cells have also been shown to express TIE2 and apelin receptor (APJ). TIE2 receptor is important for endothelial tight junction maturation and pericytes migration via angiopoietin (ANGPT)1 induction (Figure 6), while the APJ receptor is important for the process of lumen formation (41–43). TIE2 is a receptor for both ANGPT1 and ANGPT2 ligands. Competitive binding of ANGPT2 to TIE2 receptor inhibits ANGPT1-induced maturation, thus maintaining a balance between vessel maturation and stalk cells proliferation (44). Another factor expressed by stalk cells is sphingosine-1-phosphate receptor (S1PR1), which signalling blocks angiogenic sprouting by inhibiting VEGFR2 and favouring endothelial cell-cell adhesion via vascular endothelial (VE)-cadherin localisation (Figure 6) (45).

Other signalling pathways known from other developmental have been implicated in the control of angiogenic sprouting. For instance BMPs have been found to be involved in this mechanisms. In particular, BMP2 has been shown to activate the expression of tip cell-associated genes such as DLL4, and BMP6 has been shown to induce SMAD1/5 signalling, promoting the expression of stalk cell–associated genes. BMP2/BMP6 signal via ALK2, which represses sprouting, and ALK3 is required for sprouting. This suggests that expression levels and respective complex formation of BMP type I receptors in ECs determine tip/stalk cell identity. (46). On the other hand, Bone Morphogenetic Protein (BMP)-9 and BMP10 signalling via activin receptor like kinase (ALK)-1 are recognised as antagonists of angiogenesis. BMP9 has been shown to prevent vascular permeability by inhibiting VEGFR2 signalling (47). Nonetheless, the mechanisms behind this process are still unclear and likely context-dependent (Figure 6).

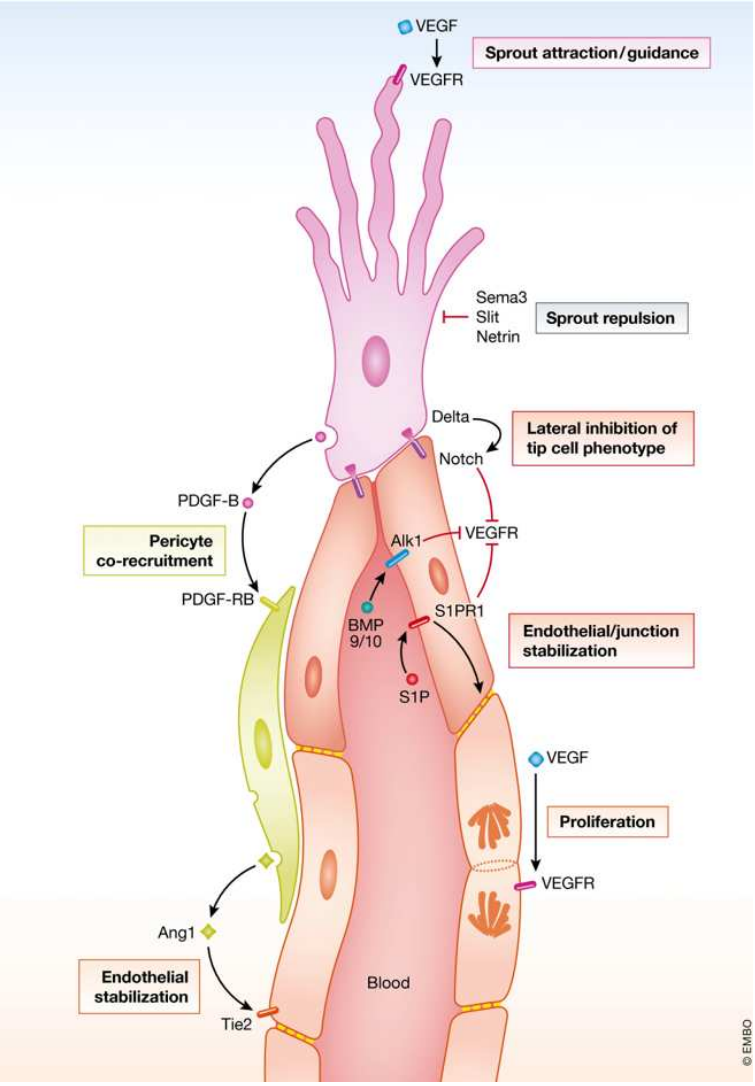


***Figure 6: Mechanochemical drivers of sprouting angiogenesis.***
*Tip cells expressing, VEGFR1, VEGFR2 and DLL4. (35). The direction of sprout depends also on other ligand/receptor interaction Ephrin/Eph, Semaphorin/Plexin, Slit/Robo and Netrin/UNC5B. DLL4/Notch activation prevents adjacent stalk cells from becoming tip cells. Stalk cells expressing VEGFR3, Notch, and TIE2 important for tight junction maturation and pericytes migration. Also, S1PR1 signalling blocks angiogenic sprouting by inhibiting VEGFR2. Circulating factors PDGFB is important for the recruitment of pericytes to newly formed vessels. Competitive binding of ANGPT1 and ANGPT2 to TIE2 receptor maintains a balance between vessel maturation and stalk cells proliferation. BMP9/BMP10 signalling via ALK1 are recognised as antagonists of angiogenesis. BMP9 has been shown to prevent vascular permeability by inhibiting VEGFR2 signalling. Image taken from "Cell–cell signaling in blood vessel development and function" by Betsholtz C., EMBO Mol. Med., 2018 (36).*

### *1.1.2.3 Factors involved in vessel maturation, quiescence and maintenance*

The vessel maturation stage is critical to warrant the return to quiescence of the activated endothelium, and the functionality of the new vascular structures. For newly formed vessels to mature they need the recruitment of mural cells, deposition of ECM and specialisation of the vessel wall for structural support and vessel function (48). Recruitment of mural cells is crucial for vessel maturation. In particular, pericytes establish direct cell-cell contact with ECs in capillaries and immature vessels providing structure and support, whereas vascular smooth muscle cells (vSMCs), enwrapping EC tubule, maintain vascular homeostasis via active vessel contraction and relaxation (49). Additionally, ECs will develop a tissue-specific phenotype adjusted to meet local homeostatic requirements (50). All of these processes are coordinated by physical forces as well as by ligands and receptors spatio-temporally regulated which will be hereafter described.

Besides exerting important function in active angiogenesis, pericytes-secreted AGPT1 and EC-secreted AGPT2 are also important during the maturation stages. VEGF stimulates ANGPT2-induced sprouting and vessel remodelling by inducing the dissociation of pericytes from ECs. Besides, stability of the maturating vessels requires the action of quiescent factors. During vasculature maturation, vessel quiescence is induced and maintained by competitive binding of ANGPT1 to Tie2 receptor impeding signal transduction subsequent destabilisation of mature vessels (51). Moreover, BMP9 and BMP10 have been defined as circulating quiescent factors involved in the development of both blood and lymphatic vessels (52). In particular BMP9 has been described as inhibitor of ECs proliferation and migration via ALK1 receptor expressed in EC **(Figure 6)** (53). Function of BMP9 and BMP10 in this context will be further discussed later.

Quiescent endothelium forms barriers between blood and surrounding tissue to control exchanges of fluids, nutrients and immune cells. To achieve so, ECs specialised in secreting transmembrane-adhesive proteins to regulate cell adhesion between each other's and surrounding cells. Among transmembrane-adhesive proteins there is VE-cadherin at the adherens junction (mediating adhesion, cytoskeletal remodelling and intracellular signalling) as well as claudin, occludin and transmembrane proteins and junctional adhesion molecule (JAM) at the tight junctions (mediating paracellular permeability) (49,54). Endothelial cells also expressed another type of cadherin: neural (N)- cadherin, which function is to promote pericytes recruitment involved in the stabilisation of newly formed vessels by forming pericyte-endothelial heterotypic interactions (55).

Besides molecular signalling influencing vascular fate, blood vessels are under the constant influence of haemodynamic forces, which are crucial for vascular homeostasis. Haemodynamic forces includes (i) shear stress, which is the force applied to the vascular wall as a response to blood flow, (ii) hydrostatic pressure, which is the force applied to the vascular wall as a response to blood pressure and (iii) cyclic stretch, which consist of the circumferential dilation of the vessel wall (56). Endothelial cells sense these mechanical forces to which they are exposed and transduce them into biological responses in a process known as mechanotransduction, which is crucial to regulate not only vascular development and remodelling but also endothelial identity (57,56). Next, arteriovenous specification will be discussed.

### 1.1.3. Arteriovenous identity

Differentiation of the major arteries and veins in the vertebrate circulatory system occurs mainly during early embryonic development prior to the onset of circulation. In some cases arteriovenous specification occurs after birth such as capillaries specification resulting from physiological process such as ovarian follicles maturation, or retina vascularisation in mice, as well as in pathological conditions such as neo-vessel growth in tumorigenic tissues or as a response to vessel growth induced by ischemia (58). The initial embryonic determination of an

artery or vein's identity is controlled by the expression of different molecular markers specifying the fate of endothelial cells. This tightly regulated process will lead to the development of two distinct components of the circulatory loop, each of which has its own distinctive structural characteristics. The processes leading to arteriovenous (A/V) differentiation will be herein described.

To date, many signalling pathways important in A/V differentiation have been recognised, among which Notch pathway activation has been proven indispensable (59). For instance, it has been shown that VEGF-A binds to its receptor VEGFR2 which will assemble with co-receptor NRP1, triggering Notch induced signalling for arterial specification. Notch signalling activation, upregulates the expression of Ephrin (Eph) B2 arterial-specific genes and downregulates venous-specific EphB4 expression **(Figure 6)** (5). Disruption of Notch signalling results in loss of arterial identity and shifting towards veins identity. During vasculogenesis, different blood vessels can be identified based on the expression of different molecular markers, even before the blood starts flowing (58). One of the best examples to this account is the expression of the transmembrane ligands EphB2/EphB4: prior to the establishment of blood flow, these two markers are specifically expressed in different blood islands that will later develop in $EphB2^{+}$ arteries and $EphB4^{+}$ veins **(Figure 6)** (58).

Also, during early vascular development, nerve association has been shown essential for the arterial differentiation patterning. In particular, nerve-derived VEGF has been shown to be important in the process of arterial specification **(Figure 6)** (60). These findings have been crucial to disrupt the hypothesis that A/V identification was merely due to haemodynamic forces. Nonetheless, the ECs plasticity, including A/V differentiation, accounts for the significance of haemodynamic forces in the determination of EC fate. It has been shown that under high flow, arterial ECs elicit mural cell recruitment, which are crucial constituents of the arterial wall, enabling the vessels to withstand high vascular pressures, accounting for haemodynamic role in A/V specification (59). Many other factors have been shown to play important roles in the ECs fate. For instance, expression of wingless/integrated (Wnt) pathway transcriptional co-activator β-catenin has been proven to promote arterial specification via upregulation of DLL4 ligand (61). Another factor involved is the sonic hedgehog (SHH) signalling molecule which acts upstream of VEGF-A, favouring arterial specification over venous identity (62).

Regarding venous specification, it has been assumed for many years that the ECs retain venous identity by default resulting in their fate being defined simply be the lack of arterial specification. However, growing evidence suggests that venous EC identity relies upon dynamic gene regulation. For instance, venous specification requires downregulation of Notch signalling induced by the vein-specific chicken ovalbumin upstream promoter-transcription factor II (COUP-TFII) **(Figure 6)** as well as activation of phosphoinositide-3 kinase-(PIK) AKT pathway

downstream VEGF-A inducing venous differentiation by inhibition of extracellular signal–regulated kinase/mitogen-activated protein kinase (ERK/MAPK) (63,64).

Also, more recently, the role of BMP signalling in venous identification has been highlighted (65). The authors of this study proposed a working model in which venous specification is activated by BMP2/BMP4 signalling via vein-specific ALK3 type I receptor (in association with different BMP type II receptors) resulting in the phosphorylation of Suppressor of Mothers against Decapentaplegic (SMAD)1/5 **(Figure 6)**. Signal translocation to the nucleus will results in transcriptional activation of EphB4 and COUP genes characteristics of venous identity (65). Failure of endothelial cells to properly undergo A/V specification may contribute to vascular malformation and dysfunction, such as in hereditary haemorrhagic telangiectasia (HHT), ultimately resulting in formation of arteriovenous malformation (AVM) consisting of shunts directly connecting arteries and veins lacking clear arteriovenous identity and function. Pathogenesis of HHT will be discussed later.

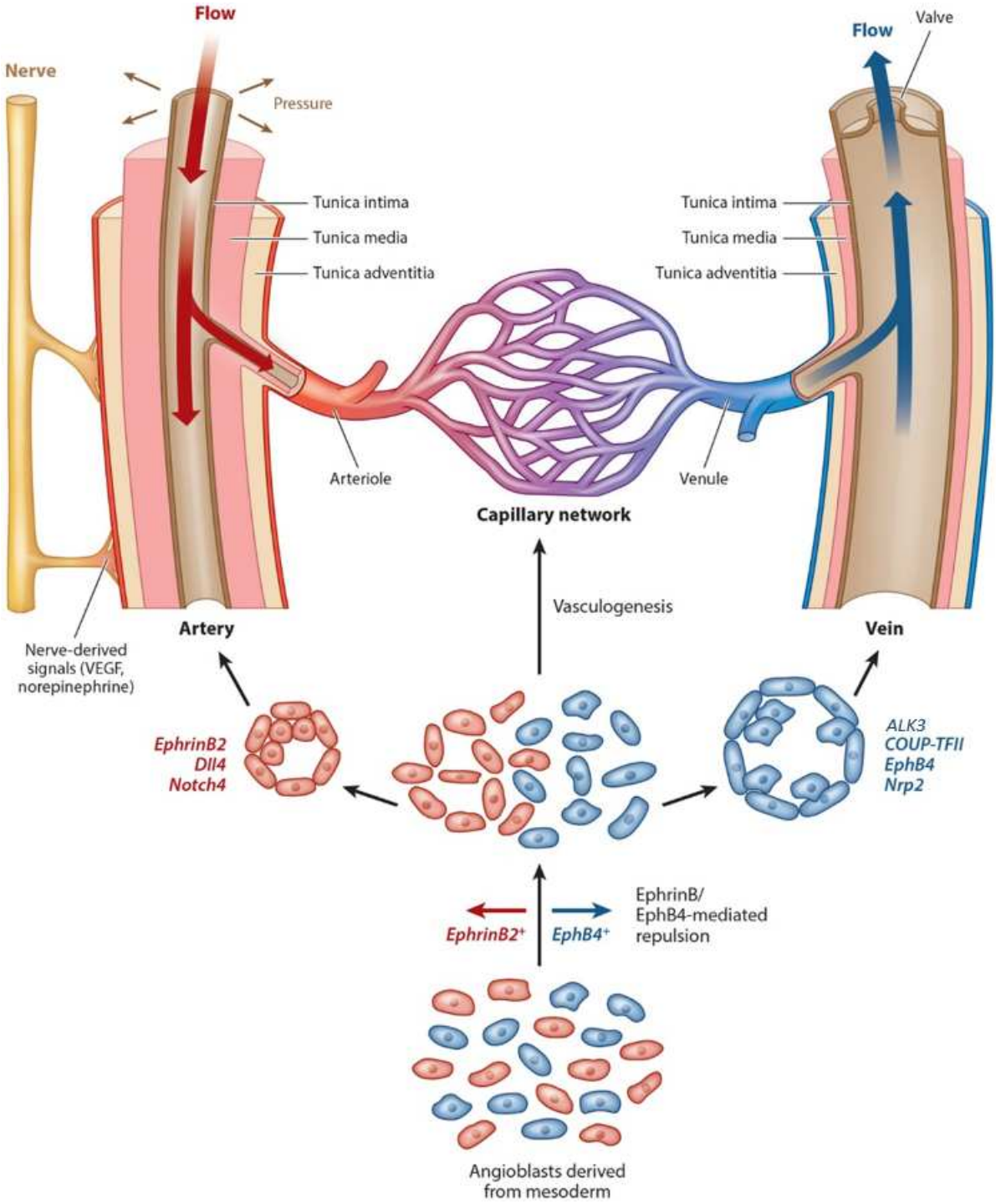


*Figure 7: Schematic illustration of arterio-venous differentiation.*

*During early vascular development, angioblasts, starts to acquire either arterial or venous identity specified by expression of specific molecular markers. Primitive vascular plexus subsequently undergoes extensive remodelling via EphB2/EphB4-mediated cell arterio-venous specification. Notch signalling activation, upregulates the expression of EphB2 arterial-specific marker and downregulates venous-specific EphB4 expression. Arterial differentiation is driven by Notch signalling activating EphB2, initiation of blood flow and VEGF nerve-derived signals, while venous specification is derived by ALK3-induced signalling, Notch de-regulation by COUP-TFII and activation of EphB4. Image adapted from "Arterial Venous Differentiation for Vascular Bioengineering" by Niklason and Dai, Annu. Rev. Biomed. Eng., 2018 (59).*

## 1.2 Lymphatic system development

The lymphatic system consist of an unidirectional conduit belonging to the circulatory system and is important for (i) preserving physiological fluid balance in tissues by absorbing interstitial fluid and macromolecules and return them to the circulation via vein/lymphatic vessels connection, (ii) modulating the inflammatory response to injury or pathogens, and (iii) cholesterol metabolism (66–68). In particular, the lymphatic vasculature is composed of a network of thin-walled, blind-ended, highly permeable initial lymphatic capillaries that take in fluid that continuously leaks out of the arterial blood capillary bed and drain its contents (lymph) into larger caliber collecting lymphatics specialised for transport. Lymph is filtered through lymph nodes before entering the thoracic and the right lymphatic ducts which, in turn, returns the lymph to the bloodstream via two pairs of bilaterally located lymphovenous valves back into the subclavian veins (68). Additionally, the lymphatic system contains lymph nodes, which work closely with the lymphatic vasculature to initiate and expand immune responses while acting as a filtration barrier to stop toxic stimuli from returning to the blood circulation (68). Congenital or acquired dysfunctional lymphatic vasculature can express in different forms, the most widely known being lymphoedema but also they can results in tumours involving the lymphatic system, or in inflammation associated with defective immune system, obesity and cardiovascular disease (69,70).

Lymphatic system arise from veins in a process known as lymphangiogenesis, which begins shortly after blood circulation is established (68). During embryonic vasculogenesis, non-specialised endothelial cells cluster together to form a primitive vascular plexus. Throughout the process of remodelling, these ECs specialise to form specific vascular structures, to develop arterio/venous identity or to form the lymphatics vessels. It is of general agreement that, following specification from mesoderm, local environmental stimuli determine the unique chemical and functional properties of ECs leading to the specialisation of blood vasculature and the formation of lymphatic vessels. In the case of lymphatic development, a subset of blood-vascular endothelial cells (BECs) in the jugular vein will acquire lymphatic identity by activating the master transcription factor in the cardinal vein Prospero-homeobox (Prox)-1 mediated by co-expression of SRY-Box Transcription Factor (Sox)-18 and COUP-TF II (68,71,72). These lymphatic endothelial cells (LECs) will after migrate out of the cardinal vein to form the jugular lymphatic sacs, which give rise to the entire lymphatic vasculature via a process of expansion and sprouting (71).

Nonetheless, some studies have shown that lymphatic endothelial cells (LECs) can also arise from non-venous sources. In particular, haemogenic endothelial derived cells have been demonstrated to supply LEC progenitors to the mesenteric lymphatic vessels, in addition to their venous source (73). Additionally, it has been shown that dorsal dermal lymphatic

vasculature is derived from a population of cells within the dermal blood capillary bed (74) as well as an unidentified, non-vein-derived cell population (75). More recently, it was shown that the lymphatic vasculature on the ventral side of the heart is largely produced from a second population of heart field progenitor cells (76,77). Moreover, recent findings have identified the paraxial mesoderm as the source of the main progenitor lineage that contributes to the majority of Prox-1 positive LECs in the mouse embryo (78).

The following subchapter will focus on the development of the mammalian lymphatic system in the process known as lymphangiogenesis, and adult homeostasis, as well as how to study the lymphatic system development and maintenance *in vivo* using transgenic mouse models.

### 1.2.1 Mechanochemical drivers of lymphangiogenesis

Lymphatic development occurs during mouse embryo development at around embryonic day (E)9.5-10 when a specific subset of EC located within the cardinal vein begins to express the master transcription factor Prox-1 mediated by the co-expression of COUP-TF II and Sox-18. (68,71,72). Next, these lymphatic ECs (LECs) progenitors will bud off from the cardinal vein to initiate the formation of primitive lymph sacs. However, a small subpopulation of LEC will remain associated to the vein to form the lymphovenous valves at the junction, which are necessary for maintaining fluid homeostasis (68).

Prox-1 is a critical factor in the process of lymphangiogenesis and acts by inducing the synthesis of VEGFR3, which will respond to VEGF-C expressed by the surrounding mesenchyme, to initiate VEGF-C/VEGFR3 signalling, crucial in lymphatic endothelial cell survival, proliferation, and migration (79). In turn, VEGFR3 also regulates Prox-1 expression by establishing a feedback loop that is crucial to maintain LECs identity and securing their continuous propagation from the lymph sacs, contributing in the formation of a functional lymphatic vascular network (68). LEC also express receptors important in the process of lymphangiogenesis including NRP2, which binds to VEGF-C and is important for (i), vessels sprouting, (ii) β1-integrin interaction required for the proliferative response of LECs to both fluid accumulation and cell stretching, and (iii) facilitating VEGFR3 phosphorylation. At around E11, podoplanin (PDPN), a transmembrane glycoprotein important for platelets interaction and separation of lymphatic networks from veins, begins to be expressed in the lymph sacs (80).

Once the primitive vascular plexus is formed, the blood and lymphatic vascular system take on different routes for development, whilst maintaining few contacts (lympho-venous valves) to ensure the unidirectional return of lymph fluid to the blood circulation. At this point, the primary lymphatic plexus undergoes extensive expansion and remodelling which will occur during both embryogenesis and postnatal life. Extension of the plexus is marked by lumenization of the vessels and initiation of the flow, which, in turn, initiates valve development

during late stages of embryogenesis, continuing during postnatal growth period. Lymphatic valves are marked by several keys transcription factors namely GATA-binding factor 2 (GATA2), forkhead box protein C2 (FOXC2) and Prox-1. Concomitant expression of FOXC2 and shear stress resulting from flow are important factors for the stabilisation of the lymphatic system providing an essential link between biomechanical forces and LEC identity (81). Following proliferation of LECs from the lymph sac, and subsequent migration into the mesenchymal tissue, begins the differentiation of the three distinct lymphatic vessel types: the collecting lymphatic vessels, the precollectors vessels and the lymphatic capillaries starting from E14.5 **(Figure 8)** (82).

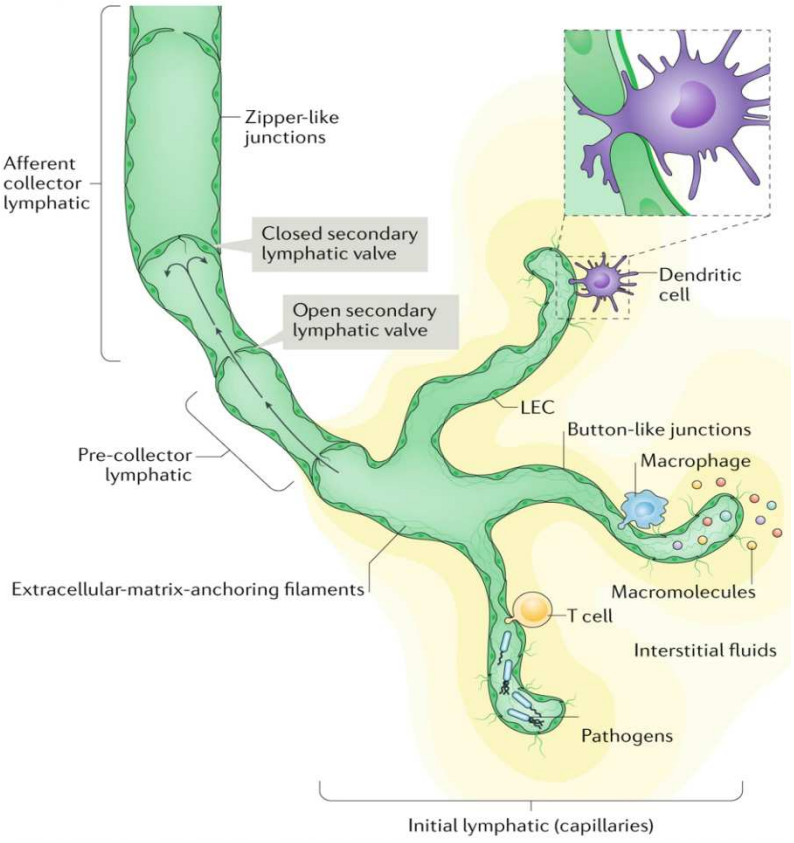


***Figure 8: Schematic overview of lymphatic network hierarchical structure.***

*Lymphatic network consists of the collecting lymphatic vessels, the precollectors vessels and the lymphatic capillaries. Lymph flow begins at the lymphatic capillaries, where loosely connected LECs drain immune cells, fluids, macromolecules and pathogens from the interstitial space, making up the lymph. The lymph flows through the pre-collector and collector vessels that are connected by impermeable zipper junctions, and bicuspid lymphatic valves preventing retrograde flow. Image taken from "The evolving cardiac lymphatic vasculature in development, repair and regeneration" by Klaourakis* et al.*, Nat. Rev. Cardiol., 2021 (82).*

Several major events mark this transition: (i) the development of intraluminal valves, (ii) the recruitment of SMCs in collecting vessels, and (iii) the formation of discontinuous "button-like" junctions in lymphatic capillaries (68). Large collecting vessels are characterised by a continuous basement membrane, zipper-like LEC junctions, SMC coverage and bicuspid lymphatic valves preventing retrograde flow. Their main function is to allow efficient unidirectional transport of lymph (83). Pre-collecting vessels connect capillaries to collecting vessels and are characterised by an intermediate phenotype between the two surrounding vessel types as they possess both oak-leaf shaped ECs (typical of capillaries), and SMC coverage and valves (characteristic of collecting vessels). Their main function is to ensure both absorption and forward motion of the lymph (83). On the other hand, lymphatic capillaries, consists of the initial sections of lymphatic

vessels at the distal part of the network and are characterised by button-like junction connected oak leaf-shaped EC lacking SMC coverage. Capillaries main function is to allow fluid passage and serve as entry points for immune cell. Anchoring filaments sprouting from the main capillaries, allow them to attach to surrounding tissues should they need for any rapid adaptation to changes in biomechanical forces (84).

### 1.2.2 Methods to study the lymphatic system development

The investigation of lymphangiogenesis using *in vitro*, *in vivo*, and, more recently*, in silico* computational models, is critical for providing novel insights and identifying the key molecular actors in the biological dysregulation of this process under physiological and pathological conditions. Although lymphangiogenesis is latent in physiological conditions, as its development is almost entirely restricted to the embryonic or postnatal stages, lymphatic vasculature can undergo intense remodelling under pathological circumstances. This remodelling includes abnormal lymphatic dysplasia, vessel dilatation, and increased permeability, all of which can be linked to lymphangiogenesis. *In vitro* models are useful for studying the mechanisms underlying lymphangiogenesis under controlled experimental conditions. However, no *in vitro* models can currently mimic the entire lymphangiogenesis process, but only parts of it. Lymphangiogenesis assays currently available, rely on 2D in vitro cultures of isolated LECs, which can be applied to investigate any individual step of the lymphangiogenic process (proliferation, migration, invasion, etc.) and morphogenesis. 3D *in vitro* models including organotypic approaches using bio-printing techniques have also been developed. These techniques increase the level of complexity and allow researchers to investigate the biological mechanisms underlying the entire lymphangiogenic process, including hemodynamic mechanisms such as flow (85). Despite its numerous advantages, *in vitro* modelling alone is insufficient for studying and understanding complex and multifactorial mechanisms because it cannot fully mimic all *in vivo* variables. At the moment, *in vivo* models are required for a thorough investigation of the lymphatic system under physiological and pathological conditions. Nonetheless, in the study of processes such as lymphangiogenesis, *in vitro* models are still powerful and make complementary allies of *in vivo* models. To study lymphangiogenesis involvement in developmental biological processes such as cell proliferation, guided migration, differentiation, and cell-to-cell communication, lymphatic-specific imaging techniques are highly required. Researchers were able to develop several lymphatic (as well as blood)-vessel specific, promoter-driven, fluorescent-reporter transgenic mice for *in vivo* as well as *in vitro* lymphatic visualisation thanks to the discovery of lymphatic-specific markers. Available transgenic mice models harbouring fluorescent proteins under the control of a lymphatic-specific marker, have been recently reviewed (86). Despite the great advantages brought by this technique, it has to be considered that the need to sacrifice animal models for tissue harvesting at each experimental time point limits the potential of imaging

techniques such as immunohistochemistry and in situ hybridization. Moreover, *ex vivo* processing of harvested and fixed tissues may introduce artefacts that can lead to a diverted explanation of the eventual observation. Still, transgenic mouse models continue to be the preferred animal model, owing to their genetic and physiological similarities with humans, as well as their ability to be monitored using fluorescent proteins (85).

## 1.3 Other routes of endothelial cell differentiations

The endothelial cells are capable of remarkable plasticity. As it was described, after vasculogenesis, the primitive plexus is remodelled into specific vascular structures that will then give rise to arteries, veins or lymphatic vessels. During organ vascularisation, the endothelial cells will further differentiate to meet the need of the specific organ. Depending on the organ, the endothelial cells can take up specific characteristics based of their function needs. For example, brain ECs are key constituent of the blood-brain barrier (BBB), whose function is to shield the organs from pathogens and controlling access of circulating molecules. For these specific requirements, the brain microvasculature is characterised by ECs with a continuous intercellular barrier defined by the tight junctions connecting adjacent cells. On the other hand, in organs such as kidney and liver, subjected to continuous blood filtration, EC develop fenestrations, which consist of ovoid transcellular holes allowing for the passage of circulating factors. In other instances, endothelial cells undergo a different fate transition leading to the development of another cell type. In this next subchapter two independent differentiation process arising from endothelial cells will be described. In particular:

- Endothelial to haematopoietic transition (EHT): resulting in the formation of hematopoietic stem and progenitor cells (HSPC) responsible for the generation of all blood cellular components;
- Endothelial to mesenchymal transition (EndMT): resulting in the formation of mesenchymal cells contributing in cardiac development.

### 1.3.1 The process of haematopoiesis

The blood and the vascular systems are closely associated in their evolutionary and developmental origins. At the same time of arterial and venous ECs specification, another subtype of endothelial cell arise: the haemogenic ECs. These cells arise during embryonic development from a small-specialised fraction of vascular endothelium, known as haemogenic endothelium (HE), developing inside a specific tissue within a narrow developmental window. Endothelial cells from the HE develops hematopoietic potential and will ultimately give rise to multilineage HSPC in a process known as endothelial to haematopoietic transition (EHT) (5,87).

Haematopoiesis is defined as the process by which the blood cellular component are formed throughout the development of the embryo and is maintained during adulthood (88,89). The haematopoietic system in adults is responsible for the formation of the common-myeloid progenitors (CMP) and the common-lymphoid progenitor (CLP) from a common hematopoietic stem cell (HSC) precursor. The myeloid progenitors will give rise to erythrocytes, thrombocytes (i.e. platelets), basophils, neutrophils, eosinophils and monocytes. The lymphoid progenitors will give rise to T, B, natural killer (NK) and innate lymphocytes (90,91) **(Figure 9)**. In vertebrates, embryonic haematopoiesis has been shown to occur in several waves each giving rise to cohorts of cells which complexity arises along with the succession of waves.

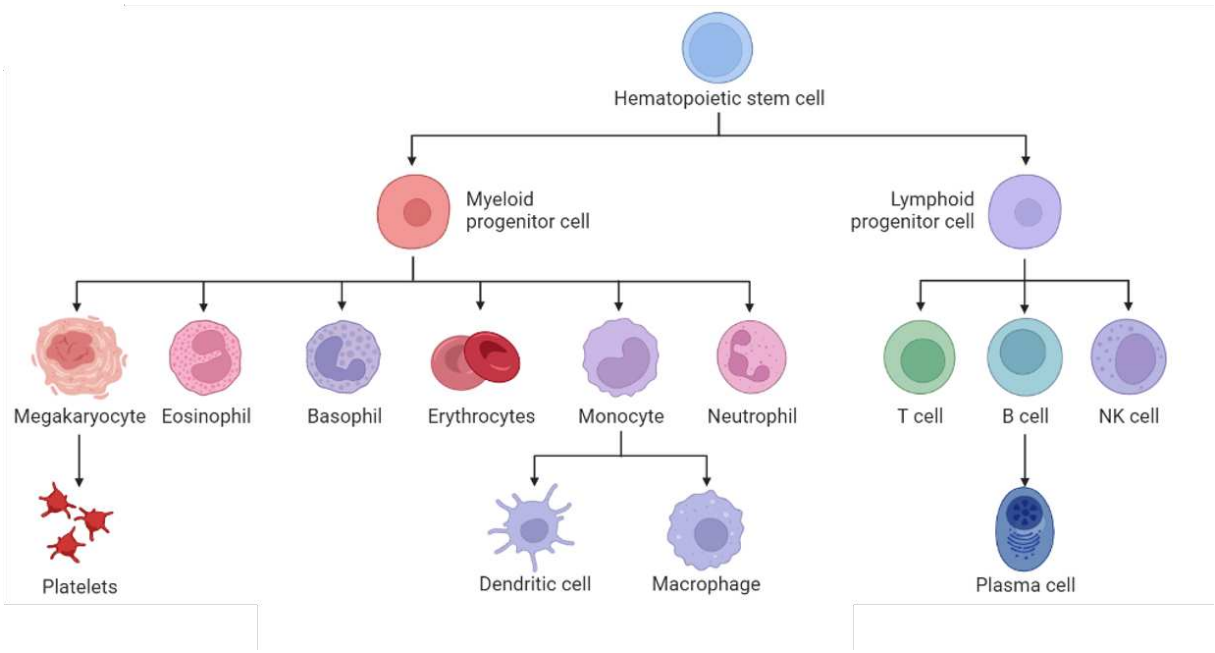


***Figure 9: Schematic overview of the haematopoietic system in adults.***

*Haematopoietic stem cells (HSCs) will give rise to common-myeloid progenitors (CMP) and the common-lymphoid progenitor (CLP) The myeloid progenitors will give rise to erythrocytes, platelets, basophils, neutrophils, eosinophils and monocytes. The lymphoid progenitors will give rise to T, B, natural killer (NK). Image created with BioRender.com.*

At around E7, after gastrulation, the extraembryonic mesoderm begins to produce the first blood and endothelial cells. Whether these cells originate from a single bipotent progenitor (haemangioblast) or whether they follow separate fates is still a matter of debate (92).

A first primitive wave of haematopoiesis emerges at this stage in the yolk sac where extra-embryonic mesoderm gives rise to primitive nucleated erythroid cells, macrophages and megakaryocytes progenitors that are generated in parallel with ECs **(Figure 10)** (87). These primitive erythroid cells are different from later erythroid progenitors in that they are bigger, nucleated, express early stage globins, and are solely distinguished in the extra-embryonic yolk sac during a restricted window lasting 48h before they disappear (93). Other sources of pro-

definitive erythroid and myeloid progenitor cells arise somewhere between E7.5 and E8.0 and include the allantois membrane and para-aortic splanchnopleura (P-SP) region which are vital to the developing organism as they provide the required support before the rise of definitive haematopoietic wave by contributing in the formation of the blood islands (93). In addition, also primitive macrophages and megakaryocytes exhibit characteristics specific to their embryonic origin, making them different from their definitive counterparts. Primitive macrophages appear to mature without going through a monocyte intermediate stage, and primal megakaryocytes have a reduced set of chromosomes and yield to a lower platelet production (94).

A second wave of yolk sac-derived haematopoiesis known as erythro-myeloid progenitor (EMP) haematopoiesis occurs the following day, at around E8.25, and results in the production of definitive erythrocytes, megakaryocytes, and most myeloid lineages **(Figure 10)**.

At about E9.0, in the yolk sac and the embryonic P-SP take place another wave of haematopoiesis that exhibit both lymphoid and myeloid potential and therefore known as lymphoid multipotent progenitor (LMPP) haematopoiesis **(Figure 10)**. The placenta then starts to generate hematopoietic progenitors between E9.0 and E9.5. The primitive wave is followed by a pro-definitive wave that will result in the formation of multipotent haematopoietic progenitor cells (MPP), which is characterised by a limited self-renewal capability yet holds the potential to differentiate into any haematopoietic cell (95,96).

The first haematopoietic stem cells (HSCs) exhibit long-term, multi-lineage capacity are readily observed in mouse embryo at around E10.5. These cells emerge at the wall of aorta-gonad-mesonephros (AGM) region **(Figure 10)** (87,94). In particular, they rise following the a process known as endothelial to hematopoietic transition (EHT), in which endothelial cells located in aortic floor lose their characteristic spindle-shaped morphology, round up and bud into the extravascular space resulting in the formation of the first HSCs **(Figure 11)**.

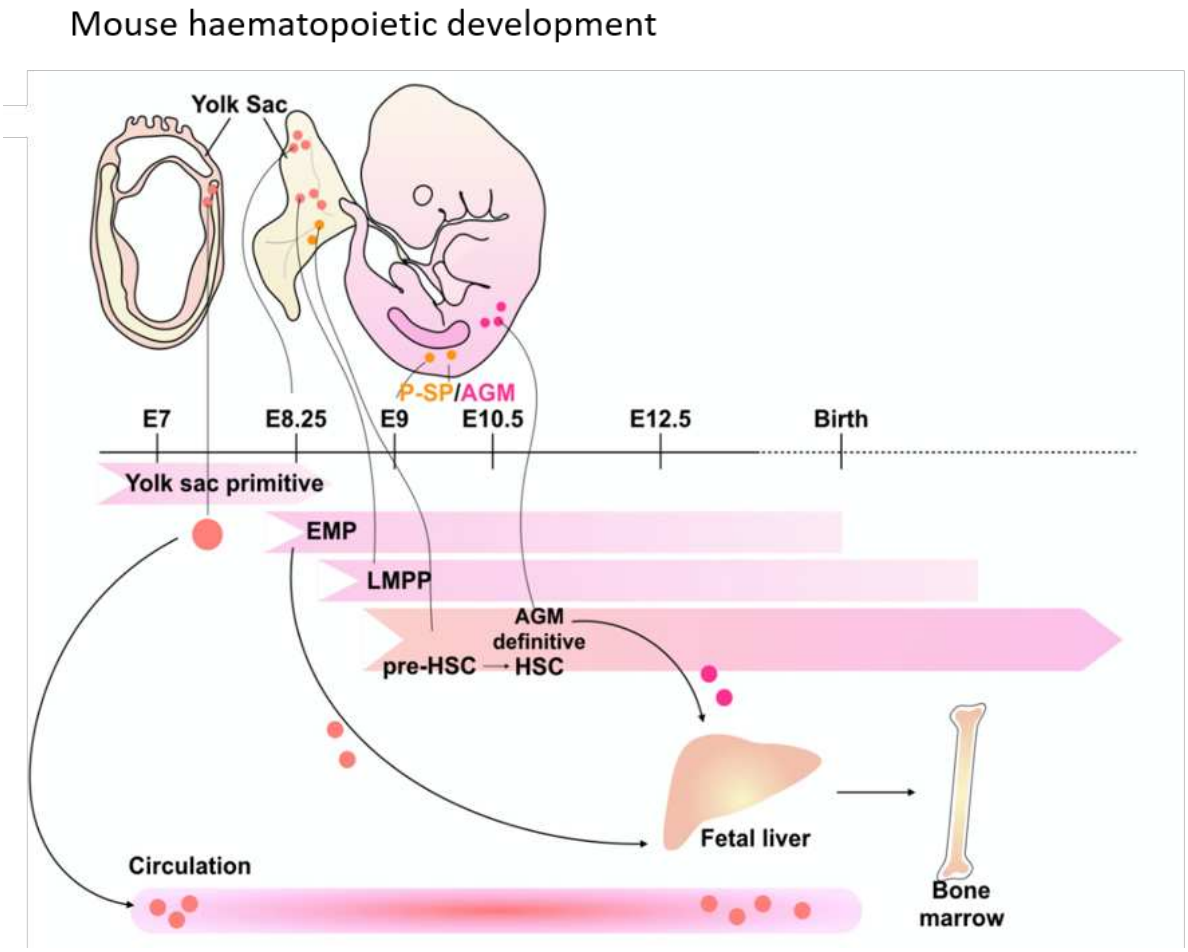


*Figure 10: Diagram representing an overview of the timing and main events of haematopoiesis in mouse embryo. At around E7, a first primitive wave of haematopoiesis emerges at in the yolk sac where extra-embryonic mesoderm gives rise to primitive nucleated erythroid cells, macrophages and megakaryocytes progenitors. A second wave of yolk sac-derived haematopoiesis occurs at around E8.25, and results in the production of definitive erythro-myeloid progenitors (EMP), and most myeloid lineages. At about E9.0, in the yolk sac and the embryonic para-aortic splanchnopleura P-SP take place another wave of haematopoiesis which exhibit both lymphoid and myeloid potential and therefore known as lymphoid multipotent progenitor (LMPP) haematopoiesis. The placenta then starts to generate hematopoietic progenitors between E9.0 and E9.5. The first haematopoietic stem cells (HSCs) exhibit long-term, multi-lineage capacity are readily observed in mouse embryo at around E10.5 and they emerge at the wall of aorta-gonad-mesonephros (AGM) region. From the AGM region, HSCs will then migrate to the foetal liver at around E10.5. The bone marrow is the main secretory organ for haematopoiesis in adults. Image created with BioRender.com.*

Once formed, these cells re-enter the circulation through the underlying vein and seed various hematopoietic niches throughout embryonic development. From the AGM region, HSCs will then migrate to the foetal liver at E10.5. At E14.0 the spleen initiates blood production and will continue to act as an extramedullary haematopoietic organ throughout adulthood at time of stress. At E18 blood production shifts to the bone marrow, which is the main location for haematopoiesis in adults **(Figure 10)** (94). Recently, it has been observed a previously unacknowledged haematopoietic wave that takes place in the bone marrow or late foetus and

young adults. This transient wave is capable of giving rise de novo to HSPCs from haemogenic endothelial cells in both chicken and mice (97).

#### *1.3.1.1 Endothelial-to-Haematopoietic Transition (EHT)*

The development of blood cellular components from the endothelium require two distinct steps: (i) haemogenic endothelial cell specification and (ii) endothelial-to-haematopoietic transition (EHT) process, which are tightly coordinated by the up regulation of a specific transcriptional haematopoietic program at the cost of the endothelial program. At around E10.5, in murine models, endothelial cells lining the AGM region in the dorsal aorta become haemogenic, following a process that will result in disrupting the tight junctions among between endothelial cells which will, in turn, round up to be then released into the blood stream. During this process, blood cells bud off from the vascular endothelium to be then released in the blood vessels (98). This description has been corroborated by fluorescent-tracing experiment that demonstrate the movement and change in shape of these cells from the vessels endothelium to circulating blood. Moreover, *in vivo* fate tracing experiments have further shown the emergence of HSC from vascular endothelial (VE)-cadherin+ ECs and their colonisation of haematopoietic organs including bone marrow, spleen and thymus (99). The steps involved in the formation of HSCs from the haemogenic endothelium depends on the upregulation of several transcriptional factors that will induce a strictly and temporally controlled haematopoietic program. Haemogenic endothelial cells (HECs) cells, which are the progenitors of the haemogenic endothelium (HE), progressively lose their endothelial identity between E8.5 and 10.5 to give rise to the multipotent HSPC (Figure 11).

The initial specification of haemogenic endothelial cells implicates some of the same signalling pathways involved in arterial-venous differentiation, though it appears to be uniquely initiated by retinoic acid signalling (5). Signalling initiated by retinoic acid controls the upregulation of c-Kit, a tyrosine kinase receptor that binds stem cell factor (SCF). C-Kit expression marks a distinctive feature of the haemogenic endothelium, allowing for the differentiation of haemogenic endothelial cells from non-blood forming endothelial cells (100). Two transcriptional factors secreted by the stem cells have been described to be absolutely crucial for the formation of HSCs, those being: Runt-related transcription factor 1 (Runx1) and GATA2. Moreover, expression of the core binding factor-β (Cbfβ) is essential for Runx1 to function and, when its missing, embryos develop the same embryonic lethal phenotype as Runx1 knock-out (KO), characterised by the complete lack of definitive haematopoiesis (101,102). Functional Runx1 expression and relative binding of proteins such as GATA, ETS, and SCL allows for a successful repression of the endothelial program favouring the development of the HE (5).

The Notch signalling pathway is important in the completion of EHT as it is responsible for the expression of GATA2. Nonetheless, Notch signalling promotes arterial program in ECs to the

expenses of the haematopoietic program. JAG1 ligand is responsible for downregulating Notch expression during the ETH. Another transcriptional factor downregulated during this process is Sox-17. Like Notch, Sox-17 is a pro-angiogenic factor therefore, it needs to be downregulated for EHT to occur. (5,87,98). Other binding factors important are ETV2 member of the ETS family, which, besides having an important role in vasculogenesis, is also important in regulating hematopoietic-associated downstream targets such as LIM only protein 2 (Lmo-2) (103,104).

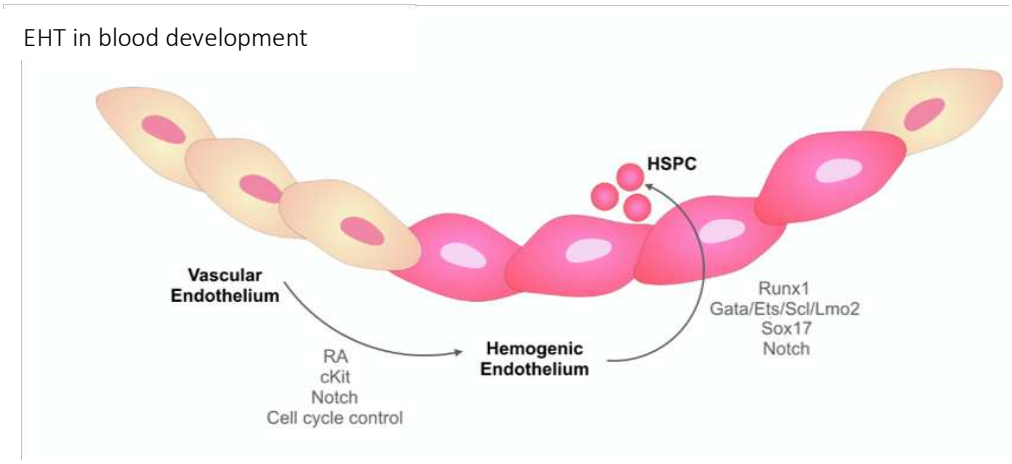


***Figure 11: Diagram showing factors involved in the process of haemogenic endothelium (HE) formation and rise of HSPC.***

*Hematopoietic progenitors develop following a process known as endothelial to hematopoietic transition (EHT) which occur at around E10.5 in murine models. Endothelial cells lining the AGM region in the dorsal aorta lose their characteristic spindle-shaped morphology, round up and bud into the extravascular space resulting in the formation of the first HSCs. The specification of haemogenic endothelial cells requires retinoic acid signalling, which leads to upregulation of c-Kit receptor marker of haematopoietic cells. Two transcriptional factors secreted by the stem cells have been described to be crucial for the formation of HSCs: Runx1 and Gata2. Notch signalling pathway is responsible for the expression of Gata2. Other important binding factors are ETS, Lmo2, and Sox-17. Image created with BioRender.com*

## 1.3.2 Endothelial to Mesenchymal Transition (EndMT)

In addition to vascular endothelial cells within hematopoietic tissues undergoing EHT and giving rise to HSPC, during development, a specialised subset of endothelial cells lining the heart tissue (endocardial cells) undergo a process known as endothelial to mesenchymal transition (EndMT). EndMT occurs in both physiological and pathological conditions, and will result in ECs changing their typical characteristics to give rise to mesenchymal cells characterised by a spindle-shaped elongated cell morphology, loss of cell-cell junctions and polarity, acquisition of cellular motility as well as invasive and contractile properties (105). The process of EndMT contributes in the formation of endocardial cushions progenitor cells that will later develop to form the mitral and tricuspid valves. EndMT also generates cardiac fibroblasts and smooth muscle cells, but not cardiac myocytes. Besides being actively involved during cardiac development, EndMT plays a role during the progression of certain pathologies. In particular,

it has been shown to be involved in diseases such as atherosclerosis and pulmonary arterial hypertension (PAH) and to play a role in the development of haemodynamic abnormalities, inflammation, hypoxia, tumour formation, and vascular fibrosis (106). Moreover, EndMT has been shown to occur during physiological angiogenic sprouting. In particular, during sprouting, ECs express many of the same genes as during the EndMT process allowing for the breakdown of basement membrane, but they retain intercellular junctions. This process, known as intermediate EndMT, requires a critical regulatory checkpoint, determining whether cells transitioning should stop at this point or go further into a full EndMT. At this stage, little is known about how this switch is regulated (107).

Endocardial cells transition into mesenchymal cells during cardiac development via EndMT in the atrioventricular canal and ventricular outflow tract regions. As EndMT progression endothelial markers such as CD31, Von Willebrand factor (vWF), collagen (COL)- IV, VEGFR and VE-cadherin are lost to make space for mesenchymal markers such as α smooth muscle actin (αSMA), extra domain A (EDA) fibronectin, N-cadherin, vimentin, fibroblast-specific protein (FSP)-1, fibroblast activating protein (FAP), and COL-I and COL-III. (105,106) **(Figure 12)**.

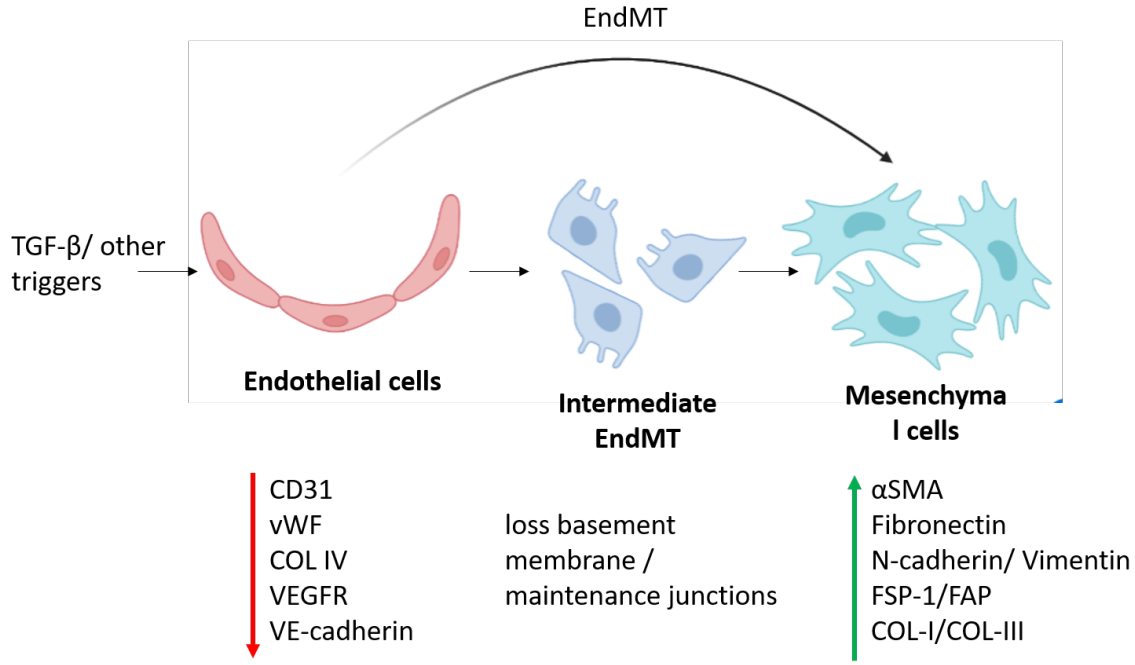


***Figure 12: Schematic diagram representing the endothelial to mesenchymal transition (EndMT).***
*The diagram depicts the morphological, phenotypic, and gene expression program changes that occurs during the process of endothelial to mesenchymal cell transition, resulting in the phenotypic switch of endothelial cells into activated myofibroblasts with increased production of various mesenchymal-specific factors such αSMA, fibronectin, N-cadherin, vimentin, FSP-1, FAP, COL-I, COL-III. Endothelial cell-specific gene products such as CD31, vWF, COL-IV, VEGFR and VE-cadherin are lost resulting from these events. Image created with BioRender.com*

The next chapter will focus on the Transforming Growth Factor β (TGF)-β members, with particular regards to the BMP family of cytokines and their involvement in different functions

from embryonic development to adult homeostatic stages. In particular, blood and lymphatic vascular implication of BMP9 and BMP10, two particular members of this family, will be discussed. Since the discovery of their high affinity towards the endothelial receptor ALK1 made by my group, studying BMP9 and BMP10 function has been the main focus of the team and the topic of my thesis.

# 2. Transforming Growth Factor β (TGF-β) superfamily proteins

TGF-β superfamily consists of a group of varied cytokines conserved in both vertebrates and invertebrates. Members of the TGF-β superfamily are ubiquitously expressed in varied tissues and encompass several functions that range from embryonic development to adult tissue homeostasis (108). In mammals, TGF-β family comprises 33 ligands and is subdivided into several subfamilies: TGF-βs (TGF-β 1 to 3), Bone morphogenetic proteins (BMPs), Growth differentiation factors (GDFs), Activins (A, B), Inhibins (A, B), nodal, and anti-Mullerian hormone proteins **(Figure 13)** (109,110).

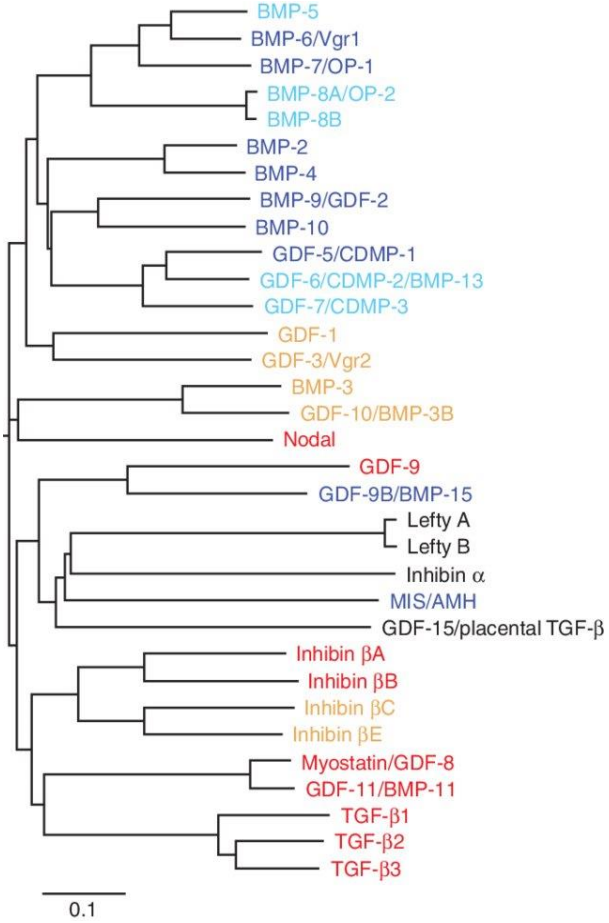


***Figure 13: Phylogenetic tree of the 33 TGF-β family polypeptides in human.***

*Phylogenetic tree representing the members of the TGF-β family obtained from the human amino acid sequences of 33 TGF-β family polypeptides retrieved from NCBI's protein database (www.ncbi.nlm.nih.gov). Activins and TGF-β members are shown in red, BMP members are shown in blue. Ligands whose receptors and Smad-signalling pathways have not been fully determined, are shown in orange or light blue. Abbreviations: BMP, Bone morphogenetic protein; OP, osteogenic protein; GDF, growth and differentiation factor; CDMP, cartilage-derived morphogenetic protein; MIS/AMH, Müllerian-inhibiting substance/anti-Müllerian hormone; TGF-β, transforming growth factor β. Image taken from "TGF-β and the TGF-β Family: Context-Dependent Roles in Cell and Tissue Physiology", Morikawa* et al.*, Cold Spring Harb. Perspect. Biol., 2016 (109).*

All 33 ligands belonging to the TGF-β family share a common conformation. In particular, they are composed of a signal peptide, which is required for secretion, a long polypeptide, and the mature polypeptide, which binds and activates the receptors as a dimer. The ligands generally transmit a signal via transmembrane serine/threonine kinase receptors which mediates the phosphorylation of serine or threonine amino-acid residues thus initiating a signal propagation via the SMAD transcription factors allowing for nuclear translocation where gene expression is regulated (108). Proteins that belong to the TGF-β superfamily are secreted and function as

homodimers or heterodimers and are readily identifiable by a characteristic spacing of seven cysteines in the mature, fully processed polypeptide.

This second introductory chapter will focus on the bone morphogenetic proteins (BMPs) comprised within the TGF-β superfamily. Despite they share with the TGF-β members fundamental conserved characteristics, the signalling pathways that they regulate varies significantly. The BMP family of ligands regulates cellular lineage commitment, morphogenesis, differentiation, proliferation, and apoptosis of various types of cells throughout the body during embryonic development and adult homeostasis. In particular, 15 isoforms have been identified in humans and they have been described in varied contexts including blood and lymphatic development/maintenance, which will be further discussed with a particular focus on BMP9 and BMP10 ligands.

## 2.1 Ligand-receptor interactions

TGF-β superfamily members signal via transmembrane receptors which can be subdivided into type I receptors (7 types also known as receptor-like kinase, i.e., ALK1–7), type II receptors (TβRII, ActRIIA, ActRIIB, and BMPRII and Amhr2) and type III co-receptors (endoglin for BMPs and betaglycan for TGF-β isoforms), which potentiate the signalling pathway (108,111). Ligands bind to selective combinations of type I and II receptors and transduce their signals via two main pathways: (i) SMAD-dependent pathway also called "canonical" pathway, and (ii) SMAD-independent pathway called "non-canonical" pathway.

As for the canonical pathway, upon ligand association to the transmembrane receptors, the type II transmembrane receptor kinases phosphorylates the type I receptors which, in turn, will mediate SMAD-dependent signalling. Ligand-receptor association triggers the activation of type I receptors via phosphorylation of a regulatory glycine/serine (GS)-rich domain. This alters the GS domain's binding specificity, increasing SMAD recruitment, resulting in phosphorylation of the receptors. SMAD proteins are highly conserved among vertebrates; eight SMAD proteins have been identified in mammals namely from SMAD1 to SMAD8 (SMAD8 is also known as SMAD9) (112). These proteins are classified into three functional groups: receptor-regulated (R)-SMADs (SMAD1/5/8 and SMAD2/3), a common (co)-SMAD (SMAD4 in vertebrates), and inhibitory (I)-SMADs (SMAD6 and SMAD7). I-SMADs have only one MAD-homology domain (MH2), whereas R-SMADs and SMAD4 have two (MH1 and MH2). Because SMADs interact with DNA via their MH1 domain, only R-SMADs and SMAD4 are directly involved in gene expression regulation. I-SMADs, on the other hand, modulate TGF-β family signalling. In particular, TGF-β and BMP induce expression of I-SMADs, in vertebrates SMAD 6/7, which, in turn, inhibit canonical SMAD-dependent TGF-β/BMP signalling establishing an important feedback loop. The specificity for the SMAD pathways is determined by the type I receptors also known as

activin receptor-like kinases (ALK). To that account, signal initiated by TGF-β, activin, or nodal via type I receptors ALK 4/5/7 will activate R-SMAD 2/3, whilst BMPs association to ALK1/2/3/6 will activate R-SMAD1/5/8 (112). Association to the R-SMADs will results in the formation of a trimeric complex with co-SMAD4, which acts as a common SMAD to all ligand-activated SMAD pathways, and mediate the transfer of the signal into the nucleus where gene expression is modulated (52). SMAD6 mostly hinders BMP signal transduction initiated by ALK3 and ALK6, while SMAD7 inhibits both TGF-β and BMP signal transduction (113).

Upon phosphorylation, R-SMADs dissociate from the receptor complex and associate with SMAD4 to form an heteromeric complex which will then translocate to the nucleus to regulate gene expression (114). R-SMADs are classified into two groups based on their specificity: the SMAD1/5/8 (responsible for "the BMP-pathway"), which is activated by ALK1/ALK2/ALK3/ALK6, and the SMAD2/3 (responsible for "the Activin/TGF- β pathway"), which is activated by ALK4/5. Significantly, SMAD2/3 and SMAD1/5/8 regulate distinct sets of target genes (Figure 14). Which SMAD branch is activated thus has profound consequences for a cell (115).

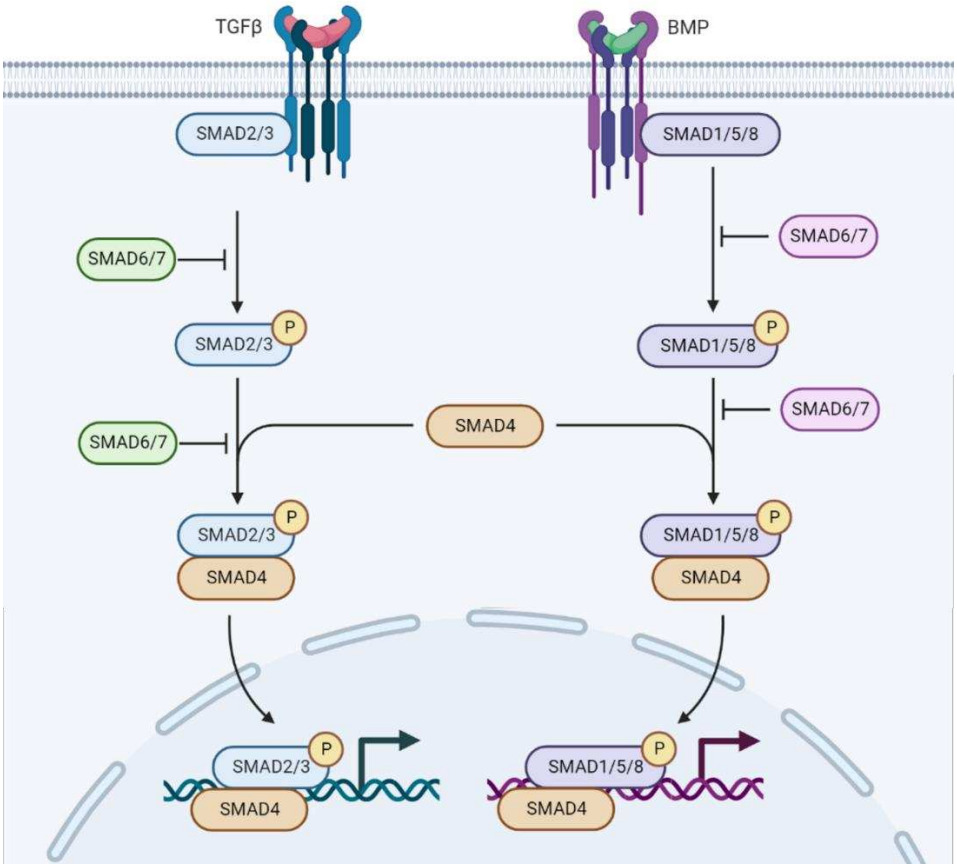


*Figure 14: Schematic representation of TGF-β and BMP signalling.*

*Schematic representation of TGF-β and BMP signalling. Ligands signal through serine/threonine transmembrane receptors. Upon ligand binding, type II receptors gets phosphorylated and transfer the signal to the type I receptors. The signal initiated will activate the R-SMADs (for the TGF-β arm SMAD 2/3, and for the BMP arm SMAD 1/5/8). R-SMADs form a complex with SMAD4 that mediates nuclear translocation where, by interacting with other transcription factors, gene target is regulated. Image created with BioRender.com*

In addition to the SMAD-dependent canonical pathway, these ligands can act via non-canonical SMAD-independent signalling pathways. In particular, these ligands can activate different MAPK signalling pathways including (i) the extracellular signal-regulated kinase (Erk) MAPK, (ii) c-Jun amino terminal kinase (JNK) and (iii) p38 MAPK, as well signalling via the IκB kinase (IKK)/ nuclear factor kappa beta (NFkB) signalling cascade , and Rho-like small GTPases proteins, or phosphatidylinositol-3 kinase (PI3K)/Akt axis. These receptor-activated, non-SMAD transducers can mediate signalling responses either as stand-alone pathways or in conjunction with SMAD to control their activity (116,117). As stand-alone, activation of non-canonical SMAD pathways, is thought to occur via the interaction with bone morphogenetic protein-receptor-associated molecule (BRAM)-1 and X-linked inhibitor of apoptosis protein (XIAP) and downstream TGFβ-activated kinase (TAK)-1/TAK1-binding protein (TAB1) complex (118). Downstream of TAK1 is the activation of NFkB, p38, JNK. Through the initiation of these pathways, BMPs are able to elicit their effects on cell proliferation, survival, apoptosis, migration, and differentiation (117).

Ligands are classified into three types based on how they interact with their type I and type II receptors. The majority of ligands bind only one receptor with high affinity, resulting in the widely accepted model of sequential signalling complex assembly. TGF-βs, activins, and some GDFs bind their type II receptors with high affinity but not their type I receptors. As a result, these ligands are thought to first form a complex with their type II receptors before engaging type I receptors. Table 1 represents the known ligand-receptors interactions of the members of the TGF-β family (114). Considering that the number of available receptors in a given cell is limited, ligands that target the same receptor must compete for binding. Because of this, high-affinity ligands can prevent low-affinity ligands from interacting with a specific receptor and inducing signalling.

*Table 1: Interactions between ligands and receptors in the TGF-β family.*

*Abbreviation: N.D: not determined (114).*

| Ligand (protein/*gene*) | Type II receptors | Type I receptors |
|---|---|---|
| Inhibin A/*INHA* | ActRIIA, ActRIIB | No type 1 receptor |
| Activin Ab/*INHBA* | BMPRII, ActRIIA, ActRIIB | ALK2, ALK4, ALK5, ALK7 |
| Activin Bb/*INHBB* | BMPRII, ActRIIA, ActRIIB | ALK2, ALK4, ALK5, ALK7 |
| Activin Cb/*INHBC* | ActRIIA, ActRIIB | No type 1 receptor |
| Activin Eb/*INHBE* | N.D. | N.D. |
| TGF-β1/*TGFB1* | TGFβRII | ALK5, ALK1 |
| TGF-β2/*TGFB2* | TGFβRII | ALK5 |
| TGF-β3/*TGFB3* | TGFβRII | ALK5, ALK1 |
| BMP-2/*BMP2* | BMPRII, ActRIIA, ActRIIB | ALK2, ALK3, ALK6 |
| BMP-3/*BMP3* | ActRIIB | No type 1 receptor |
| BMP-4/*BMP4* | BMPRII, ActRIIB | ALK3, ALK6 |
| BMP-5/*BMP5* | N.D. | ALK2, ALK3, ALK6 |
| BMP-6 (VGR1)/*BMP6* | BMPRII, ActRIIA, ActRIIB | ALK2, ALK3, ALK6 |
| BMP-7 (OP-1)/*BMP7* | BMPRII, ActRIIA, ActRIIB | ALK2, ALK3, ALK6 |
| BMP-8A (OP-2)/*BMP8A* | N.D. | N.D. |
| BMP-8B (OP-3)/*BMP8B* | N.D. | N.D. |
| BMP-9/*GDF2* | BMPRII, ActRIIA, ActRIIB | ALK1, ALK2 |
| BMP-10/*BMP10* | BMPRII, ActRIIA, ActRIIB | ALK1-3, ALK6 |
| GDF-1/*GDF1* | ActRIIA, ActRIIB | ALK4, ALK7 |
| GDF-3 (VGR2)/*GDF3* | ActRIIA, ActRIIB | ALK4, ALK7 |
| GDF-5 (BMP-14)/*GDF5* | BMPRII, ActRIIA | ALK3, ALK6 |
| GDF-6 (BMP-13)/*GDF6* | BMPRII, ActRIIA | ALK3, ALK6 |
| GDF-7 (BMP12)/*GDF7* | BMPRII, ActRIIA | ALK3, ALK6 |
| GDF-8 (Myostatin)/*MSTN* | ActRIIA, ActRIIB | ALK4, ALK5, ALK7 |
| GDF-9/*GDF9* | BMPRII | ALK5, ALK6 |
| GDF-9B/*BMP15* | BMPRII | ALK3, ALK6 |
| GDF-10 (BMP-3b)/*GDF10* | TGFβRII, ActRIIA | ALK4, ALK5 |
| GDF-11 (BMP-11)/*GDF11* | ActRIIA, ActRIIB | ALK4, ALK5, ALK7 |
| GDF-15 *c/GDF15* | No type II receptor | No type I receptor |
| MIS/*AMH* | AMHRII | ALK2, ALK3, ALK6 |
| Nodal/*NODAL* | BMPRII, ActRIIA, ActRIIB | ALK4 |
| Lefty1/*LEFTY1* | ActRIIA, ActRIIB | No type 1 receptor |
| Lefty2/*LEFTY2* | ActRIIA, ActRIIB | No type 1 receptor |

## 2.1.1 Classification of the BMPs

BMPs made their first appearance in the scientific field when, in 1965, Dr. Urist described them as a bone natural constituent, liable for the repair and regeneration of the organ (119,120). He named this component BMP: bone morphogenetic protein, introducing the new term to describe this bone inductive capacity. BMP family members can be subdivided into several subgroups based on structural homology **(Figure 15)** (112). These include: the BMP 2/4 group, the BMP 5/6/7/8 group, the BMP 9/10 group, and the BMP12/13/14 group. BMP-1 has a metalloproteinase domain involved in regulating the formation of the extracellular matrix and is not classified as a member of the TGF-β family (121). On the other hand, BMP3, as well as GDF9 and BMP15 ligands, has been shown to activate ALK4 and ALK5 resulting in the initiation of SMAD2/3 pathways inducing signals similar to that of TGFβ /activins but distinct from those induced by other BMPs. Moreover, BMP-3 has also been described as an antagonist of BMP2/BMP4 activity by binding to ActRIIB receptor (122,123).

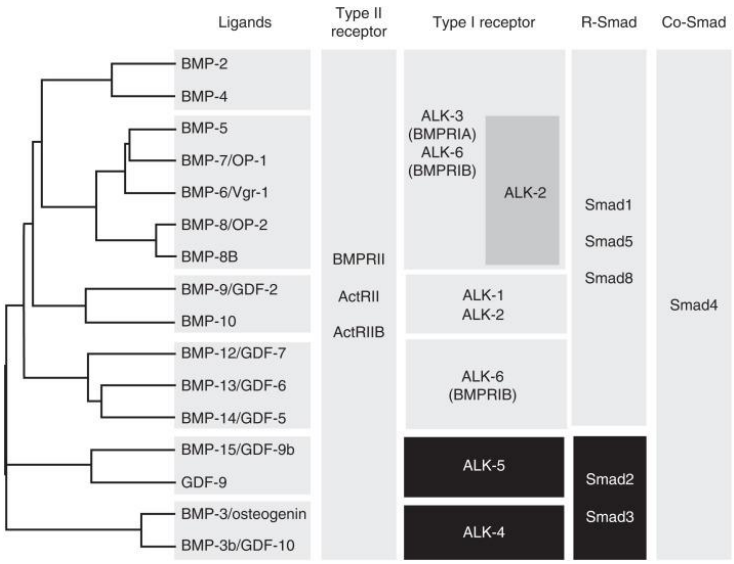


***Figure 15: Diagram representing sub-group differentiation of BMP/GDFs based on their structural homology.***
*Structurally related ligands, receptors, and SMAD proteins are grouped in same boxes: BMP 2/4 group, BMP 5/6/7/8 group, BMP 9/10 group, BMP12/13/14 group, BMP15/GDF9 and BMP3. BMP3, as well as GDF9 and BMP15, has been shown to activate TGF-ßs, ALK4 and ALK5 resulting in the activation of SMAD2/3 differently from SMAD1/5/8 activation by other BMPs. Image taken from "Bone Morphogenetic Proteins", Katagiri and Watabe, Cold Spring Harb Perspect Biol., 2016 (112).*

Like all TGFβ members, BMPs are synthesised as large precursors composed of a prodomain (33kDa) flanked by signal peptide and a C-terminal mature domain (12.5 kDa) linked by a disulphide bond. Cleavage by subtilisin-related pro-protein convertases, generates the mature dimers (124,125). Active forms can be found with either the prodomain non-covalently attached to the mature domain (complex form), or as a mature dimer, which is usually the commercially available form **(Figure 16)** (125–127). The crystal structures of BMP homodimers revealed that the overall structure of BMPs is "wrist and knuckle" and that that core structures of the BMP dimers are characterised by the cysteine-knot typical of the other TGFβ members (112).

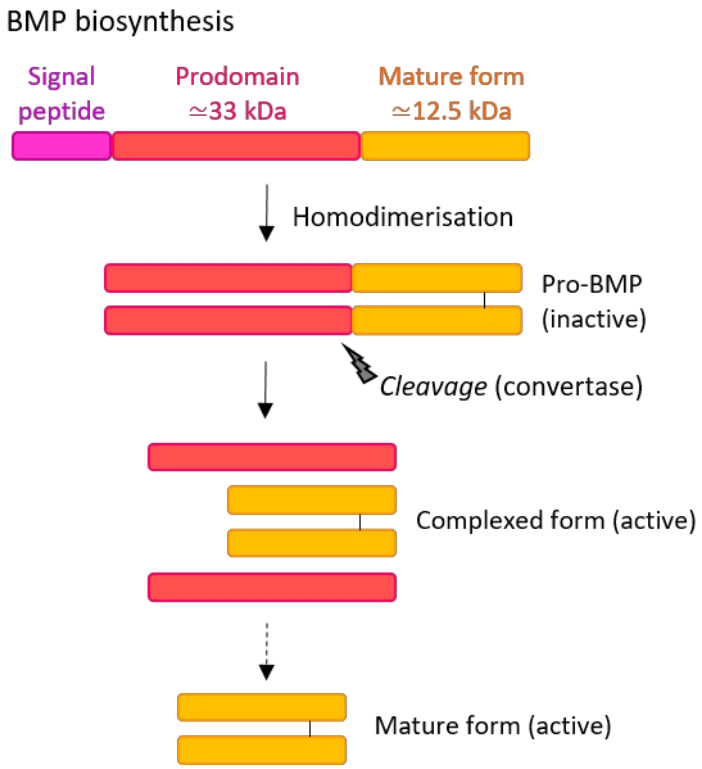


***Figure 16: Schematic representation of BMP biosynthesis and processing.***
*BMPs are synthesized as pre-pro-proteins composed of a signal peptide, a pro domain (≃ 33 kDa) and a mature form (≃ 12.5 kDa) that are disulfide-bonded to form pro-BMPs. Pro-BMPs are generally considered as inactive precursors. Upon cleavage by pro–protein convertases, the prodomains remains linked to the mature BMP dimer via a non-covalent bond (complexed form). Inactive Pro-BMPs as well as active complexed form and mature form are found in the bloodstream. Image created with BioRender.com.*

Because BMPs are commercially available as homodimers, most studies define their activities as homodimers and make the assumption that they function physiologically as homodimers. However, growing evidence, much of it from developmental genetics, suggests that TGF-β family proteins can also act as heterodimers with activities that can be stronger or distinct from homodimers, as will be discussed later.

### 2.1.2 BMPs regulatory proteins and targets

The wide array of distinct activities of the members of the BMP family are determined not only by signalling via type I and type II receptors, to which these ligands have different affinities, but also by a variety of binding proteins and enzymes. These extracellular agonists and antagonists greatly diversify signalling activity by regulating, not only whether the ligands bind to their cellular receptors, but also whether other components exist within ligand-receptor complexes. These regulators are involved in many functions including modifying ligand's processing, secretion, stability, diffusion, and presentation. Many of these regulatory molecules share with the ligands a cysteine knot growth factor (CKGF) domain, providing for their stability.

Signalling pathways initiated by the BMP molecules are tightly controlled at different levels, going from the extracellular space to the nucleus and, by either directly or indirectly interacting with the ligands. In particular, in the extracellular compartment, BMP signalling can be inhibited

by BMP antagonists, which work by directly binding to BMP and preventing it from binding to specific receptors. In some instances, BMPs increase the expression of some antagonists, such as noggin and Gremlin, establishing therefore a negative feedback loop. Another inhibitor of the BMP signalling is the BMP and activin membrane-bound inhibitor (BAMBI), a TGF-β family pseudo-receptor, which also inhibits BMP signalling at the cell membrane. BAMBI lacks the intracellular domain of serine-threonine kinase receptors and inhibits ligand-induced signalling by preventing signalling receptor complex formation. BAMBI expression is induced by BMP and TGF-β, making it another example of TGF-β family signal negative feedback. Other intracellular modulators are, SMAD6/SMAD7, the E3 ubiquitin ligases SMURF1 and SMURF2, as well as transcriptional co-repressors such as c-Ski, SnoN, and Tob (112). Notably, for BMP9 and BMP10, to date, no antagonist has been identified (52).

Aside from antagonists, some extracellular BMP agonists have also been identified. For example, the metalloproteinase BMP1, which function is to break down procollagen, has been described as a potential BMP activator because it cleaves chordin/BMP complex to release active BMPs. In addition, mature BMPs forms can associate to heparin; for that, sulphated polysaccharides like heparin, heparan sulphate, and dextran sulphate have been shown to enhance BMP2, BMP4, and BMP7 induced osteoblast differentiation. Another important regulator of the BMP signalling is the crossveinless (CV)-2, also known as BMP binding endothelial regulator (BMPER), which, like chordin, has been shown to function as both a BMP signal agonist and antagonist. When CV-2 is depleted in ECs, sprouting phenotypes and BMP signals are reduced (112,128).

BMP signals are also positively regulated by their co-receptor, glycosylphosphatidylinositol (GPI)-anchored membrane proteins of the repulsive guidance molecule (RGM) family RGMa, RGMb (also known as DRAGON), and RGMc (also known as hemojuvelin or HFE2). Transcriptional coactivators, such as p300 and CBP, are required in the nucleus for the transcriptional activity of phosphorylated BMP-specific R-Smads. Several transcription factors, including Runx2, interact with R-SMADs to promote BMP-induced gene expression (112). These agonists and antagonists of BMP signal have been shown to be cell-type specific and to play important functions in the biological activities of BMPs.

One of the most important BMP targets are the inhibitor of differentiation also known as inhibitor of DNA binding (ID) proteins, induced in various cell types. All four ID proteins (ID1–4) have similar biological activities and expression profiles and can act both as negative regulators of cell differentiation and positive regulators of cell proliferation (129). During osteoblast differentiation of early mesenchymal cell, various genes that regulate transcription and signal transduction were identified as immediate early genes (regulated within 2 hours of BMP stimulation), including ID1-ID3, I-SMAD6/7, old astrocyte specifically induced substance gene (OASIS), paired-related homeobox gene (Prx2), TGFβ -inducible early gene (TIEG), and snail

family transcriptional repressor (SNAI). The intermediate and late (regulated from 6 to 24 h after BMP stimulation) response genes, on the other hand, are associated with processes of osteoblastic differentiation, including genes for transcription factors HEY1 and TCF7, which mediate Notch and Wnt signalling, respectively. During angiogenesis, BMP-4 promotes the expression of ID1, a common target of BMP signals, as well as the expression of angiogenesis-related genes such as VEGFR2 and Tie2 (112).

### 2.1.3 BMPs sites of expression

Although the majority of BMPs are expressed in a variety of tissues during embryogenesis, some members' expression becomes restricted to specific tissues after birth. In adult mice, BMP3/BMP4/ BMP5, and BMP6 are abundantly expressed in the lung, whereas BMP7 is found in the kidney. Also, BMP3 is highly expressed in osteoblasts and osteocytes, which are terminally differentiated osteoblasts, while BMP6 is abundant in hypertrophic chondrocytes. In the early stages of fracture healing, BMP4 expression is transiently induced in callus-forming cells. BMP9 is produced by liver hepatic stellate cells and circulates in plasma in both active and inactive forms, while BMP10 is mainly expressed in the embryonic heart during development and restricted to the right atria in the adults and, thought to lesser extent, in the liver and can be also found circulating in the plasma (112,52). These results suggest that BMPs are capable of both inducing local and systemic activity by being secreted in the circulation. The next subchapter will take a closer look on BMP9 and BMP10 ligands and their vascular-related functions.

## 2.2 BMP9 and BMP10

BMP9 and BMP10 ligands have been shown to be closely related members of the TGF-β superfamily sharing 65% sequence identity at the protein level. Like all the BMP members, they are both synthesised as large precursors composed of a prodomain (BMP9: aa 23–319; BMP10 aa 22–316) flanked by signal peptide, and a C-terminal mature domain (BMP9: aa 320–429; BMP10 aa 317–424) linked by a disulphide bond. Upon cleavage by subtilisin-related pro-protein convertases, the prodomain will remain attached to the mature domain via non-covalent bonds **(Figure 16)** (52).

BMP9 and BMP10 initiate the signalling cascade by forming an heterotetrameric complex composed by two copies of type I receptors (ALK1) and two copies of type two receptors (BMPR2, ActR2A, or ActR2B). These two ligands will propagate the signal through the phosphorylation of SMAD 1/5/8 as well as SMAD-independent pathways modulating the expression of genes in the nucleus including ID (1 to 3), BMPRII and target genes of the Notch pathways (i.e. hairy and enhancer of split (HES)/HEY). The signalling pathway activated through

ALK1 and co-receptor endoglin highly expressed in endothelial cells is known to be crucial in vascular development (52).

In the early '00s it was discovered that constitutive ALK1 and endoglin (ENG) KO mice die *in utero* at around E11.5 resulting from severe vascular impairment and AVM development (130–133). This finding, along with the identification of BMP9 and BMP10 as ligands for ALK1 receptor few years later, introduced the BMP9-BMP10/ALK1 signalling pathway in the field of angiogenesis. Genetic mutation in BMP9/BMP10 signalling axis mediated by ALK1 and ENG has been shown to be implicated in two vascular conditions: hereditary haemorrhagic telangiectasia (HHT) and pulmonary arterial hypertension (PAH) which will be later discussed.

### 2.2.1 Ligands and regulation of their activity

BMP9 is mainly secreted by the hepatic stellate cells in the liver and is known to be the most osteogenic ligand among the BMPs (52). Also, BMP9 mRNA expression has been described in lungs and the brain (septum) (134,135). Furthermore, BMP9 has been shown to possess functions in different biological mechanisms including: stem cell differentiation, angiogenesis, lymphangiogenesis , vessel homeostasis, neurogenesis, tumorigenesis and metabolism (52). In turn, BMP10 is mainly secreted in embryos by the heart and in adults by the right atria and, albeit to a much lesser extent, by the liver (136). It is known that BMP10 plays an important roles in cardiovascular development (cardiomyocytes proliferation and heart size regulation), closure of the ductus arteriosus, angiogenesis and ventricular trabeculation (52). However, in comparison to BMP9, not much is known on its regards. This is due to the fact that *in vivo* functional assessment of BMP10 using transgenic mouse models *Bmp10*$^{-/-}$ cannot be achieved as these animals die in utero between E9.5 and E10.5 due to failed cardiac trabeculation and early vascular defects (52,137). Interestingly, while BMP9 is able to compensate for BMP10 vascular role, it cannot cover for its specific function on cardiac development (138). In the past years, the scientific community is paying more and more attention to the function of this ligand. For instance, in the zebrafish model, BMP10 is considered the most important ALK1 ligand to maintain the post-embryonic vasculature (139).

Different conformation of the prodomain bound complex of BMP9 and BMP10 are thought to influence the activity of the ligands. To this account, it has been proposed that conformational flexibility can results in differential activities of closely related isoforms. In particular, characterised structure of prodomain (pro)-BMP9 indicates that this complex can adopt both "close-arm" and "open-arm" conformations, which may correspond to latent and non-latent states, respectively (140). The transition between the two states could be controlled by binding to ECM proteins that act as BMP reservoirs. To this regards, it has been shown that when BMP7 is bound to fibrillin-1, it adopts a "close-arm" conformation and prevents BMP receptors from

accessing the growth factor (141). Because the BMP10 prodomain has been shown to form stable complexes with fibrillin-1 and fibrillin-2 proteins of the ECM, it is plausible that a similar mechanism for BMP9 and BMP10 homodimers takes place, resulting in a “open-arm” or a "close-arm" conformation (142). *In vivo* it has been shown that a purification step of mice plasma, using an anti-BMP10 column, results in higher levels of detected BMP10 in comparison to raw plasma, suggesting the presence of dormant BMP10 reservoir that is unmasked via the purification step process (136).

BMP9 and BMP10, are involved in a wide variety of function from embryogenesis to adult homeostasis. For that, their regulation is crucial and occurs via different routes ranging from epigenetic methylation and miRNA-mediated RNA regulation, protein ubiquitination, pseudo-receptors and secreted extracellular antagonists preventing signalling activation (143). Interestingly, both BMP9 and BMP10 do not respond to noggin, a BMP-natural antagonist and it is not sure whether a BMP9/BMP10 antagonist actually exists. This could explain the higher osteogenic potential of BMP9 compared to other BMPs. To this regards; the modulator, CV-2, has been reported as a plausible candidate to the role of BMP9/10 antagonists, however, a recent work shows disagreements as it reports impossibility of CV2 to bind to BMP9 (144–146).

### 2.2.2 BMP9 and BMP10 receptor specificity targeted gene expression

BMP9 and BMP10 bind to the type I receptor ALK1 with sub-nanomolar affinity ($EC_{50}$ of around 50 pg/mL), which is much higher than those of other BMPs to their cognate type I receptors ($EC_{50}$ of around 50 ng/mL). Moreover, BMP9 and BMP10 bind directly, with high affinity, to the co-receptor endoglin that is strongly expressed in endothelial cells and function as a signalling enhancer (53,52). Besides, the two ligands hold specific affinities (though lower compared to that of ALK1) for other cognate receptors. In particular, BMP9 binds to ALK2 and BMP10 has been shown to bind ALK3 and ALK6 *in vitro* (147,148). Interestingly, BMP9 seems to be biased toward ActRIIB whilst displaying a lesser specificity to ActRIIA and BMPRII, whereas BMP10 display similar affinities to the three type II receptors (149,150). Also, it has been shown that type I hetero-complexes can lead to SMAD-dependent or independent signalling (ALK1/ALK5 and ALK2/ALK3) (151). Besides being implicated in non-canonical signalling (involving ECs downstream factors JNK, p38 and PI3K), BMP9 and BMP10 have also been shown to be implicated in the Notch signalling and the Hippo pathway (52). Moreover, in addition to the several combination of BMP9/10 with type I and type II receptor possibly leading to different signalling pathways, another important factor contributing to the regulation of BMP9 and BMP10 signal transduction is blood flow. In particular, studies have shown that BMP9 signalling regulates flow-induced PI3K/AKT1 signalling to prevent AVM formation (152,153). Considering that these ligands are secreted into the circulatory system, how they behave when subjected to different hemodynamic forces is of high relevance.

Over the years, many gene targets of BMP9/BMP10 signalling have been described both *in vitro* (by BMP9/BMP10 cell stimulation) and *in vivo* by analysing gene expression upon blocking or genetically deleting either ligand. Overall, RNA sequencing analysis revealed that the most relevant targets of BMP9/BMP10 are the transcriptional repressors ID1-3, inhibitory SMAD6/7, receptors ENG and BMPRII, as well as the Notch targets HES/HEY (53,154,155,146). Moreover, the expression of several important factors involved in blood and lymphatic vessel development, maturation and functioning have been found to be influenced by BMP9/BMP10 signalling, and these are:

- Angiogenetic factors: up-regulation of VEGFR2 and ANGPT2 and downregulation of VEGFR1 (52);
- Lymphatic maturation factors: FOXC2 and lymphatic vessel endothelial hyaluronic acid receptor (LYVE)-1 (156);
- Regulators of endothelial to mesenchymal transition (EndMT): SNAI-1/2, zinc finger E-box binding homeobox (ZEB)-2 and twist family BHLH transcription factor (TWIST)-1 (157,158);
- Vasoconstriction regulators: up-regulation of endothelin and adrenomedullin, down-regulation of apelin shown in chick chorioallantoic membrane (CAM) assay (159–162);
- Chemokines, interleukins (IL), and cell surface adhesion molecules: up-regulation of IL6, IL8 (also known as C-X-C motif chemokine ligand (CXCL)-8), selectin-E (SELE) and downregulation of C-C motif chemokine ligand (CCL)-2 regulators of endothelial permeability and monocyte/macrophages recruitment (163,164).

### 2.2.3 BMP9 and BMP10 during embryogenesis

During embryogenesis, specific expression of BMP9 and BMP10 follows different timelines. In particular, in mouse models, BMP10 is detected as early as at E8.5 which coincides with the onset of ALK1 expression, whilst, liver specific BMP9 expression occurs around E9.75–10 (138). Therefore, there is a specific time frame, between E8.5 and E9.75–10, where only BMP10 is present. It is important to keep this detail in mind to avoid misinterpretation of ligand function.

To this regards, as it was previously mentioned, constitutive BMP10 KO mice fail to develop due to impaired cardiac growth and profound vascular development characterised by an enlarged pericardium, absence of vessels in the yolk sac and formations of AVMs between the dorsal aorta and the cardinal veins at E9.5 (137). In this work they showed that inserting the *Bmp9* gene into the *Bmp10* locus, prevents formation of vascular defect but not defective cardiac morphogenesis leading to the conclusion that BMP9 and BMP10 can have a redundant function during embryonic vascular development, but BMP10 hold a specific role in cardiac

morphogenesis that cannot be replaced by BMP9. BMP10 cardiac specific function will be discussed in the next sub-chapter.

Differently from BMP10 KO mice, generation of BMP9 KO results in litters born at expected Mendelian ratios that grew into normal fertile adults although they displayed defective development of lymphatic vasculature resulting in impaired valve maturation and lymphatic vessel function, from embryonic development to adult stages (137,156). Lymphatic role of BMP9 ligand will be later discussed. Nonetheless, it is important to keep in mind that, although it seems that BMP10 cannot compensate for the loss of BMP9 in this situation, an eventual function of BMP10 in lymphatic maturation and homeostasis has not yet been studied and this is partly due to the difficulties encountered to study function of BMP10 *in vivo* using transgenic mouse models.

### *2.2.3.1 Cardiac implications – BMP10 specific role*

Cardiac development comprises a series of tightly orchestrated molecular and morphogenetic events such as cardiogenic induction and patterning, cardiomyocyte growth and differentiation, multiple cell lineage specification and terminal differentiation and chamber maturation. Briefly, in mice, cardiac development start around E7, when mesoderm cardiac-derived progenitors migrate to the anterior region of the embryo disposing in a crescent shape composed by two main cardiac progenitor: the first heart field (FHF) and second heart field (SHF) **(Figure 17 A-B)**. Between E.8.5 and E9, the heart undergoes a rightward looping changing the initial anterior-posterior axis of the primitive heart to a left–right orientation **(Figure 17 C-D)**. Following, the trabeculation process occurs, which is characterised by the ventricular cardiomyocytes growing towards the ventricular lumen forming a complex sponge-like meshwork (trabeculae). The endocardium penetrates through this formed trabeculae and is followed by invagination at specific points to form endocardial "out-pockets" **(Figure 17 E)**. The main function of ventricular trabeculation is to increase the myocardial mass and facilitate oxygen and nutrient exchange in the heart muscle, prior to coronary vascularisation. At around E.9.5 the four different heart chambers can be distinguished and they are finally formed at E13.5 **(Figure 17 F)**. Subsequent remodelling will lead to the formation of a fully mature heart by E18.5 (165–167).

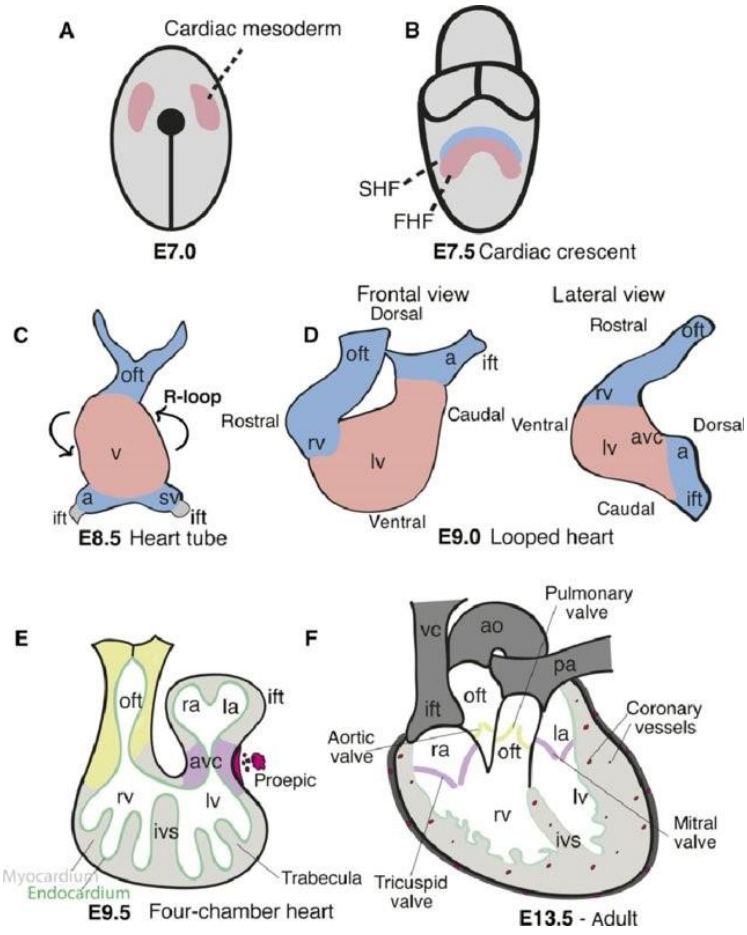


***Figure 17: Schematic illustration of mouse heart development.***

*(A, B) Ventral views of the developing mouse embryo. At E7.0, mesoderm-derived cardiac progenitors migrate to the anterior region of the embryo disposing in a crescent shape composed by two main cardiac progenitor: the first heart field (FHF) and second heart field (SHF). (C-E) At E.8.5, the heart undergoes a rightward looping changing the initial anterior-posterior axis of the primitive heart to a left–right orientation, initiating the process of trabeculation. At around E.9.5 the four different heart chambers starts to be distinguished: atrium (ra, right atrium; la, left atrium), atrioventricular canal (avc), ventricles (lv and rv) and cardiac outflow tract (oft) connecting ventricles with the aortic sac. In the developing ventricle, cardiomyocytes from the myocardial outer layer start to differentiate into trabeculae. Endocardial cells (green line) delineate the myocardium of the chambers (ventricle and atria, in grey) and the myocardium of valve primordia (avc, purple; oft, yellow). (F) Transversal section of an E13.5 with fully formed chambers. Image taken from "Notch signalling in ventricular chamber development and cardiomyopathy", D'Amato* et al.*, FEBS J., 2016 (165).*

Several endocardial growth factors have been identified in the process of trabeculation formation and compaction including neuregulin and its ErbB receptors, VEGF, angiopoietin-1 and, more recently, BMP10 (137,138,168–172). In particular, BMP10 is transiently expressed in the forming trabecular myocardium from E9.0 to E13.5, a crucial time span in which cardiac development shifts from patterning to growth and chamber maturation. BMP10 KO mice, exhibited strong defects starting from E9.5 ultimately leading to embryonic death by E10.5 (137). In their work, Chen *et al*., confirmed that BMP10 has a specific function in the growth of both ventricular wall and trabeculation leading to chamber maturation. In particular, BMP10 regulates Nkx2.5 and MEF2C induced cardiomyocytes proliferation by preventing activation of negative cell cycle regulator $p57^{kip2}$(137). Recently, *in vitro* and *in vivo* analysis revealed that BMP10 is capable to signal through the signal transducer and activator of transcription (STAT)-3 promoting cardiomyocyte survival and suppressing cardiac fibrosis (173).

### *2.2.3.2 Lymphatics implication – BMP9 "specific" role*

ALK1 receptor, towards which BMP9 and BMP10 hold a high affinity, is expressed in both blood and lymphatic ECs. Injection of soluble ALK1-Fc in neonates revealed defective lymphatic capillaries development and, at later stages, resulted in impaired lymphatic maturation (174). ALK1 inducible KO (iKO) pups injected at postnatal day (P)4 and P6, revealed lymphatic vessels hypoplasia and an increased number of filopodia at P8 and this defect has been show to by linked to BMP9 signalling (175). Moreover, BMP9 KO mice present lymphatic defects during embryonic development, postnatal and adult homeostasis (176). In particular, neonates revealed hyperplastic mesenteric collecting vessels expressing LYVE-1 (capillary marker). Moreover, analysis of mesenteric valves at E18.5, P0 and P4 shown significant reduction and aberrant maturation confirmed by defects in expression of genes involved in this process. In adults, mice had decreased lymphatic draining efficiency that could be explained by the lack of lymphatic valves and vessels enlargement (176). Moreover, *in vitro* analysis revealed that BMP9 mediates the inhibition of Prox-1 expression which could suggest that BMP9/ALK1 axis is important in lymphatic endothelial identity (175,177).

*In vitro* stimulation of lymphatic ECs using either BMP9 or BMP10 induces the expression of inhibitory SMAD6 via SMAD1/5/8 suggesting that not only BMP9, but also BMP10 is capable of negatively regulating the formation of lymphatic vessels (174). Due to the difficulties encountered to study the function of BMP10 *in vivo* using transgenic mouse models, the role of BMP10 in lymphatic maturation and homeostasis has not been analysed yet.

## 2.2.4 BMP9 and BMP10 role in angiogenesis - *In vitro* functions

Both BMP9 and the less-studied BMP10 have been mostly described as quiescent factors. In particular their inhibitory function has been described in the context for ECs proliferation, migration, tube formation, sponge angiogenesis and metatarsal outgrowth (52). Notwithstanding, different reports have shown *in vitro* diverging function of BMP9 among endothelial cells from different origins. To this account, *in vitro* studies of primary cells (human microvascular endothelial cells dermal (HMVEC-D), bovine aorta endothelial cells (BAEC) and human umbilical vein endothelial cells (HUVEC) have depicted BMP9 to function as a quiescent factor via inhibiting cells proliferation and migration, inducing ECs fate and inhibit tube formation in HUVECs (178–181). Conversely, stimulation of embryonic stem cells with BMP9 results in activation of angiogenesis and induced tube formation, in human pulmonary artery endothelial cells (HPAECs) and more recently, in HUVECs (182–184). Recently, BMP9 function has been shown to activate epidermal growth factor-like domain (EGFL)-7 mediated sprouting angiogenesis on ECs derived from human embryonic stem cells (183). Additionally, BMP9 has been shown to prevent vascular permeability by inhibiting VEGFR2 signalling and VE-cadherin

internalization and by favouring expression of junctional protein occludin (47). Moreover, cultured EC derived from human pulmonary artery revealed that BMP9 is able to inhibit permeability induced by tumour necrosis factor alpha (TNFα), lipopolysaccharide (LPS), or thrombin and protects these cells from apoptosis (155). *In vitro* analysis of BMP10 revealed same functions as BMP9 and is considered a quiescent factor acting on both blood and lymphatic ECs besides holding a specific cardiac function that cannot be taken up by BMP9, as previously described (137,173,174,178). This dual function of these ligands is evidently due to the heterogeneity of blood vessels, and the availability of surface receptors and ligands.

### 2.2.5 BMP9 and BMP10 role in angiogenesis - *In vivo* functions

*In vivo,* BMP9 and BMP10 have been shown to hold either similar or specific functions. This duality depends on their site of expression, kinetics, as well as the different accessibility of target cells surface receptors expression.

Regarding BMP9, despite having been described as an autocrine and paracrine mediator both inducing and inhibiting angiogenesis, *in vivo* BMP9 KO did not display any strong alterations in blood vessels formation and angiogenesis, differently from the lymphatic vessels that, as previously described, are significantly affected at different stages of maturation. Of note, both BMP9 and BMP10 have been shown to be important for the proper closure of the ductus arteriosus (DA), a foetal arterial shunt connecting the pulmonary artery with the aortic arches, thus bypassing non-ventilating lungs during embryonic development (157). More recently, BMP9 KO has been generated using clustered regularly interspaced short palindromic repeats (CRISPR). BMP9 KO revealed no obvious vascular defects, however, it has shown discontinuous SMC layer surrounding vessels in different organs, and abnormal retention of lipids (steatosis) in the liver (184,185).

In the past years, the concept of genetic modifiers is taking hold within the field of vascular biology. Genetic modifiers are described as genome variants that may alleviate or exacerbate the severity of the disease, resulting in different phenotypic outcomes (186). For example, a strain-dependent effect for either deletion of BMP9 or ENG has been identified with a stronger phenotype in the 129/Ola background compared to C57BL/6 and BALB/c background. In particular, in 129/Ola background, BMP9 has been shown to be important for liver endothelial cell fenestration via plasmalemma vesicle associated protein (PLVAP) and GATA-4 as well as prevention of fibrosis (187). However, in contrast to this, other studies revealed that BMP9 KO mice have reduced CCL4-induced liver fibrosis (188,189). In heterozygous KO ENG mice models, clinical signs of HHT disease (which will be further discussed later) were higher in 129/Ola background compared to C57BL/6 backcrosses and intercrosses among the two strains (190). BMP9 function has also been studied using the zebrafish model leading, in this case too, to

controversial results. While some studies show that BMP9 deficient zebrafish model do not reveal any overt phenotype, a recent study prove that BMP9 plays a role in vascular wall maturity and remodelling (184).

Function of BMP10 in the closure of the DA has been proven using neutralising antibodies against the ligand (157). In particular, blocking BMP10 in BMP9 KO mice has been shown to result into a reopening of the DA after birth deriving from defective EndMT (157). Also, these mice revealed defects during physiological postnatal angiogenesis in the retina (191). It has been documented that using neutralising antibodies against both BMP9 and BMP10 eventually leads to AVMs in the retinal vascular-developing bed and in the intestines (192,193). However, genetic deletion of BMP9 combined with blockade of BMP10 postnatally did not reveal AVM formation (191). This suggests that acute blockade is not the same as permanent blockade and may indicate a possible adaptation to BMP9 loss in BMP9-KO mice which, for example, could be due to expression of another ALK1 ligand. On the other hand, in zebrafish it has been shown that circulating BMP10 is the main physiological ligand acting via ALK1 and that its expression is required for vascular maintenance and for stabilising the caliber of nascent arteries, while BMP9 is dispensable (139,194).

Germline deletion of BMP10 led to *in utero* death resulting from impaired cardiac development and vascular defects. Nonetheless, there is a specific timeframe, from E8.5 to E9.75–E10, in which only BMP10 is present. Expression of BMP9 as early as E8.5 in the place of BMP10 did not reveal any vascular defect showing that lack of redundancy is due BMP9 unavailability and not a specific function of BMP10 (138). Functional studies of BMP10 *in vivo* gained more attention over the past years, since the generation of the iKO model, allowing to overcome the embryonic lethality previously described. Adult BMP10 iKO models in C57BL/6 background have not revealed any obvious vascular phenotype (195).

### 2.2.6 The heterodimer BMP9-BMP10

In 2018 Tillet *et al.*, showed that BMP9 and BMP10 can heterodimerise via a disulphide bridge in the C-terminal mature domain. This heterodimer has been confirmed to be active and can be located in both human and mouse plasma, and is responsible for the circulatory activity (136). In particular, plasma obtained from BMP9 KO or BMP10 iKO mice models failed to activate ALK1 in either 3T3 fibroblast cells transfected to express ALK1 or endothelial cells. This finding provided strong evidence that ALK1 activity results from the BMP9/10 heterodimer-induced signalling and that this form is likely to be a key regulator of blood vessel homeostasis. The heterodimerisation of BMP9/10 via disulphide bridge suggests a common production site of both BMPs. Indeed, analysis of mRNA expression of BMP9 and BMP10 in the liver revealed that mRNA for both ligands is present in hepatic stellate cells suggesting that the liver could be

the hypothesised common source of BMP9 and BMP10 (136). Yet, this hypothesis requires further validation.

Though TGFβs and BMPs have been described mostly as homodimeric proteins, they have been shown to be able to heterodimerise to some extent. This feature provides them with the advantage of higher specific activity than that of the homodimers. For example, in zebrafish, BMP signalling is solely induced by BMP2/7 heterodimer, and although single homodimers of BMP2 and BMP7 are produced, they do not seem to induce activity (196). In *Xenopus*, BMP4 and BMP7 preferentially form heterodimers rather than either homodimers when co-expressed in the same cell types (197). During mice embryonic development, BMP2/7 and BMP4/7 heterodimers are the predominant functional signalling ligand in several tissues (198). BMP2/6 heterodimers show enhanced ability to activate downstream signalling for human embryonic stem cell differentiation (199).

Overall, there is a large body of growing data describing the pleiotropic autocrine, paracrine, and endocrine functions of BMP9 and BMP10 homodimers. This introduction did not cover all the situations that sees the involvement of BMP9 and BMP10, but was rather meant to describe their role in the context of vascular biology. To date, the working model is that both ligands, circulating in the blood at biologically active concentrations, act via ALK1 as quiescence factors on the blood endothelium. Figure 18 represents a general summary of the different function of BMP9 and BMP10 that have been described in this subchapter.

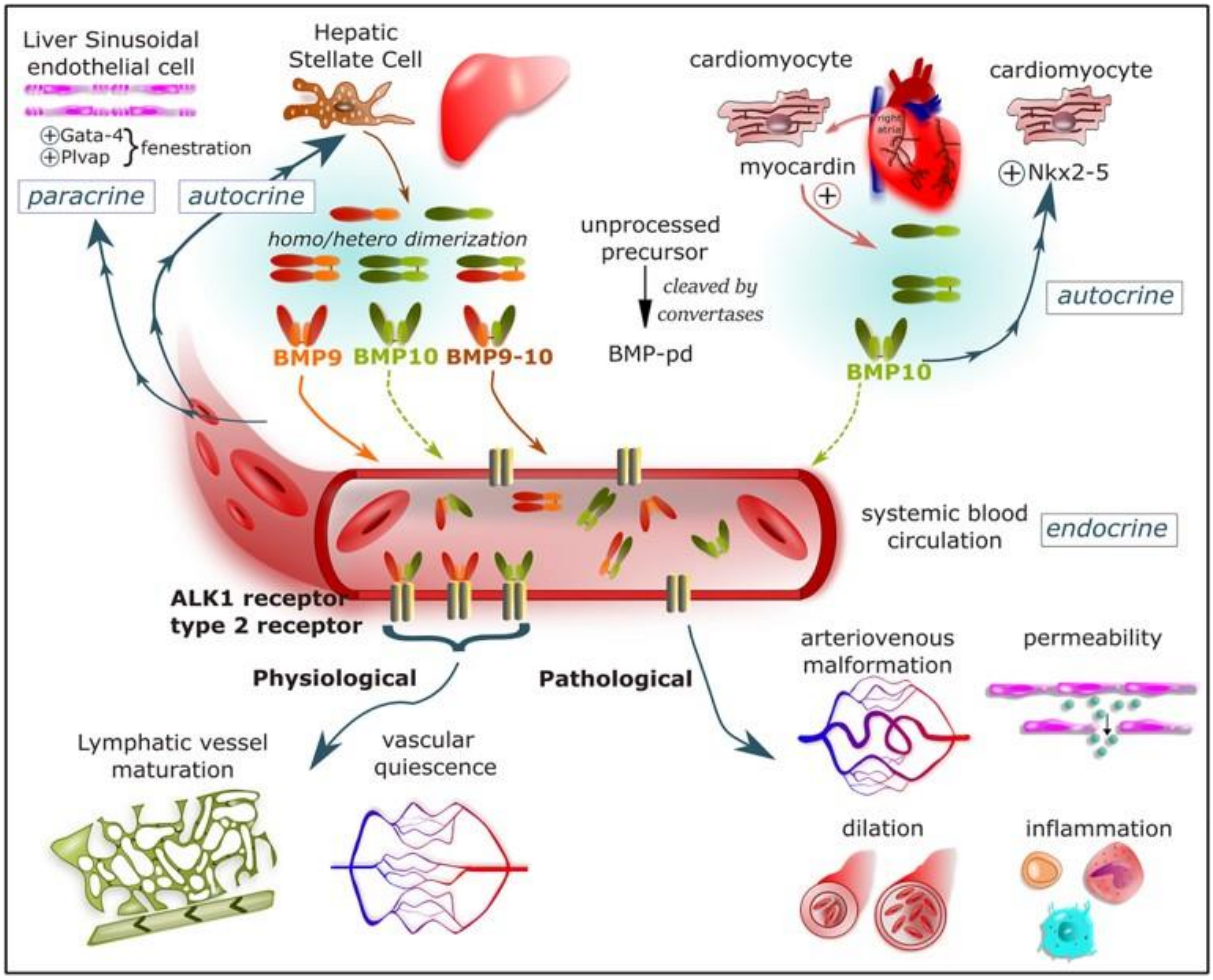


*Figure 18: Schematic summary of BMP9 and BMP9-10 functions in vascular homeostasis.*

*After birth, BMP10 homodimer is mostly expressed by cardiomyocytes of the right atria of the heart under the control of myocardin. BMP10 contributes to heart morphogenesis during development and control expression of Nkx2-5. Both BMP9 and BMP10 homodimers and BMP9/10 heterodimer are produced by hepatic stellate cells in the liver. BMP9 exerts a paracrine role by regulating liver sinusoidal ECs fenestration via PLVAP and GATA-4 regulation and an autocrine activity on hepatic stellate cells. Homo and heterodimers are found in the circulatory blood in unprocessed and prodomain-bound forms and they exert their function via signal through two type I ALK1 and two type II receptors (BMPRII, ActRIIA, or ActRIIB). Signalling via this axis allows maintenance of vascular quiescence and lymphatic vessel maturation. In the absence of BMP9 and/or BMP10 multifaceted phenotype have been observed* in vivo *among which, vessel dilation, inflammation, AVM and increased vascular permeability. Image taken from "BMP9 and BMP10: Two close vascular quiescence partners that stand out", Desroches-Castan* et al.*, Dev. Dyn., 2022 (52).*

## 2.2.7 Diseases associated to BMP9-BMP10 signalling pathways

Genetic mutations encoding genes and receptors involved in BMP9/BMP10 signalling pathway mediated by ALK1 and ENG have been shown to result in two vascular diseases namely: hereditary haemorrhagic telangiectasia (HHT) also known as Osler-Weber-Rendu syndrome and pulmonary arterial hypertension (PAH) which will be described in this last part of introductory chapter.

### *2.2.7.1 Hereditary Haemorrhagic Telangiectasia (HHT)*

HHT is an autosomal dominant disease leading to a complex, haemorrhagic multisystemic vascular dysplasia which, in January 2022 has been estimated to affect 85,000 European citizen in a 1/6000 ratio. The condition is characterised by two major types of vascular malformations. The first is spontaneous recurrent telangiectasia developing at specific sites i.e. nose (causing nosebleeds (epistaxis)), mouth, finger tips and gastrointestinal tract that onsets in youngsters and worsen with age. The second is the development of AVMs in both visceral and mucocutanous vascular beds leading to physiological distresses. AVMs consists of direct shunts between arteries and veins occurring in vital organs such as the lungs, liver, or brain that can rupture at any moment, resulting in serious complications such as ischemic injury and stroke. Hepatic AVMs, which can remain dormant for a long time, can lead in rare occasions to severe heart failure, portal hypertension or pulmonary hypertension (PH) and the only possible treatment is liver transplantation (200).

HHT results from heterozygous loss-of-function mutations occurring in one of three different genes, which are major factors of the BMP9/BMP10 signalling axis in ECs. These genes are:

- *ENG* encoding for co-receptor endoglin (ENG), leading to HHT type 1 (HHT1);
- *ACVRL1* encoding for ALK1 receptor, leading to HHT type 2 (HHT2);
- *SMAD4* encoding for SMAD4 protein, leading to development of juvenile polyposis (JP), which is a condition that shares some features with HHT, including AVMs.

Most mutations in *ENG* and *ACVRL1*, which together account for nearly the same percentage of mutations causing the disease, result in haploinsufficiency and, the associated reduced levels of the respective proteins, leads to excessive angiogenesis, which is the underlying cause of HHT1 and HHT2, respectively (201). Sequencing analysis revealed missense mutations in *GDF2* gene encoding for BMP9 in three unrelated individuals with suspected HHT who had previously tested negative for ENG, ACVRL1, and SMAD4 (202). Recently, homozygous *GDF2* nonsense mutations have been identified to result in a loss of circulating BMP9 and BMP10 (further confirming the presence of the heterodimer in humans responsible for the circulating activity) and are associated with either PAH or an “HHT-like” syndrome in children (203).

The clinical consensus (curaçao) diagnostic criteria for HHT had defined four criteria to diagnose HHT. Diagnosis is considered certain if three or more criteria are met, possible if two criteria are met and unlikely if only one is met. The criteria are: (i) spontaneous and recurrent epistaxis; (ii) multiple telangiectasias at specific sites (lips, oral cavity, fingers, and nose); (iii) visceral (gastrointestinal, pulmonary, hepatic, cerebral, and spinal) AVMs; and (iv) first-degree relatives diagnosed with HHT according to these criteria (204).

HHT phenotypic manifestations revealed high variability, in which the number and location of telangiectasias and AVMs vary widely even within the same family. This significant phenotypic variation suggests a role of genetic modifiers on the HHT phenotype. To this account, variants in two particular genes have been shown to exacerbate HHT phenotype. These two genes are: protein tyrosine phosphatase non-receptor type 14 (PTPN14), which is associated with pulmonary AVMs in HHT patients, and A disintegrin and metalloprotease 17 (ADAM17), which variants have also been associated with the presence of pulmonary AVMs in HHT1 but not in HHT2 and may aggravate TGF-β-regulated vascular conditions (205,206).

Overall, molecular mechanisms underlying HHT pathogenesis are not fully understood, and this reflects in the shortage of effective treatments. Currently, HHT therapeutic treatments are aimed to alleviate disease symptoms. However, no mechanism-based targeted therapy is currently available. Current drugs either (i) correct HHT patients' angiogenic defects (bevacizumab anti-VEGF antibody, tyrosine kinase inhibitors, or PI3K inhibitors), or (ii) reactivate the altered BMP9/10 signalling pathway (Tacrolimus, Sirolimus) (207).

Several hypotheses around the molecular pathogenesis currently exist but necessitate further validations. It is plausible to think that additional genetic modifiers, that have not been yet identified, also play a role in the development of vascular lesions in HHT. Moreover, further analysis are needed to corroborate the hypothesis of haploinsufficiency, as well as the second-hit mutation, the contribution of environmental triggers and epigenetic factors, ultimately promoting the progress of lesions.

### *2.2.7.2 Pulmonary Arterial Hypertension (PAH)*

PAH, a subtype of the broader condition known as pulmonary hypertension (PH), is a progressive disorder characterised by strong remodelling of pulmonary arteries which results in high in mean pulmonary arterial pressure (mPAP) (≥ 20 mmHg) leading to high blood pressure (hypertension) (≤ 15 mmHg) at resting state, ultimately causing heart failure and death. It is a much rarer condition compared to HHT with an incidence of 15-60 cases per million. Early symptoms are non-specific but generally consists of dyspnoea resulting from effort and fatigue, fluid retention (oedema), and episodes of systemic hypoperfusion (low flow) with angina (chest pain) or syncope (sudden loss of consciousness): all the symptoms are almost entirely related to a progressive right heart failure (208).

Right heart failure results from a progressive increase in pulmonary vascular resistance (PVR), which describes the resistance that the blood must overcome to go through the pulmonary vasculature. Increase in PVR leads to dilation and eventual failure of the right heart, which is unable to meet the increased vascular resistance. In the lungs, the alveoli, consist of sacs formed by a single-celled thin alveolar epithelial cell layer on the outer edge and thin

endothelial cell layer on the inner edge and is defined as the gas exchange unit, allowing for rapid exchange of carbon dioxide and oxygen between circulating red blood cells (RBC) and air. The resulting thin layer of blood exposed to such large surface area of air is crucial for efficient gas exchange and requires a very high flow at a very low pressure to minimise alveolar damage and pulmonary oedema. For that, the right ventricle is structured to accommodate a large volume of blood (preload) and pump blood against a low resistance (low afterload). PAH progression is parallel to the decrease of vessels diameter and PVR increase, which results in cardiac output (CO) decrease, ultimately leading to progressive right heart failure (208).

There is no cure for this condition yet. Currently, the first line of therapy consist of a combination of drug therapy targeting more than one biological pathway which are: (i) enhancers of the nitric oxide-guanosine monophosphate pathway (sildenafil, tadalafil, or riociguat), (ii) antagonists of the prostacyclin pathway (epoprostenol or treprostinil), and antagonists of the endothelin pathway (bosentan and ambrisentan) (209).

PAH is subdivided into different groups based on their underlying aetiology which can either be (i) idiopathic, (ii) resulting from germline mutation, (iii) resulting from long term exposure to calcium channel blockers, or (iv) associated with either medical conditions (i.e. connective tissue disease, HIV, or congenital heart disease) (209,210). Heritable PAH accounts for approximately 10% of the cases and in at least 70% to 80% of cases it results from heterozygous germline mutations in the *BMPR2* gene which encodes for a type 2 BMP receptor that forms a complex with ALK1 (178,179). Also, about 10–20% of idiopathic PAH cases are associated with mutations in *BMPR2* gene (211). Patients with PAH and *BMPR2* mutations present at a younger age with more severe disease, and are at increased risk of death, compared with those without *BMPR2* mutations. Moreover, the effect of *BMPR2* mutation on survival suggests a role for BMPR2 dysfunction in the clinical progression of the disease that that cannot be replaced by another type II receptors (211).More rarely, other genetic heterozygous mutations have been identified over the years as contributors to the development of the disease. These are:

- Mutation of different SMAD family members: *SMAD1*, *SMAD4*, and *SMAD9* (212);
- Mutations in *CAV-1* gene, encoding for caveolin-1 imp is to co-localise of BMP receptors (213);
- Mutations in the K subfamily potassium channel member (*KCNK*)-*3* encoding for a potassium channel that has a role in membrane potential and regulates pulmonary vascular tone (214);
- Loss-of-function mutations in T-box (*TBX*)-*4* gene encoding for a transcription factor of the T-box family important throughout development (215);
- Mutation in *ACVRL1* and *ENG*, mainly causative of HHT, have also been found in PAH patients (216,217);

- Biallelic mutations in the eukaryotic translation initiation factor 2 alpha kinase (*EIF2AK*)-*4* gene, mainly causative of pulmonary veno-occlusive disease and pulmonary capillary haemangiomatosis, were described in patients with idiopathic and heritable PAH (218);
- Mutation at the *GDF2* gene encoding for BMP9 have been described as a predisposing factor to PAH (219,220);
- Mutation in the *BMP10* gene of in two young patients (11 and 28 years old) with severe PAH have also been identified one of them presenting congenital heart disease (221).

Mutations in all of these genes, apart from *EIF2AK*, are inherited in an autosomal dominant manner and have reduced penetrance, meaning that not all individuals carrying a mutation will manifest symptoms of PAH. The incomplete penetrance observed suggests that additional genetic, epigenetic, and/or environmental triggers contribute to the onset of the disease. Yet, whether mutation in the BMP10 is causative for the onset and development of the disease is not certain, and further studies are required. The identification of PAH patients carrying BMP9 mutations revealed reduced BMP9 levels suggesting that supplementation of BMP9 in these individuals could be a possible treatment approach to restore functional ALK1/BMPR2 endothelial signalling. Nonetheless, the safety of this potential treatment remains to be yet assessed. Figure 19 represents an overview of the two pathological conditions HHT and PAH in the context of BMP/ALK1/ENG signalling pathway.

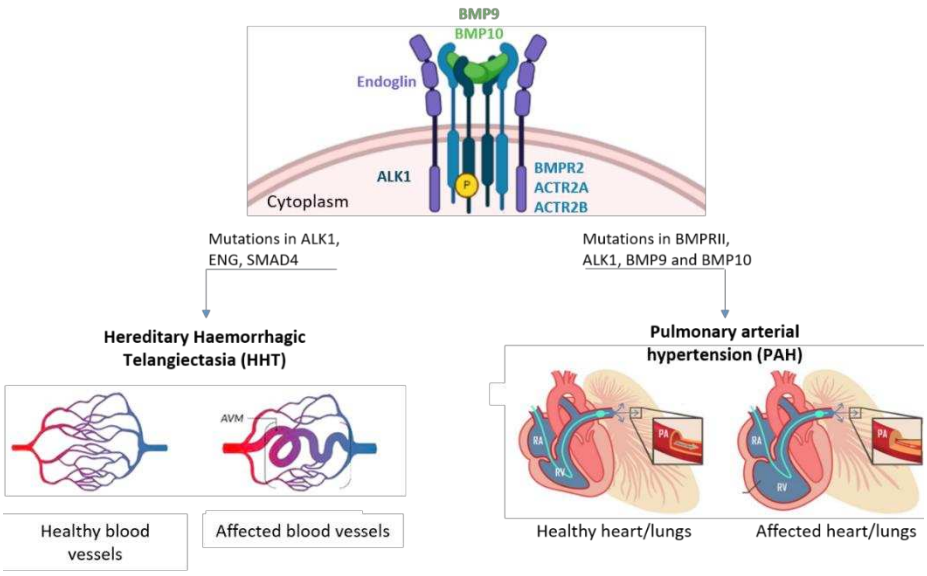


***Figure 19: Mutations in the BMP9/BMP10-ALK1 pathway leads to cardiovascular diseases.*** *Diagram showing the heterotetrameric complex composed of BMP9/10 ligands bound, two type I receptors (ALK1) and two type II receptors (BMPR2, ActR2A, or ActR2B) and co-receptor endoglin. Heterozygous mutations in the gene encoding for ALK1, ENG genes and SMAD4 (more rare) are associated with Hereditary Hemorrhagic Telangiectasia (HHT) disease characterised by formation of AVMs in several organs. Mutations in genes encoding BMPRII, ALK1, and rarely BMP9 and BMP10 (two patients with identified mutations) results to predisposition to Pulmonary Arterial Hypertension (PAH) disease progression characterised by vasoconstriction of pulmonary arteries eventually leading to right heart failure. Image created with BioRender.com. Diagram of heart/lungs during PAH adapted from "Pulmonary arterial hypertension: the clinical syndrome", Lai et al., Circ. Res., 2014 (210).*

# 3. Mouse models to study in vivo gene function

In the field of biological research, mouse models are essential to the study and understanding of mammalian gene functions. While at the beginning, the "forward research" approach enabled scientists to study a gene function based on phenotypic characteristics, the advent of genetic engineering allowed shifting to a "reverse genetic" approach where the phenotypic consequences derived from a known specific genetic mutation could be studied.

Nowadays, a growing body of new technologies are being developed to regulate biological information at every level, from engineering specific changes in DNA to inhibiting gene transcription to regulating protein activity. Gene inactivation can be achieved by either generating a constitutive (or conventional) KO model in which the gene of interest is permanently inactivated in the whole animal, or by generating a conditional KO (cKO) where the inactivation of the target gene can be temporally (inducible) and/or spatially (tissue or cell specific) controlled.

Generation of constitutive KO models can be obtained by genetically engineering the genome of embryonic stem (ES) cells and subsequent injecting it into the morulae (8-16 cells stage) or blastocysts (64 cells stage) or by microinjecting an exogenous gene into the pronucleus of one cell-stage zygote. Transfected cells can be then implanted into pseudo-pregnant female mice, which in turn give rise to into an offspring that bear the desired gene deletion. After back-crossing to assess the success of the germline transmission of the KO allele and eventual inter-crossing to obtain homozygosity, the phenotypic results of the genetic mutation can be analysed. The creation of constitutive KO models, leads to cohorts bearing irreversible genetic mutations that will be transmitted to the next generations (222). The most common application of this technique is the generation of ubiquitous KO models, in which the gene is deleted in every cell in an irreversible process.

On the other hand, it also is possible generate transgenic mice that retain wild-type gene expression and are responsive to conditional, spatio and/or temporal controlled deletion. This approach is particularly useful when the gene of interest is either crucial for developmental stages, or results in sudden death when both allelic copies are deleted. A great advantage of conditional mutagenesis versus constitutive germ-line mutation is the ability to efficiently convert a functional allele into a mutant allele in a particular tissue/cell type (recombinase expression under control of tissue/cell specific promoter) and/or at a particular time during developmental stages (inducible). As my thesis project was based on *in vivo* studies using the cyclization recombinase/locus of X-over, P1 (Cre/loxP) system to generate cKO mice models, the technique will be described in the next sub-chapter.

## 3.1. The Cre/loxP mediated recombination

The Cre/loxP system, firstly described in the *E. coli* bacteriophage P1, is characterised by two components: (i) the tyrosine recombinase Cre enzyme and (ii) the loxP sites to which the Cre binds with a high specificity. A Cre monomer in composed by 343 amino acid residues and has two main domains: an N-terminal domain and a C-terminal domain containing the Cre active site. For the Cre-mediated recombination to occur, two dsDNA flanked by loxP sites are involved. A loxP site is made up of 34 base pairs (bp) of which, the 13 bp at the two terminal sites are inverted palindromic repeats flanking a central 8 bp core spacer sequence (5'-ATAACTTCGTATA-NNNTANNN-TATACGAAGTTAT-3'; N: general nucleotide). The two palindromic repeats are the specific recognition sites for the Cre, while the spacer, providing for the orientation of the loxP, is the site in which recombination occurs. In particular, when the two flanking sequences are asymmetrically aligned (head-to-tail), recombination will result in gene deletion. In contrast, if the target sequence pairs are symmetrically aligned (head-to-head), recombination will result in gene inversion. If the target sequences are on different chromosomes, recombination results in chromosomal translocation **(Figure 20)** (223).

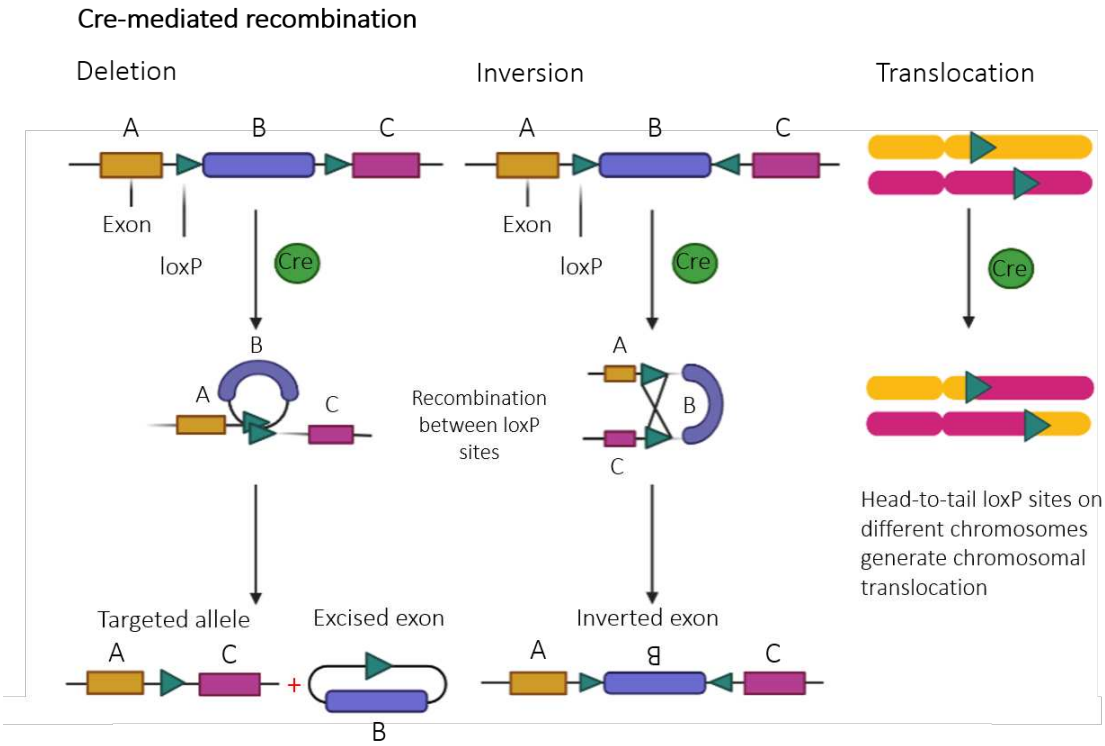


***Figure 20: Different possibilities of Cre-mediated DNA recombination.***

*From left to right cre-mediated recombination can results in either DNA deletion, inversion, or translocation based on the orientation of loxP sites. When loxP sites (green triangles) have the same direction, the gene (B) is deleted, if the direction of the loxP site is opposite the gene is inverted and if loxP are on different allele the flanked gene is translocated. Image created with BioRender.com*

Target gene recombination occurs as follows: firstly, two Cre monomers bind at each end of the 13 bp palindromic sequence causing the DNA to bend **(Figure 21)**. This result in the formation of a Cre tetramer where the four active sites at the C-terminal domain are bound to the two double strand (ds) DNA. Within the Cre tetramer, one monomer at each site becomes active and each tyrosine residue attacks the phosphodiester bond of DNA's backbone mediating the cleavage and exchange of one pair of strands releasing a 5'OH that, in turn, attacks the neighbouring strand to form a Holliday junction intermediate **(Figure 21)**. Following the isomerisation of the Holliday junction, the second pair of Cre monomers will activate, resulting in the catalysation of the same reaction, ultimately resulting in the targeted DNA recombination **(Figure 21)** (223,224).

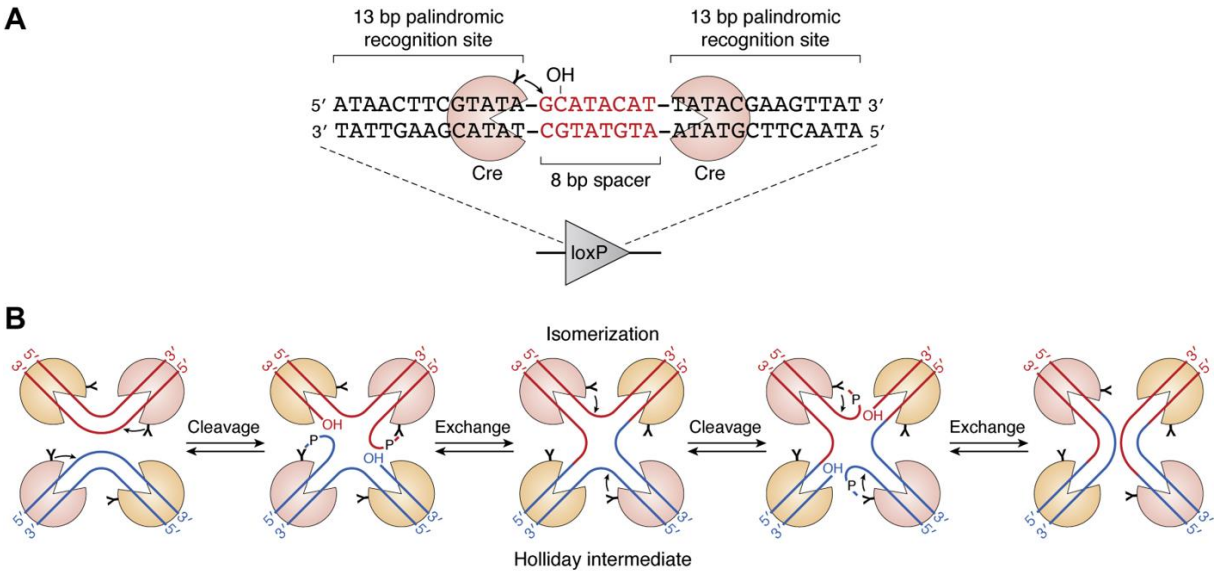


*Figure 21: Schematic diagram representing Cre/loxP-mediated recombination.*
*(A) The loxP DNA sites recognised by the Cre recombinase are made up of 34 bp of which, the 13 bp at the two terminal sites are inverted palindromic repeats flanking a central 8 bp core spacer sequence. The two palindromic repeats are the specific recognition sites for the Cre, while the spacer, providing for the orientation of the loxP, is the site in which recombination occurs. (B) Cre monomer in composed by 343 amino acid residues and has two main domains: an N-terminal domain and a C-terminal domain containing the Cre active site. For Cre-mediated recombination, two dsDNA flanked by loxP sites are involved (red and blue). At each end, two Cre monomers bind at each 13 bp palindromic sequence causing the DNA to bend. This result in the formation of a Cre tetramer. Within the Cre tetramer, one monomer at each site becomes active and each tyrosine residue attacks the phosphodiester bond of DNA's backbone mediating the cleavage and exchange of one pair of strands releasing a 5'OH that, in turn, attacks the neighbouring strand to form a Holliday junction intermediate. Following isomerization of the Holliday junction leads to the activation the second pair of Cre monomers that will catalyse the same reaction resulting in the formation of recombinant DNA products. Image taken from "Strategies for site-specific recombination with high efficiency and precise spatiotemporal resolution" by Xueying, T. and Bin, Z. J. Biol. Chem. 2021 (223).*

In the context of vascular biology, genetic mouse models allow for conditional gene ablation in specific subsets of cells lining the vascular beds such as ECs or pericytes, therefore allowing for a spatio-temporal analysis of various signalling pathways in different blood vessel cell types.

This allows, among many things, to study the functions of specific genes in the context of vascular malformations (VM).

Many such cKO models, also called inducible knock-out (iKO), relies on a modified Cre-lox system allowing for spatio-temporal control of the genetic alteration. To obtain this iKO model, scientists modified the Cre enzyme by fusing it with the estrogen receptor (CreER) containing a mutated ligand binding domain (225). The resulting fused CreER recombinase (also known as CreERT (Cre Estrogen Receptor, Tamoxifen)), in present in the cytoplasm and bound to heat shock protein 90 (HSP90) under physiological conditions. Upon delivery of synthetic steroids (i.e. tamoxifen or 4-hydroxytamoxifen (4-OHT)), binding of Cre to HSP90 is disrupted, allowing for steroid-mediated CreERT translocation into the nucleus, where it will recognise and excise floxed DNA sequence **(Figure 22)**.

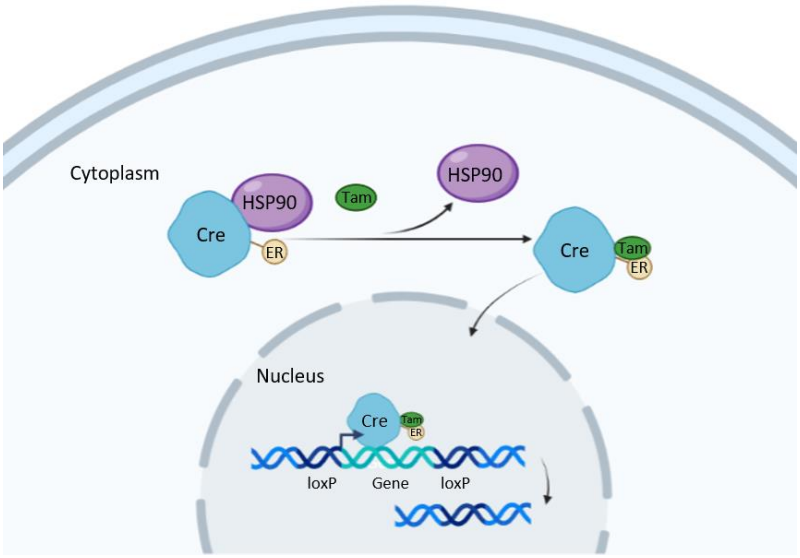


***Figure 22: Schematic illustration of inducible Cre-loxP recombination system.***
*In the absence of tamoxifen, fusion protein CreER, interacts with heat shock protein 90 (HSP90) and remains in the cytoplasm. Tamoxifen (Tam) delivery disrupts the interaction of HSP90 with CreER to mediate Cre nuclear translocation. In the nucleus, the CreER identifies the loxP sites and recombine the floxed gene. Image created with BioRender.com*

An inducible CreERT system controlled by tissue/cell-specific regulatory elements (promoters and enhancers) and temporally inducible by delivery of synthetic steroids such as tamoxifen will allow for a precise spatio-temporal control over the genetic alteration of the animal consenting to study function of genes that, if inactivated in the germ line, will cause early lethality.

## 3.2 Models to study vascular development and diseases

Depending on the scientific question addressed, there are different models that permit the study of angiogenesis. In general, the mechanism of angiogenesis can be addressed by *in vitro, ex vivo* and *in vivo* studies. *In vitro* studies allows for the analysis of processes contributing to angiogenesis and relies on the growth of endothelial cells in culture such as matrix degradation, proliferation, migration, survival and morphogenesis (226). Moreover, to allow for the rapid

screening of different molecules inhibiting or stimulating angiogenesis, *ex vivo* retina explant cultures can be utilised before *in vivo* validation (227). On the other hand, to study physiological or pathological angiogenesis (e.g. during tumour growth), different *in vivo* models can be applied.

Over many other animal models used in research, the mouse system offers several clear advantages including its genetic closeness to the human genome, the relative ease of its genome manipulation, the large litter yield size, as well as the accessibility to numerous strains. Over the past three decades, transgenic mouse models have proven to be a powerful tool to understand the mechanisms behind a broad spectrum of biological processes moderated by specific genes, including vasculature development, maturation, quiescence and homeostasis as well as their roles in the development of diseases. Our understanding of vascular biology relies mostly on the use of mouse models that have been genetically modified to express a mutation in their genome, either leading to a genetic loss-of-function (LOF) or gain-of-function (GOF). Nonetheless, the relevance of these models is frequently hindered by the inaccessibility of tissue in live animals, and much of what we know is derived from fixed material or indirect assays. To this account, the zebrafish model offers a number of advantages over the mouse model because of its rapid development, optical transparency, simple genetic manipulation strategies, and conserved molecular pathways in the context of vascular biology (228).

As my thesis evolved around the study of transgenic mice, the following subchapters will recapitulate the mouse models that have been used to study vascular development and diseases. In particular, the mouse retina model to study postnatal vascularisation, a gold standard in the field of vascular biology research, will be hereafter described.

### 3.2.1 Mouse retina as a model to study postnatal angiogenesis

The mouse retina is a widely used organ for angiogenesis research as it allows for the investigation of vessels growth under both physiological and pathological conditions. In contrast to humans, mice are born with an immature retinal vasculature that develops postnatally in parallel to the regression of the hyaloid vessels present at birth (229). The mouse retina is composed of three main tissue layers (superficial, deep and intermediate) situated at the back of the eyeball, and it functions by converting the light entering the eye into electrical signals that the optic nerve will transmit to the brain. Thanks to its ease of accessibility and dissection for imaging, the retina model allows for the study of postnatal angiogenesis without the difficulties connected to embryonic studies. Also, because of its postnatal vascular development, both the establishment and regression of blood vessels can be studied in a tightly controlled setting in the context of numerous vascular conditions (229,230). Different mice

strain can follow slightly different temporal and spatial patterns during retina vasculature development. The following description of retinal development will concern the C57Bl/6 strain.

The retinal vascular plexus is formed during the first week after birth and it occurs via a radial extension of the vessels starting from the central optic nerve toward the periphery following hypoxia-induced VEGF gradient, released from the neural bed in the peripheral a vascular zone, eventually reaching the boundaries of the retina around P8 **(Figure 23)** (229,231).

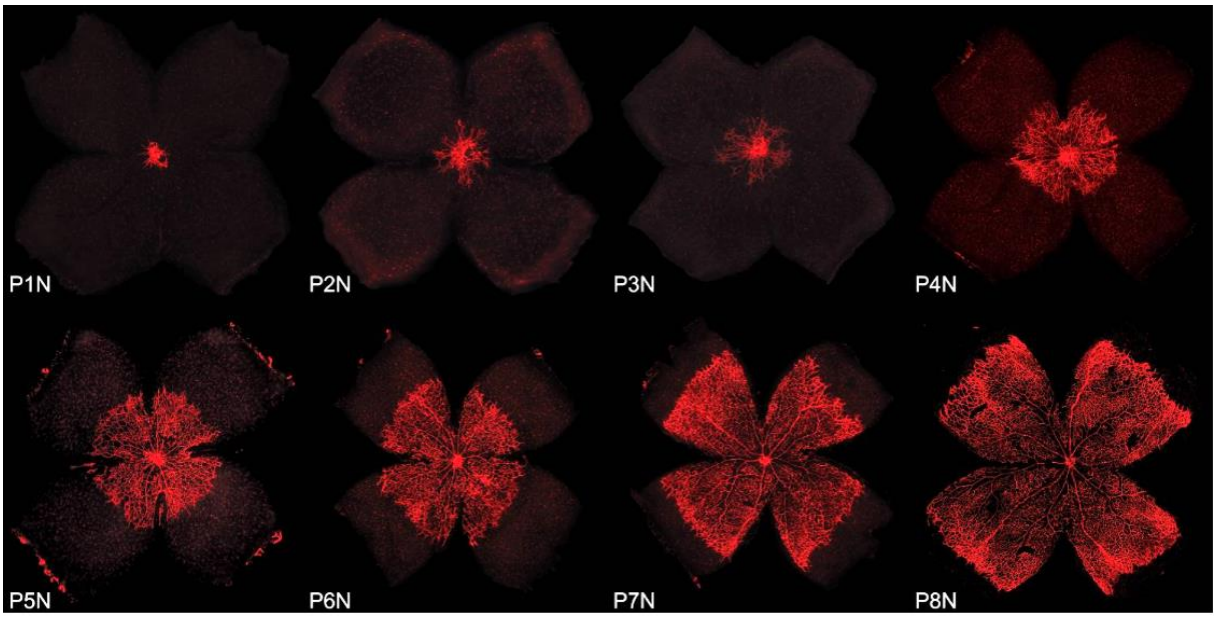


*Figure 23: Representation of vascular retina development in 3C57Bl/6 strain.*
*Retina vasculature stained with isolectin B4 (red). Primitive vascular plexus undergoes extensive remodelling starting from the central optic nerve toward the periphery following hypoxia-induced VEGF gradient released from the neural bed in the peripheral a vascular zone eventually reaching the boundaries of the retina around P8 Abbreviation N=normoxia. Image taken from "The Mouse Retina as an Angiogenesis Model" by Stahl* et al*., Invest. Ophthalmol. Vis. Sci., 2010 (229).*

From P7 the capillaries at the frontal superficial plexus starts sprouting to form the deep and intermediate vascular plexi respectively. The deep plexus reach the boundaries of the retina at around P12 and is immediately followed by the growth and expansion of the intermediate layer between P12 and P15. By P17, the superficial, intermediate, and deep plexus can be readily observable throughout the whole surface of the retina. Between P21 and P25, these three vessel layers further mature to form an intricate interconnecting vessel plexus **(Figure 24)** (229).

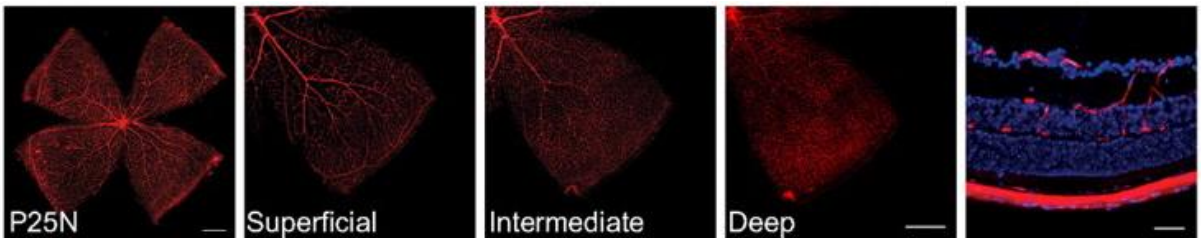


*Figure 24: Representation of fully formed retina at P25 C57Bl/6 strain at P25.*

*Retina vasculature stained with isolectin B4 (red) at P25 showing the fully matured tree vascular layers (superficial, intermediate and deep) and cross section stained with isolectin B4 (red) and with DAPI (blue) illustrating the mature retinal vasculature. Abbreviation N=normoxia. Image taken from "The Mouse Retina as an Angiogenesis Model" by Stahl* et al*., Invest. Ophthalmol. Vis. Sci., 2010 (229).*

### *3.2.1.1 Retina arterio-venous differentiation*

Arterio-venous differentiation in the retina vascular bed starts around P2 when the primitive capillary plexus is formed (232). During retinal angiogenesis, arteries and veins specification arise from a capillary plexus only in the occurrence of blood flow. From P3, differentiation between arteries and veins appear in an alternating arrangement. The process leading to arterio-venous specification in the postnatal angiogenic retina is still not completely elucidated. Nonetheless, the involvement of shear stress is known to be crucial in the process. Moreover, *in vivo* lineage tracing experiment have shown that arterial EC are derived from tip cells at the capillary front. This suggests that tip cells migrates against blood flow to access to the arteries, again proving the importance of haemodynamic forces in A/V specification (Figure 25) (233–235). As a further support to this model of reverse migration, a time-course lineage tracing experiment described in a recent report revealed that venous EC move in opposite direction to blood flow and sequentially differentiate into capillary, tip, and arterial EC (236). In particular, in this work, Lee *et al.*, showed that in the P7 vasculature ≈80% of the total ECs derived from veins, demonstrating ECs-venous origin in retina active angiogenesis. The current agreed model proposes that blood flow attracts EC migration from low flow vessels (veins and capillaries) toward high flow vessels (arteries).

Recently, in the context of ALK1 signalling, it has been shown that deletion of ALK1 in capillaries and veins using Mfsd2a CreERT2, but not from arteries or tip cells, led to disruption of Golgi polarization against the flow direction and caused retinal and cerebral AVMs (237). Disruption of flow leads to the accumulation of ECs in capillaries, causing enlargement of these vessels and, eventually, AVM formation. Disruption of flow-migration and resulting accumulation of ECs in capillaries could cause capillary enlargement thereby resulting in AVM formation.

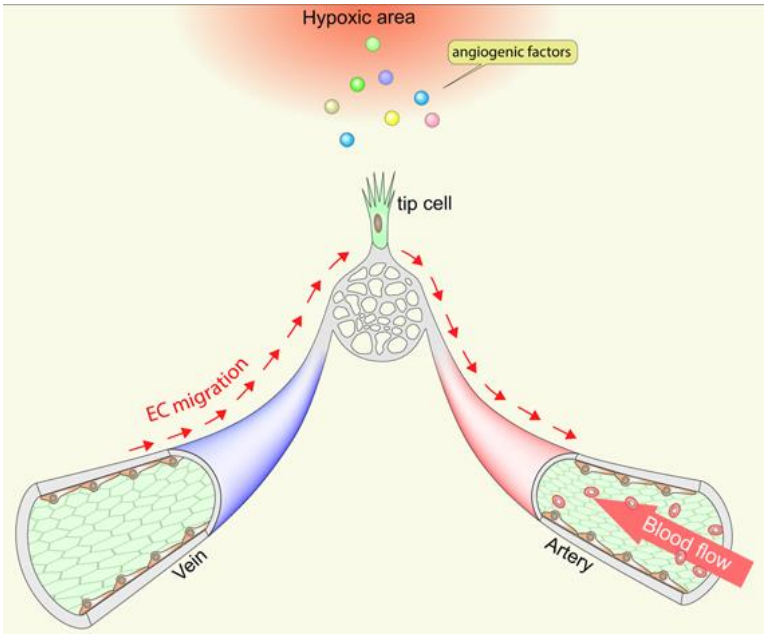


***Figure 25: Schematic illustration of EC migration during active angiogenesis.*** *Venous endothelial cells migrate against blood flow and differentiate into tip and arterial EC. Angiogenic factors released by cells at the vascular front guide angiogenesis. This initiates migration of venous EC towards the vascular front following reverse migration against the blood flow. Venous ECs are the primary source of capillary, tip and arterial ECs. Image taken from "Flow goes forward and cells step backward: endothelial migration" by Lee* et al., *2022 (235).*

### *3.2.1.2 Mouse models of vascular malformations (VM) in the context of BMP9/BMP10 ALK1-induced signalling*

Vascular malformations (VM), including congenital vascular anomalies (VA), are classified based on the vessel-type affected: veins, arteries, lymphatic vessels, or any combination thereof. Among them, arteriovenous malformations (AVMs) are characterised by shunts directly connecting arteries and veins bypassing entirely any normal capillary connection (238). AVM-composing vessels are twisted, dilated, and connected in an unorganised manner. As mentioned, development of AVMs is associated with HHT, a congenital disease that arises from mutations occurring in ENG/ALK1/SMAD4 genes which are major players of the BMP9/BMP10 signalling axis in ECs. AVMs can occur in different tissues in the body, the most life-treating being brain or and spinal cord AVM. Unfortunately, nowadays therapeutic options for these conditions are limited to surgery, radiosurgery and embolization, and are often mostly effective on smaller lesions (238). For that, there is a need to develop a representative model of this disease to be able to identify the underlying molecular and pathophysiological mechanisms in order to develop new therapeutic approaches.

Indeed, the identification of numerous signalling pathways associated with the formation of vascular lesions led to the generation of various transgenic animal models (230). Nonetheless, this purpose is still not entirely achieved as, to date, there is no transgenic animal that fully reproduces human AVMs. The complexity of AVM study is due to their intricate heterogeneity. Although it is believed that many VMs develop from inherited genetic mutations, it has been found that sporadic VM may arise from the combination of congenital mutations and what are known as "second hit" spontaneous mutations, particularly found in ECs. This spatio-temporal

complexity leading to the development of vascular malformations is an active area of research for which new genetic mouse models are urgently needed.

As HHT is associated with heterozygous loss of function mutations in genes encoding for receptor ALK1 or co-receptor ENG, the first step toward generating a mouse model to study this condition was to generate ALK1 and ENG heterozygous KO. However, these mice only displayed mild phenotypes with variable HHT-like vascular defects, among different genetic backgrounds (133). On the other hand, generation of mice with inducible homozygous deletion for ALK1 and ENG, resulted in a more robust and reliable phenotypes, including the appearance of AVMs (239–242). To note, the phenotype developed in the presence of an additional trigger such as inflammatory environment and/or an angiogenic stimuli. These findings, combined with the observation ALK1 and ENG KO mice die *in utero* from severe vascular impairment and AVM development (130–133), further proved the importance of ALK1/ENG signalling axis in the context of angiogenesis, and that, when dysfunctional, it leads to the development of HHT-like phenotypes, including the formation of AVMs in mice.

As it was shown that BMP9 and BMP10 are the functional ligands to ALK1/ENG signalling pathway, the roles of these two ligands in the development of AVMs has also been analysed. It has been documented that using neutralising antibodies against both BMP9 and BMP10, eventually led to AVMs in the retina vascular-developing bed and in intestines (192,193). However, genetic deletion of BMP9 combined with blockade of BMP10 postnatally did not reveal AVM formation (191).

SMAD4 mutations have been identified in patients with juvenile polyposis, a syndrome that shares some features with HHT, including AVMs. SMAD4 is a downstream effector of BMP induced signalling. Genetic studies of SMAD4 iKO mice revealed a phenotype highly similar to that of ALK1/ENG deletion and to that of blockade of BMP9/BMP10 featuring retinal, cerebral and intestinal AVMs. (153,243)

Table 2 lists the current mouse models available to investigate key genetic candidates of BMP9-10/ALK1/ENG/SMAD4 signalling pathway known to be involved in HHT pathology and development of vascular malformations and, in some instances leading to formation of AVM, which can therefore be studied.

*Table 2 Non-exhaustive list of principle constitutive and inducible transgenic mouse models to study vascular malformations induced by defects in BMP9-10/ALK1/ENG/SMAD4 signalling pathway.*

*Abbreviations: Acvlr1: Activin A Receptor Like Type 1; Chd5: Cadherin 5; E: Embryonic; HOHF: High Output Heart Failure; ENG: Endoglin; L1: Line1 Transposon; PAVMs: Pulmonary Arteriovenous Malformation; R26: Rosa26; SCL: Stem Cell Leukemia.*

| Mouse Driver Line | Genetic manipulation | Site of vascular defect | Selected References |
|---|---|---|---|
| *Acvlr1*$^{-/-}$ Global KO | Embryonic germline homozygous deletion of ALK1. | AVM formation between E10.5 and 11.5, vessel lumen dilation, fusion of capillary plexus, defective differentiation and recruitment of VSMC. 100% mortality in embryo. | (130,131,133) |
| *Acvlr1*$^{+/-}$ Global KO | Embryonic germline heterozygous deletion of ALK1. | Age-dependent vascular lesions and AVM in the skin, extremities, oral cavity and in the internal organ (lung, liver, gut, spleen and brain). 100% mortality. | (244,245) |
| *Acvlr1*$^{lox/lox}$ Global KO R26-CreERT | Constitutive ubiquitous ALK1 deletion. | Adults (> 2 months old) die 9–21 days after a single TM injection. Gut and lung haemorrhage, skin AVMs upon wound-induced healing. 100% mortality. | (239) |
| *Acvlr1*$^{lox/lox}$ EC specific KO L1-Cre | Conditional ALK1 deletion in ECs of brain, lung and guts. | AVMs, haemorrhage in brain, lung and gut and mortality observed in late gestational period (E17.5) .100% mortality. | (239,246) |
| *Acvlr1*$^{lox/lox}$ EC specific KO Cdh5-CreERT | Conditional ALK1 deletion in ECs postnatally. | Retinal AVMs, lung haemorrhage, adult caecal haemorrhage. 100% mortality. | (192,240) |
| *Acvlr1*$^{lox/lox}$ SMC specific KO Pdgfb-CreERT | Conditional ALK1 deletion in ECs in adult. | Brain AVMs upon VEGF stimulation lung haemorrhage and visceral AVMs. 100% mortality. | (247) |
| *Acvlr1*$^{lox/lox}$ SMC specific KO SM22α-CreERT | Conditional ALK1 deletion in vSMCs and ECs. | Brain and spinal AVMs. High mortality. Massive reduction of pulmonary vSMCs but no effect in aorta and coronary arteries | (248) |
| *Acvlr1*$^{lox/lox}$ EC specific KO Scl-CreERT | Conditional ALK1 deletion in ECs in adults | Skin AVMs following wounding, visceral AVMs. 100% mortality. | (241) |
| *Eng*$^{-/-}$ Global KO | Embryonic global homozygous ENG deletion | Embryonic yolk sac vascular defects, umbilical vein dilation haemorrhage, heart defects. 100% mortality in embryo. | (249,250) |
| *Eng*$^{+/-}$ Global KO | Embryonic global heterozygous ENG deletion | Brain AVMs, telangectasia, vessel dilation. Viable. | (250) |
| *Eng*$^{lox/lox}$ EC specific KO Cdh5-CreERT | Conditional KO in ECs in neonates or adult stages | Adults reduced angiogenesis and increase in vein diameter upon VEGF stimulation. Viable Neonates from P5 to P7 retinal AVMs, increased EC proliferation. | (242) |
| *Eng*$^{lox/lox}$ Global KO R26-CreERT | Conditional KO in all cell types upon induction in neonates or adult stages | Neonates die at 4 to 10 days after invalidation. Adults AVMs dependent on VEGF stimulation or wounding. Viable | (241,251) |

| | | | |
|---|---|---|---|
| *Eng*$^{lox/lox}$<br>SMC specific KO<br>SM22α-CreERT | Conditional KO in vSMCs and ECs | Scattered AVMs, brain and spinal cord micro-haemorrhages. 50% mortality by 6 weeks. | (251) |
| *Eng*$^{lox/lox}$<br>EC specific KO<br>Scl-CreERT | Conditional KO in ECs | Skin AVMs upon wounding. Viable. | (241) |
| *Smad4*$^{-/-}$<br>Global KO | Embryonic germline homozygous SMAD4 deletion | Incomplete mesoderm formation. 100% mortality during gastrulation (E6. 5) | (252) |
| *Smad4*$^{lox/lox}$<br>Cdh5-CreERT | Postnatal deletion of SMAD4 in ECs | Retinal AVMs, likely PAVMs, increase EC proliferation and size, enlargement of veins and arteries. | (243) |
| *Smad4*$^{lox/lox}$<br>Tie2Cre | Embryonic deletion of SMAD4 in ECs | Enlarged pericardium, defective endocardial cushion development, haemorrhage, decreased dorsal aorta diameter, enlarged veins.100% mortality by E10.5. | (253) |
| *Bmp9*$^{-/-}$<br>Global KO | Embryonic germline homozygous BMP9 deletion | Enlarged lymphatic capillaries and mesenteric collecting vessels in the pup and the adult. Viable. | (156) |
| *Bmp10*$^{-/-}$<br>Global KO | Embryonic germline homozygous BMP10 deletion | Embryonic enlarged pericardium, absent vitelline vessels, arrested vascular development, cardiac defects. 100% mortality (E10.5). | (254) |

This table summarises the major studies on transgenic mouse models in the context of vascular malformations induced by defects in BMP9-10/ALK1/ENG/SMAD4 signalling pathway prior to the beginning of this thesis project. As it can be observed, not much is known concerning the function of BMP9 and BMP10. Ultimately, my thesis project, aimed to unveil the function of these two ligands in the context of vascular malformation and possibly bring a new model to study the mechanisms behind the development of vascular malformations.

The need of developing transgenic mice models applies also in the context of another disease which sees this pathway involved: pulmonary arterial hypertension. Given the heterogeneous nature of pulmonary hypertension, no single transgenic animal model is likely to make a universally accurate model capable of phenocopying all the different facets of the condition. Nonetheless, several animal models have been developed over the years to, at least, reproduce the clinical state of this disease. The models are generated based on the principle that exposure to diverse environmental stimuli can induce a pulmonary vasculopathy comparable to the counterpart human condition. Some important key feature are shared among these models of PAH, including the progressive increase in mean pulmonary arterial pressure (mPAP), the right ventricle systolic pressure (RVSP) resulting from vascular remodelling (e.g. muscularisation and thinning of the pulmonary vascular tree) and increased pulmonary vascular resistance. Table 3 represents the animal models available to the study of pulmonary arterial hypertension.

*Table 3: Summary of most commonly used mice and rat models for PAH.*

| Model | Species | Precapillary arteriopathy | Plexiform lesions | RV remodelling/ RV function | Systemic effects | Mortality | Selected reference |
|---|---|---|---|---|---|---|---|
| Monocrotaline / Inflammatory model PAH | Rat Dose (60–80 mg/kg) | Yes | No | Maladaptive/ Reduced | Yes | Yes | (255,256) |
| | Rat Dose (20–40 mg/kg) | Yes | No | Adaptive/ Maintained | Yes | No | (257,258) |
| Chronic hypoxia/ High-altitude, chronic lung disease | Rat | Yes | No | Adaptive/ Maintained | Yes | No | (259,260) |
| | Mouse | Yes | No | Adaptive/ Maintained | Yes | No | (261,262) |
| Sugen+ hypoxia/ PAH model | Rat | Yes | Yes | Maladaptive/ Reduced | Yes | Strain-dependent | (263,264) |
| | Mouse | Yes | No | Adaptive/ Moderately reduced | Yes | No | (265,266) |
| Pulmonary artery banding/ Isolated RV pressure overload | Rat/ Mouse Mild constriction | No | No | Adaptive/ Maintained | No | No | (267,268) |
| | Rat/ Mouse Severe constriction | No | No | Maladaptive/ Reduced | No | Yes | (269–271) |

Regarding rat models for PAH, chronic hypoxia-induced PAH rat model is among the most commonly used animal models of PAH. For instance, it has been shown that treatment of wild-type (WT) BMPRII to PAH-rat lung endothelium ameliorates the condition (272). Nonetheless, despite being considered the best model for studying pulmonary vasoconstriction and vascular hypertrophy, chronic hypoxia-induced PAH rat model is not entirely representative human PAH. On the other hand, although mice usually reveal less severe PH and RV dysfunction compared to rats, they have been more analysed compared to the latter due to the ease of genetic manipulation. Indeed, analysis of these animal models allowed the scientific community to make considerable progress over the past years. For instance, analysis of chronic hypoxia (CH)- or monocrotaline (MCT) administered- PAH models, led to the development of vasodilator therapy for PAH (273). Also, it has been shown that BMPR2 loss in HPAECs changed the kinetics of BMP9-mediated SMAD canonical signalling: in particular, BMPR2 loss blocks the endothelial

response to BMP9, resulting in increase of proliferation (274). This finding could have potential implications for the proposed translation of BMP9 as a treatment for PAH.

Models that combine multiple hits common to PAH patients, would allow to better reproduce severe vascular lesions more relevant to the pathogenesis of human PAH bringing the research community one step closer to novel therapies. More recently, development of transgenic rats, including BMPR-II and KCNK3 mutant lines, opened new routes to the study of this disease (275,276). Combinations of both genetic defects with a secondary hit (e.g. hypoxia) results in robust phenotype allowing both phenotypic and mechanistics analysis of cellular and molecular signalling pathways involved in the pathogenesis.

Overall, HHT and PAH conditions involve the same signalling pathway occurring in ECs, yet they are quite different from each other. Still many questions remain to be answered before being able to find new therapeutic approaches for these conditions. In the case of BMP10 involvement in PAH, biochemical and functional characteristics of the identified mutations are not yet known. Moreover, because BMP9 and BMP10 are dimeric proteins, it is important to consider that heterozygous mutations in BMP9 or BMP10 could have a dominant negative effect on their homo- and heterodimers forms.

# Aims

My thesis project was born from Vascular Anomalies (V.A.) Cure, a European collaboration founded by Marie Skłodowska-Curie Actions. V.A. Cure has assembled 7 world-leading academic laboratories and 5 companies, that collaboratively aimed to: (i) identify novel genes involved in VAs in patients, (ii) unravel molecular mechanisms behind the diseases using *in vitro* models, (iii) apply deep tissue analysis to dissect mechanisms in pathophysiological conditions using *in vivo* models, and (iv) test identified treatment strategies. This collaborative effort would ultimately lead to understanding not only vascular anomalies, but also aberrant vascular function in other vascular-related diseases. The consortium founded 14 different PhD projects around Europe and supported the interaction between students and PI among the different laboratories via annual meetings and secondments allowing the student to visit another institution and carry some experiments related to the project, taking advantage of the host's specific expertise. Of course, due to the travelling restrictions imposed during the COVID-19 crisis, annual meeting and planned secondments could only be partially fulfilled.

My thesis project, aimed to unveil the respective roles of BMP9 and BMP10 in blood and lymphatic vascular homeostasis using *in vivo* transgenic mouse models.

In particular, the main objectives were:

a) Determine the role of BMP10 in both adult blood vascular homeostasis and in postnatal vascular developmental process;
b) Determine the origin of circulating homo- and heterodimer forms and deciphering the functions of cardiac BMP10 vs hepatic BMP10 in the context of postnatal vascular development and maintenance.

a) Determine the role of BMP10 in both adult blood vascular homeostasis and in postnatal vascular developmental process

The first part of the project was aimed to unveil the function of BMP10 in adult blood vascular homeostasis and postnatal vascular developmental process. At the time of the beginning of my PhD, the long-term effect of deletion of either BMP10 or both BMP9 and BMP10 ligands had not been thoroughly elucidated, mainly due to the difficulties encountered in studying the function of this ligand *in vivo,* due to the premature embryonic death of constitutive BMP10 KO. To study that we utilised either the Rosa Cre BMP10 iKO to analyse whether this ligand had a specific function (in both pups and adults vascular development/homeostasis) or we crossed the BMP9 KO to the Rosa Cre BMP10 iKO to obtain a conditional double KO (cDKO) model (Rosa Cre cDKO). This led to a publication by Bouvard *et al.* that will be presented in "Part I - Introduction to 1st article (contribution as 3rd author)".

Regarding the study of the BMP10 function during postnatal vascular development using Rosa Cre BMP10 iKO, at the beginning of my PhD project, my group had gathered some preliminary data in which they observed that inducing the deletion of BMP10 quickly lead to growth arrest an anaemia and that the haematopoietic organs were strongly affected (bone marrow, spleen and thymus). These observations led us to believe that BMP10 played a major role in postnatal haematopoiesis. Therefore, we set up to analyse the function of BMP10 in this context, however we came to the realisation that the phenotype that we were observing was a result of Cre toxicity. We believe that the issue of Cre toxicity has been widely disregarded in the field of vascular biology, and, while we realised this problem prior to publish a paper, we realised that the majority of published articles using the Rosa CreERT2 model lack the use of the right controls, and that this could lead to misleading conclusions. Nevertheless, during this past year, the issue of Cre toxicity is getting more and more attention, but still many groups are not aware of this problem and do not use the right controls in their experiments. For this reason, we are trying to publish a paper in Scientific Report journal showing the deleterious effect of the Rosa CreERT2 activation in pups that will be discussed in "Part II – Consequences of BMP10 deletion in young mice using Rosa26 CreERT2 line"

As the study of the functional role of BMP10 at this stage using the Rosa CreERT2 mouse model was not feasible, we had to re-orientate the project. For that, we used two new mice model of tissue-specific BMP10 KO to determine the origin of the circulating forms and to characterise their function in the context of postnatal angiogenesis and lymphatic network formation.

b) Determine the origin of circulating homo- and heterodimer forms and deciphering the functions of cardiac BMP10 vs hepatic BMP10 in the context of postnatal vascular development and maintenance

During the last year of the PhD, we set up determine the source of the circulating homodimer BMP10 and the heterodimer BMP9/BMP10 and to characterise their functions. At the time I started the PhD, my team had recently described the presence of the circulating active heterodimer composed of BMP9 and BMP10. We aimed to unveil the source of both BMP10 and BMP9/10 heterodimer. For that, we generated tissue specific BMP10 KO models by crossing out *Bmp10*$^{lox/lox}$ model with either cardiac specific inducible αMHC –MerCreMer or liver specific Lrat Cre (Table 4).

Lastly, in the context of postnatal angiogenesis, we had some preliminary data from M2 student Elisa Redman showing that both BMP9 and BMP10 are necessary for functional development of the retina vascular bed (using the Rosa Cre cDKO). We aimed to understand which BMP10 (cardiac vs hepatic) has a role in this context. To study the function of tissue specific BMP10 in the context of postnatal angiogenesis we crossed each of the three BMP10 mouse lines that we had (whole-body Rosa Cre BMP10 iKO; cardiac-specific MerCreMer BMP10 iKO; liver-specific Lrat Cre BMP10 KO) with BMP9 KO to obtain Rosa cDKO, MerCreMer cDKO and Lrat DKO. On the other hand, we planned to study the function of BMP10 in lymphatic network formation and maintenance. To study the lymphatic function of BMP10 we used the three single KO lines of BMP10 that we generated to first analyse whether BMP10 had a function in the formation of this vascular bed (Rosa Cre) and, if confirmed, to address whether the role came from cardiac (MerCreMer) or hepatic (Lrat Cre) BMP10.

In Table 4 are represented the models that I used over the course of the project.

*Table 4: Transgenic mice models used during PhD thesis.*

| Mouse Driver Line | Characteristics | Specificity | Strain abbreviation | Reference |
|---|---|---|---|---|
| *Bmp9*$^{-/-}$ Global KO | Embryonic germline homozygous BMP9 deletion | Whole body constitutive KO | BMP9 KO | (191) |
| *Bmp10*$^{lox/lox}$ Global iKO R26-CreERT2 | Conditional inducible ubiquitous BMP10 deletion | Whole body inducible Cre activation | Rosa Cre BMP10 iKO | (195) |
| *Bmp10*$^{lox/lox}$ Cardiac specific iKO αMHC -MerCreMer | Conditional inducible cardiac BMP10 deletion | Cardiac specific inducible Cre activation | MerCreMer BMP10 iKO | (277) |
| *Bmp10*$^{lox/lox}$ Liver specific KO Lrat Cre | Liver BMP10 deletion Cre | Liver specific Cre activation during gestation | Lrat Cre BMP10 KO | (278) |

# Results

## Part I - Introduction to 1st article (contribution as 3rd author)

### Different cardiovascular and pulmonary phenotypes for single- and double-knock-out mice deficient in BMP9 and BMP10 (279).

*In vivo* functions of BMP9 and BMP10 have been previously addressed in the context of both postnatal active angiogenesis (191) and closure of ductus arteriosus (157) using neutralising antibodies against BMP10 in BMP9 KO mice. BMP9 KO mice, on the other hand, are viable although they present some lymphatic defects (176). However, the long-term effect of deletion of either BMP9 or BMP10 had not been thoroughly elucidated mainly due to the difficulties encountered in studying the function of this ligand *in vivo* due to the premature embryonic death of constitutive BMP10 KO.

In the context of PAH disease (discussed in "2.2.7.2 Pulmonary Arterial Hypertension (PAH)") several mutations in the BMP9-10/ALK1/ENG pathway have been identified over the years. Recently, mutations in the genes BMP9 and BMP10 have also been recognised (219–221). Therefore we hypothesised that the loss of these ligands could be of importance in the pathogenesis of the disease. *In vivo* studies of the function of these two ligands in the context of PAH had not been yet carried out. For that, in this study we set up to analyse the function of BMP9 and BMP10 in adult single (R26CreERT2 *Bmp10*$^{lox/lox}$) and double (*Bmp9*$^{-/-}$; R26CreERT2 *Bmp10*$^{lox/lox}$) knock-out mice under normoxic and hypoxic conditions (to induce PAH) to investigate for the first time the roles of BMP9 and BMP10 in pulmonary and cardiovascular homeostasis. Of note the BMP9 KO we used was constitutive while BMP10 is inducible under tamoxifen injection.

We found out that, under normal physiological conditions, deletion of either BMP9 or BMP10 does not result in any overt phenotype (apart from lymphatic phenotype in BMP9 KO already described (176)), hence proving that although BMP10 is crucial for cardiac formation during

embryogenesis (138), it is dispensable in adult animals. On the other hand, double knock-out mice, in which BMP10 deletion had been induced at eight-weeks of age, although viable, revealed vascular defect. In particular, analysis of these mice at 5 months, resulted in cardiomegaly with signs of dilated cardiomyopathy that progressively leads to heart failure, as well as splenomegaly, and pulmonary hemosiderosis. The development of high-output resulted from decrease in systemic arterial blood pressure caused by strong vessel dilations, which were identified especially in the lungs, intestines, and brain. Of note, these organs are known to have the highest level of ALK1, which again underlies the importance of this signalling axis. At a molecular level, RNAseq analysis of the lungs of the double-KO mice revealed differential expression of genes involved in inflammation and vascular homeostasis. Overall, these DKO mice share some features with HHT (although no AVMs could be found) and could make a useful mouse model for long-term studies given their viability. While our manuscript was being revised, a different mouse model with a double deletion of BMP9 and BMP10 (specifically in the right atria), was published. The phenotype described by the team resembled ours showing vasodilatation and a decrease systemic blood pressure (280).

Moreover, we tested the function of these ligands under hypoxia-induced PAH. Interestingly, when the mice were subjected to hypoxia, single-KO for BMP9 and BMP10 responded differently. Chronic hypoxia causes pulmonary vasoconstriction, which leads to adaptive muscularisation of the pulmonary arterial vascular tree. In our work, we showed that BMP9 KO models were protected from PAH-induced pulmonary muscularisation. A recent publication from our group has shown that BMP9 KO mice had lower mRNA levels of the vasoconstrictor endothelin (ET)-1, which we confirmed, and increased levels of the two potent vasodilator factors apelin and adrenomedullin (ADM) (161). Overall, these findings are in agreement with the suggestion of BMP9 protective function in the context of PAH. On the other hand, when single BMP10 iKO mice were exposed to chronic hypoxia, they developed significant cardiac enlargement, which was not observed in BMP9 KO mice. These findings indicate that BMP10 does indeed play an important role in cardiac remodelling in adulthood, which could not be revealed under normal physiological conditions.

My contribution to the work revolved around *in vivo* analysis of transgenic mice models to analyse the function of BMP10 on the maintenance of adult vascular homeostasis. In particular, I contributed in the assessment of phenotypic characterisation of single and double KO mice for BMP9 and BMP10 to characterise the gross phenotype of dissected organs, and analyse the vascular beds after latex blue injection, a medium used for better visualisation of arteries and veins.

ESC European Society of Cardiology

Cardiovascular Research (2022) **118**, 1805–1820
https://doi.org/10.1093/cvr/cvab187

# Different cardiovascular and pulmonary phenotypes for single- and double-knock-out mice deficient in BMP9 and BMP10

**Claire Bouvard [1]*, Ly Tu [2,3], Martina Rossi[1], Agnès Desroches-Castan [1], Nihel Berrebeh [2,3], Elise Helfer [1], Caroline Roelants[1,4], Hequn Liu [1], Marie Ouarné[1†], Nicolas Chaumontel[1], Christine Mallet[1], Christophe Battail [1], Andreas Bikfalvi [5], Marc Humbert [2,3,6], Laurent Savale[2,3,6], Thomas Daubon[5,7], Pascale Perret [8], Emmanuelle Tillet[1], Christophe Guignabert [2,3‡], and Sabine Bailly [1‡]**

[1]Laboratoire Biosanté U1292, Université Grenoble Alpes, INSERM, CEA, IRIG-Biosanté UMR_S 1292, 38000 Grenoble, France; [2]School of Medicine, Université Paris-Saclay, Le Kremlin-Bicêtre, France; [3]INSERM UMR_S 999, Hôpital Marie Lannelongue, Le Plessis-Robinson, France; [4]Inovarion, 75005 Paris, France; [5]INSERM U1029, Institut National de la Santé et de la Recherche Médicale, 33615 Pessac, France; [6]AP-HP, Department of Respiratory and Intensive Care Medicine, Hôpital Bicêtre, Le Kremlin-Bicêtre, France; [7]Univ. Bordeaux, CNRS, IBGC, UMR5095, 33000 Bordeaux, France; and [8]Laboratory of Bioclinical Radiopharmaceutics, Université Grenoble Alpes, INSERM, UMRS_1039, LRB, 38000 Grenoble, France

*Received 1 October 2020; editorial decision 23 May 2021; online publish-ahead-of-print 4 June 2021*

**Aims** *BMP9* and *BMP10* mutations were recently identified in patients with pulmonary arterial hypertension, but their specific roles in the pathogenesis of the disease are still unclear. We aimed to study the roles of BMP9 and BMP10 in cardiovascular homeostasis and pulmonary hypertension using transgenic mouse models deficient in *Bmp9* and/or *Bmp10*.

**Methods and results** Single- and double-knockout mice for *Bmp9* (constitutive) and/or *Bmp10* (tamoxifen inducible) were generated. Single-knock-out (KO) mice developed no obvious age-dependent phenotype when compared with their wild-type littermates. However, combined deficiency in *Bmp9* and *Bmp10* led to vascular defects resulting in a decrease in peripheral vascular resistance and blood pressure and the progressive development of high-output heart failure and pulmonary hemosiderosis. RNAseq analysis of the lungs of the double-KO mice revealed differential expression of genes involved in inflammation and vascular homeostasis. We next challenged these mice to chronic hypoxia. After 3 weeks of hypoxic exposure, *Bmp10*-cKO mice showed an enlarged heart. However, although genetic deletion of *Bmp9* in the single- and double-KO mice attenuated the muscularization of pulmonary arterioles induced by chronic hypoxia, we observed no differences in *Bmp10*-cKO mice. Consistent with these results, endothelin-1 levels were significantly reduced in *Bmp9* deficient mice but not *Bmp10*-cKO mice. Furthermore, the effects of BMP9 on vasoconstriction were inhibited by bosentan, an endothelin receptor antagonist, in a chick chorioallantoic membrane assay.

**Conclusions** Our data show redundant roles for BMP9 and BMP10 in cardiovascular homeostasis under normoxic conditions (only combined deletion of both *Bmp9* and *Bmp10* was associated with severe defects) but highlight specific roles under chronic hypoxic conditions. We obtained evidence that BMP9 contributes to chronic hypoxia-induced pulmonary vascular remodelling, whereas BMP10 plays a role in hypoxia-induced cardiac remodelling in mice.



* Corresponding author. Tel: +33 4 38 78 42 25; fax: +33 4 38 78 50 58, E-mail: claire.bouvard@univ-grenoble-alpes.fr
† Present address. Instituto de Medicina Molecular, Faculdade de Medicina, Universidade de Lisboa, Lisbon, Portugal.
‡ The last two authors contributed equally to this work.

## Graphical Abstract

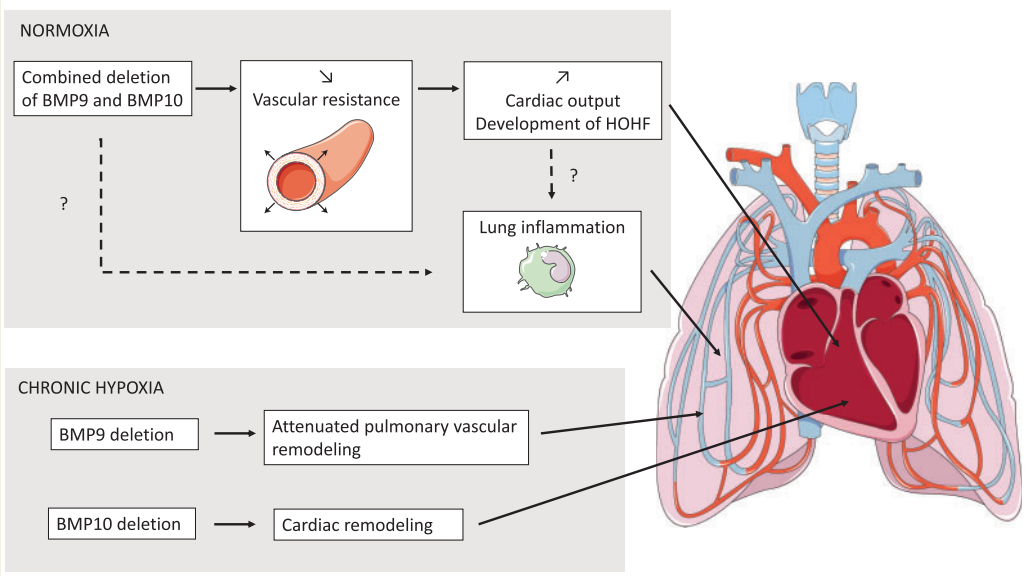


**Keywords** Pulmonary hypertension • Pulmonary vascular remodelling • Vascular anomalies • High-output heart failure • Bone morphogenetic proteins



# 1. Introduction

Pulmonary arterial hypertension (PAH) refers to an incurable rare and lethal cardiopulmonary disorder that affects both the structure and function of blood vessels of the heart and lungs.[1,2] Although the aetiology and underlying mechanisms are still unknown, many PAH-predisposing factors have been recently identified, including mutations in the genes encoding BMPRII and ALK1 (*BMPR2* and *ACVRL1*, respectively)[3,4] and, more recently, in those encoding one of the major ligands of BMPRII/ALK1 heterocomplexes, namely BMP9 and BMP10 (*BMP9*, also named *GDF2*, and *BMP10*, respectively).[5–9] Consequently, the loss or dysfunction of BMPRII/ALK1 signalling are currently considered to be the major molecular defects responsible for the predisposition to PAH and disease progression. Heterozygous mutations in the *ACVRL1* and *ENG* genes and, less frequently, *BMP9* mutations have also been shown to be associated with hereditary haemorrhagic telangiectasia (HHT), another rare disease, characterized by various vascular defects, including epistaxis, blood vessel dilation (telangiectasia), and arteriovenous malformations (AVMs) in several organs.[10–12] The mechanism by which defects in this signalling pathway predispose individuals to HHT and/or PAH and alters cardiovascular function and pulmonary blood flow is still unknown.

BMP9 and BMP10 share a high degree of sequence identity (64% in the mature domain) and have been found to have both redundant and specific roles due to their expression profiles and receptor affinities.[13] BMP9 is mainly produced by hepatic stellate cells (HSCs),[14,15] whereas BMP10 is produced mainly by the heart[16–18] and only at low levels by HSCs.[15] They are both present in the circulating blood[18–20] and were shown to bind to the endothelial-specific receptor ALK1 with subnanomolar affinities,[21,22] supporting a critical role for BMP9 and BMP10 in vascular remodelling. However, their binding affinities for type 2 receptors differ,[21] suggesting that they could also play specific roles. Consistent with this notion, gene deletion studies have shown that C57BL/6 mice lacking *Bmp9* are viable and fertile, with no overt defect in cardiac or blood vessel development,[23] whereas *Bmp10* knock-out (KO) mice die during embryonic development due to defective cardiac development[24] and show vascular defects.[20] The analysis of $Bmp10^{9/9}$ knock-in mice, for which the coding sequence of *Bmp10* was replaced by that of *Bmp9*, showed that although BMP9 and BMP10 appear to play redundant roles in early embryonic vascular development, BMP10 has an exclusive function in embryonic cardiac development that cannot be replaced by BMP9.[20] We have also demonstrated that BMP9 and BMP10 exhibit redundant roles in postnatal retinal vascularization and ductus arteriosus closure.[23,25] In our previous study, we unexpectedly showed that genetic deletion or inhibition of BMP9 (using an inhibitory antibody or the soluble ALK1 receptor as a ligand trap) had beneficial effects against the onset and progression of pulmonary hypertension (PH) in several experimental animal models.[26] These results appear to contradict those published by another group that demonstrated the capacity of recombinant BMP9 to attenuate PH in animal models.[27,28] Overall, these findings suggest that BMP9 and BMP10 may play a role in cardiovascular homeostasis and are involved in the development of PAH, but that further work is necessary to understand their respective roles. Although the phenotype of adult *Bmp9* knockout mice has been previously described,[26] the long-term effects of the loss of *Bmp10* or that of both *Bmp9* and *Bmp10* in adult mice have never been thoroughly studied.

We aimed to investigate and compare the roles of BMP9 and BMP10 in cardiovascular homeostasis and PH using adult single-KO and double-KO mice for *Bmp9* (constitutive deletion) and/or *Bmp10* (tamoxifen-induced deletion to bypass embryonic lethality) under both normoxic and hypoxic conditions to induce PH.

# 2. Methods

Methods are detailed in the Supplementary material online.

## 2.1 *Bmp9*-KO, *Bmp10*-cKO, and DKO mouse models

We generated C57BL/6 mice lacking *Bmp10* and/or *Bmp9* as previously described.[23,29] Briefly, constitutive deletion of *Bmp9* resulted from the replacement of exon 2 by a neomycin-resistance cassette. Because *Bmp10* deletion leads to early embryonic lethality, we used the tamoxifen-inducible Cre system to generate *Bmp10*-cKO mice (Rosa26-CreER$^{T2}$; *Bmp10*$^{lox/lox}$) by crossing Rosa26-CreER$^{T2}$ mice (generously provided by Pr P. Chambon, IGBMC, Illkirch, France) with *Bmp10*$^{lox/lox}$ mice, which possess loxP sites flanking exon 2. We generated double-KO (DKO) mice by crossing the Rosa26-CreER$^{T2}$; *Bmp10*$^{lox/lox}$ mice with *Bmp9*-KO mice. All mice were viable. The offspring genotypes were determined by PCR as previously reported.[29] All mice (3–4 weeks old for the PH experiments and 8 weeks old for all other experiments) were treated with tamoxifen (Sigma) by intraperitoneal injection once a day for five days at a dose of 50 mg/kg to induce Cre recombination in the *Bmp10*-cKO and DKO transgenic mice or to serve as controls. Mice were housed in a pathogen-free barrier facility under a 14-h light/10-h dark cycle and temperature-controlled environment with standard diet and water ad libitum.

## 2.2 Ethical approval and methods for anaesthesia and euthanasia

All animal procedures were designed to conform to the guidelines of Directive 2010/63/EU of the European Parliament on the protection of animals used for scientific purposes and the protocols used were approved by institutional ethics committees (APAFIS#17604-2018092716378446 v4; APAFIS #18715-2019013018234 52 v2). Gaseous anaesthesia (isoflurane 4% for induction and 1.5–2.5% for maintenance) was used for echocardiography, right heart catheterization, and fluorescent microsphere injections. Euthanasia was performed using pentobarbital injection (180 mg/kg) or by exsanguination under isoflurane.

## 2.3 Statistical analysis

The data are expressed as the means ± standard error of the mean (SEM). Mann–Whitney tests were used to assess the statistical significance of differences between two groups. Comparisons concerning more than two groups were calculated by analysis of variance followed by the Tukey test for data with a normal distribution or the Kruskal–Wallis and Dunn tests for data with a non-normal distribution. Differences were considered significant for $P < 0.05$. Analyses were performed using PRISM software (GraphPad).

# 3. Results

## 3.1 Phenotypic and molecular characterization of single-(KO) and DKO mice

We first studied adult single-KO and DKO mice for *Bmp9* and *Bmp10* under unstressed conditions to decipher the role of BMP9 and BMP10 in cardiovascular homeostasis. The deficiency in BMP9 and/or BMP10 was previously demonstrated[15,29] and verified here by measuring plasma concentrations of BMP9, BMP10, and BMP9-BMP10 heterodimers by ELISA (Supplementary material online, *Figure S1a*) and *Bmp9* and *Bmp10* mRNA levels in the liver (Supplementary material online, *Figure S1b*), right atria (Supplementary material online, *Figure S1c*), and lungs (Supplementary material online, *Figure S1d*). As expected, *Bmp9* was mainly expressed in the liver and *Bmp10* in the right atria and at a lower levels in the liver. *Bmp9* transcripts were absent from the *Bmp9*-KO and DKO mice and *Bmp10* mRNA levels were down-regulated in the *Bmp10*-cKO and DKO mice. We observed no compensatory changes between *Bmp9* and *Bmp10* expression (Supplementary material online, *Figure S1b–d*). Notably, circulating levels of BMP9 in *Bmp10*-cKO and BMP10 in *Bmp9*-KO mice were reduced but this might be due to the fact that the BMP9 and BMP10 ELISAs also detected the BMP9-10 heterodimeric form, as previously demonstrated[15] (Supplementary material online, *Figure S1a*).

Adult *Bmp9*-KO, *Bmp10*-cKO, and DKO mice were viable, and their body weight was not significantly different from that of wild-type (WT) mice (Supplementary material online, *Figure S2a* and *b*). Upon dissection, the single KO mice appeared to be normal, whereas the hearts and spleens of the DKO mice were significantly larger than those of all the other groups (*Figure 1A–F*, Supplementary material online, *Figure S2*). The greater size of the DKO hearts resulted from an increase in the size of both the right and left ventricles (*Figure 1E and F*, Supplementary material online, *Figure S3a* and *b*). Analysis of spleen sections stained with H&E did not reveal any obvious structural differences (Supplementary material online, *Figure S3c*). In contrast to the other groups of mice, DKO mouse lungs appeared strikingly reddish and/or brownish (although a few brown spots were occasionally noticed on single-KO lungs) (*Figure 1G*) and Prussian blue staining revealed the presence of iron-laden macrophages in DKO lungs (*Figure 1H*). We previously observed liver defects in another mouse model lacking *Bmp9* (in the 129Ola genetic background).[30] Thus, we examined this organ more closely. The colour and general aspect of the liver in the various groups appeared normal upon dissection. Picrosirius red staining showed a slight but significant increase in liver perivascular fibrosis in the *Bmp10*-cKO and DKO mice (Supplementary material online, *Figure S3d* and e), but hyaluronic acid (HA), ALT, and AST plasma levels were normal for all mice (Supplementary material online, *Figure S3f*, *Table S1*). We analysed standard serum chemistry and haematology parameters but observed no significant differences relative to WT mice (Supplementary material online, *Tables S1* and *S2*). Of note, the phenotype of DKO mice was similar for male and female C57BL/6 mice (Supplementary material online, *Figure S2*).

To better characterize the mice at the molecular level, we assessed mRNA levels of the main BMP9/10 receptors, *Acvrl1* (encoding the receptor ALK1), *Eng* (encoding the co-receptor endoglin), and *Bmpr2*, as well as the two BMP target genes, *Id1* [encoding the protein ID1

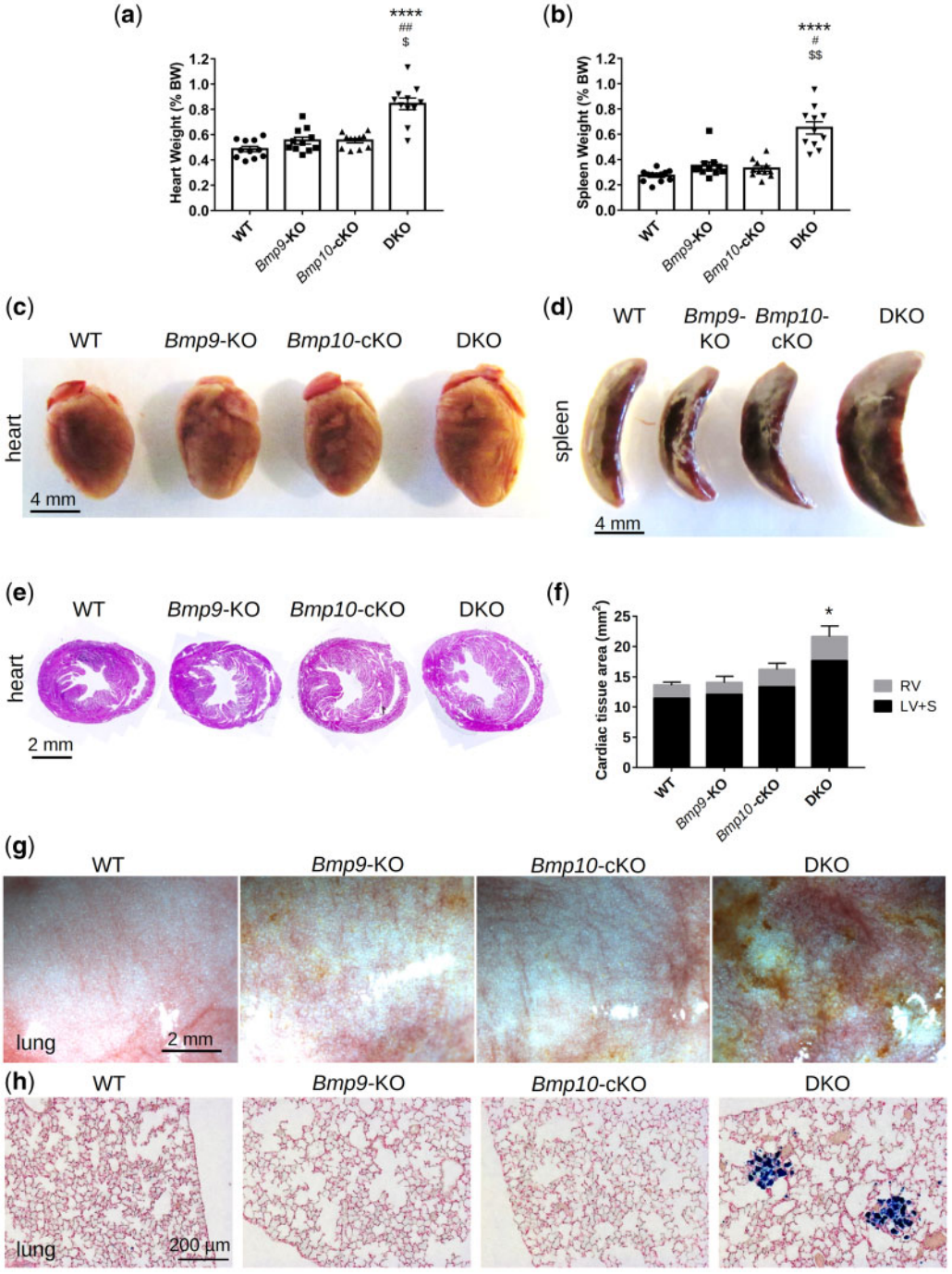


**Figure 1** Combined loss of *Bmp9* and *Bmp10* leads to cardiomegaly, splenomegaly, and pulmonary hemosiderosis in DKO mice. Heart weight (*A*) and spleen weight (*B*) normalized to body weight and representative photographs of hearts (*C*) and spleens (*D*) ($n = 11$–$12$/group, male mice, scale bar = 4 mm). Representative photomicrographs of H&E-stained transverse heart sections (*E*) and quantitative analysis of the left ventricle + septum (LV+S), right ventricle (RV), and total cardiac tissue area (*F*) ($n = 4$/group, female mice, scale bar = 2 mm). Representative photomicrographs of fresh lungs (scale bar = 2 mm) (*G*) and lung sections stained with Prussian blue (scale bar = 200 µM) (*H*). All mice were injected with tamoxifen at the age of 2 months and euthanized at the age of 5 months. Data are presented as the means ± SEM and were analysed using Kruskal–Wallis tests followed by Dunn's tests. $^{*}P < 0.05$, $^{****}P < 0.0001$ vs. WT; $^{\#}P < 0.05$, $^{\#\#}P < 0.01$ vs. *Bmp9*-KO; $^{\$}P < 0.05$, $^{\$\$}P < 0.01$ vs. *Bmp10*-cKO.

(inhibitor of DNA binding 1)] and *Smad6* (encoding the inhibitory protein Smad6) in lung, liver, and heart (right atria and left ventricle) tissue. We observed no significant differences between KO and WT mice, except for *Eng* (also a target gene in the BMP9/10 pathway) and *Smad6*, which were significantly down-regulated in the left ventricle and lungs of DKO mice, respectively (Supplementary material online, *Figure S4a–d*). We also analysed the BMP9/10 signalling pathways in the KO mice by western blotting. pSmad1/5/8 and pSmad2/3 protein levels were

significantly down-regulated in the lungs of *Bmp9*-KO and DKO mice but the difference vs. WT mice did not reach statistical significance in *Bmp10*-cKO mice (Supplementary material online, *Figure S4f*). There were no differences in heart tissue (data not shown).

## 3.2 DKO mice present signs of dilated cardiomyopathy with high output that progressively leads to heart failure

We next performed echocardiographic and cardiac histological examinations to further characterize the observed cardiac phenotype when *Bmp9* and *Bmp10* were deleted. Doppler-echocardiographic assessment of the left ventricular (LV) structure and function was performed in anaesthetized adult WT and DKO mice (4 and 11 months old). It revealed an increase in LV internal diameter and volume during systole and diastole in DKO mice, without significant changes in the thickness of the ventricle walls (LV anterior wall, posterior wall, septum) (*Figure 2A and B*). Consistent with our observations, the calculated LV mass/body weight ratio was higher in DKO mice (*Figure 2C*). We found no differences in heart rate between DKO and WT mice (*Figure 2D*). Stroke volume and cardiac output were also significantly higher in the DKO than WT group (*Figure 2E and F*). The LV dilation observed in the DKO mice (increase in LV internal diameter and volume) significantly progressed over time (*Figure 2A and B*). Although the ejection fraction and fractional shortening were not significantly different between the WT and DKO groups at 4 months, they had significantly decreased in the DKO group by 11 months (*Figure 2G and H*). These observations suggest that DKO mice develop dilated cardiomyopathy with high output that progressively leads to heart failure. Consistent with these findings, plasma levels of atrial natriuretic peptide (ANP) and brain natriuretic peptide (BNP) were significantly higher in 5-month-old DKO mice than in single-KO and WT mice (*Figure 2I and J*). Measurement of the size of individual cardiomyocytes showed them to be significantly enlarged in the DKO mice (*Figure 2K and L*) but there were no obvious signs of cardiac fibrosis upon Picrosirius red staining at the age of five months (Supplementary material online, *Figure S5a* and *b*).

## 3.3 Combined loss of *Bmp9* and *Bmp10* leads to a reduction of arterial blood pressure, vascular abnormalities, and alveolar capillary dilatation

We next conducted experiments to identify the underlying mechanisms that could lead to the development of high-output heart failure (HOHF) in DKO mice. Because a fall in systemic arterial blood pressure (BP) is a feature of HOHF,[31] systemic arterial BP was first assessed in conscious mice using a non-invasive BP system (tail-cuff method, Kent Scientific Corporation). Systemic, diastolic, and mean BP were significantly lower in DKO than WT and single-KO mice (*Figure 3A–C*). We next determined whether the fall in systemic arterial BP was related to systemic arteriovenous shunting and/or peripheral vasodilatation. To detect systemic shunts, we injected 45-µm fluorescent microbeads into the systemic circulation via the left cardiac ventricle. The microbeads were efficiently trapped in the systemic vasculature in WT and single-KO mice, for example in the brain, but also readily crossed to the lungs in the DKO mice, leading to a massive accumulation of beads in the lungs (*Figure 3D*), supporting the presence of arteriovenous shunting or important dilations in the systemic vasculature. To detect pulmonary shunts, we intravenously injected 15-µm fluorescent microbeads. The fluorescent microbeads were efficiently trapped in the pulmonary arterioles and capillaries in WT and single-KO mice but not in 70% of DKO mice, in which the beads were able to reach other organs, such as the brain (*Figure 3E*), suggesting the presence of shunts or large dilations in the pulmonary vasculature. Using latex blue intra-ventricular injection, we observed that the latex progressed further in the vascular tree and small blood vessels in the intestines and brains of DKO than WT and single KO, mice suggesting dilated vessels in the DKO mice (*Figure 3F* and Supplementary material online, *Figure S6a* and *b*). Consistent with these observations, histological analysis of 500-nm thick lung sections revealed a two- to three-fold significant increase in the average size of the lung capillaries of DKO mice relative to that of WT mice (*Figure 3G and H*). In accordance with these results, the blood volume that could be collected from the DKO mice was significantly higher than that of the other groups (Supplementary material online, *Figure S6c*), perhaps partially explaining the observed splenomegaly and increased cardiac output.

Certain conditions, such as chronic anaemia and hyperthyroidism, can also be associated with elevated cardiac output. Thus, we measured haemoglobin levels (Supplementary material online, *Table S2*) and examined thyroid glands (Supplementary material online, *Figure S6d*), but no differences were noted.

Overall, our data show that the combined loss of *Bmp9* and *Bmp10* results in a decrease in peripheral vascular resistance in DKO mice, resulting in an increase in cardiac output, cardiomegaly, and the development of a HOHF phenotype with age.

## 3.4 RNAseq analysis reveals differential expression of genes involved in inflammation, angiogenesis, blood pressure, cilium organization and motility, and cardiac chamber development

We performed an RNAseq analysis of the lungs of WT and DKO mice to better understand what was happening in the DKO mice, specifically in the lungs, which are highly vascularized, and of specific interest in PH. Among the 17 853 identified genes, we observed 537 differentially expressed genes (DEGs) with adjusted *P*-values <0.05 and absolute log2 fold changes >log2 (1.5). The DEGs were distributed between 343 over-expressed and 194 under-expressed genes in DKO relative to WT mice. A bi-clustering heatmap designed to visualize the expression profile of the top 40 DEGs according to their statistical significance (lowest adjusted *P*-values) is presented in *Figure 4A*. We used DAVID tools to analyse the list of the 537 DEGs (Supplementary material online, *Figure S7* and *Table S3*), grouped the most relevant biological process gene ontology (GO) terms into six categories and highlighted the involved genes in volcano plots (*Figure 4B*, Supplementary material online, *Table S4*). We found 82 DEGs related to inflammation and the immune response, 38 to ion transport, 30 to extracellular matrix disassembly, 30 to cell adhesion, 18 to angiogenesis, and 14 to BP and vasoreactivity (*Figure 4B*, Supplementary material online, *Table S3*). Enriched molecular function GO terms confirmed these results (Supplementary material online, *Figure S7*). We also found several biological process GO terms linked to insulin secretion, haemostasis, cilium, iron ions, organ morphogenesis, and multicellular organism development (Supplementary material online, *Figure S7*). The Pi3K/AKT pathway, which has been shown to be activated when *Acvrl1* is deleted,[32] was enriched in both GO biological process and KEGG analyses (Supplementary material online, *Figure S7*). We performed gene set enrichment analysis (GSEA) on the full list of genes ranked by log2 fold change using the functional Gene Ontology/Biological Process database. The categories with the top positive

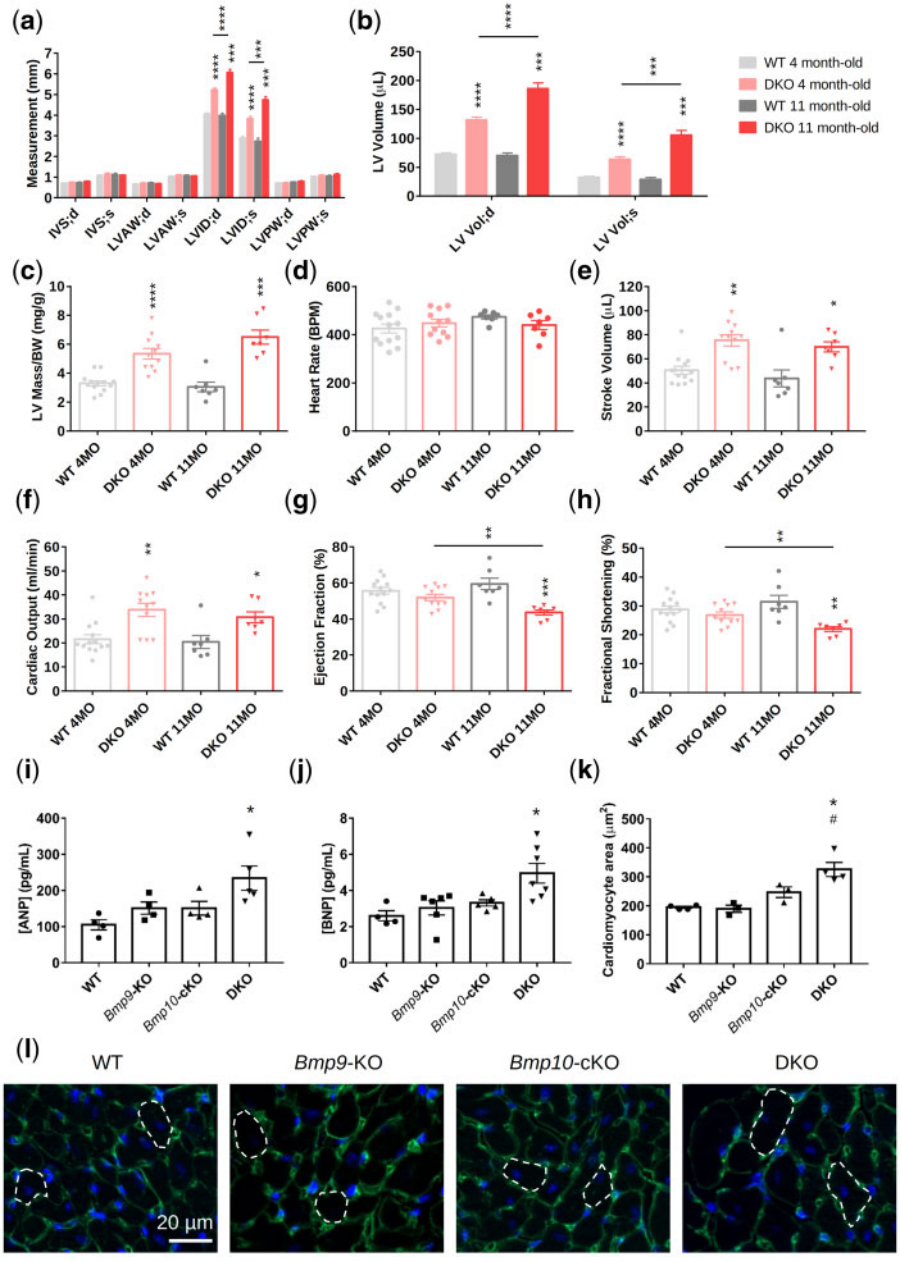


**Figure 2** Combined loss of *Bmp9* and *Bmp10* leads to high cardiac output and cardiac hypertrophy in DKO mice. (*A–H*) Echocardiographic analysis of the left ventricle of 4- and 11-month-old WT and DKO female mice ($n = 7–13$/group). End-systolic (s) and end-diastolic (d) measurements of the interventricular septum (IV S), left ventricular anterior wall (LVAW), left ventricular posterior wall (LVPW) thickness, and the left ventricular internal diameter (LVID) (*A*), calculation of the left ventricular volume (LV Vol) (*B*), left ventricular mass/body weight (LV mass/BW) (*C*), heart rate (*D*), stroke volume (*E*), cardiac output (*F*), ejection fraction (*G*), and fractional shortening (*H*). All mice were injected with tamoxifen at the age of 2 months. Data are presented as the mean ± SEM and were analysed using Mann–Whitney tests to compare DKO vs. WT or 4-month-old vs. 11-month-old mice. $^{*}P < 0.05$, $^{**}P < 0.01$, $^{***}P < 0.001$, $^{****}P < 0.0001$. (*I–L*) Plasma analysis and immunofluorescence. ANP (atrial natriuretic peptide) (*I*) and BNP (brain natriuretic peptide) (*J*) plasma levels ($n = 4–7$ male mice/group). Quantitative analysis of cardiomyocyte size (*K*) and representative photomicrographs (*L*) of transverse heart sections stained with FITC-conjugated wheatgerm agglutinin to outline individual cardiomyocytes ($n = 3–4$ female mice/group, 100 cardiomyocytes/mouse). Mice were injected with tamoxifen at the age of 2 months and analysed at the age of 4–5 months. Data are presented as the means ± SEM and were analysed using Kruskal–Wallis tests followed by Dunn's tests. $^{*}P < 0.05$ vs. WT; $^{\#}P < 0.05$ vs. *Bmp9*-KO.

normalized enrichment score were related to inflammation (the first was the response to interleukin 1) and those with the top negative scores were linked to cilium organization and motility, cardiac chamber/ventricular system development, and response to BMP (*Figure 4C*). We next performed quantitative real-time reverse transcription polymerase chain reaction (RT-qPCR) of several DEGs or genes identified by the GSEA analysis using a different cohort of mice and studied their expression in both single and DKO mice (Supplementary material online, *Figure*

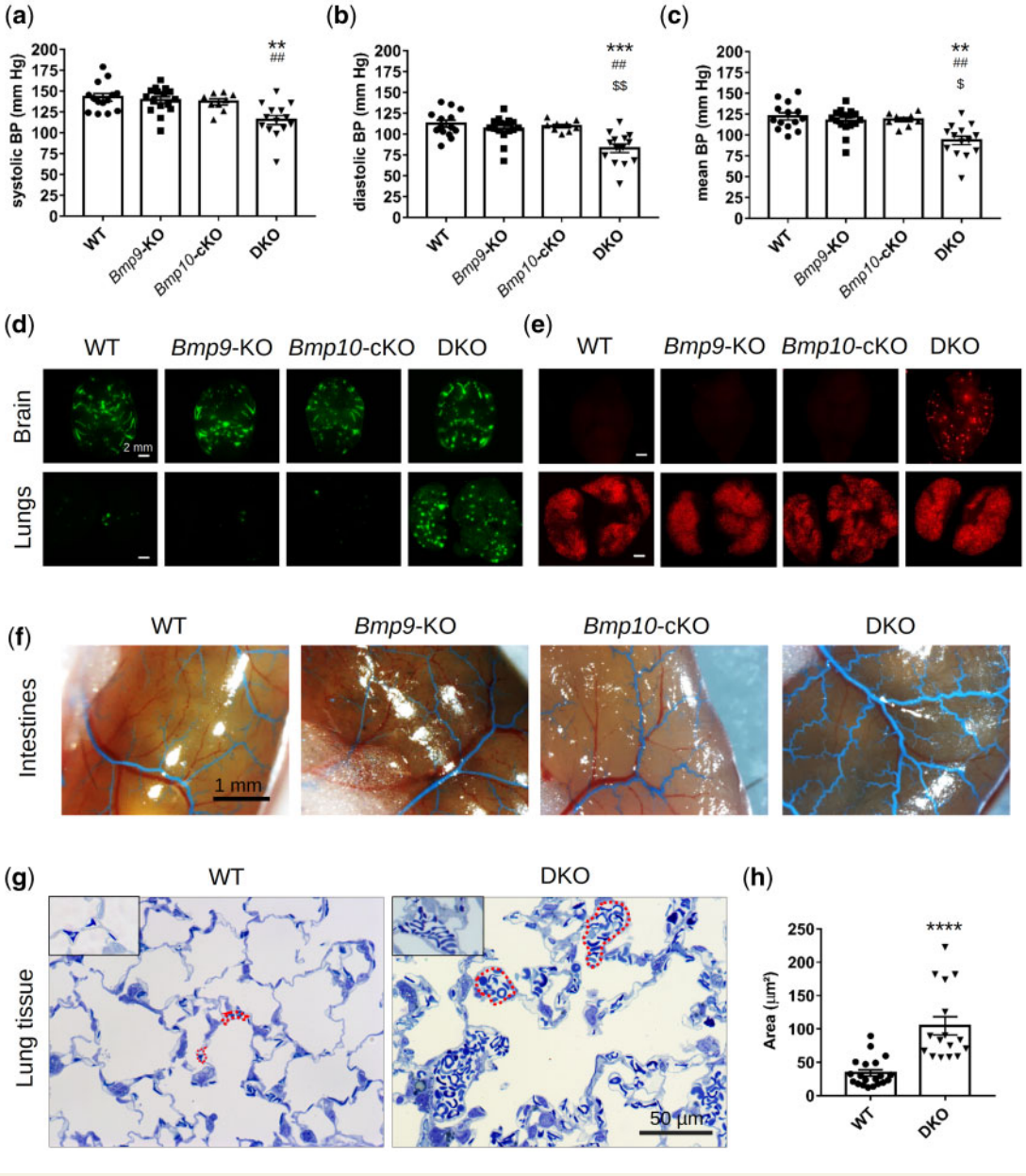


**Figure 3** Combined loss of *Bmp9* and *Bmp10* leads to a reduction in arterial blood pressure (BP), vascular anomalies, and alveolar capillary dilatation in DKO mice. Non-invasive measurements of systolic (*A*), diastolic (*B*), and mean (*C*) BP in conscious adult mice ($n = 9$–16 male mice/group). Data are presented as the mean ± SEM and were analysed using Kruskal–Wallis tests followed by Dunn's tests. $^{**}P < 0.01$, $^{***}P < 0.001$ vs. WT. $^{\#\#}P < 0.01$ vs. *Bmp9*-KO. $^{\$}P < 0.05$, $^{\$\$}P < 0.01$ vs. *Bmp10*-cKO. Representative photomicrographs of brain and lungs of mice that received an injection of 45-µm fluorescent beads in the left cardiac ventricle ($n = 5$ female and 5 male mice/group, scale bar = 2 mm) (*D*) and of mice that received an intravenous injection of 15-µm fluorescent beads ($n = 4$ female and 3 male mice/group) (*E*). Representative photomicrographs of the intestines of latex-blue injected mice (*F*) ($n = 3$–5 male and 3–5 female mice/group, scale bar = 1 mm). Representative photomicrographs (*G*) and quantitative analysis (*H*) of the size of capillaries from 500-nm thick lung sections stained with epoxy tissue stain. The red dotted lines outline several capillaries (scale bar = 50 µm). Data represent the mean capillary area of $n = 16$–20 independent lung sections from three different female mice/group. Data are presented as the means ± SEM and were analysed using Mann–Whitney tests. $^{****}P < 0.0001$ vs. WT. Mice were injected with tamoxifen at the age of 2 months and analysed at the age of 5 months.

*S8a* and *b*). We confirmed elevated expression of two genes encoding key inflammatory mediators, *Ccl2* (encoding CCL2, also known as monocyte chemoattractant protein-1) and *Ccl3* (encoding CCL3, also known as macrophage inflammatory protein 1-alpha), but not *Cxcl5*. We also confirmed the reduced expression of two genes in the lungs of DKO mice involved in BP and vasoreactivity, *Smad6* and *Edn1* (encoding endothelin 1) (*Figures 4B and 7B*, Supplementary material online, *Figure S4a*). Consistent with these results, a reduction in endothelin-1 (ET-1) protein levels was also confirmed in the plasma of DKO mice (*Figure 7A*). We could not confirm the down-regulation of two genes involved in cilium

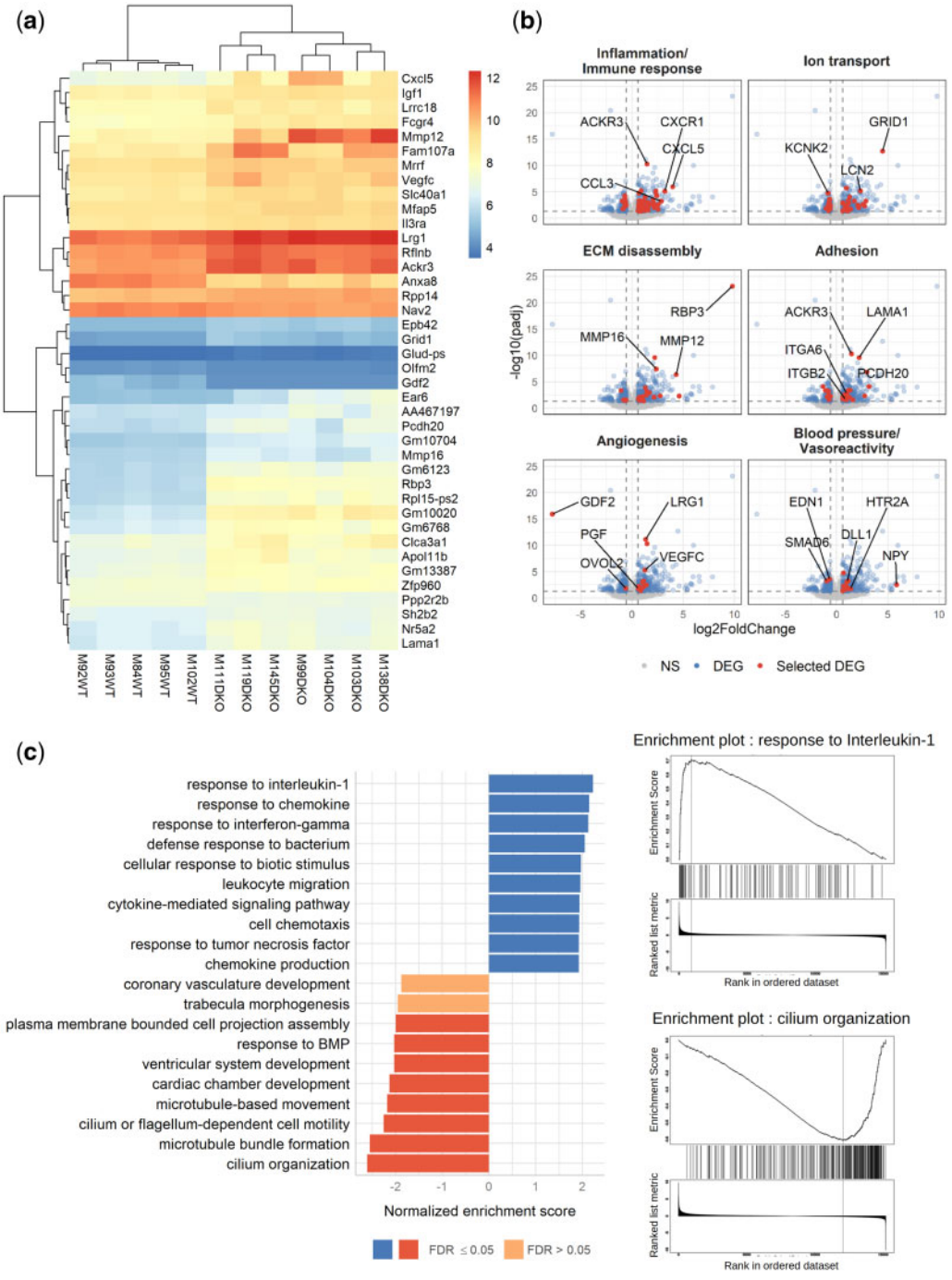


**Figure 4** RNAseq analysis of WT and DKO mouse lung tissue reveals modulation of the transcription of genes involved in inflammation, angiogenesis, blood pressure, cilium organization, and cardiac development. Five WT and seven DKO male mice were injected with tamoxifen at the age of 2 months and analysed at the age of 5 months. (*A*) A bi-clustering heatmap was used to visualize the expression profile of the top 40 differentially expressed genes (DEGs) between the WT and DKO conditions, with the lowest adjusted *P*-value by plotting their log2 transformed expression values (colour scale) for each sample. (*B*) Visualization of the comparison of the global transcriptional change across groups was visualized by volcano plots. Each data point in the scatter plot represents a gene. The log2 fold change of each gene is represented on the *x*-axis and the -log10 of its adjusted *P*-value on the *y*-axis. Genes that were not significantly differentially expressed (NS) are represented in grey, DEGs in blue, and a selection of DEG involved in specific biological processes in red (gene ontologies used for these volcano plots are listed in the Supplementary material online, *Table S3*). (*C*) Gene-set enrichment analysis (GSEA) performed using the functional database gene ontology/biological process non-redundant. The top 10 positive (blue) and negative (red) categories are presented. Each bar represents a gene ontology, the normalized enrichment score is represented on the *x*-axis, and the colour of the bar represents the FDR *P*-value. Enrichment plots for the top positive and negative terms are shown on the right. .

motility, *Hydin* and *Dnah5* (data not shown). Surprisingly, our RNAseq analysis performed in the lungs highlighted the cardiac chamber development GO term. We thus performed an RT-qPCR analysis in heart tissue (left ventricle) from single KO and DKO mice of *Nkx2-5* (encoding the homeobox transcription factor Nkx2-5) and *Tbx-20* (encoding a T-box transcription factor Tbx20), two transcription factors that are important in cardiac development and known to be regulated by BMP10.[24,33] The mRNA levels of both transcription factors were reduced in the DKO mice, but only the decrease of Nkx2-5 reached statistical significance (Supplementary material online, *Figure S8b*). To further validate the inflammation/Immune response GO term, we next used the Cibersortx digital cytometry tool,[34] along with a mouse lung single-cell RNAseq dataset,[35] to estimate the relative abundance of various cell populations from our lung RNAseq analysis. Consistent with our histological observations (*Figure 1H*), we observed a significant increase in the estimated percentage of alveolar and interstitial macrophages in DKO versus WT mice (Supplementary material online, *Figure S8c* and *d*). We also observed an increase in the estimated percentage of vein cells, that may likely be a consequence of pulmonary vasodilation or possible venous congestion due to the development of HOHF in this DKO mouse model (*Figure 3G*, Supplementary material online, *Figure S8c* and *d*). Consistent with our GSEA results, which highlighted the cilium organization GO term, the estimated percentage of ciliated cells was reduced (*Figure 4C*, Supplementary material online, *Figure S8c* and *d*). Overall, these results show that there is strong inflammation in the lungs of the DKO mice and that genes that are crucial for cardiovascular homeostasis are deregulated in the absence of *Bmp9* and *Bmp10*.

### 3.5 Hypoxia-induced pulmonary vascular and cardiac remodelling in *Bmp9*-KO, *Bmp10*-cKO, and DKO mice

Chronic hypoxia induces adaptive pulmonary arterial muscularization and right ventricular hypertrophy[26,36] and we previously showed that *Bmp9*-KO mice are partially protected from such remodelling.[26] Thus, we next determined and compared the susceptibility of *Bmp9*-KO, *Bmp10*-cKO, and DKO mice to develop PH in response to chronic hypoxia (10% $FiO_2$) for 3 weeks (*Figures 5 and 6*).

We confirmed that *Bmp9*-KO mice do not develop spontaneous PH under normoxic conditions and that they are mildly protected against PH induced by chronic hypoxia, as reflected by a significant decrease in the values of the right ventricular systolic pressure (RVSP) and Fulton index [RV/(LV+S)], indicators of right ventricular hypertrophy (*Figure 5A and B*), and the percentage of medial wall thickness and muscularized distal pulmonary arteries (*Figure 6A*).

Under normoxic conditions, *Bmp10*-cKO mice did not develop spontaneous PH. There were no significant differences in the RVSP values, percentage of medial wall thickness or muscularized distal pulmonary arteries, or Fulton index [RV/(LV+S)] between *Bmp10*-cKO and WT mice (*Figures 5D and E, 6B*). After 3 weeks of exposure to hypoxia, we observed a similar increase in RVSP values, Fulton index, and the percentage of medial wall thickness and muscularized distal pulmonary arteries of the *Bmp10*-cKO mice relative to the those of the WT mice (*Figures 5D and E, 6B*). Interestingly, the heart weight of *Bmp10*-cKO mice exposed to chronic hypoxia was greater than that of hypoxic WT mice and those maintained in normoxia (*Figure 5F*). Of note, there was no significant increase in heart weight of *Bmp9*-KO mice when challenged with chronic hypoxia (*Figure 5C*).

Under normoxic conditions, the DKO mice did not develop spontaneous PH, similarly to the *Bmp9*-KO and *Bmp10*-cKO mice (*Figures 5G and H, 6C*). However, they exhibited HOHF, as reflected by a marked increase in the Fulton index [RV/(LV+S)] and heart weight (*Figure 5H and I*). DKO mice chronically exposed to hypoxia exhibited an attenuated increase in RVSP values and the percentage of medial wall thickness and muscularized distal pulmonary arteries relative to hypoxic WT mice (*Figures 5G and 6C*).

Overall, these results show that *Bmp10* deletion does not offer protection from PH, whereas *Bmp9* deletion or double *Bmp9*/*Bmp10* deletion can partially protect against the pulmonary vascular remodelling induced by chronic hypoxia.

### 3.6 BMP9 is an endothelin-1-mediated vasoconstrictor

ET-1 is a potent vasoconstrictor peptide that contributes to the pulmonary vascular remodelling associated with PH. Consistent with our previous work and publications showing that BMP9 can affect ET-1 expression,[26] we found significantly lower circulating ET-1 protein levels in the plasma of *Bmp9*-KO and DKO mice than in that of WT mice, but not in *Bmp10*-cKO mice (*Figure 7A*). This result is consistent with the RNAseq analysis showing the differential expression of genes involved in vasoreactivity, including *Edn1* (*Figure 4B*, Supplementary material online, *Table S3*). Lung ET-1 mRNA levels were also significantly lower in DKO than WT mice but not in *Bmp10*-cKO mice (*Figure 7B*). Consistent with this notion, we previously showed that BMP9 is a potent vasoconstrictor using the chicken embryo chorioallantoic membrane (CAM) assay.[19] To better characterize the important regulators of vascular tone regulated by BMP9, we tested three different inhibitors of vasoconstriction, namely bosentan (endothelin receptor antagonist), captopril (angiotensin-converting enzyme inhibitor), and terguride (serotonin receptor antagonist) in the CAM assay in response to BMP9. Vessels were visualized by injecting fluorescein-labelled dextran (FITC-dextran) into the CAM vessels. In accordance with our previous work,[19] BMP9 induced the vasoconstriction of the blood vessels in the treated area, interrupting the passage of FITC-dextran in these vessels (*Figure 7C and D*). BMP9-induced vasoconstriction was inhibited by Bosentan (at the 500-μM dose) (*Figure 7C and D*) but not captopril or terguride (Supplementary material online, *Figure S9*). These data support that ET-1 is a key component of BMP9-induced vasoconstriction.

## 4. Discussion

The first link between PAH and germline mutations in *BMPR2* was established 20 years ago. Since then, several mutations in this pathway have been added to the list of genes involved in PAH (e.g. *ACVRL1, ENG*, and *SMAD9*) and, more recently, mutations in the genes *BMP9* (also called *GDF2*) and *BMP10*, encoding the two high-affinity ligands for ALK1/BMPRII.[3–8] It was thus hypothesized that the loss of these ligands could be an essential driver of disease pathogenesis. This was underscored by the demonstration that the administration of recombinant BMP9 can attenuate the development of PH in animal models.[27] However, in 2019, in contrast to what was expected, we found that blocking BMP9 had beneficial effects and prevented the muscularization of pulmonary arteries in PH animal models.[26] Interestingly, defects in this pathway have also been associated with vascular abnormalities, such as excessive capillary fusion (AVM), hyperdilation, reduced vascular muscularization, and excessive/abnormal angiogenesis and vessel patterning.[23,37,38] However, the

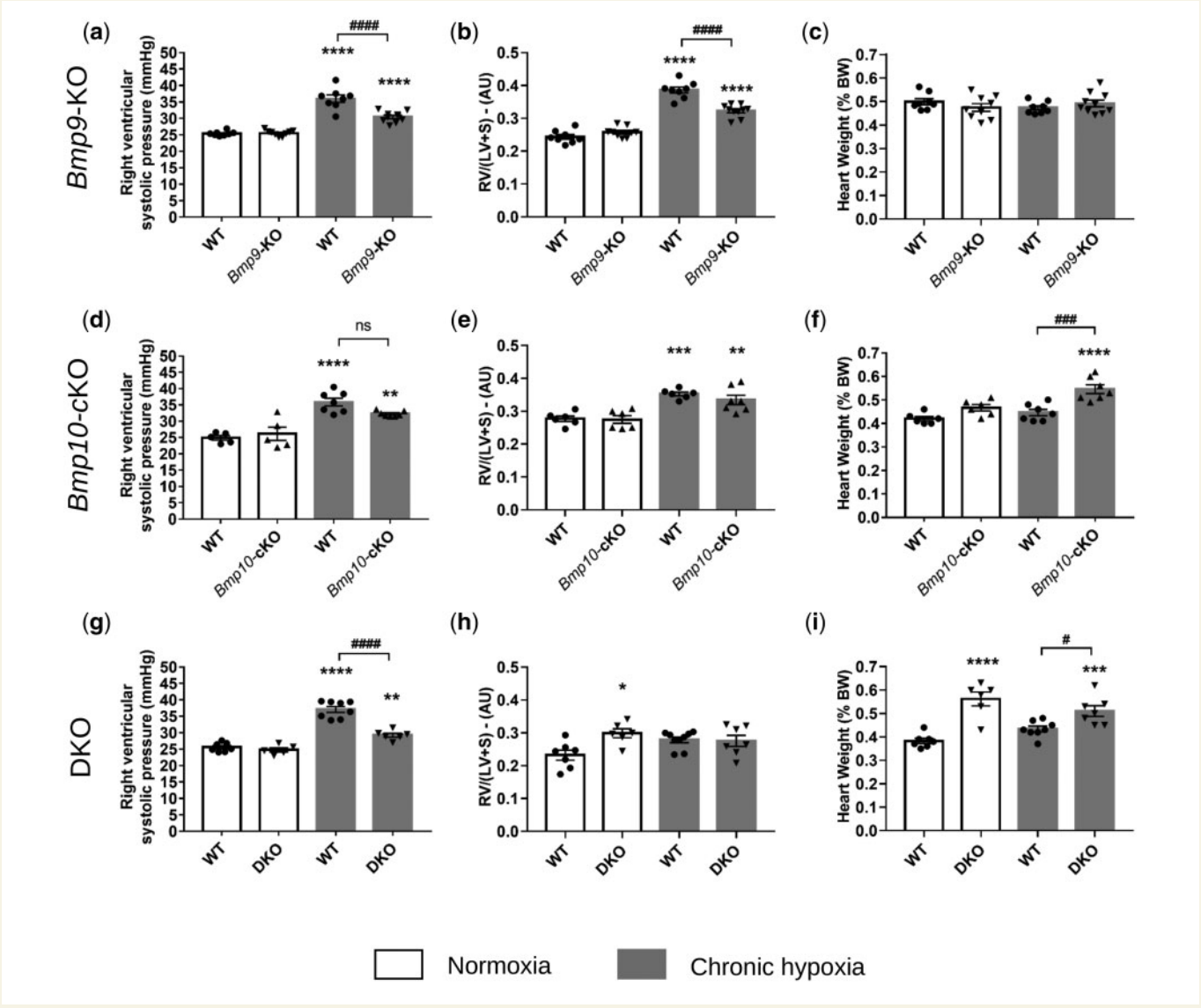


**Figure 5** *Bmp9*-KO, *Bmp10*-cKO, and DKO mice do not develop spontaneous PH under normoxic conditions and exhibit different susceptibility to the development of chronic hypoxia induced PH and cardiac remodelling. (*A, D, G*) Values of right ventricular systolic pressure (RVSP), (*B, E, H*) right ventricular hypertrophy, expressed by the Fulton Index RV/(LV+S), (*C, F, I*), and of heart weight of WT vs. *Bmp9*-KO mice (*A–C*), WT vs. *BMP10*-cKO mice (*D–F*), and WT vs. DKO mice (*G–I*). Data are presented as the means ± SEM of $n = 5–10$ male mice per group and were analysed using by ANOVA followed by Tukey's test. $^{*}P < 0.05$, $^{**}P < 0.01$, $^{***}P < 0.001$, $^{****}P < 0.0001$ vs. WT under normoxia; $^{\#}P < 0.05$, $^{\#\#\#}P < 0.001$, $^{\#\#\#\#}P < 0.0001$ vs. WT under chronic hypoxia. AU, arbitrary unit; LV, left ventricle; ns, non-significant; RV, right ventricle; S, septum.

phenotypes of adult mice lacking *Bmp9* and/or *Bmp10* have never been thoroughly described and compared. The aim of the present study was to address, for the first time, the roles of BMP9 and BMP10 in pulmonary and cardiovascular homeostasis, more specifically, in the context of PAH, using adult single and double knockout mice under normoxic and hypoxic conditions (to induce PH). The deletion of *Bmp9* was constitutive and that of *Bmp10* induced at the adult stage to bypass embryonic lethality. We found that none of these transgenic mice developed spontaneous PH under unstressed conditions. *Bmp9* and *Bmp10* single knockout homozygous mutant adult mice were viable and fertile and exhibited no overt phenotype. However, deletion of *Bmp*10 in *Bmp*9-KO mice (DKO mice) led to several abnormalities of the cardiovascular and pulmonary systems (reduced BP, cardiomegaly, pulmonary inflammation and hemosiderosis). Furthermore, although the loss of *Bmp10* had no impact on the degree of pulmonary vascular remodelling induced by chronic hypoxia, *Bmp9*-KO and DKO mice chronically exposed to hypoxia exhibited less pronounced remodelling of the pulmonary vascular bed than their WT littermates. On the other hand, the loss of *Bmp10* under chronic hypoxia induced cardiomegaly. Overall, our data indicate both redundant and specific roles for BMP9 and BMP10 in vascular remodelling.

Under physiological conditions, the loss of one of the ligands (BMP9 or BMP10) did not lead to overt cardiovascular defects in adult C57Bl/6 mice, suggesting that one can compensate for the loss of the other. However, the combined loss of *Bmp*9 and *Bmp*10 had dramatic consequences on pulmonary and cardiovascular homeostasis and led to the

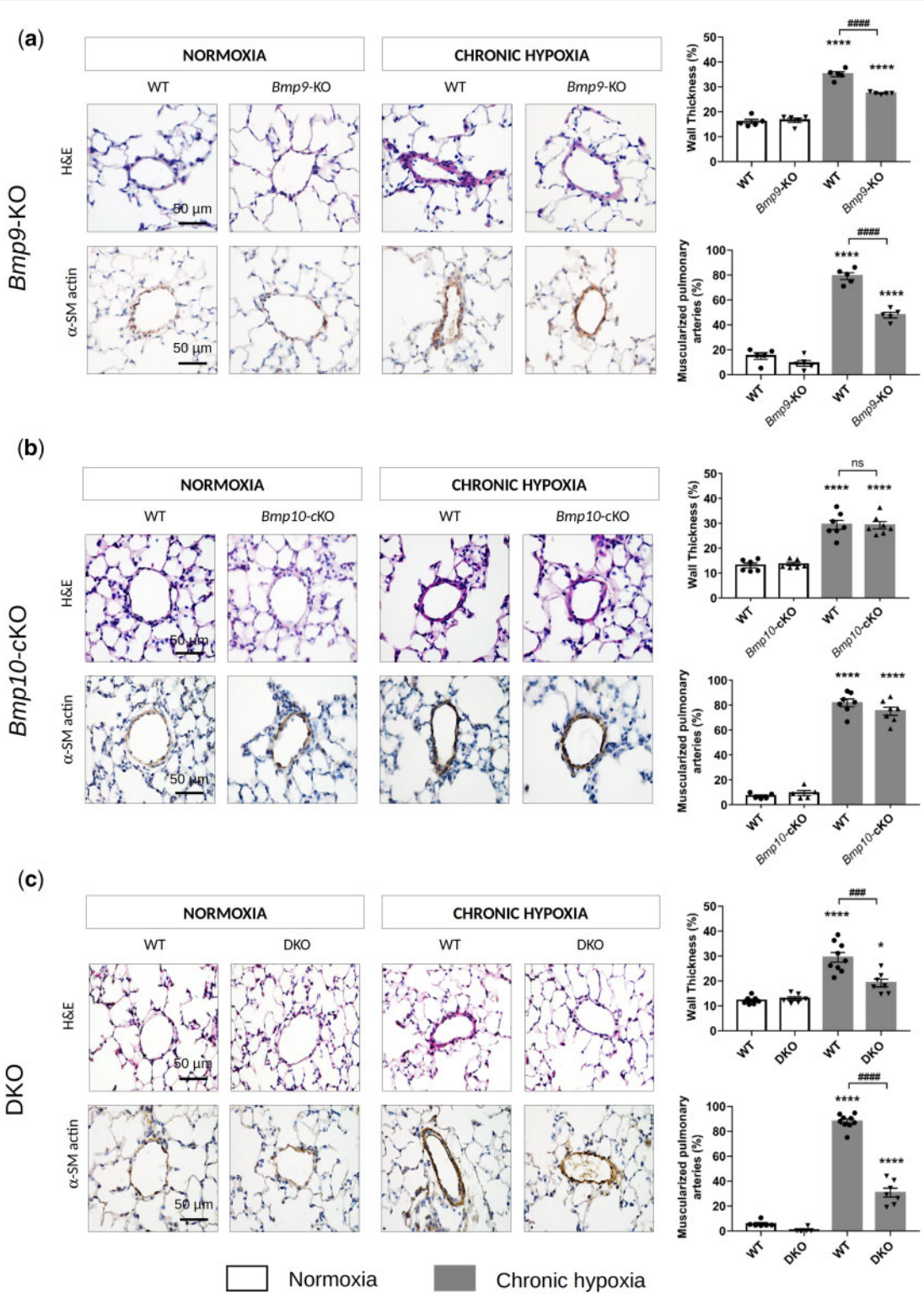


**Figure 6** Loss of *Bmp9* but not *Bmp10* decreases the susceptibility of developing of chronic hypoxia-induced PH, as it protects against pulmonary arterial remodelling. Representative images of haematoxylin-eosin (H&E) staining and α-smooth muscle (SM)-actin and quantification of the percentage of muscularized and wall thickness of distal pulmonary arteries in the lungs of WT vs. *Bmp9*-KO mice (*A*), WT vs. *Bmp10*-cKO mice (*B*), and WT vs. DKO mice (*C*). Scale bar = 50 μm for all sections. Data are presented as the means ± SEM of $n = 5–9$ male mice per group and were analysed by ANOVA followed by Tukey's test. $^{*}P < 0.05$, $^{****}P < 0.0001$ vs. WT under normoxia; $^{\#\#\#}P < 0.001$, $^{\#\#\#\#}P < 0.0001$ vs. WT under chronic hypoxia.

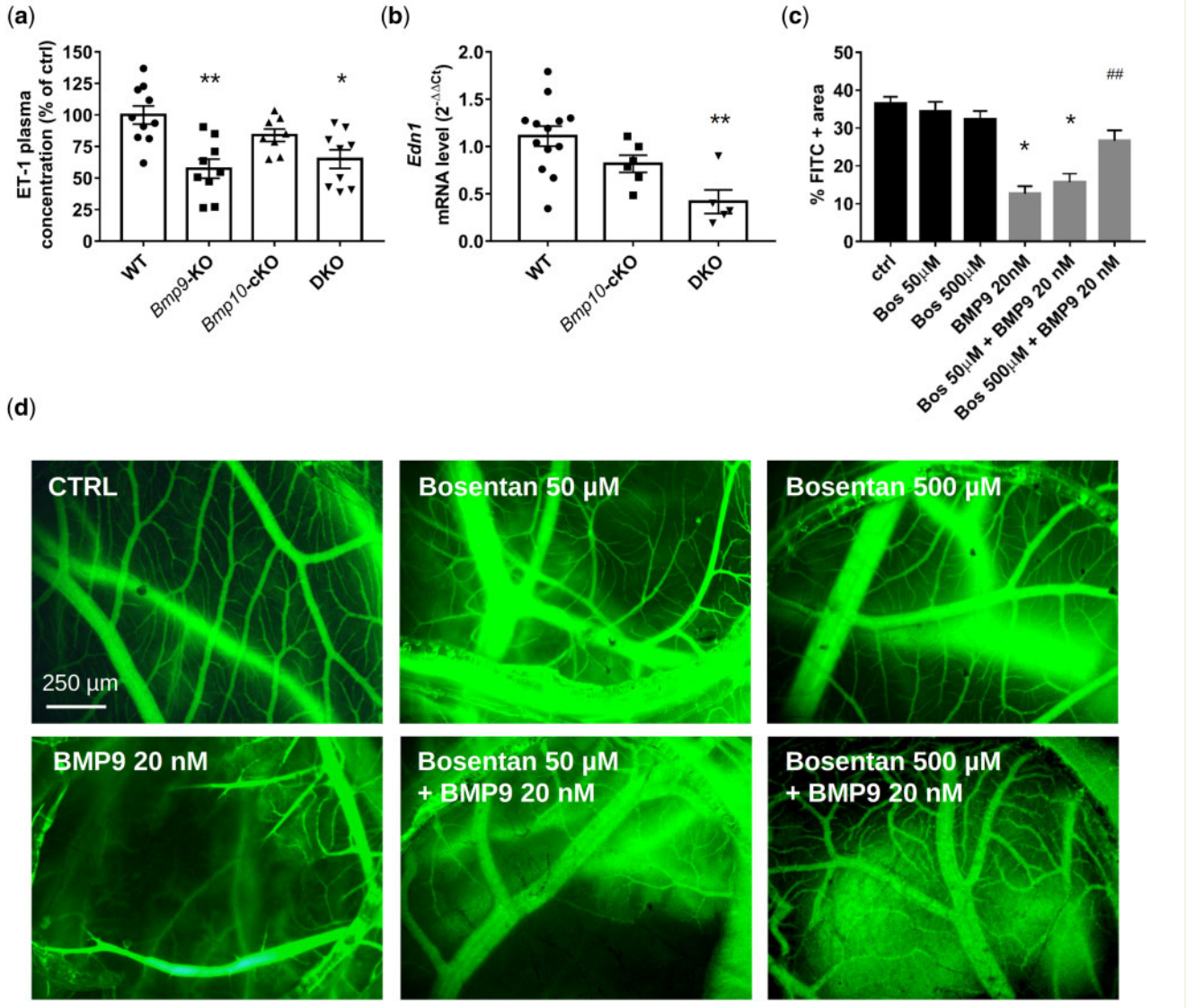


**Figure 7** Loss of *Bmp9* in mice is associated with reduced endothelin-1 (ET-1) abundance and ET-1 plays a crucial role in BMP9-induced vasoconstriction in chick chorioallantoic membrane. ET-1 plasma (*A*) levels in WT, *Bmp9*-KO, *Bmp10*-cKO, and DKO mice ($n = 8$–10 male mice/group) and lung mRNA (*B*) in WT, *Bmp10*-cKO, and DKO mice ($n = 5$–13 male mice/group). Mice were injected with tamoxifen at the age of 2 months and analysed at the age of 5 months. Data are presented as the mean ± SEM and were analysed using Kruskal–Wallis tests followed by Dunn's tests. $^{*}P < 0.05$, $^{**}P < 0.01$ vs. WT. Quantitative analysis (*C*) and representative photomicrographs (*D*) of FITC-Dextran-injected blood vessels from chick chorioallantoic membranes treated with bosentan (0, 50, and 500 µM), in combination with BMP9 (20 nM) or not for 24 h (scale bar = 250 um). Data are presented as the means ± SEM of $n = 3$–6 eggs/group and were analysed using Kruskal–Wallis tests followed by Dunn's tests. $^{*}P < 0.05$ vs. vehicle treated control and $^{\#\#}P < 0.01$ vs. the 20 nM BMP9 condition.

progressive development of HOHF, with cardiomegaly and increased cardiomyocyte size and ANP and BNP levels. We show that systemic BP is reduced in DKO mice, which is a sign of a reduced peripheral vascular resistance that can cause HOHF. This can arise from vasodilation and/or arteriovenous shunting. Indeed, we observed that blood vessels were dilated, especially in the lungs, intestines, and brain, which is intriguing, as the BMP9/BMP10 receptor ALK1 is predominantly expressed by endothelial cells in these organs (EC Atlas[39]) We also observed the abnormal passage of fluorescent microbeads from pulmonary arteries to pulmonary veins and from systemic arteries to systemic veins in DKO mice. Our results are in accordance with those of a recent study be Wang *et al.*,[40] published while our manuscript was under revision, showing vasodilatation, a decrease in peripheral arterial wall thickness, and lower systemic BP in a different mouse model with a double deletion of *Bmp*9 and *Bmp*10. Interestingly, the loss of endothelial *Eng* in adult mice also leads to HOHF and AVMs, but the underlying mechanism appears to be different. Indeed, the authors show an exaggerated endothelial response to VEGF signalling, favouring the formation of AVMs in the pelvic area,[41] whereas, in our study, the vascular dilations or shunts were not limited to one specific location. Our results are also different from those obtained from the loss of *Acvrl1* in adult mice, which is associated with pulmonary and gastrointestinal haemorrhage, severe anaemia, and the

development of HOHF, ultimately leading to death within three weeks.[42,43] Here, DKO mice survived for several months after tamoxifen administration. This could either be due to differences in the efficiency of tamoxifen-induced deletion, genetic differences, or to BMP9/10-independent ALK1 functions. These DKO mice share certain features with HHT and could be a valuable mouse model in the field of vascular anomalies, allowing long-term studies on adult mice.

The marked hemosiderosis (presence of iron-laden macrophages) and inflammation observed in DKO lungs could have been caused by heart failure (leading to venous congestion and alveolar bleeding) or compromised endothelial integrity or pulmonary circulation or could have resulted from a direct effect on inflammation. Consistent with these results, RNA-seq analysis showed that the main up-regulated functions were linked to inflammation (key inflammatory chemokines, such as CCL2 and CCL3, were confirmed by RTqPCR to be up-regulated in the DKO mice), with an increased estimated percentage of alveolar and interstitial macrophages in the DKO mice, supporting that BMP9 and BMP10 likely play important roles in inflammation. The relationship between this pathway and inflammation is also supported by recent publications suggesting that BMP9 and BMP10 can prevent macrophage recruitment, in part, via the inhibition of CCL2.[44] Blood vessel-related functions (angiogenesis, regulation of BP) were also significantly deregulated in the RNAseq analysis and these results are in accordance with the observed phenotype (vasodilation, reduced systemic BP) and the down-regulation of ET-1 in the plasma.

In addition to the alteration in peripheral vascular resistance contributing to the development of HOHF in the DKO mice, we cannot exclude direct effects of the combined loss of BMP9 and BMP10 on the heart. BMP10 is known to be predominantly expressed in the heart, where it plays a central role in cardiomyogenesis in prenatal and postnatal life.[20,24] However, it has also been implicated in the maintenance of vascular development, homeostasis, and remodelling.[20,23,25,45,46] Consistent with such roles, we found reduced expression of the gene encoding the cardiogenic transcription factor NKX2-5 in the heart of the DKO mice. Although it is currently well accepted that BMP9 could potentially compensate for the loss of *Bmp10* at the vascular level, to a certain degree, this does not appear to be the case for the cardiomyogenic program.[20,23,25] *Bmp10*-KO mice indeed die between E9.5 and E10.5, with profound defects in cardiac development[24]; the receptor and signalling molecules involved are yet to be determined. BMP10 binds with high affinity to ALK1, of which the expression is restricted to endothelial cells, but which has also been shown to bind in a complex with ALK3, which is expressed by cardiomyocytes and a subset of endothelial cells of the heart (EC Atlas[39]) Here, we provide the first *in vivo* demonstration that the loss of *Bmp10* in adult C57Bl/6 mice does not have any overt phenotypic defects in cardiac tissue or function under unstressed conditions. However, these mice developed marked cardiac enlargement when chronically exposed to hypoxia, supporting that BMP10 plays a crucial role in cardiac remodelling in adulthood. Consistent with our present findings, it was previously shown that disruption of the downstream effector Smad4 in cardiomyocytes leads to cardiac hypertrophy and heart failure.[47]

We previously showed that mice lacking *Bmp9* do not develop spontaneous PH and that its inhibition attenuates chronic hypoxia-induced pulmonary vascular remodelling.[26] Here, we confirm these results in the *Bmp9*-KO and DKO mice and additionally show that the loss of *Bmp10* has no impact on the percentage of medial wall thickness and muscularized distal pulmonary arteries. These results suggest a specific role of BMP9 in this context. Similarly, we have previously shown that BMP9, but not BMP10, plays a role in tumour angiogenesis using the same knockout mouse models.[29] This may be due to a difference between BMP9 and BMP10 in terms of their affinity for BMP receptors, quantity, availability, or the activity of ligands or receptor complexes in a given organ and in response to hypoxia. Interestingly, we found a significant reduction in pSmad1/5/8 and pSmad2/3 protein levels in lung tissues from mice lacking *Bmp9* (i.e. *Bmp9*-KO and DKO mice), but not those lacking *Bmp10*. Consistent with these results, ET-1 levels were reduced in mice lacking *Bmp9*, but not mice lacking *Bmp10*, supporting previous results obtained by our group and others showing that the BMP9 pathway is involved in lung vascular tone through the modulation of central vasoactive factors.[5,26,48,49] RNA-seq analysis also showed modulation of the expression of genes involved in vasoreactivity, including *Edn1*. We previously reported that BMP9 can induce vasoconstriction in the CAM. Here, we confirmed and extended this notion by showing that such BMP9-induced vasoconstriction is abolished in the presence of bosentan, a dual endothelin receptor antagonist. These results reinforce the hypothesis of altered vasoconstriction in *Bmp9*-KO lung vessels, which could protect the mice from the development of PH and are consistent with the current therapeutic strategies that rely on vasodilators, such as bosentan.

Our data obtained in *Bmp9*-KO mice may appear to be at odds with human genetic data and have been extensively discussed,[50–52] but were confirmed here in the DKO mice. It should be kept in a mind that a limitation of mouse studies is that they develop mild PH with no plexiform lesions. Therefore it would be informative to confirm these findings in rat models of severe PH. BMPs signal through several heterocomplexes composed of type I and type II receptors, which can be modulated by accessory receptors and endogenous ligand traps. BMP signalling is thus complex and context-dependent and the low penetrance of most of the mutations that affect the BMPR-II pathway must be considered.[53] The recent discovery of *BMP9* and *BMP10* mutations in PAH patients further supports the involvement of this signalling pathway in the development of PAH, but the underlying mechanisms in humans are still unknown. Certain *BMP9* mutations have recently been associated with impaired processing and secretion and reduced activity in plasma, whereas others have no functional consequences.[54] Biochemical characterization for *BMP10* mutations has not been yet reported, but given the importance of *BMP10* in heart morphogenesis, these mutations could cause primary cardiac problems that increase the risk of developing PH. Indeed, one of the rare patients with a *BMP10* mutation presented with features of congenital heart disease.[55] Moreover, the relationship between BMP9 and BMP10 plasma levels and the risk of developing PAH is not clear and is yet to be clearly demonstrated.

Twenty years after the discovery of *BMPR2* mutations, there are still no clinically approved treatments for PAH that target BMP signalling. Our data suggest that although blocking BMP9 could be beneficial in PH, blocking BMP10 may have no effect on pulmonary vascular remodelling and could have detrimental effects on cardiac remodelling, and blocking both BMP9 and BMP10 over a long period of time might have adverse effects, such as excessive vasodilation, HOHF, and lung inflammation. Although we previously showed protective effects of the BMP9/BMP10 ligand trap ALK-1 ECD in rat models, this treatment was only administered for 2 weeks.[26] In accordance with our results, it was recently shown that long-term treatment with BMP9 induced aberrant endothelial to mesenchymal transition in PAH pulmonary endothelial cells due to exacerbated pro-inflammatory signalling.[56] Overall, these observations warrant caution for therapeutic strategies targeting this pathway in terms of specificity, dose, and length of treatment.

In conclusion, our data suggest redundant roles for BMP9 and BMP10 in cardiovascular homeostasis under normoxic conditions (as only the combined loss of both *Bmp9* and *Bmp10* led to reduced vascular resistance, reduced BP, cardiomegaly, and development of the HOHF phenotype) but also highlight specific roles under chronic hypoxic conditions. We obtained evidence that BMP9 contributes to chronic hypoxia-induced pulmonary vascular remodelling, whereas BMP10 plays a role in hypoxia-induced cardiac remodelling in mice.

## Supplementary material

Supplementary material is available at *Cardiovascular Research* online.

## Authors' contributions

Conception or design: C.B., L.T., C.G., and S.B.; drafting of the manuscript: C.B., C.G., and S.B.; conducted experiments and/or performed data analysis: all. All authors reviewed and revised the final version and approved submission of the manuscript.

## Acknowledgements

The authors thank Raphaël Thuillet, Mina Ottaviani, Mustapha Chelgham, Antoine Wawrzyniak, the CEA-Grenoble medical biology lab, and Matthieu Rolland for technical assistance and advice. The authors also thank Helen Arthur for sharing the protocol for arteriovenous shunt detection using fluorescent beads and Hervé Pointu, Soumalamaya Bama, Irène Jeannin, and Charlène Magallon for their help in the maintenance of our mouse colonies.

**Conflict of interest:** Over the last three years, C.G. reports grants from Acceleron and Janssen and grants and personal fees from Merck, outside the submitted work. M.H. and L.S. report grants, personal fees, and non-financial support from Actelion, Bayer, GlaxoSmithKline, and MSD outside of the submitted work. M.H. is a member of the Scientific Advisory Board of Morphogen-IX. All other authors have no conflicts of interest to disclose.

## Funding

This research was supported by grants from the French National Agency for Research (ANR), ANR-17-CE14-0006 (B9inPH) and ANR-15-IDEX-02 (IDEX-IRS2018 ANGIOBMP), and in part by the CEA (Commissariat à l'Energie Atomique et aux Energies Alternatives, DRF/IRIG/DS), the National Institute for Health and Medical Research (INSERM), the University of Grenoble and the University of Paris-Saclay, the Association Maladie de Rendu-Osler (AMRO/HHT-France), the Fondation pour la Recherche Médicale (EQU202003010188), and the H2020-msca-ITN-2018 (V.A.Cure-814316). The authors acknowledge the animal facility platform supported by GRAL, a programme of the Chemistry Biology Health (CBH) Graduate School of University Grenoble Alpes (ANR-17-EURE-0003). This work was partially performed by a laboratory member of the France Life Imaging network (grant ANR-11-INBS-0006). N.B. is a recipient of a PhD fellowship from the Ile-de-France region (ARDoc Health).

## Data availability

Datasets are available in the online supplement and have been deposited on the arrayexpress website https://www.ebi.ac.uk/arrayexpress/experiments/E-MTAB-10392/, last accessed date : June 7th 2021.

## References

1. Simonneau G, Montani D, Celermajer DS, Denton CP, Gatzoulis MA, Krowka M, Williams PG, Souza R. Haemodynamic definitions and updated clinical classification of pulmonary hypertension. *Eur Respir J* 2019;**53**:1801913.
2. Humbert M, Guignabert C, Bonnet S, Dorfmuller P, Klinger JR, Nicolls MR, Olschewski AJ, Pullamsetti SS, Schermuly RT, Stenmark KR, Rabinovitch M. Pathology and pathobiology of pulmonary hypertension: state of the art and research perspectives. *Eur Respir J* 2019;**53**:1801887.
3. Evans JD, Girerd B, Montani D, Wang XJ, Galie N, Austin ED, Elliott G, Asano K, Grunig E, Yan Y, Jing ZC, Manes A, Palazzini M, Wheeler LA, Nakayama I, Satoh T, Eichstaedt C, Hinderhofer K, Wolf M, Rosenzweig EB, Chung WK, Soubrier F, Simonneau G, Sitbon O, Graf S, Kaptoge S, Di Angelantonio E, Humbert M, Morrell NW. BMPR2 mutations and survival in pulmonary arterial hypertension: an individual participant data meta-analysis. *Lancet Respir Med* 2016;**4**:129–137.
4. Morrell NW, Aldred MA, Chung WK, Elliott CG, Nichols WC, Soubrier F, Trembath RC, Loyd JE. Genetics and genomics of pulmonary arterial hypertension. *Eur Respir J* 2019;**53**:1801899.
5. David L, Mallet C, Mazerbourg S, Feige JJ, Bailly S. Identification of BMP9 and BMP10 as functional activators of the orphan activin receptor-like kinase 1 (ALK1) in endothelial cells. *Blood* 2007;**109**:1953–1961.
6. Rhodes CJ, Batai K, Bleda M, Haimel M, Southgate L, Germain M, Pauciulo MW, Hadinnapola C, Aman J, Girerd B, Arora A, Knight J, Hanscombe KB, Karnes JH, Kaakinen M, Gall H, Ulrich A, Harbaum L, Cebola I, Ferrer J, Lutz K, Swietlik EM, Ahmad F, Amouyel P, Archer SL, Argula R, Austin ED, Badesch D, Bakshi S, Barnett C, Benza R, Bhatt N, Bogaard HJ, Burger CD, Chakinala M, Church C, Coghlan JG, Condliffe R, Corris PA, Danesino C, Debette S, Elliott CG, Elwing J, Eyries M, Fortin T, Franke A, Frantz RP, Frost A, Garcia JGN, Ghio S, Ghofrani HA, Gibbs JSR, Harley J, He H, Hill NS, Hirsch R, Houweling AC, Howard LS, Ivy D, Kiely DG, Klinger J, Kovacs G, Lahm T, Laudes M, Machado RD, MacKenzie Ross RV, Marsolo K, Martin LJ, Moledina S, Montani D, Nathan SD, Newnham M, Olschewski A, Olschewski H, Oudiz RJ, Ouwehand WH, Peacock AJ, Pepke-Zaba J, Rehman Z, Robbins I, Roden DM, Rosenzweig EB, Saydain G, Scelsi L, Schilz R, Seeger W, Shaffer CM, Simms RW, Simon M, Sitbon O, Suntharalingam J, Tang H, Tchourbanov AY, Thenappan T, Torres F, Toshner MR, Treacy CM, Vonk Noordegraaf A, Waisfisz Q, Walsworth AK, Walter RE, Wharton J, White RJ, Wilt J, Wort SJ, Yung D, Lawrie A, Humbert M, Soubrier F, Tregouet DA, Prokopenko I, Kittles R, Graf S, Nichols WC, Trembath RC, Desai AA, Morrell NW, Wilkins MR; UK NIHR BioResource Rare Diseases Consortium; UK PAH Cohort Study Consortium; US PAH Biobank Consortium. Genetic determinants of risk in pulmonary arterial hypertension: international genome-wide association studies and meta-analysis. *Lancet Respir Med* 2019;**7**:227–238.
7. Wang G, Fan R, Ji R, Zou W, Penny DJ, Varghese NP, Fan Y. Novel homozygous BMP9 nonsense mutation causes pulmonary arterial hypertension: a case report. *BMC Pulm Med* 2016;**16**:17.
8. Wang XJ, Lian TY, Jiang X, Liu SF, Li SQ, Jiang R, Wu WH, Ye J, Cheng CY, Du Y, Xu XQ, Wu Y, Peng FH, Sun K, Mao YM, Yu H, Liang C, Shyy JY, Zhang SY, Zhang X, Jing ZC. Germline BMP9 mutation causes idiopathic pulmonary arterial hypertension. *Eur Respir J* 2019;**53**:1801609.
9. Graf S, Haimel M, Bleda M, Hadinnapola C, Southgate L, Li W, Hodgson J, Liu B, Salmon RM, Southwood M, Machado RD, Martin JM, Treacy CM, Yates K, Daugherty LC, Shamardina O, Whitehorn D, Holden S, Aldred M, Bogaard HJ, Church C, Coghlan G, Condliffe R, Corris PA, Danesino C, Eyries M, Gall H, Ghio S, Ghofrani HA, Gibbs JSR, Girerd B, Houweling AC, Howard L, Humbert M, Kiely DG, Kovacs G, MacKenzie Ross RV, Moledina S, Montani D, Newnham M, Olschewski A, Olschewski H, Peacock AJ, Pepke-Zaba J, Prokopenko I, Rhodes CJ, Scelsi L, Seeger W, Soubrier F, Stein DF, Suntharalingam J, Swietlik EM, Toshner MR, van Heel DA, Vonk Noordegraaf A, Waisfisz Q, Wharton J, Wort SJ, Ouwehand WH, Soranzo N, Lawrie A, Upton PD, Wilkins MR, Trembath RC, Morrell NW. Identification of rare sequence variation underlying heritable pulmonary arterial hypertension. *Nat Commun* 2018;**9**:1416.
10. Johnson DW, Berg JN, Baldwin MA, Gallione CJ, Marondel I, Yoon SJ, Stenzel TT, Speer M, Pericak-Vance MA, Diamond A, Guttmacher AE, Jackson CE, Attisano L, Kucherlapati R, Porteous ME, Marchuk DA. Mutations in the activin receptor-like kinase 1 gene in hereditary haemorrhagic telangiectasia type 2. *Nat Genet* 1996;**13**:189–195.
11. McAllister KA, Grogg KM, Johnson DW, Gallione CJ, Baldwin MA, Jackson CE, Helmbold EA, Markel DS, McKinnon WC, Murrell J. Endoglin, a TGF-beta binding protein of endothelial cells, is the gene for hereditary haemorrhagic telangiectasia type 1. *Nat Genet* 1994;**8**:345–351.

12. Wooderchak-Donahue WL, McDonald J, O'Fallon B, Upton PD, Li W, Roman BL, Young S, Plant P, Fülöp GT, Langa C, Morrell NW, Botella LM, Bernabeu C, Stevenson DA, Runo JR, Bayrak-Toydemir P. BMP9 mutations cause a vascular-anomaly syndrome with phenotypic overlap with hereditary hemorrhagic telangiectasia. *Am J Hum Genet* 2013;**93**:530–537.
13. Tillet E, Bailly S. Emerging roles of BMP9 and BMP10 in hereditary hemorrhagic telangiectasia. *Front Genet* 2014;**5**:456.
14. Breitkopf-Heinlein K, Meyer C, König C, Gaitantzi H, Addante A, Thomas M, Wiercinska E, Cai C, Li Q, Wan F, Hellerbrand C, Valous NA, Hahnel M, Ehlting C, Bode JG, Müller-Bohl S, Klingmüller U, Altenöder J, Ilkavets I, Goumans M-J, Hawinkels LJAC, Lee S-J, Wieland M, Mogler C, Ebert MP, Herrera B, Augustin H, Sánchez A, Dooley S, Ten Dijke P. BMP-9 interferes with liver regeneration and promotes liver fibrosis. *Gut* 2017;**66**:939–954.
15. Tillet E, Ouarne M, Desroches-Castan A, Mallet C, Subileau M, Didier R, Lioutsko A, Belthier G, Feige JJ, Bailly S. A heterodimer formed by bone morphogenetic protein 9 (BMP9) and BMP10 provides most BMP biological activity in plasma. *J Biol Chem* 2018;**293**:10963–10974.
16. Neuhaus H, Rosen V, Thies RS. Heart specific expression of mouse BMP-10 a novel member of the TGF-beta superfamily. *Mech Dev* 1999;**80**:181–184.
17. Susan-Resiga D, Essalmani R, Hamelin J, Asselin MC, Benjannet S, Chamberland A, Day R, Szumska D, Constam D, Bhattacharya S, Prat A, Seidah NG. Furin is the major processing enzyme of the cardiac-specific growth factor bone morphogenetic protein 10. *J Biol Chem* 2011;**286**:22785–22794.
18. Jiang H, Salmon RM, Upton PD, Wei Z, Lawera A, Davenport AP, Morrell NW, Li W. The prodomain-bound form of bone morphogenetic protein 10 is biologically active on endothelial cells. *J Biol Chem* 2016;**291**:2954–2966.
19. David L, Mallet C, Keramidas M, Lamande N, Gasc JM, Dupuis-Girod S, Plauchu H, Feige JJ, Bailly S. Bone morphogenetic protein-9 is a circulating vascular quiescence factor. *Circ Res* 2008;**102**:914–922.
20. Chen H, Brady Ridgway J, Sai T, Lai J, Warming S, Chen H, Roose-Girma M, Zhang G, Shou W, Yan M. Context-dependent signaling defines roles of BMP9 and BMP10 in embryonic and postnatal development. *Proc Natl Acad Sci USA* 2013;**110**:11887–11892.
21. Townson SA, Martinez-Hackert E, Greppi C, Lowden P, Sako D, Liu J, Ucran JA, Liharska K, Underwood KW, Seehra J, Kumar R, Grinberg AV. Specificity and structure of a high affinity activin receptor-like kinase 1 (ALK1) signaling complex. *J Biol Chem* 2012;**287**:27313–27325.
22. Salmon RM, Guo J, Wood JH, Tong Z, Beech JS, Lawera A, Yu M, Grainger DJ, Reckless J, Morrell NW, Li W. Molecular basis of ALK1-mediated signalling by BMP9/BMP10 and their prodomain-bound forms. *Nat Commun* 2020;**11**:1621.
23. Ricard N, Ciais D, Levet S, Subileau M, Mallet C, Zimmers TA, Lee SJ, Bidart M, Feige JJ, Bailly S. BMP9 and BMP10 are critical for postnatal retinal vascular remodeling. *Blood* 2012;**119**:6162–6171.
24. Chen H, Shi S, Acosta L, Li W, Lu J, Bao S, Chen Z, Yang Z, Schneider MD, Chien KR, Conway SJ, Yoder MC, Haneline LS, Franco D, Shou W. BMP10 is essential for maintaining cardiac growth during murine cardiogenesis. *Development* 2004;**131**:2219–2231.
25. Levet S, Ouarne M, Ciais D, Coutton C, Subileau M, Mallet C, Ricard N, Bidart M, Debillon T, Faravelli F, Rooryck C, Feige JJ, Tillet E, Bailly S. BMP9 and BMP10 are necessary for proper closure of the ductus arteriosus. *Proc Natl Acad Sci USA* 2015;**112**:E3207–E3215.
26. Tu L, Desroches-Castan A, Mallet C, Guyon L, Cumont A, Phan C, Robert F, Thuillet R, Bordenave J, Sekine A, Huertas A, Ritvos O, Savale L, Feige J-J, Humbert M, Bailly S, Guignabert C. Selective BMP-9 inhibition partially protects against experimental pulmonary hypertension. *Circ Res* 2019;**124**:846–855.
27. Long L, Ormiston ML, Yang X, Southwood M, Graf S, Machado RD, Mueller M, Kinzel B, Yung LM, Wilkinson JM, Moore SD, Drake KM, Aldred MA, Yu PB, Upton PD, Morrell NW. Selective enhancement of endothelial BMPR-II with BMP9 reverses pulmonary arterial hypertension. *Nat Med* 2015;**21**:777–785.
28. Nikolic I, Yung LM, Yang P, Malhotra R, Paskin-Flerlage SD, Dinter T, Bocobo GA, Tumelty KE, Faugno AJ, Troncone L, McNeil ME, Huang X, Coser KR, Lai CSC, Upton PD, Goumans MJ, Zamanian RT, Elliott CG, Lee A, Zheng W, Berasi SP, Huard C, Morrell NW, Chung RT, Channick RW, Roberts KE, Yu PB. Bone morphogenetic protein 9 is a mechanistic biomarker of portopulmonary hypertension. *Am J Respir Crit Care Med* 2019;**199**:891–902.
29. Ouarne M, Bouvard C, Boneva G, Mallet C, Ribeiro J, Desroches-Castan A, Soleilhac E, Tillet E, Peyruchaud O, Bailly S. BMP9, but not BMP10, acts as a quiescence factor on tumor growth, vessel normalization and metastasis in a mouse model of breast cancer. *J Exp Clin Cancer Res* 2018;**37**:209.
30. Desroches-Castan A, Tillet E, Ricard N, Ouarne M, Mallet C, Belmudes L, Coute Y, Boillot O, Scoazec JY, Bailly S, Feige JJ. Bone morphogenetic protein 9 is a paracrine factor controlling liver sinusoidal endothelial cell fenestration and protecting against hepatic fibrosis. *Hepatology* 2019;**70**:1392–1408.
31. Mehta PA, Dubrey SW. High output heart failure. *QJM* 2009;**102**:235–241.
32. Ola R, Dubrac A, Han J, Zhang F, Fang JS, Larrivee B, Lee M, Urarte AA, Kraehling JR, Genet G, Hirschi KK, Sessa WC, Canals FV, Graupera M, Yan M, Young LH, Oh PS, Eichmann A. PI3 kinase inhibition improves vascular malformations in mouse models of hereditary haemorrhagic telangiectasia. *Nat Commun* 2016;**7**:13650.
33. Sun L, Yu J, Qi S, Hao Y, Liu Y, Li Z. Bone morphogenetic protein-10 induces cardiomyocyte proliferation and improves cardiac function after myocardial infarction. *J Cell Biochem* 2014;**115**:1868–1876.
34. Newman AM, Steen CB, Liu CL, Gentles AJ, Chaudhuri AA, Scherer F, Khodadoust MS, Esfahani MS, Luca BA, Steiner D, Diehn M, Alizadeh AA. Determining cell type abundance and expression from bulk tissues with digital cytometry. *Nat Biotechnol* 2019;**37**:773–782.
35. Travaglini KJ, Nabhan AN, Penland L, Sinha R, Gillich A, Sit RV, Chang S, Conley SD, Mori Y, Seita J, Berry GJ, Shrager JB, Metzger RJ, Kuo CS, Neff N, Weissman IL, Quake SR, Krasnow MA. A molecular cell atlas of the human lung from single-cell RNA sequencing. *Nature* 2020;**587**:619–625.
36. Tamura Y, Phan C, Tu L, Le Hiress M, Thuillet R, Jutant EM, Fadel E, Savale L, Huertas A, Humbert M, Guignabert C. Ectopic upregulation of membrane-bound IL6R drives vascular remodeling in pulmonary arterial hypertension. *J Clin Invest* 2018;**128**:1956–1970.
37. Garcia de Vinuesa A, Abdelilah-Seyfried S, Knaus P, Zwijsen A, Bailly S. BMP signaling in vascular biology and dysfunction. *Cytokine Growth Factor Rev* 2016;**27**:65–79.
38. Oh SP, Seki T, Goss KA, Imamura T, Yi Y, Donahoe PK, Li L, Miyazono K, ten Dijke P, Kim S, Li E. Activin receptor-like kinase 1 modulates transforming growth factor-beta 1 signaling in the regulation of angiogenesis. *Proc Natl Acad Sci USA* 2000;**97**:2626–2631.
39. Kalucka J, de Rooij L, Goveia J, Rohlenova K, Dumas SJ, Meta E, Conchinha NV, Taverna F, Teuwen LA, Veys K, Garcia-Caballero M, Khan S, Geldhof V, Sokol L, Chen R, Treps L, Borri M, de Zeeuw P, Dubois C, Karakach TK, Falkenberg KD, Parys M, Yin X, Vinckier S, Du Y, Fenton RA, Schoonjans L, Dewerchin M, Eelen G, Thienpont B, Lin L, Bolund L, Li X, Luo Y, Carmeliet P. Single-cell transcriptome atlas of murine endothelial cells. *Cell* 2020;**180**:764–779 e720.
40. Wang L, Rice M, Swist S, Kubin T, Wu F, Wang S, Kraut S, Weissmann N, Bottger T, Wheeler M, Schneider A, Braun T. BMP9 and BMP10 act directly on vascular smooth muscle cells for generation and maintenance of the contractile state. *Circulation* 2021;**143**:1394–1410.
41. Tual-Chalot S, Garcia-Collado M, Redgrave RE, Singh E, Davison B, Park C, Lin H, Luli S, Jin Y, Wang Y, Lawrie A, Jakobsson L, Arthur HM. Loss of endothelial endoglin promotes high-output heart failure through peripheral arteriovenous shunting driven by VEGF signaling. *Circ Res* 2020;**126**:243–257.
42. Park SO, Wankhede M, Lee YJ, Choi EJ, Fliess N, Choe SW, Oh SH, Walter G, Raizada MK, Sorg BS, Oh SP. Real-time imaging of de novo arteriovenous malformation in a mouse model of hereditary hemorrhagic telangiectasia. *J Clin Invest* 2009;**119**:3487–3496.
43. Morine KJ, Qiao X, Paruchuri V, Aronovitz MJ, Mackey EE, Buiten L, Levine J, Ughreja K, Nepali P, Blanton RM, Karas RH, Oh SP, Kapur NK. Conditional knockout of activin like kinase-1 (ALK-1) leads to heart failure without maladaptive remodeling. *Heart Vessels* 2017;**32**:628–636.
44. Upton PD, Park JES, De Souza PM, Davies RJ, Griffiths MJD, Wort SJ, Morrell NW. Endothelial protective factors BMP9 and BMP10 inhibit CCL2 release by human vascular endothelial cells. *J Cell Sci* 2020;**133**:jcs239715.
45. Capasso TL, Li B, Volek HJ, Khalid W, Rochon ER, Anbalagan A, Herdman C, Yost HJ, Villanueva FS, Kim K, Roman BL. BMP10-mediated ALK1 signaling is continuously required for vascular development and maintenance. *Angiogenesis* 2020;**23**:203–220.
46. Laux DW, Young S, Donovan JP, Mansfield CJ, Upton PD, Roman BL. Circulating Bmp10 acts through endothelial Alk1 to mediate flow-dependent arterial quiescence. *Development* 2013;**140**:3403–3412.
47. Wang J, Xu N, Feng X, Hou N, Zhang J, Cheng X, Chen Y, Zhang Y, Yang X. Targeted disruption of Smad4 in cardiomyocytes results in cardiac hypertrophy and heart failure. *Circ Res* 2005;**97**:821–828.
48. Star GP, Giovinazzo M, Langleben D. Bone morphogenic protein-9 stimulates endothelin-1 release from human pulmonary microvascular endothelial cells: a potential mechanism for elevated ET-1 levels in pulmonary arterial hypertension. *Microvasc Res* 2010;**80**:349–354.
49. Park JE, Shao D, Upton PD, Desouza P, Adcock IM, Davies RJ, Morrell NW, Griffiths MJ, Wort SJ. BMP-9 induced endothelial cell tubule formation and inhibition of migration involves Smad1 driven endothelin-1 production. *PLoS One* 2012;**7**:e30075.
50. Morrell NW, Upton PD, Li W, Yu PB. Letter by Morrell et al. regarding article, "Selective BMP-9 inhibition partially protects against experimental pulmonary hypertension". *Circ Res* 2019;**124**:e81.
51. Guignabert C, Tu L, Feige JJ, Humbert M, Bailly S. Response by Guignabert et al. to letter regarding article, "Selective BMP-9 inhibition partially protects against experimental pulmonary hypertension". *Circ Res* 2019;**124**:e82–e83.
52. Ormiston ML, Godoy RS, Chaudhary KR, Stewart DJ. The janus faces of bone morphogenetic protein 9 in pulmonary arterial hypertension. *Circ Res* 2019;**124**:822–824.
53. Larkin EK, Newman JH, Austin ED, Hemnes AR, Wheeler L, Robbins IM, West JD, Phillips JA 3rd, Hamid R, Loyd JE. Longitudinal analysis casts doubt on the presence of genetic anticipation in heritable pulmonary arterial hypertension. *Am J Respir Crit Care Med* 2012;**186**:892–896.

54. Hodgson J, Swietlik EM, Salmon RM, Hadinnapola C, Nikolic I, Wharton J, Guo J, Liley J, Haimel M, Bleda M, Southgate L, Machado RD, Martin JM, Treacy CM, Yates K, Daugherty LC, Shamardina O, Whitehorn D, Holden S, Bogaard HJ, Church C, Coghlan G, Condliffe R, Corris PA, Danesino C, Eyries M, Gall H, Ghio S, Ghofrani H-A, Gibbs JSR, Girerd B, Houweling AC, Howard L, Humbert M, Kiely DG, Kovacs G, Lawrie A, MacKenzie Ross RV, Moledina S, Montani D, Olschewski A, Olschewski H, Ouwehand WH, Peacock AJ, Pepke-Zaba J, Prokopenko I, Rhodes CJ, Scelsi L, Seeger W, Soubrier F, Suntharalingam J, Toshner MR, Trembath RC, Vonk Noordegraaf A, Wort SJ, Wilkins MR, Yu PB, Li W, Gräf S, Upton PD, Morrell NW. Characterization of GDF2 mutations and levels of BMP9 and BMP10 in pulmonary arterial hypertension. *Am J Respir Crit Care Med* 2020;**201**:575–585.
55. Eyries M, Montani D, Nadaud S, Girerd B, Levy M, Bourdin A, Tresorier R, Chaouat A, Cottin V, Sanfiorenzo C, Prevot G, Reynaud-Gaubert M, Dromer C, Houeijeh A, Nguyen K, Coulet F, Bonnet D, Humbert M, Soubrier F. Widening the landscape of heritable pulmonary hypertension mutations in paediatric and adult cases. *Eur Respir J* 2019;**53**:1801371.
56. Szulcek R, Sanchez-Duffhues G, Rol N, Pan X, Tsonaka R, Dickhoff C, Yung LM, Manz XD, Kurakula K, Kiełbasa SM, Mei H, Timens W, Yu PB, Bogaard H-J, Goumans M-J. Exacerbated inflammatory signaling underlies aberrant response to BMP9 in pulmonary arterial hypertension lung endothelial cells. *Angiogenesis* 2020;**23**:699–714.

## Translational perspective

Twenty years after the discovery of *BMPR2* mutations, there are still no clinically approved treatments for pulmonary arterial hypertension (PAH) that target BMP signalling. Our data suggest, using *Bmp9* and *Bmp10* single and double-knockout mice, that although blocking BMP9 could be beneficial in pulmonary hypertension, blocking BMP10 may have no effect on pulmonary vascular remodelling and could have detrimental effects on cardiac remodelling. Overall, these observations warrant caution for therapeutic strategies targeting this pathway and support that further studies are needed to understand how this complex pathway is involved in maintaining cardiovascular homeostasis in health and contributes to PAH and hereditary haemorrhagic telangiectasia (HHT).

# SUPPLEMENTAL MATERIALS

## MATERIALS & METHODS

### Blood pressure measurements and echocardiographic assessment of left ventricular function

Systemic blood pressure (BP) was blindly determined in conscious mice by a non-invasive computerized tail-cuff method (CODA Kent Scientific) according to the manufacturer's instructions. For echocardiography, mice were anesthetized under gaseous anaesthesia (isoflurane-Vetflurane, Virbac 1.8-2% in a 1:1 mixture of oxygen:air). Hairs of the thoracic area were removed (hair-removing cream for sensitive skin), and the animal was positioned on a heating platform linked to the echography system (Vevo® 2100, VisualSonics) allowing the registration of ECG and respiratory rate. MS-550D (40 MHz) transducer was used for image acquisition; this transducer is specifically dedicated to mouse cardiac imaging (VisualSonics). Standard parameters were obtained using M-mode on "small-axis" views (SAX) and "long-axis" views. Parameters allowed the calculation of thickness of cardiac walls, ventricular volumes (during systole and diastole), estimated left ventricle mass, ejection fraction, fractional shortening, cardiac output and stroke volume.

### Invasive right heart catheterization and assessment of pulmonary vascular changes

Mice were randomized and either studied in room air at 8-14 weeks of age, or were exposed to hypoxia ($FiO_2$=10%) for 3 weeks. At the end of these protocols, hemodynamic parameters were blindly measured in unventilated anesthetized mice (isoflurane) using a closed chest technique, by introducing a 1.4-F Millar catheter (ADInstruments, Paris, France) into the jugular vein and directing it to the right ventricle (RV) to assess the right ventricular systolic pressure (RVSP) [1-3]. Euthanasia was performed by exsanguination under isoflurane. The RV hypertrophy was calculated using the Fulton Index [weight ratio of right ventricle and (left ventricle + septum)] and the percentage of wall thickness [(2 × medial wall thickness/ external diameter) × 100] and of muscularized vessels were performed as previously described [3, 4]. The pulmonary circulation was flushed with 5mL of buffered saline at 37°C, and then the left lung was prepared for histological analyses and the right lung was quickly harvested, immediately snap-frozen in liquid nitrogen and kept at -80°C.

### Microvessel perfusion

Fluorescent 45 µm microspheres (Polysciences, Inc) were injected into the left cardiac ventricle of anesthetized (isoflurane) to investigate left to right shunting (systemic arteriovenous shunts), or 15 µm microspheres (Life technologies) were injected intravenously to investigate pulmonary shunts in mice as previously described [5], Euthanasia was performed using an injection of pentobarbital 180 mg/kg, mice were dissected and fluorescent beads trapped in the tissue vasculature were examined using a Zeiss Axiobserver microscope.

Another group of animals was used to visualize the vasculature following perfusion with latex blue. Briefly, mice received a pentobarbital intraperitoneal injection (180 mg/kg). Abdominal and thoracic cavities were open, left and right atria were cut, the left ventricle was punctured with a 26-gauge needle, and a blue latex dye (Connecticut Valley Biological Supply Co.) was slowly and steadily injected. The vasculature was observed and organs of

interest were collected, rinsed in PBS and fixed with 10% formalin overnight at 4°C. Tissue clearing procedure was performed to enhance sample transparency and maximize delineation of the vascular casts using urea/Quadrol/Triton X-100 and triethanolamine/urea/sucrose solutions. Images were acquired using a Leica S8APO stereomicroscope.

**RNA sequencing and real-time quantitative-PCR**

Mouse lung tissue was flash frozen in liquid nitrogen and stored at -80°C. RNA extraction, RNA sample quality assessment, RNA library preparation, sequencing and raw data analysis were conducted at GENEWIZ, Inc. (South Plainfield, NJ, USA).

Total RNA was extracted from frozen tissue using the Qiagen RNeasy Plus Mini kit. RNA samples were quantified using Qubit 2.0 Fluorometer (Life Technologies, Carlsbad, CA, USA) and RNA integrity was checked with Agilent TapeStation (Agilent Technologies, Palo Alto, CA, USA).

rRNA depletion was performed using Ribozero rRNA Removal Kit (Illumina, San Diego, CA, USA). RNA sequencing library preparation used NEBNext Ultra RNA Library Prep Kit for Illumina by following the manufacturer's recommendations (NEB, Ipswich, MA, USA). Briefly, enriched RNAs were fragmented for 15 minutes at 94 °C. First strand and second strand cDNA were subsequently synthesized. cDNA fragments were end repaired and adenylated at 3'ends, and universal adapter was ligated to cDNA fragments, followed by index addition and library enrichment with limited cycle PCR. Sequencing libraries were validated using the Agilent Tapestation 4200 (Agilent Technologies, Palo Alto, CA, USA), and quantified by using Qubit 2.0 Fluorometer (Invitrogen, Carlsbad, CA) as well as by quantitative PCR (Applied Biosystems, Carlsbad, CA, USA).

The sequencing libraries were clustered on one lane of a flowcell. After clustering, the flowcell was loaded on the Illumina HiSeq 4000 instrument (or equivalent) according to manufacturer's instructions. The samples were sequenced using a 2x150 Paired End (PE) configuration. Image analysis and base calling were conducted by the HiSeq Control Software (HCS). Raw sequence data (.bcl files) generated from Illumina HiSeq was converted into fastq files and de-multiplexed using Illumina's bcl2fastq 2.17 software. One mis-match was allowed for index sequence identification.

After investigating the quality of the raw data, sequence reads were trimmed to remove possible adapter sequences and nucleotides with poor quality using Trimmomatic v.0.36. The trimmed reads were mapped to the the Mus musculus GRCm38 reference genome available on ENSEMBL using the STAR aligner v.2.5.2b. Gene counts were calculated from uniquely mapped reads using feature Counts from the Subread package v.1.5.2. Only unique reads that fell within exon regions were counted.

The gene hit counts table was then used for downstream differential expression analysis. A differential gene expression analysis between WT and DKO groups of samples was performed using the R-package DESeq2 (Wald test). Genes with adjusted p-values < 0.05 and absolute log2 fold changes > log2(1.5) were called as differentially expressed genes (DEG). A bi-clustering heatmap was used to visualize the expression profile of the top 40 differentially expressed genes with the lowest adjusted p-value by plotting their log2 transformed expression values in samples using the R-package pheatmap. A gene ontology analysis was performed on the statistically significant set of genes using DAVID functional annotation tool (https://david.ncifcrf.gov/summary.jsp). Gene Set Enrichment Analysis (GSEA) was performed on the full list of genes ranked by log2 fold change using the WEB-

based Gene SeT AnaLysis Toolkit (http://www.webgestalt.org/) with the functional database geneontology / Biological Process noRedundant.

We performed estimations of cell type abundances from our bulk lung transcriptomes using the method Cibertsortx [6]. To accomplish this, we used single-cell reference transcriptome profiles collected from mice lungs (Travaglini et al [7] ). We filtered from these single-cell data the cell types identified by less than 40 cells, and generated a signature matrix composed of 10,000 cells sampled from the remaining cell types. This signature matrix was then used by Cibersortx, with S-mode batch correction, to predict cell type factions from our bulk lung transcriptomes. The heatmap showing cell type abundances per sample was produced with the pheamap function in R.

Level of lung mRNA level encoding endothelin-1 were measured by qRT-PCR according to the method previously described [3]. To assess the mRNA level of other genes, mRNA was extracted using an RNeasy kit (Macherey, Nagel), reverse transcription was performed using iScript kit from Biorad and quantitative PCR was performed using SsoAdvanced SYBR green kit from Biorad. The Delta-Delta Ct (**ΔΔ**Ct) method was used to obtain relative expression levels, normalized to *Rpl13a* levels. Primer sequences can be found in table S5.

**Blood analysis, Western Blot, histology, and immunostaining**

Whole blood or plasma was collected from 5-month-old mice. The total volume of blood collected via cardiac puncture was measured using a 2.5 mL graduated syringe. EDTA whole blood was analyzed using an XNL 550 automated hematology analyzer (Sysmex). Li-heparin plasma (collected after 4 hours of fasting) was analyzed using AU-480 automated clinical chemistry analyzer (Beckman Coulter). Concentrations of atrial natriuretic peptide (ANP), brain natriuretic peptide (BNP), endothelin (ET)-1 and of hyaluronic acid (HA) in plasma were evaluated using specific ELISA Kits from Ray Biotech for ANP and BNP and from R&D for all the others, according to the manufacturer instructions. ELISA for BMP9, BMP10 or for the heterodimer BMP9-BMP10 were performed as previously described [8].

Tissues were homogenized and sonicated in RIPA buffer containing protease and phosphatase inhibitors and 30 µg of protein was used to detect pSmad 1/5/8 (1/500, 13820 Cell Signaling), pSmad2/3 (1/200, 8828 Cell Signaling), and β-actin (1/400, A3854 Sigma).

Hematoxylin-Eosin (H&E; Sigma), Picrosirius red (Sigma) or Prussian blue (Merck) staining of the heart, lung, liver, spleen, and kidney tissues were performed using routine procedures. Images were acquired using Zeiss Axioplan or Axioscan microscopes and analyzed using Zen, Axiovision or Image J softwares. Cardiomyocyte size was determined by measuring the cross-sectional area of 100 cardiomyocytes in the left ventricular wall. Briefly, transverse heart sections (40-µm thickness) were blocked with PBS 3% BSA, stained with fluorescein conjugated Wheat Germ Agglutinin (WGA) (5 µg/mL, W834 Invitrogen) in PBS 1% BSA and with Hoechst (1/1000, 33342 Sigma) for nuclear counterstaining. Images were acquired with a Zeiss ApoTome microscope (objective x40) and analyzed using Zen software (Zeiss). Diameters of pulmonary capillary vessels were determined in semi-thin lung sections (500-nm thickness) stained with epoxy tissue stain (EMS). Briefly, 1-2 $mm^3$ pieces of lung tissue were fixed overnight in 2% glutaraldehyde at 4°C, post-fixed in Osmium buffer, dehydrated and embedded in epoxy resin (EMS). Sections were then stained and images were acquired using a Zeiss axiovision microscope and analyzed using Image J software.

Immunohistochemistry staining for alpha-smooth muscle actin (α-SM actin) were performed as previously described [3]. Briefly, lung sections (4-µm thickness) were deparaffined and stained with (HE), or incubated with

retrieval buffer. Then, sections were saturated with blocking buffer and incubated overnight with α-SM actin antibodies (1:200, sc32251, Santa Cruz), followed by corresponding secondary fluorescent-labeled antibodies (Thermo Fisher Scientific). Nuclei were labelled using DAPI (Thermo Fisher Scientific). Mounting was performed using ProLong Gold antifade reagent (Thermo Fisher Scientific). All images were taken using a LSM700 confocal microscope (Zeiss, Marly-le-Roi, France).

**Chick Chorioallantoic Membrane (CAM) assay**

Fertilized Gallus gallus (Chicken) eggs were incubated at 37°C in a 65% humidified environment. They were rotated during 3 days (25° every 4h). On day 3, a window was created in the eggshell and sealed with medical tape. On day 10, a plastic ring (made from Nunc Thermanox coverslips) was placed on the surface of the CAM in each egg and received 50 µL of control vehicle (PBS BSA 0.1% DMSO 0.5%) or treatment solution containing 50 or 500 µM of Bosentan (R&D), 50 or 500 µM of Captopril (Tocris) or 0.5, 50 or 500 µM of Terguride (Abcam) in association with 20 nM of BMP9 (R&D) or not. The CAM was observed and imaged under a macroscope (AZ-100 multizoom, Nikon) after 4h and 24h of treatment. After 24h of treatment, 100 µL of FITC-Dextran solution was injected into the CAM vessels. Fluorescence images were taken using the 2X objective of the macroscope and automated quantification of the area of FITC positive vessels within the rings was performed using Angiotool software.

## SUPPLEMENTARY FIGURE LEGENDS

Figure S1: BMP9, BMP10 and BMP9-BMP10 heterodimer concentration in mouse plasma measured by ELISA (n=8-10 mice/group). (**a**) *Bmp9* and *Bmp10* mRNA levels in liver (**b**) heart (right atria) (**c**) and lungs (**d**), normalized to *Rpl13a*. Data are presented as mean ± SEM of n=8-10 male mice per group and analyzed using a Kruskal Wallis test followed by a Dunn's test. *p<0.05, **p<0.01, ***p<0.001, ****p<0.0001 vs WT

Figure S2: Combined loss of *Bmp9* and *Bmp10* leads to cardiomegaly and splenomegaly for both male and female mice. Body weight, femur length and weight of the heart, liver, kidney and spleen of male (**a**) and female (**b**) mice. All mice were injected with tamoxifen at the age of 2 months and sacrificed at the age of 5 months. Data are presented as mean ± SEM of n=9-11 mice/group and analyzed using a Kruskall Wallis test followed by a Dunn's test. **p<0.01, ****p<0.0001 vs WT. #p<0.05; ##p<0.01, ###p<0.001 vs Bmp9-KO. $p<0.05; $$p<0.01 vs Bmp10-cKO.

Figure S3: Weight of the right ventricle (RV) (**a**) or left ventricle + septum (LV+S) (**b**) from WT and DKO mice (n=6-7/group). Data are presented as mean ± SEM and analyzed using a Mann-Whitney test. **p<0.01 vs WT. Representative photomicrographs of spleen sections stained with hematoxylin and eosin, scale bar 500 µm (**c**) and of liver sections stained with Picrosirius red, scale bar 100 µm (**d**). Quantitative analysis of the percentage area of liver sections stained in red (**e**). Plasma concentration of hyaluronic acid (HA) determined by ELISA (**f**). All mice were injected with tamoxifen at the age of 2 months and sacrificed at the age of 5 months. Data are presented as mean ± SEM of n=4-8 mice/group and analyzed using a Kruskal Wallis test followed by a Dunn's test. *p<0.05 vs WT. .#p<0.05 vs Bmp9-KO.

Figure S4: Relative mRNA levels of *Acvrl1, Eng, Bmpr2, Id1, Smad6,* in lung (**a**), liver (**b**) right atria (**c**) and left ventricle (**d**), normalized to *Rpl13a*. Representative western blots and quantitative analysis of pSmad1/5/8 and pSmad2/3 protein level in lung tissue, normalized to β-actin levels (**e**) Data are presented as mean ± SEM of n=6-10 male mice per group and analyzed using a Kruskal Wallis test followed by a Dunn's test. *p<0.05, **p<0.01, ****p<0.0001 vs WT

Figure S5: No obvious signs of cardiac fibrosis were observed after deletion of *Bmp9* and/or *Bmp10*. Heart sections stained with Picrosirius red represented as a mosaic of photomicrographs to show the entire section, scale bar 200 µm (**a**) or single photomicrographs, scale bar 100 µm (**b**). Mice were injected with tamoxifen at the age of 2 months and sacrificed at the age of 4 months. n=4/group

Figure S6: Representative photomicrographs of clarified intestines (**a**) and brains (**b**) from latex blue WT and DKO injected mice (n=4-6/group). Extracted blood volume of WT, Bmp9-KO, Bmp10-cKO and DKO mice (n=11-14 mice/group) (**c**). Data are presented as mean ± SEM and analyzed using a Kruskal Wallis test followed by a Dunn's test. **p<0.01 vs WT, #p<0.05 vs Bmp9-KO. $$p<0.01 vs Bmp10-cKO (**c**). Representative photomicrographs of the thyroid gland (**d**) of WT and DKO mice (n=8/group). All mice were injected with tamoxifen at the age of 2 months and sacrificed at the age of 4-5 months. Scale bar 1mm.

Figure S7: RNAseq analysis was performed on lung tissue from n=5 WT and n=7 DKO mice that were injected with tamoxifen at the age of 2 months and sacrificed at the age of 5 months. Genes with adjusted p-values < 0.05 and absolute log2 fold changes > log2(1.5) were called as differentially expressed genes (DEG). A gene ontology analysis was performed on these DEG using DAVID functional annotation tool (https://david.ncifcrf.gov/summary.jsp). Enriched gene ontologies sorted by modified Fisher Exact p-value (EASE score) were plotted, each data point in the dot plot represents a gene ontology, the -log10 p-value is on the x-axis, the size of the dot represents the number of DEG and the color scale the percentage of DEG involved in the gene ontology term.

Figure S8: Relative mRNA levels (normalized to *Rpl13a*) of *Ccl2, Ccl3, Cxcl5* from lung (**a**) and of *Tbx20, Nkx2-5* from left ventricle (**b**). Data are presented as mean ± SEM of n=6-10 male mice per group and analyzed using a Kruskal Wallis test followed by a Dunn's test. *p<0.05, **p<0.01 vs WT

Heatmap of predicted percentages of the different cell types in lungs from WT and DKO mice (n=5 WT and n=7 DKO mice per group) obtained using Cibersortx tool (**c**). Cell type abundances that were significantly different in DKO vs WT mice were visualized using bar plots (**d**). Data are presented as mean ± SEM and analyzed using a Mann-Whitney test *p<0.05, **p<0.01 vs WT.

Figure S9: Representative photomicrographs and quantitative analysis of FITC-Dextran injected blood vessels from chick chorioallantoic membranes treated with captopril (Capt) at 0, 50 and 500 µM, or terguride (Ter) at 0.5, 50 and 500 µM in combination with BMP9 (20 nM) or not for 24 hours. Scale bar 250 µm. For captopril treated eggs, data are presented as mean ± SEM of n=3-4 eggs/condition and analyzed using a Mann Whitney test. *p<0.05 vs captopril treated condition without BMP9. For terguride treated eggs automated quantitative analysis was not possible for several eggs due to high background and mortality at 24h, therefore no statistical analysis was performed.

205 **SUPPLEMENTARY TABLES**

206

207 Table S1: Clinical chemistry and metabolic exploration. Biochemical analysis of plasma from n=6 WT, n=8 *Bmp9*-
208 KO, n=5 *Bmp10*-cKO and n=7 DKO mice. All mice were injected with tamoxifen at the age of 2 months and blood
209 was collected at the age of 5 months. LDH = lactate dehydrogenase, AST = aspartate aminotransferase, ALT =
210 alanine aminotransferase.

211

| | | **WT** | | ***Bmp9*-KO** | | ***Bmp10*-cKO** | | **DKO** | |
|---|---|---|---|---|---|---|---|---|---|
| | | **MEAN** | SEM | **MEAN** | SEM | **MEAN** | SEM | **MEAN** | SEM |
| **Glucose** | **mmol/l** | **16.68** | 1.53 | **15.04** | 1.32 | **17.00** | 0.64 | **12.23** | 1.37 |
| **Urea** | **mmol/l** | **7.37** | 0.40 | **6.61** | 0.40 | **7.18** | 0.38 | **7.01** | 0.40 |
| **Sodium** | **mmol/l** | **152.17** | 0.60 | **150.63** | 0.65 | **149.80** | 0.20 | **152.43** | 0.84 |
| **Potassium** | **mmol/l** | **4.57** | 0.19 | **5.29** | 0.39 | **4.38** | 0.20 | **4.99** | 0.31 |
| **Chloride** | **mmol/l** | **113.00** | 0.93 | **113.88** | 0.58 | **112.60** | 0.68 | **115.43** | 1.27 |
| **Total proteins** | **g/l** | **49.33** | 0.84 | **48.88** | 0.74 | **48.60** | 0.60 | **46.71** | 1.15 |
| **Albumin** | **g/l** | **27.33** | 0.49 | **27.13** | 0.69 | **27.20** | 0.20 | **25.29** | 0.92 |
| **Calcium** | **mmol/l** | **2.18** | 0.01 | **2.15** | 0.01 | **2.14** | 0.02 | **2.12** | 0.02 |
| **Phosphorus** | **mmol/l** | **2.14** | 0.10 | **2.03** | 0.13 | **1.95** | 0.10 | **2.51** | 0.19 |
| **Total bilirubin** | **µmol/l** | **3.18** | 0.88 | **4.11** | 1.25 | **2.16** | 0.23 | **3.44** | 1.02 |
| **Creatine kinase** | **U/l** | **159.33** | 70.35 | **162.00** | 122.83 | **155.40** | 25.42 | **104.86** | 22.22 |
| **LDH** | **U/l** | **683.17** | 209.29 | **569.71** | 132.23 | **465.80** | 113.35 | **637.29** | 108.10 |
| **AST** | **U/l** | **99.83** | 21.77 | **89.86** | 19.38 | **101.60** | 9.42 | **90.71** | 13.58 |
| **ALT** | **U/l** | **46.00** | 15.74 | **23.71** | 5.63 | **44.20** | 7.30 | **18.86** | 5.29 |
| **ALP** | **U/l** | **61.33** | 3.96 | **66.88** | 7.73 | **51.80** | 3.62 | **53.71** | 3.98 |
| **Total cholesterol** | **mmol/l** | **3.10** | 0.31 | **2.61** | 0.24 | **3.09** | 0.15 | **2.48** | 0.18 |
| **Triglyceride** | **mmol/l** | **0.60** | 0.06 | **0.48** | 0.03 | **0.57** | 0.06 | **0.46** | 0.04 |
| **Creatinine** | **µmol/l** | **8.33** | 0.49 | **9.00** | 1.48 | **7.40** | 0.51 | **7.86** | 0.34 |

212

213

214

215

216

Table S2: Hematological analysis. All mice were injected with tamoxifen at the age of 2 months and blood was collected at the age of 5 months (n=5 WT, n=6 *Bmp9*-KO, n=5 *Bmp10*-cKO and n=7 DKO mice). WBC = white blood cells, RBC = red blood cells, HGB = hemoglobin, HCT = hematocrit, MCV = mean corpuscular volume, MCH = mean corpuscular hemoglobin, MCHC = mean corpuscular hemoglobin concentration, PLT = platelets, MPV = mean platelet volume

| | | **WT** | | ***Bmp9*-KO** | | ***Bmp10*-KO** | | **DKO** | |
|---|---|---|---|---|---|---|---|---|---|
| | | **MEAN** | SEM | **MEAN** | SEM | **MEAN** | SEM | **MEAN** | SEM |
| **WBC** | $x10^3$ cells/µL | **15.70** | 0.96 | **16.59** | 1.58 | **16.34** | 1.32 | **15.35** | 1.27 |
| **RBC** | $x10^6$ cells/µL | **10.67** | 0.40 | **9.09** | 0.26 | **10.76** | 0.18 | **9.04** | 0.29 |
| **HGB** | g/dL | **15.36** | 0.45 | **13.33** | 0.32 | **15.48** | 0.32 | **13.63** | 0.54 |
| **HCT** | % | **50.38** | 1.42 | **44.53** | 1.12 | **51.42** | 1.06 | **45.00** | 1.53 |
| **MCV** | fL | **47.26** | 0.52 | **49.02** | 0.76 | **47.78** | 0.31 | **49.77** | 0.77 |
| **MCH** | pg | **14.42** | 0.13 | **14.68** | 0.19 | **14.38** | 0.07 | **15.06** | 0.31 |
| **MCHC** | g/dL | **30.46** | 0.11 | **29.63** | 0.39 | **30.10** | 0.10 | **30.24** | 0.22 |
| **PLT** | $x10^3$ cells/µL | **826.40** | 62.84 | **711.00** | 92.20 | **748.25** | 43.47 | **534.14** | 75.61 |
| **MPV** | fL | **6.66** | 0.05 | **6.78** | 0.09 | **6.70** | 0.05 | **6.84** | 0.07 |

Table S3: Selection of enriched gene ontology terms and associated differentially expressed genes represented in figure S7

| GO number | GO term | Count | % | PValue | DEG |
|---|---|---|---|---|---|
| GO:0006954 | inflammatory response | 34 | 6.75 | 1.06E-12 | CXCL1, C3AR1, CCL3, CXCL5, TNFRSF26, CXCL3, CCR1, PTGS1, CXCL2, CCL9, FPR1, CCL8, MMP25, CCL6, SLC11A1, CHIL4, CCL22, NAIP2, CHIL1, CCL20, CHIL3, ZC3H12A, SPP1, LIPA, OLR1, TLR13, CHST4, CCL17, PRKCQ, TNFRSF9, PLA2G7, TRP73, CLEC7A, BMPR1B |
| GO:0007155 | cell adhesion | 28 | 5.56 | 9.12E-06 | CADM3, CADM2, PCDH20, ITGAE, ITGB2, IGSF11, ITGAX, FAT3, TNR, GPNMB, SPP1, KIRREL3, TYRO3, CLCA2, OLR1, BMX, ACKR3, TINAGL1, CD84, LAMA1, LYVE1, ITGA6, DSG2, FREM2, FREM1, CD33, RELN, ADAM15 |
| GO:0030574 | collagen catabolic process | 7 | 1.39 | 1.01E-05 | CTSK, MMP8, MMP19, MMP16, CTSS, MMP13, ADAM15 |
| GO:0070374 | positive regulation of ERK1 and ERK2 cascade | 15 | 2.98 | 6.91E-05 | CCL3, CCR1, CCL9, CCL8, ACKR3, ESR2, CCL6, CCL17, CCL22, CCL20, CHIL1, TREM2, GPNMB, HTR2B, HTR2A |
| GO:0007204 | positive regulation of cytosolic calcium ion concentration | 12 | 2.38 | 4.15E-04 | CXCL1, C3AR1, CCKAR, GNA15, CCL3, P2RY2, CCR1, CXCL3, CXCL2, EDN1, FPR1, HTR2A |
| GO:0022617 | extracellular matrix disassembly | 5 | 0.99 | 0.0012 | SH3PXD2B, LAMA1, MMP19, MMP13, MMP12 |
| GO:0014065 | phosphatidylinositol 3-kinase signaling | 5 | 0.99 | 0.0020 | EDN1, IGF1, PIK3R5, HTR2B, HTR2A |
| GO:0055072 | iron ion homeostasis | 6 | 1.19 | 0.0021 | LCN2, SLC11A1, STEAP4, EPB42, SLC40A1, B2M |
| GO:0045766 | positive regulation of angiogenesis | 9 | 1.79 | 0.0051 | VEGFC, C3AR1, GDF2, LGALS3, CHIL1, PGF, LRG1, ZC3H12A, ITGB2 |
| GO:0003341 | cilium movement | 5 | 0.99 | 0.0069 | DNAH11, DNAH7B, HYDIN, DNAH5, DNAH6 |
| GO:0006811 | ion transport | 23 | 4.56 | 0.0096 | KCNH1, STEAP4, CLCA2, SLC6A15, CFTR, KCNJ10, SLCO2B1, FXYD6, KCNK2, LRRC26, LCN2, SLC11A1, ATP2B2, SLC23A1, TTYH2, KCNN3, SLC4A1, SLC38A1, SLC40A1, ATP6V0D2, SLC4A5, GRID1, GABRP |
| GO:0030335 | positive regulation of cell migration | 11 | 2.18 | 0.0142 | C3AR1, IGF1R, SEMA6B, CCL3, PLET1, ITGA6, TIAM1, CCR1, EDN1, IGF1, GPNMB |
| GO:0007229 | integrin-mediated signaling pathway | 7 | 1.39 | 0.0162 | NME2, ITGAX, ITGA6, ADAMTS20, ITGAE, ITGB2, ADAM15 |
| GO:0001525 | angiogenesis | 12 | 2.38 | 0.0164 | VEGFC, GDF2, OVOL2, PGF, LEPR, MMP19, ZC3H12A, ACKR3, TNFAIP2, VASH1, MMRN2, ADAM15 |
| GO:0007599 | hemostasis | 5 | 0.99 | 0.0178 | ANXA8, PROZ, F8, SERPIND1, F7 |
| GO:0030073 | insulin secretion | 4 | 0.79 | 0.0404 | CCKAR, IL1RN, FFAR1, PCLO |
| GO:0008217 | regulation of blood pressure | 5 | 0.99 | 0.0465 | C3AR1, NPY, PTGS1, EDN1, DLL1 |
| GO:0001938 | positive regulation of endothelial cell proliferation | 5 | 0.99 | 0.0588 | VEGFC, GDF2, PGF, LRG1, HTR2B |
| GO:0007275 | multicellular organism development | 31 | 6.15 | 0.0673 | DHH, TNFRSF26, PGF, PAX5, OVOL2, FAT3, ZC3H12A, LHX6, UNC5D, TCF23, NGEF, ZFP423, MMP19, ACKR3, DLL1, SIX4, VEGFC, TNFRSF9, SEMA6B, HOXD8, m, NXN, FREM2, DBP, FREM1, GADD45G, WIF1, RELN, TNFAIP2, GAP43, KIF26B |
| GO:0045907 | positive regulation of vasoconstriction | 4 | 0.79 | 0.0749 | TBXAS1, SMAD6, PTGS1, HTR2A |

Table S4: Lists of GO enriched terms and associated differentially expressed genes represented in figure 4b. Downregulated genes are represented in blue and upregulated genes are represented in blue.

| category | GO number | GO term | Nb of DEG | DEG |
|---|---|---|---|---|
| **inflammation / immune response** | GO:0006954<br>GO:0070098<br>GO:0030593<br>GO:0006955<br>GO:0071346<br>GO:0006935<br>GO:0071347<br>GO:0060326<br>GO:0002376<br>GO:0002548<br>GO:0048247<br>GO:0071356<br>GO:0045087<br>GO:0035458<br>GO:0090023<br>GO:2000660<br>GO:2001180 | inflammatory response<br>chemokine-mediated signaling pathway<br>neutrophil chemotaxis<br>immune response<br>cellular response to interferon-gamma<br>chemotaxis<br>cellular response to interleukin-1<br>cell chemotaxis<br>immune system process<br>monocyte chemotaxis<br>lymphocyte chemotaxis<br>cellular response to tumor necrosis factor<br>innate immune response<br>cellular response to interferon-beta<br>positive regulation of neutrophil chemotaxis<br>negative regulation of interleukin-1-mediated signaling pathway<br>negative regulation of interleukin-10 secretion | 82 | CXCL1, MRC1, C3AR1, LCN2, ADGRE1, CCL22, LGALS3, GBP6, IL1R2, CD84, CCL3, PRKCQ, OLR1, TLR13, F830016B08RIK, IL1RN, TNFRSF9, CXCL5, TNFRSF26, CCL20, BMX, IIGP1, CXCL3, CCR1, CXCL2, VPREB3, STAR, LILRB4A, CCL9, CCL8, OAS2, TGTP2, EDN1, CHIL1, MALT1, TGTP1, CCL6, TRIM10, GM4951, FPR1, H2-Q7, CCL17, FCGR1, FCGR3, IL12B, ZC3H12A, B2M, ACKR3, C1QA, PTGS1, ITGB2, SUSD2, CLEC4N, CXCR1, MMP25, SLC11A1, CHIL4, NAIP2, CHIL3, SPP1, LIPA, CHST4, PLA2G7, TRP73, CLEC7A, BMPR1B, ACKR4, IGF1R, NFIL3, SMAD6, CTSS, TINAGL1, C1QB, CD300A, SERPINA3G, CD300LF, CLEC4D, CLEC5A, CD300LD, OAS1A, TREM2, ADAM15 |
| **ion transport** | GO:0007204<br>GO:0051928<br>GO:0006811 | positive regulation of cytosolic calcium ion concentration<br>positive regulation of calcium ion transport<br>ion transport | 38 | KCNH1, STEAP4, CLCA2, SLC6A15, CFTR, KCNJ10, SLCO2B1, FXYD6, KCNK2, LRRC26, LCN2, SLC11A1, ATP2B2, SLC23A1, TTYH2, KCNN3, SLC4A1, SLC38A1, SLC40A1, ATP6V0D2, SLC4A5, GRID1, GABRP, CXCL1, C3AR1, CCKAR, GNA15, CCL3, P2RY2, CCR1, CXCL3, CXCL2, EDN1, FPR1, HTR2A, ATP2B2, FFAR1, LPAR3 |
| **ECM disassembly** | GO:0030574<br>GO:0006508<br>GO:0022617 | collagen catabolic process<br>proteolysis<br>extracellular matrix disassembly | 30 | DHH, RBP3, MMP8, MMP25, PROZ, DPP6, PCSK5, CLCA2, ADAMTS20, MMP19, MMP17, MMP16, MALT1, CTSS, F7, TINAGL1, MMP13, MMP12, CTSK, CTSD, RELN, PRSS23, PHEX, ADAMDEC1, ADAM15, ASPRV1, ADAMTS4, CTSK, SH3PXD2B, LAMA1 |
| **adhesion** | GO:0007155<br>GO:0007229 | cell adhesion<br>integrin-mediated signaling pathway | 30 | CADM3, CADM2, PCDH20, ITGAE, ITGB2, IGSF11, ITGAX, FAT3, TNR, GPNMB, SPP1, KIRREL3, TYRO3, CLCA2, OLR1, BMX, ACKR3, TINAGL1, CD84, LAMA1, LYVE1, ITGA6, DSG2, FREM2, FREM1, CD33, RELN, ADAM15, NME2, ADAMTS20 |
| **angiogenesis** | GO:0045766<br>GO:0001525<br>GO:0001938 | positive regulation of angiogenesis<br>angiogenesis<br>positive regulation of endothelial cell proliferation | 18 | VEGFC, C3AR1, GDF2, LGALS3, CHIL1, PGF, LRG1, ZC3H12A, ITGB2, OVOL2, LEPR, MMP19, ACKR3, TNFAIP2, VASH1, MMRN2, ADAM15, HTR2B |
| **blood pressure / vasoreactivity** | GO:0045019<br>GO:0007200<br>GO:0008217<br>GO:0045907 | negative regulation of nitric oxide biosynthetic process<br>phospholipase C-activating G-protein coupled receptor signaling pathway<br>regulation of blood pressure<br>positive regulation of vasoconstriction | 14 | GLA, ACP5, ZC3H12A, C3AR1, GNA15, P2RY2, FPR1, HTR2A, NPY, PTGS1, EDN1, DLL1, TBXAS1, SMAD6 |

233 Table S5. List of Primer

234 Primers for quantitative RT-PCR were designed using Primer-Blast on GenBank sequences and are separated by
235 at least one intron or span an exon-exon junction for intron containing genes.

| Gene | GenBank sequences | Forward (5'-3') | Reverse (5'-3') |
|---|---|---|---|
| ***Rpl13a*** | NM_009438.5 | CCCTCCACCCTATGACAAGA | TTCTCCTCCAGAGTGGCTGT |
| ***Id1*** | NM_010495.3 | CGCTCAGCACCCTGAACGGC | TCCGGTGGCTGCGGTAGTGT |
| ***Acvlr1*** | NM_009612.3 | CCTCACGAGATGAGCAGTCC | GGCGATGAAGCCTAGGATGTT |
| ***Bmpr2*** | NM_007561.4 | TGGCAGTGAGGTCACTCAAG | TTGCGTTCATTCTGCATAGC |
| ***Eng*** | NM_001146348.1 | GCCAAAGTGTGGCAATCAGG | TGGTCGTCAGTGTCTTCAGC |
| ***Bmp10*** | NM_009756.3 | TCCATGCCGTCTGCTAACATCATC | ACATCATGCGATCTCTCTGCACCA |
| ***Smad6*** | NM_008542.3 | CTGCGGGCCAGAATCACCGC | GCTCGGCTTGGTGGCATCCG |
| ***Edn-1*** | NM_010104.4 | GGCCCAAAGTACCATGCAGA | TGCTATTGCTGATGGCCTCC |
| ***Nkx2-5*** | NM_008700.2 | GACCCTCGGGCGGATAAAAA | CCATCCGTCTCGGCTTTGT |
| ***Tbx20*** | NM_194263.2 | GTTTGCCAAAGGATTCCGGG | CCGGGCATAGGAATGCTTCT |
| ***Cxcl5*** | NM_009141.3 | CGGTTCCATCTCGCCATTCA | GCTATGACTGAGGAAGGGGC |
| ***Ccl3*** | NM_011337.2 | ATATGGAGCTGACACCCCGA | AGCAAAGGCTGCTGGTTTCA |
| ***Ccl2*** | NM_011333.3 | CTGCATCTGCCCTAAGGTCT | AGTGCTTGAGGTGGTTGTGG |
| ***Bmp9 (Gdf-2)*** | NM_019506.4 | CAATGACCGCAGCAATGGG | AAGCATGGTCTCCTGCTCAT |

236

237

## SUPPLEMENTARY REFERENCES


1. Guignabert C, Alvira CM, Alastalo TP, Sawada H, Hansmann G, Zhao M, Wang L, El-Bizri N, Rabinovitch M. Tie2-mediated loss of peroxisome proliferator-activated receptor-gamma in mice causes PDGF receptor-beta-dependent pulmonary arterial muscularization. *Am J Physiol Lung Cell Mol Physiol* 2009;**297**:L1082-1090.
2. Guignabert C, Izikki M, Tu LI, Li Z, Zadigue P, Barlier-Mur AM, Hanoun N, Rodman D, Hamon M, Adnot S, Eddahibi S. Transgenic mice overexpressing the 5-hydroxytryptamine transporter gene in smooth muscle develop pulmonary hypertension. *Circ Res* 2006;**98**:1323-1330.
3. Tu L, Desroches-Castan A, Mallet C, Guyon L, Cumont A, Phan C, Robert F, Thuillet R, Bordenave J, Sekine A, Huertas A, Ritvos O, Savale L, Feige J-J, Humbert M, Bailly S, Guignabert C. Selective BMP-9 Inhibition Partially Protects Against Experimental Pulmonary Hypertension. *Circulation Research* 2019;**124**:846-855.
4. Bordenave J, Thuillet R, Tu L, Phan C, Simonneau G, Huertas A, Hibert M, Bonnet D, Humbert M, Frossard N, Guignabert C. Neutralization of CXCL12 reverses established pulmonary hypertension in the sugen-hypoxia rat model. *Eur Respir J* 2017;**50**:PA2385.
5. Tual-Chalot S, Garcia-Collado M, Redgrave RE, Singh E, Davison B, Park C, Lin H, Luli S, Jin Y, Wang Y, Lawrie A, Jakobsson L, Arthur HM. Loss of Endothelial Endoglin Promotes High-Output Heart Failure Through Peripheral Arteriovenous Shunting Driven by VEGF Signaling. *Circ Res* 2020;**126**:243-257.
6. Newman AM, Steen CB, Liu CL, Gentles AJ, Chaudhuri AA, Scherer F, Khodadoust MS, Esfahani MS, Luca BA, Steiner D, Diehn M, Alizadeh AA. Determining cell type abundance and expression from bulk tissues with digital cytometry. *Nat Biotechnol* 2019;**37**:773-782.
7. Travaglini KJ, Nabhan AN, Penland L, Sinha R, Gillich A, Sit RV, Chang S, Conley SD, Mori Y, Seita J, Berry GJ, Shrager JB, Metzger RJ, Kuo CS, Neff N, Weissman IL, Quake SR, Krasnow MA. A molecular cell atlas of the human lung from single-cell RNA sequencing. *Nature* 2020;**587**:619-625.
8. Tillet E, Ouarne M, Desroches-Castan A, Mallet C, Subileau M, Didier R, Lioutsko A, Belthier G, Feige JJ, Bailly S. A heterodimer formed by bone morphogenetic protein 9 (BMP9) and BMP10 provides most BMP biological activity in plasma. *J Biol Chem* 2018;**293**:10963-10974.

Figure S1

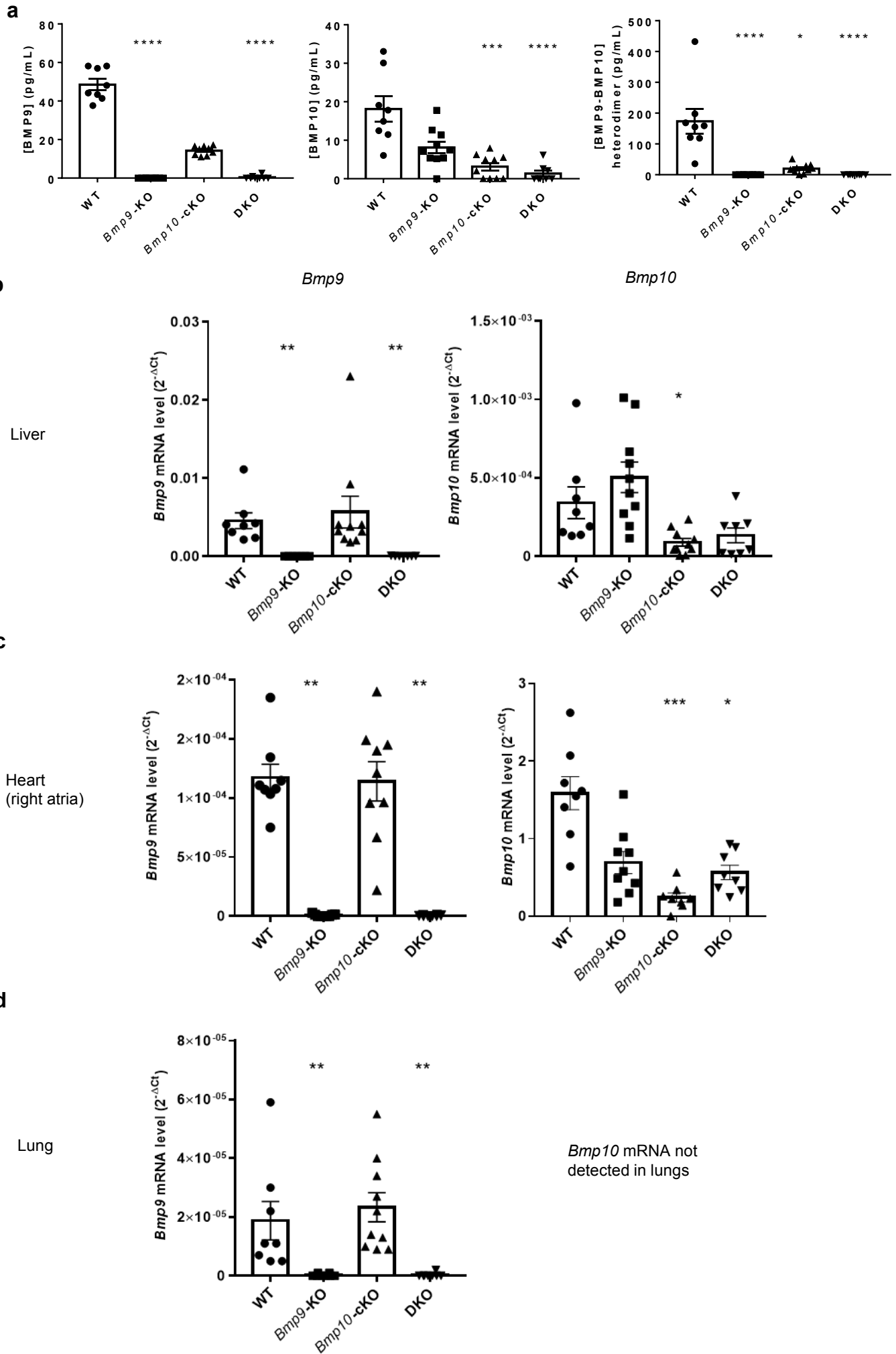
a
[BMP9] (pg/mL)
[BMP10] (pg/mL)
[BMP9-BMP10] heterodimer (pg/mL)
WT
Bmp9-KO
Bmp10-cKO
DKO
b
Bmp9
Bmp10
Liver
Bmp9 mRNA level (2^-ΔCt)
Bmp10 mRNA level (2^-ΔCt)
c
Heart (right atria)
d
Lung
Bmp10 mRNA not detected in lungs

Figure S2

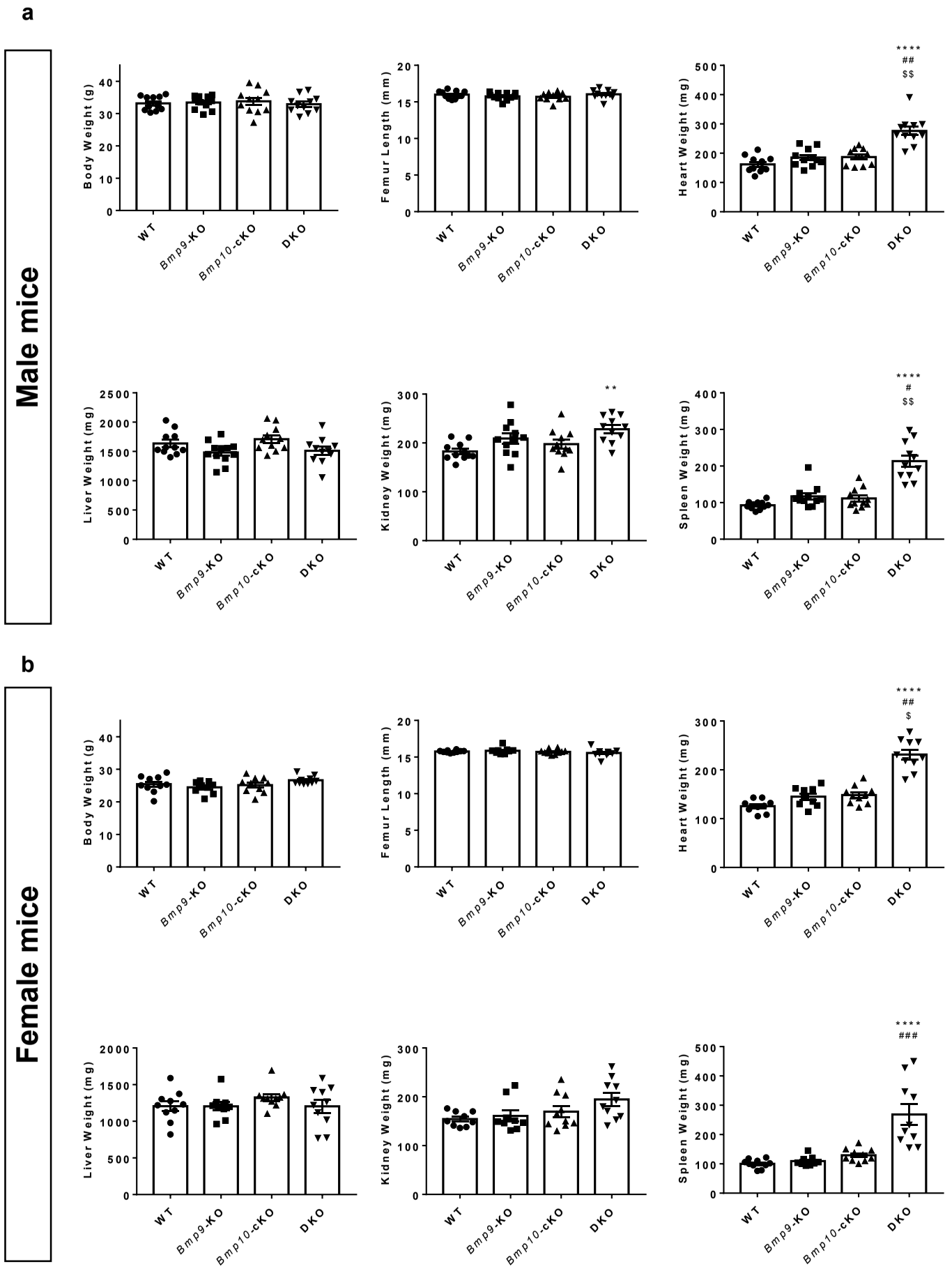
a
Male mice
Body Weight (g)
Femur Length (mm)
Heart Weight (mg)
Liver Weight (mg)
Kidney Weight (mg)
Spleen Weight (mg)
WT
Bmp9-KO
Bmp10-cKO
DKO
b
Female mice
Body Weight (g)
Femur Length (mm)
Heart Weight (mg)
Liver Weight (mg)
Kidney Weight (mg)
Spleen Weight (mg)
WT
Bmp9-KO
Bmp10-cKO
DKO

Figure S3

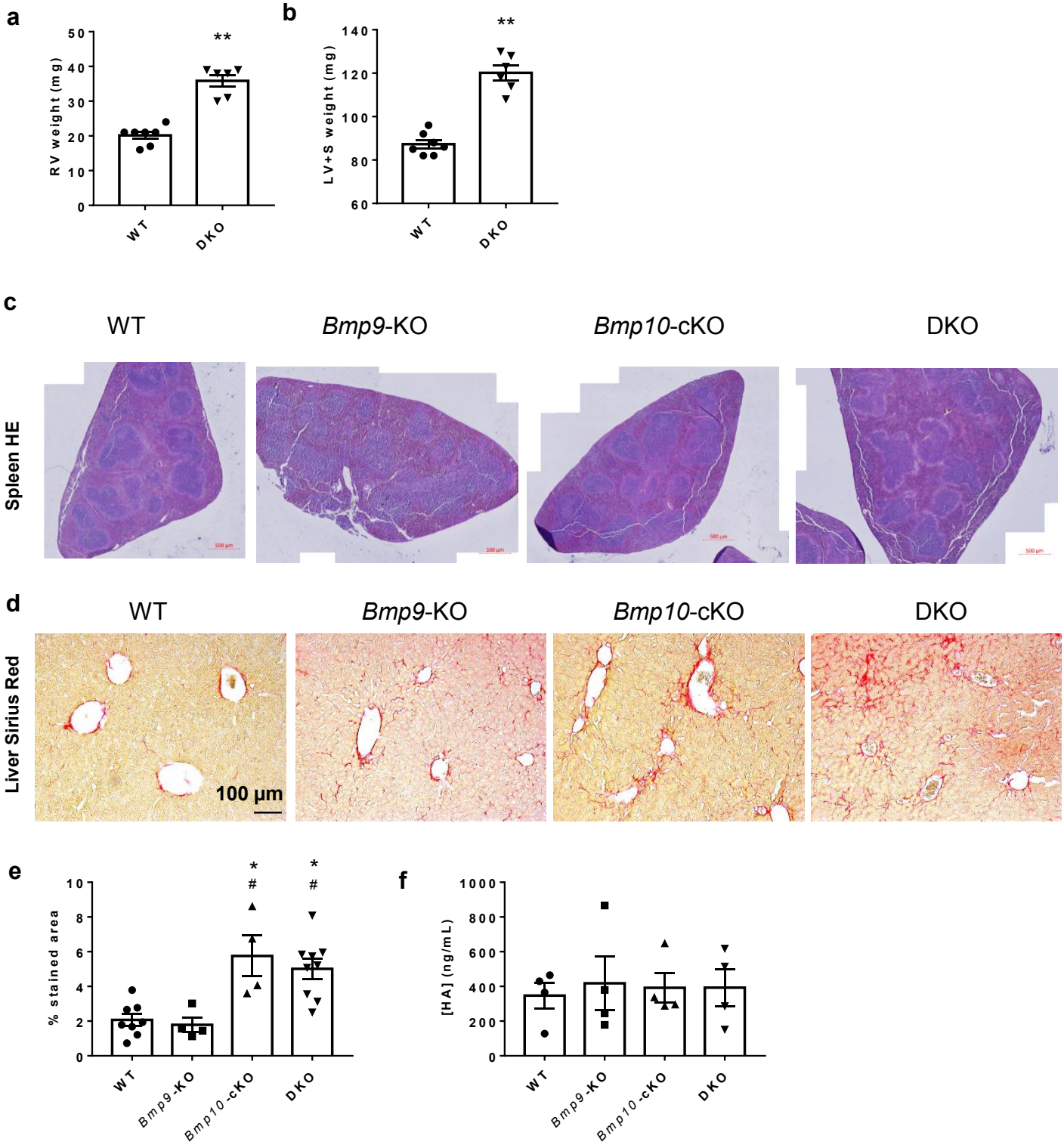
a
RV weight (mg)
50
40
30
20
10
0
**
WT
DKO
b
LV+S weight (mg)
140
120
100
80
60
**
WT
DKO
c
WT
Bmp9-KO
Bmp10-cKO
DKO
Spleen HE
d
WT
Bmp9-KO
Bmp10-cKO
DKO
Liver Sirius Red
100 μm
e
% stained area
10
8
6
4
2
0
*
#
*
#
WT
Bmp9-KO
Bmp10-cKO
DKO
f
[HA] (ng/mL)
1000
800
600
400
200
0
WT
Bmp9-KO
Bmp10-cKO
DKO

Figure S4

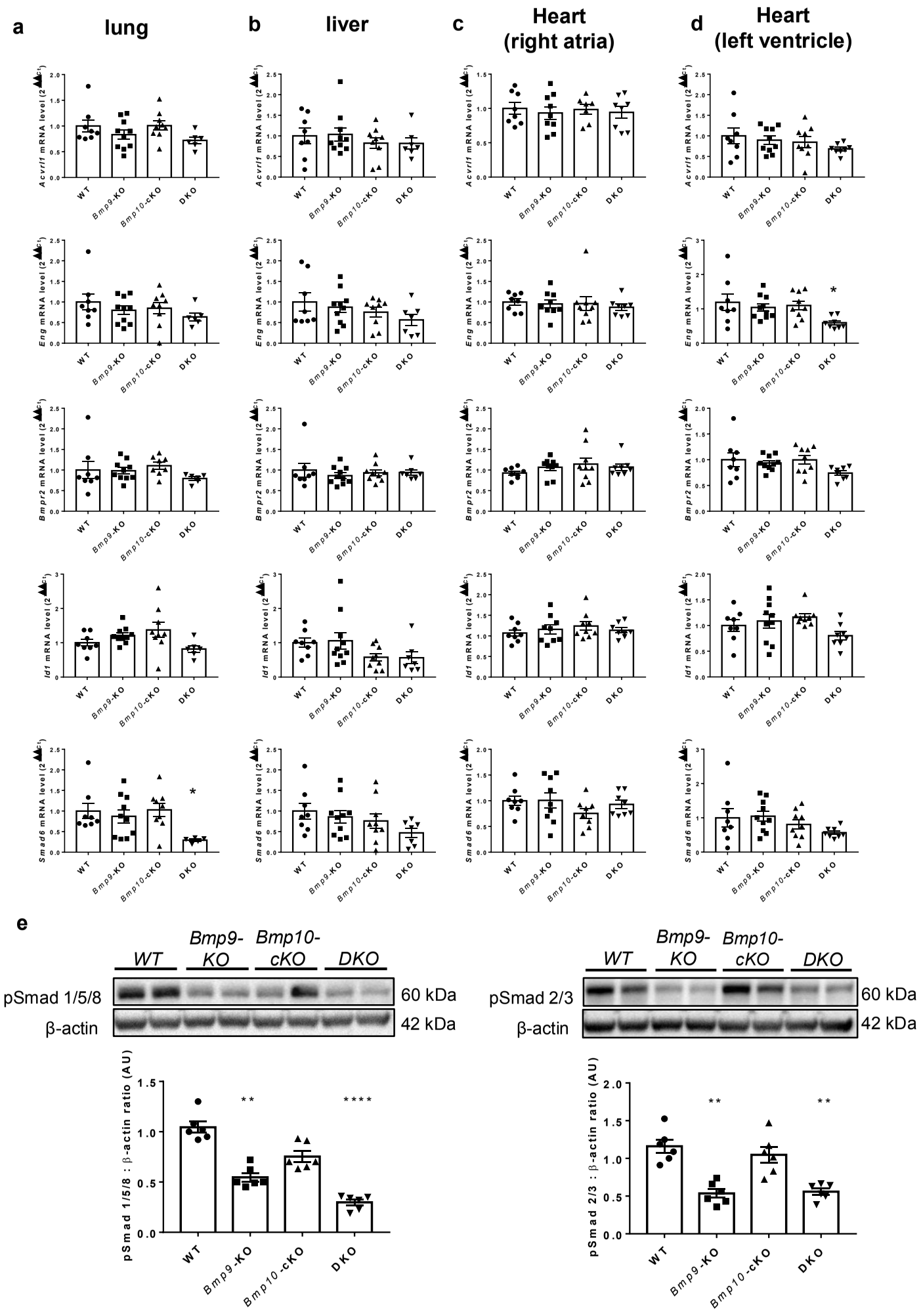
a
lung
b
liver
c
Heart (right atria)
d
Heart (left ventricle)
Acvrl1 mRNA level (2-ΔCt)
Eng mRNA level (2-ΔCt)
Bmpr2 mRNA level (2-ΔCt)
Id1 mRNA level (2-ΔCt)
Smad6 mRNA level (2-ΔCt)
WT
Bmp9-KO
Bmp10-cKO
DKO
e
WT
Bmp9-KO
Bmp10-cKO
DKO
pSmad 1/5/8
β-actin
60 kDa
42 kDa
pSmad 1/5/8 : β-actin ratio (AU)
pSmad 2/3
pSmad 2/3 : β-actin ratio (AU)

Figure S5

**a**

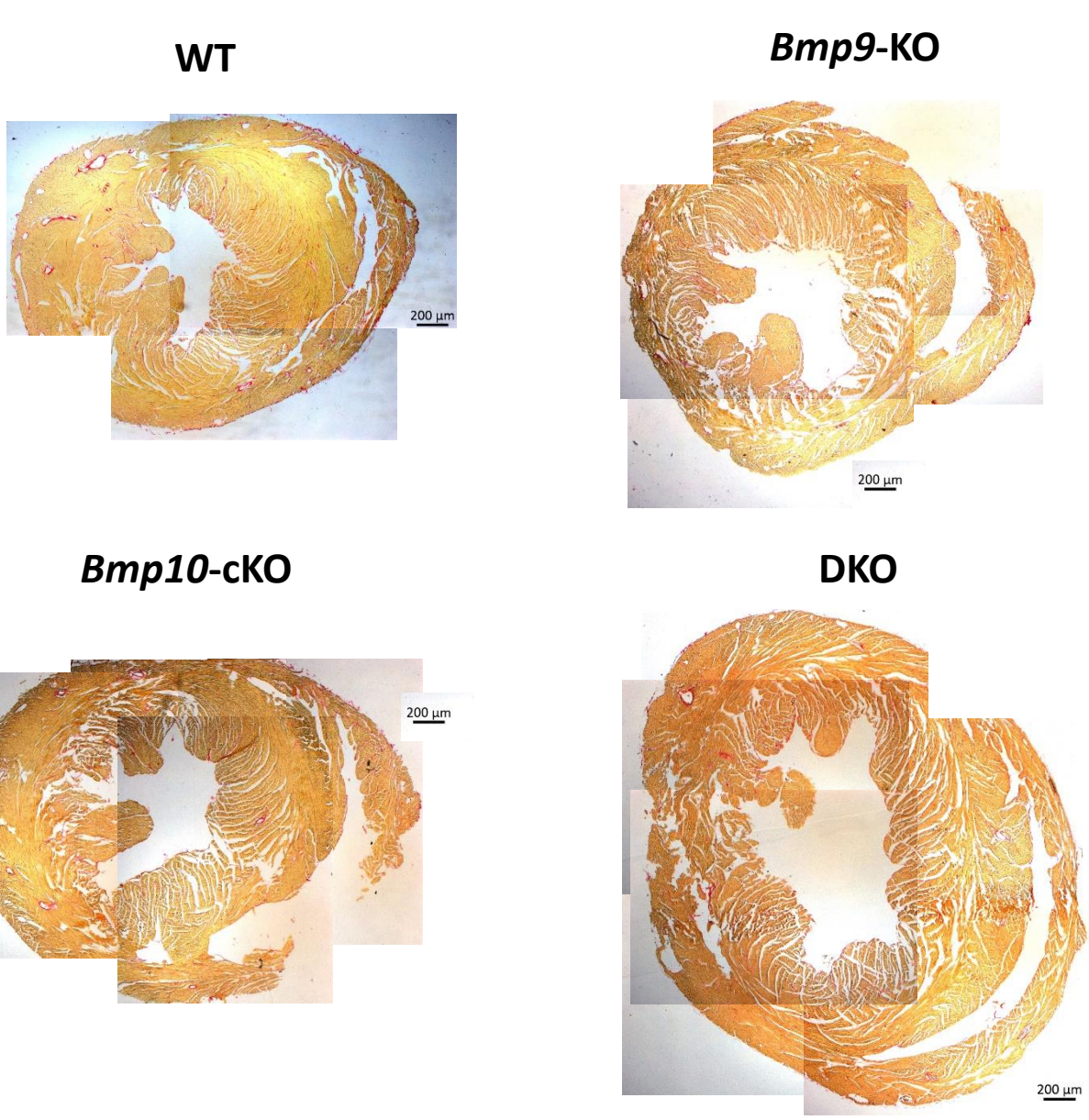
WT
Bmp9-KO
Bmp10-cKO
DKO
200 μm
200 μm
200 μm
200 μm

**b**

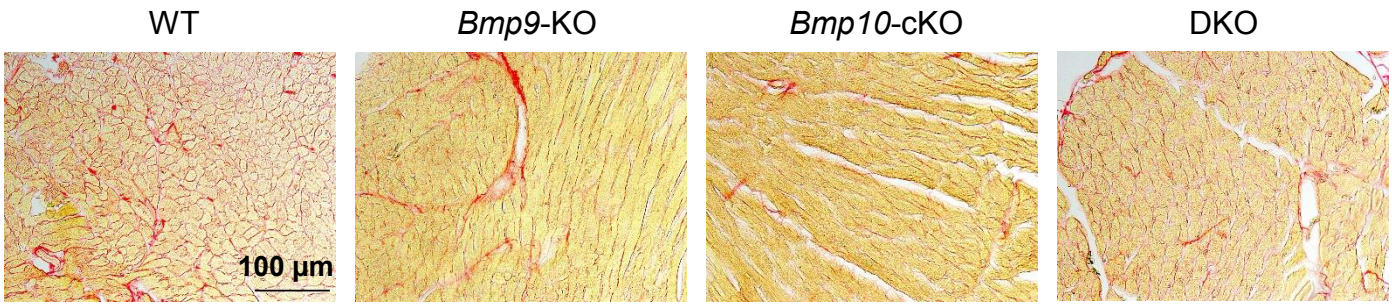
WT
Bmp9-KO
Bmp10-cKO
DKO
100 μm

Figure S6

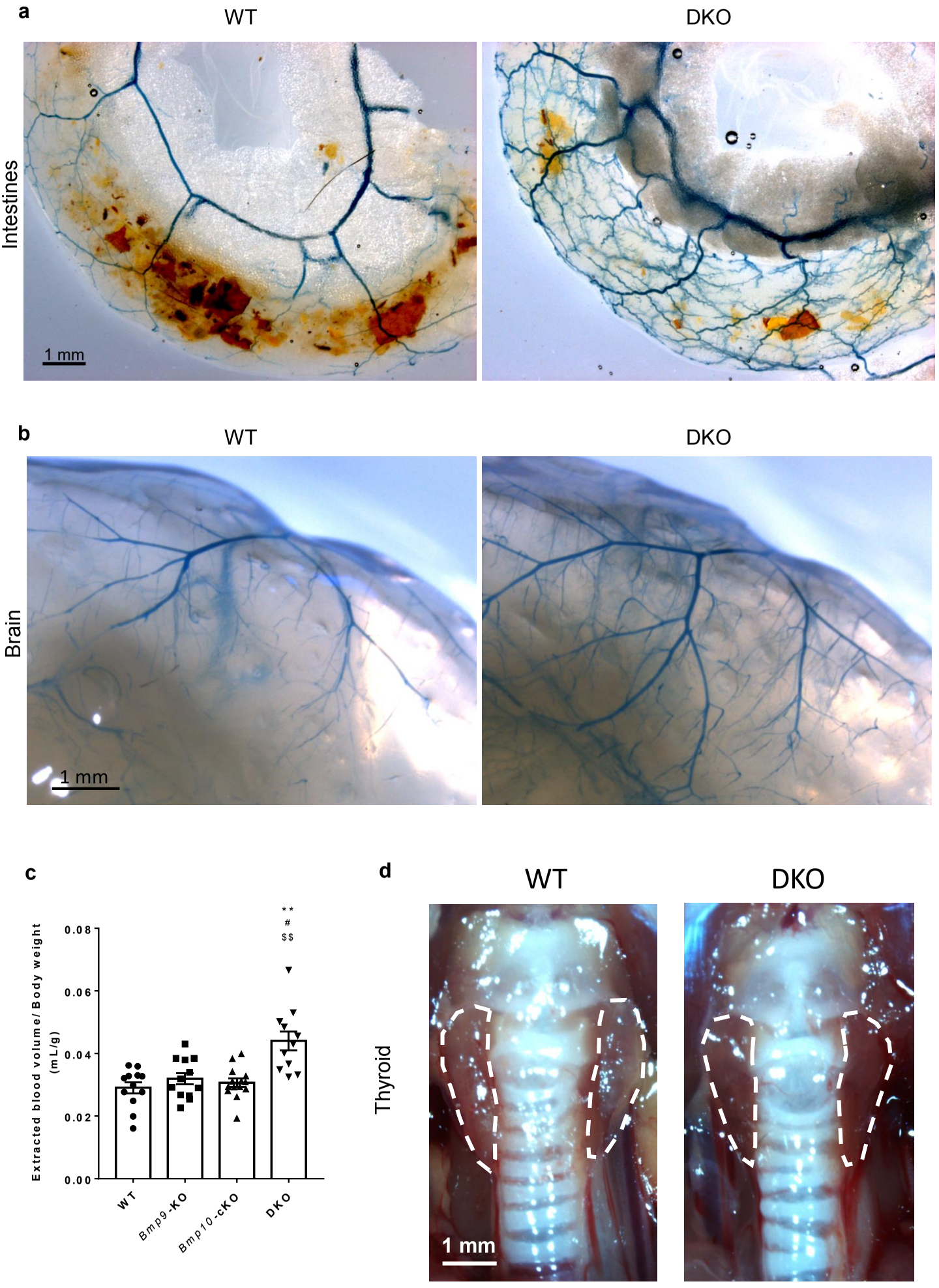
a
WT
DKO
Intestines
1 mm
b
WT
DKO
Brain
1 mm
c
Extracted blood volume/ Body weight (mL/g)
0.08
0.06
0.04
0.02
0.00
**
#
$$
WT
Bmp9-KO
Bmp10-cKO
DKO
d
WT
DKO
Thyroid
1 mm

Figure S7

## Gene Ontology Biological Process : top20

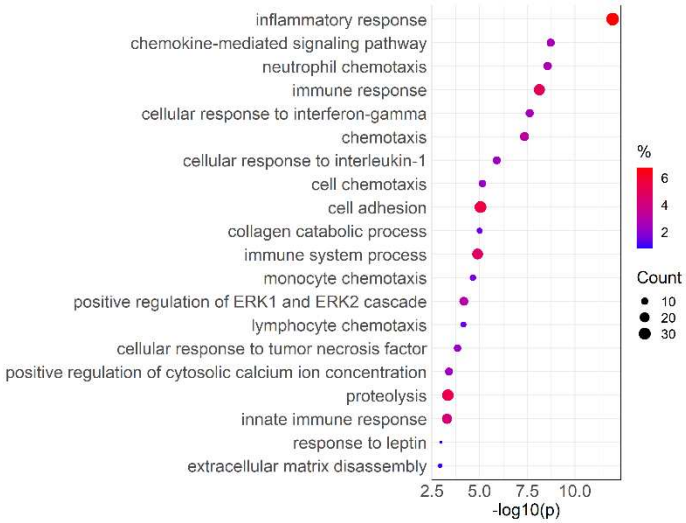


## Gene Ontology Biological Process : selection

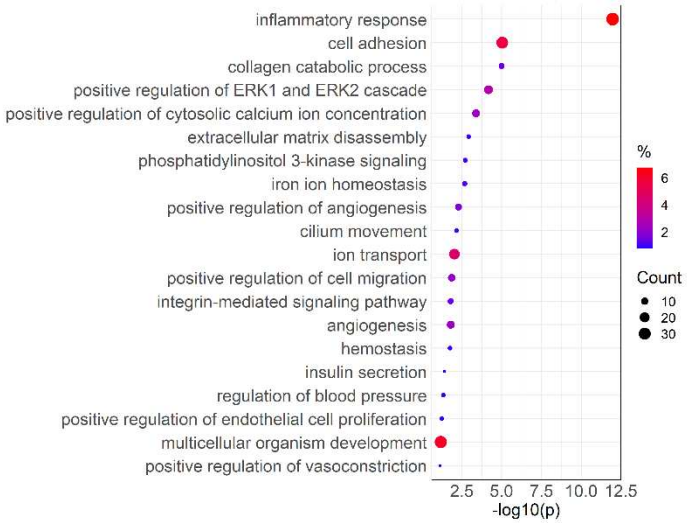


## Gene Ontology Molecular Function : top20

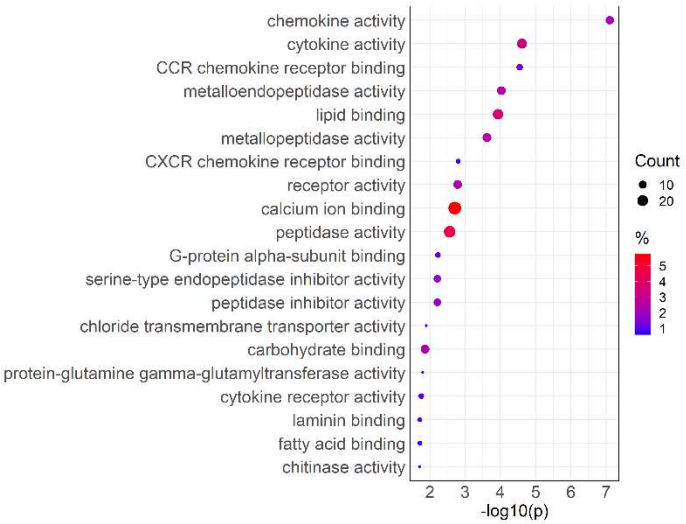


## Gene Ontology Cellular Component : top20

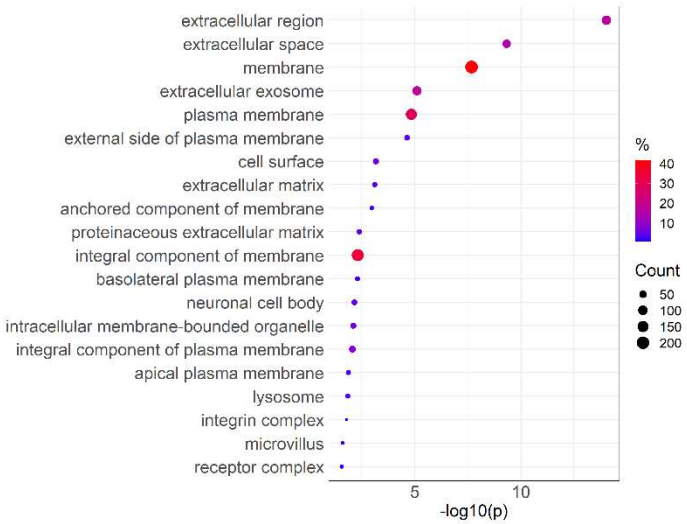


## KEGG

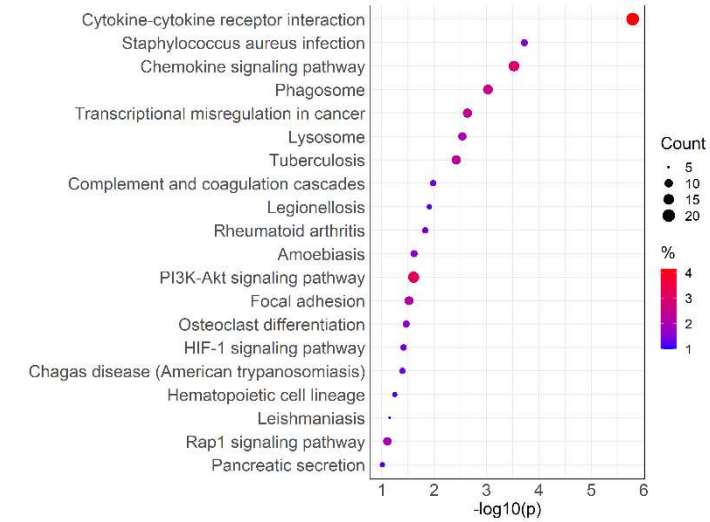

Figure S8

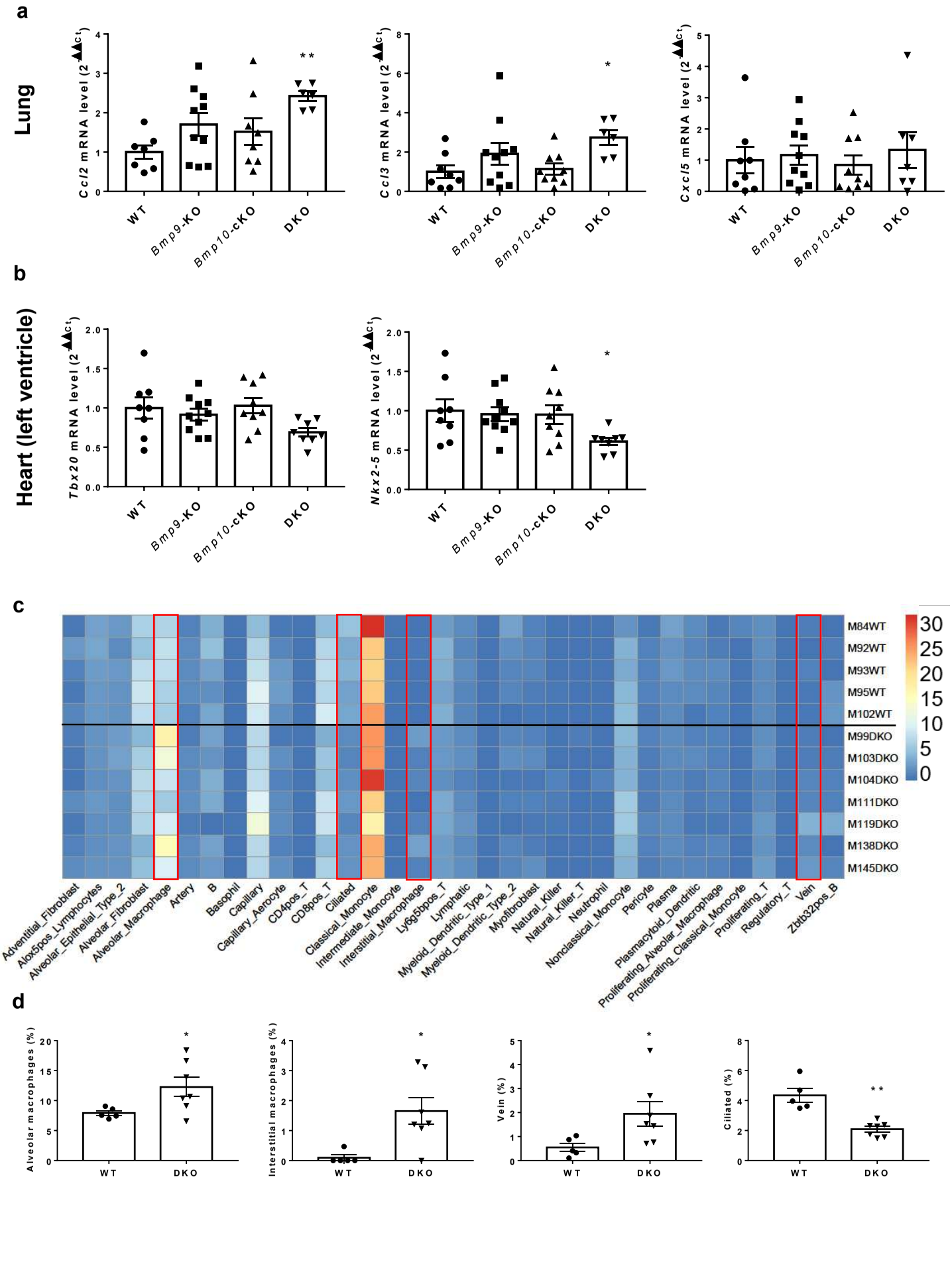
a
Lung
Ccl2 mRNA level (2-ΔΔCt)
Ccl3 mRNA level (2-ΔΔCt)
Cxcl5 mRNA level (2-ΔΔCt)
WT
Bmp9-KO
Bmp10-cKO
DKO
b
Heart (left ventricle)
Tbx20 mRNA level (2-ΔΔCt)
Nkx2-5 mRNA level (2-ΔΔCt)
c
M84WT
M92WT
M93WT
M95WT
M102WT
M99DKO
M103DKO
M104DKO
M111DKO
M119DKO
M138DKO
M145DKO
Adventitial_Fibroblast
Alox5pos_Lymphocytes
Alveolar_Epithelial_Type_2
Alveolar_Fibroblast
Alveolar_Macrophage
Artery
B
Basophil
Capillary
Capillary_Aerocyte
CD4pos_T
CD8pos_T
Ciliated
Classical_Monocyte
Intermediate_Monocyte
Interstitial_Macrophage
Ly6g5bpos_T
Lymphatic
Myeloid_Dendritic_Type_1
Myeloid_Dendritic_Type_2
Myofibroblast
Natural_Killer
Natural_Killer_T
Neutrophil
Nonclassical_Monocyte
Pericyte
Plasma
Plasmacytoid_Dendritic
Proliferating_Alveolar_Macrophage
Proliferating_Classical_Monocyte
Proliferating_T
Regulatory_T
Vein
Zbtb32pos_B
d
Alveolar macrophages (%)
Interstitial macrophages (%)
Vein (%)
Ciliated (%)

Figure S9

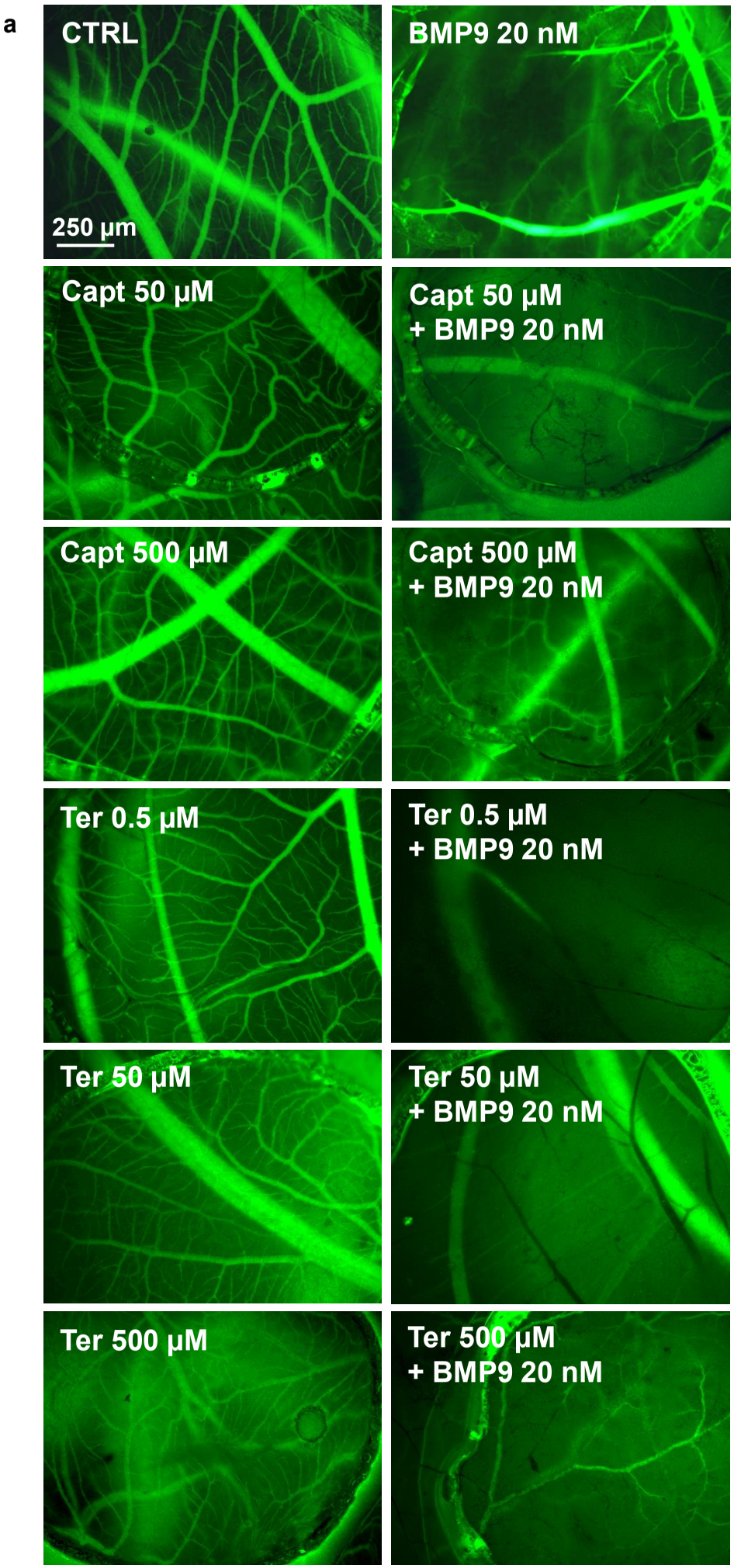
a
CTRL
BMP9 20 nM
250 µm
Capt 50 µM
Capt 50 µM
+ BMP9 20 nM
Capt 500 µM
Capt 500 µM
+ BMP9 20 nM
Ter 0.5 µM
Ter 0.5 µM
+ BMP9 20 nM
Ter 50 µM
Ter 50 µM
+ BMP9 20 nM
Ter 500 µM
Ter 500 µM
+ BMP9 20 nM

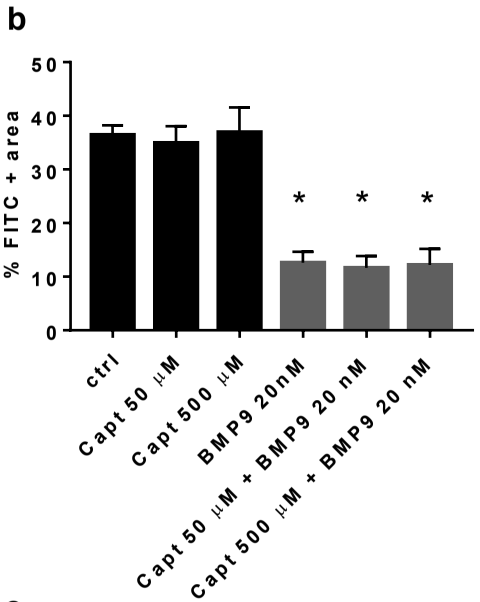
b
% FITC + area
0
10
20
30
40
50
*
*
*
ctrl
Capt 50 µM
Capt 500 µM
BMP9 20nM
Capt 50 µM + BMP9 20 nM
Capt 500 µM + BMP9 20 nM

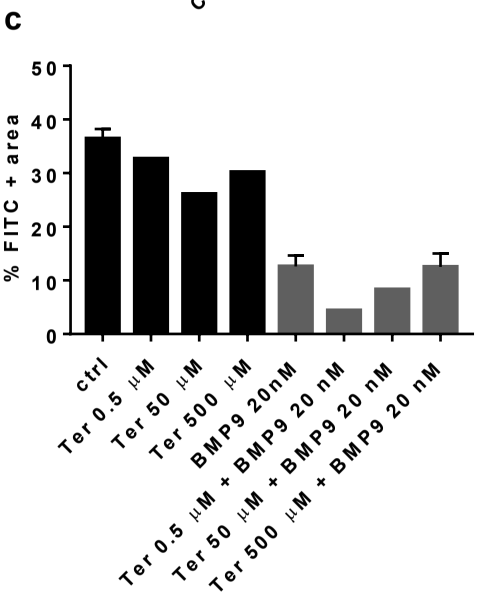
c
% FITC + area
0
10
20
30
40
50
ctrl
Ter 0.5 µM
Ter 50 µM
Ter 500 µM
BMP9 20nM
Ter 0.5 µM + BMP9 20 nM
Ter 50 µM + BMP9 20 nM
Ter 500 µM + BMP9 20 nM

# Part II – Consequences of BMP10 deletion in young mice using Rosa26 CreERT2 line

## 1. Rosa CreERT2 BMP10 iKO displayed haematopoiesis defect

This part of the project was aimed to study the function of BMP10 during postnatal development. It is generally agreed that BMP9 and BMP10 signalling via ALK1 is mainly responsible for maintenance of vascular quiescence in mature endothelium and that they both hold redundant roles in postnatal angiogenesis (138,176,191) as well as during adult vascular homeostasis under normal physiological conditions (279). Nonetheless, the function of BMP10 had not been yet thoroughly analysed in the context of postnatal vascular development. The data obtained from us, and other groups involved the use of neutralising antibodies against BMP10. Therefore, we set up to analyse the function of BMP10 postnatally *in vivo* using the tamoxifen-inducible Rosa26 CreERT2, *Bmp10*$^{lox/lox}$ previously described.

By deleting BMP10 by tamoxifen injection from postnatal day 9 (P9) to P11, we found that these young animals display a sudden growth arrest starting around P15 and fail to survive 9-10 days after the last tamoxifen injection. Gross phenotypic analysis revealed that the haematopoietic organs bone marrow spleen and thymus were strongly affected in the Rosa Cre iKO (KO) compared to the BMP10$^{lox/lox}$ WT littermate **(Figure 26 A-C)**. In particular, the organs are overall pale, spleen and thymus are smaller, and the cell counts are significantly lower in the KO models **(Figure 26 B)**.

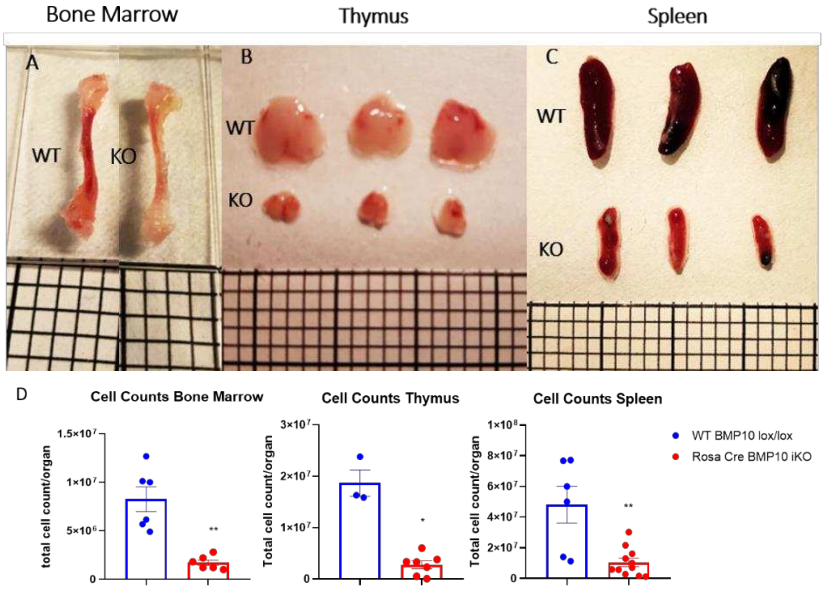


***Figure 26: Rosa CreERT2 BMP10 iKO displayed strong defects in haematopoietic organs.***
*Representative pictures of (A) long bones tibiae, (B) thymus, and (C) spleen haematopoietic organs of BMP10$^{lox/lox}$ WT vs Rosa Cre BMP10 iKO. Animals were injected with 75 mg/kg of tamoxifen from P9 to P11 and euthanised at P20. (D) Relative cell counts in bone marrow, thymus and spleen. Data is expressed as mean ± SEM. Mann-Whitney tests were used to asses statistical significance (ns p-value > 0.05; * p-value ≤ 0.05; ** p-value ≤ 0.01; *** p-value ≤ 0.001; **** p-value ≤ 0.0001).*

These observations led us to believe that BMP10 plays a major role in postnatal haematopoiesis. We hypothesised that BMP10 function could not be replaced by BMP9 probably due a different receptor specificity or a secretion source (BMP10 is expressed by both right atria cardiomyocytes and liver hepatic stellate cells while BMP9 is only expressed by liver hepatic stellate cells) (52). Specific affinity for both type I and type II receptors could be the key for BMP9 and BMP10 tissue-specific functions.

In order to better understand the mechanisms behind the observed phenotype; we performed a flow cytometric analysis to assess the levels of lineage committed progenitors (Figure 27), as well as a complete blood count (CBC) analysis to check the levels of blood circulating cells (data not shown). We analysed the levels of $Ter119^{+}CD71^{+}$ erythroblasts (RBC precursors), $B220^{+}CD19^{+}$ B cell precursors and $CD11b^{+}Gr\text{-}1^{+}$ myeloblasts. We observed that the erythroblasts are completed depleted in the Rosa Cre BMP10 iKO. To follow, B cell precursors were significantly decreased, and the myeloblasts are slightly affected by BMP10 deletion (Figure 27). These results were in line with the results obtained from the CBC analysis.

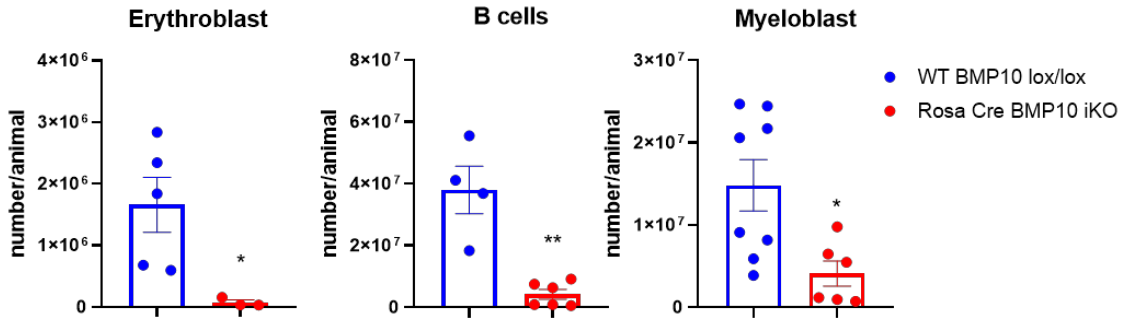


*Figure 27: Lineage precursors cells in bone marrow are affected in Rosa Cre BMP10 iKO.*
*Relative quantification expressed in total number of cells per animal of WT $Bmp10^{lox/lox}$ vs Rosa Cre BMP10 iKO (red) animals at P20 of $Ter119^{+}CD71^{+}$ erythroblasts, $B220^{+}CD19^{+}$ B cell precursors and $CD11b^{+}Gr\text{-}1^{+}$ . Data is expressed as mean ± SEM. Mann-Whitney tests were used to asses statistical significance (ns p-value > 0.05; * p-value ≤ 0.05; ** p-value ≤ 0.01; *** p-value ≤ 0.001; **** p-value ≤ 0.0001).*

At this point, the following step was to assess the function of BMP10 on the formation of haematopoietic stem and progenitor cells (HPSC). The HSPC reside within a restricted cell population known as LSK ($Lineage^{-}Sca1^{+}cKit^{+}$) which is defined as "early" haematopoietic progenitors. These cells are characterised by: (i) lack of expression of markers for committed progenitors, (ii) expression of receptor surface Sca1 and (iii) expression of receptor surface cKit (CD117). To differentiate the HSPC subgroups within the LSK population we relied on two markers from the signalling lymphocytic activation molecule (SLAM) family of receptors.

The SLAM family of receptors is a group of type I transmembrane receptors that includes SLAM (CD150; SLAMF1), 2B4 (CD244; SLAMF4), Ly-9 (CD229; SLAMF3), natural killer T- and B-cell antigen (NTB-A; SLAMF6; Ly108 in the mouse), CD84 (SLAMF5), and CD2-like receptor activating cytotoxic cells (CRACC; CD319; SLAMF7). SLAM-family receptors are widely expressed in immune cells, but not in non-immune cells (281). Antibodies against SLAM receptors are a great tool to quantify different immune cells. In particular, we relied on CD150 and CD48, which allows for the identification of four functionally different fraction of cells among the heterogeneous LSK population. These four cell types are:

- Restricted Hematopoietic Progenitors (HPC)-1 characterised by $CD150^{-}CD48^{+}$;
- Restricted Hematopoietic Progenitors (HPC)-2 characterised by $CD150^{+}CD48^{+}$
- Hematopoietic Stem Cells (HSCs) characterised by $CD150^{+}CD48^{-}$;
- Multipotent Progenitors (MPPs) characterised by $CD150^{-}CD48^{-}$.

These sub-groups are distinguished based on their differences in changes in cell cycle kinetics, self-renewal capacity, and reconstituting potential (281). HPC-1 consists of restricted lymphoid progenitors that lacked megakaryocytic potential. HPC-2 contain a heterogeneous collection of restricted progenitors i.e. erythrocytes, megakaryocytes, myelocytes and B cells progenitors and they constitute a transitional population between HSCs and MPPs. HSC possess the ability of both multi-potency and self-renewal and can give rise to MPPs cell population that no longer possess self-renewal ability yet keeping full-lineage differentiation potential (282,91).

Figure 28 represent the results obtained from flow cytometric analysis of these four respective cells subgroups in our WT vs Rosa Cre BMP10 iKO models. In particular, both the percentage of cells within the population that did not expressed any lineage committed markers $CD4^{-}/CD8a^{-}/B220^{-}/Gr1^{-}/Ter11^{-}$) and the total number of the cells within the bone marrow of each animals were quantified. Overall, it seemed that the percentage of lineage negative cells were slightly increased in the Rosa Cre BMP10 iKO. On the other hand, within the LSK population, undifferentiated haematopoietic progenitors HPC1, HSC and MPP were not affected by the deletion of BMP10. However, we could appreciate a significant increase in the percentage of HPC-2 population.

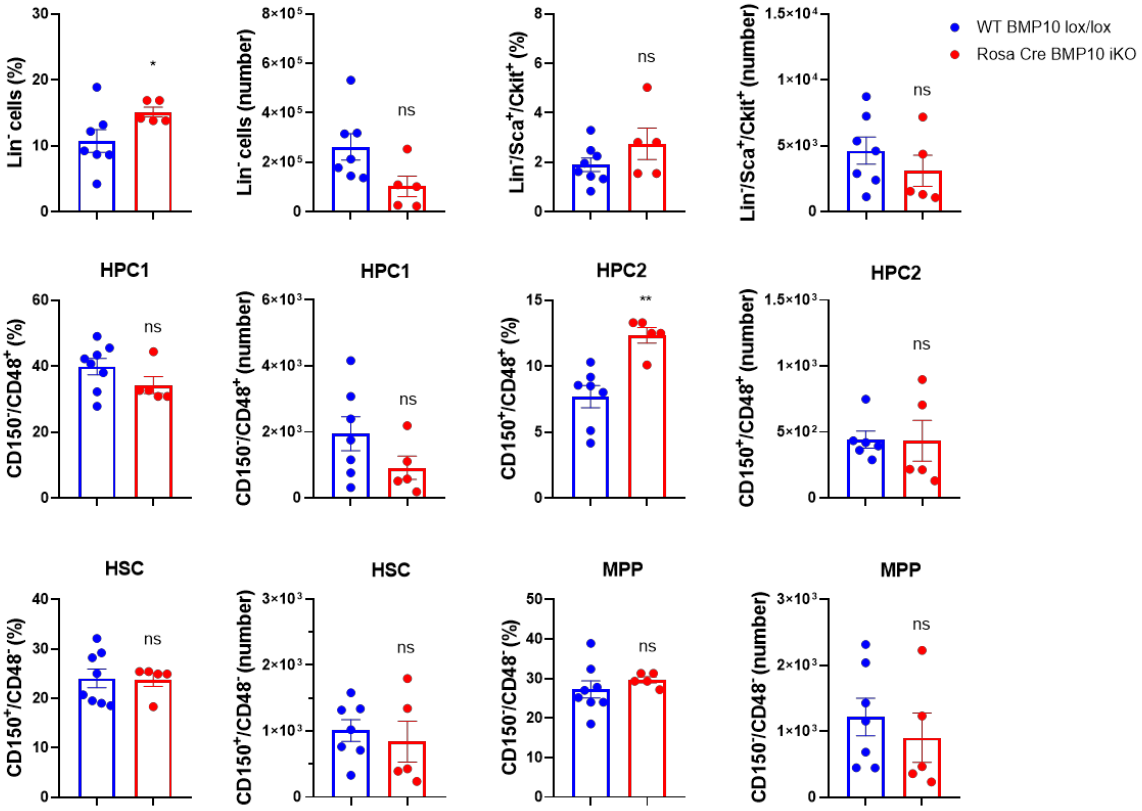


*Figure 28: Rosa Cre BMP10 iKO models revealed a slight increase in percentage of lineage non-committed cells and HPC-2 CD150$^{+}$CD48$^{+}$.*

*Relative quantification expressed as % (left) and total number (right) of hematopoietic stem cells at different stages using SLAM family markers of WT BMP10 lox/lox (blue) vs Rosa Cre BMP10 iKO (red). Progenitors analysed from top to bottom: Lin- (CD4$^{-}$/CD8a$^{-}$/B220$^{-}$/Gr1$^{-}$/Ter119$^{-}$) (% and total number); LSK (Lin$^{-}$/Sca$^{+}$/Ckit$^{+}$) (% and total number); HPC1 (CD150$^{-}$/CD48$^{+}$) (% and total number); HPC2 (CD150$^{+}$/CD48$^{+}$) (% and total number); HSC (CD150$^{+}$/CD48$^{-}$) (% and total number); MPP (CD150$^{-}$/CD48$^{-}$) (% and total number). Data is expressed as mean ± SEM. Mann-Whitney tests were used to asses statistical significance (ns p-value > 0.05; * p-value ≤ 0.05; ** p-value ≤ 0.01; *** p-value ≤ 0.001; **** p-value ≤ 0.0001).*

Being HPC-2 composed of low levels of cells of multiple restricted lineages including erythrocytes, megakaryocytes, myelocytes and B cells progenitors, this observed increased could be explained from a result of a compensatory mechanisms aimed to balance for the loss of the lineage committed cells.

## 2. Bone marrow vasculature defect observed in Rosa Cre BMP10 iKO

Having starting gathering some information on the postnatal deletion of BMP10, we ventured the hypothesis that, considering that BMP10 is a strong affinity ligand for ALK1 receptor found in ECs, it could be plausible that the deletion of BMP10 could have a vasculature repercussion which would in turn impact the formation and maturation of HSCs in the organ.

The bone marrow is the major site of hematopoiesis in adults. Over the years, it has been shown that there is a tight interdependence between endothelial cells and haematopoietic stem cells in the bone marrow. Besides their well-characterised role as a conduit for cells, nutrients, gases and waste, blood vessels provide niches for maintenance of a steady-state haematopoietic stem cells (HSCs) microenvironment by releasing of angiocrine factors (283). Moreover, the importance of blood vessels in bone repair, bone mass loss and bone marrow reconstruction after irradiation have recently been highlighted (284,285). The vascular niches in the bone marrow are characterised by the intricate co-existence of heterogeneous vascular and perivascular cell types important for the maintenance of stem and progenitor cells.

Long bones are subdivided into three main regions known as epiphysis, metaphysis, and diaphysis **(Figure 29)** (286). In the metaphysis of the bone, arteries branch into smaller arterioles and terminate in type H capillaries ($Emcn^{high}$ and $CD31^{high}$). On the other hand, the diaphyseal region is characterised by the presence of type L sinusoids ($Emcn^{low}$ and $CD31^{low}$). This differentiation have been made on the basis of morphological, molecular and functional criteria (287). Lineage tracing experiment revealed that type H cells can give rise to type L cells (287). Moreover, while type H are known to be physically coupled with osteoprogenitors, while type L ECs are closely associated with hematopoietic stem cells residing in perivascular niches (288).

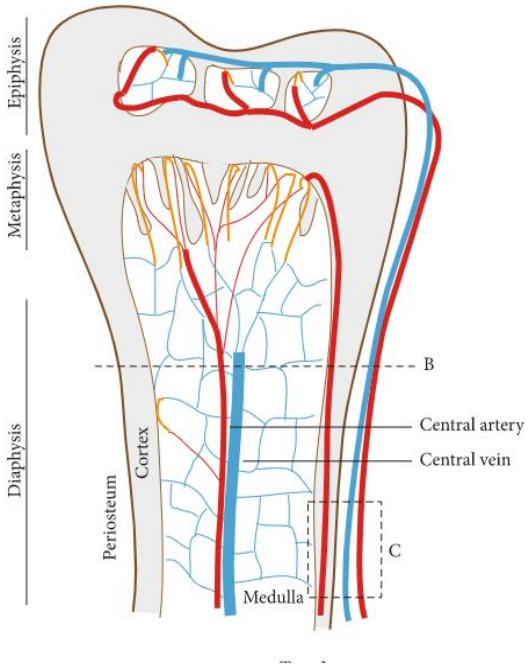


***Figure 29: Diagram showing the blood vessel arrangement in the bone.***

*Long bones are subdivided into three main regions known as epiphysis, metaphysis, and diaphysis. In the metaphysis of the bone, arteries branch into smaller arterioles and terminate in capillaries. On the other hand, the diaphyseal region is composed of sinusoidal vessels characterised by specific morphological, molecular and functional criteria. Image taken from "Structure and Functions of Blood Vessels and Vascular Niches in Bone", by Saravana K. Ramasamy, Stem Cells International, 2017 (286).*

Analysis of the bone marrow vasculature of our Rosa Cre BMP10 iKO revealed a highly disorganised bone marrow network restricted to the sinusoidal vessels of the bone diaphyseal area **(Figure 30)**.

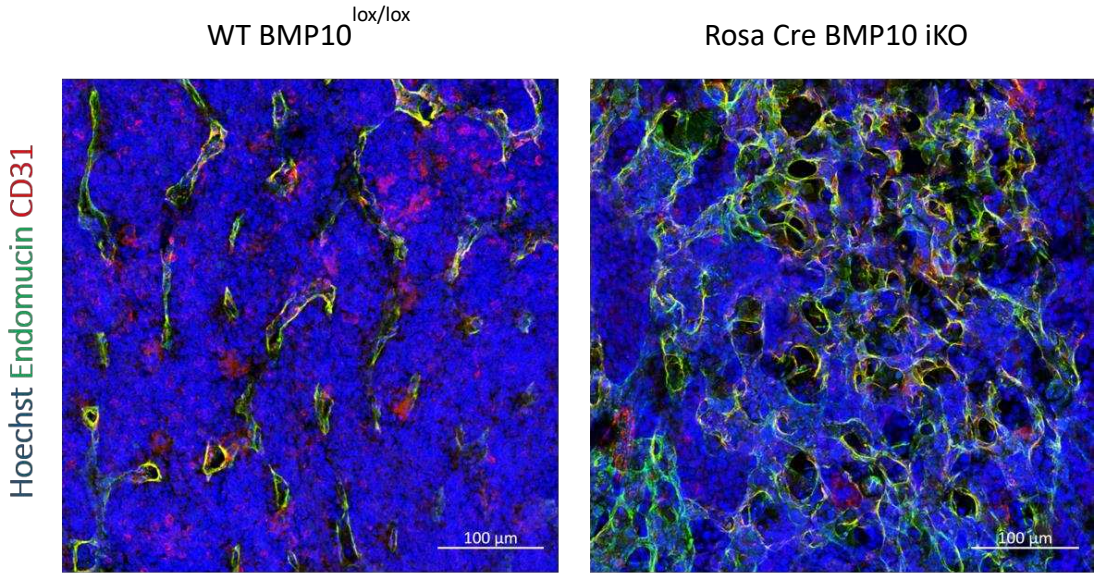


***Figure 30: Increase and dilation of diaphyseal sinusoidal vessels in Rosa Cre BMP10 iKO.***

*Representative maximum-intensity projections confocal images of WT* Bmp10$^{lox/lox}$*(left) vs Rosa Cre BMP10 iKO (right) representing the vascular bed of the diaphysis in the bone marrow stained with Endomucin /CD31/Hoechst showing an increase in vascularization and a vessel hyper dilation in the bone marrow.*

Additionally, flow cytometric data revealed a significant increase in Endomucin (Emcn)$^+$/CD31$^+$ in both percentages and total number of cells **(Figure 31)** (even though the total bone marrow cells in the Rosa Cre BMP10 iKO was significantly reduced).

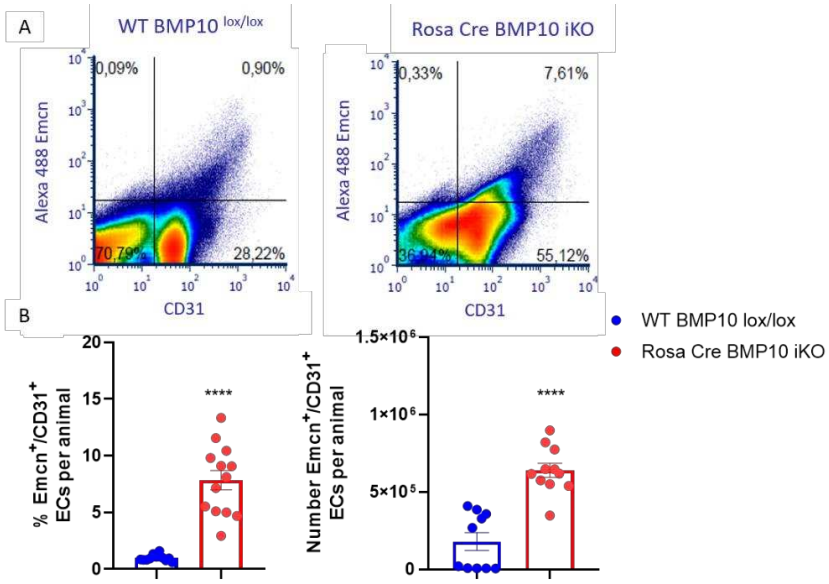


***Figure 31: Increase of bone marrow Emcn$^+$CD31$^+$ endothelial cells in Rosa Cre BMP10 iKO.***

*(A) Representative flow cytometry pseudocolor graph showing Emcn$^+$CD31$^+$ ECs in total bone marrow cells digested with collagenase at P20 for WT Bmp10$^{lox/lox}$ controls (left) vs iKO Bmp10 (right). Gate settings exclude dead cells from the analysis. (B) Relative quantification expressed as percentage of Emcn$^+$CD31$^+$ cells and respective number of Emcn$^+$CD31$^+$ per animal based on total cell count. Data is expressed as mean ± SEM. Mann-Whitney tests were used to asses statistical significance (ns p-value > 0.05; * p-value ≤ 0.05; ** p-value ≤ 0.01; *** p-value ≤ 0.001; **** p-value ≤ 0.0001).*

These findings strengthen our hypothesis that BMP10 alone could be a critical factor for the vasculature maintenance of bone marrow capillaries and that, in its absence, the vasculature of the bone marrow could not develop properly thus indirectly affecting the maintenance and formation of haematopoietic stem and progenitor cells.

## 3. Rosa Cre BMP10 iKO phenotype does not coincide with loss of activity and cannot be reproduced by blocking ALK1 receptor

In an attempt to study the development of the vasculature phenotype and whether it coincided with loss of circulating BMP10 activity, we performed a kinetic study where we retrieved long bones for immunofluorescence and plasma at different time points to measure circulating BMP10/ALK1-induced activity from animals injected with tamoxifen. For this study, we induced deletion of BMP10 from P9 to P11 and sacrificed the animals at P12, P15, P17 and P19-P20 to start gathering more information on the mechanistics leading to the observed phenotype. We observed that the vasculature phenotype was already apparent at P12 (one-day after last tamoxifen injection) however, at that time point, the animals were still not devoid of circulating BMP10 **(Figure 32)**. Such a strikingly fast phenotype that did not coincide with loss of BMP10 was a first warning that the observed phenotype did not actually result from loss of the ligand.

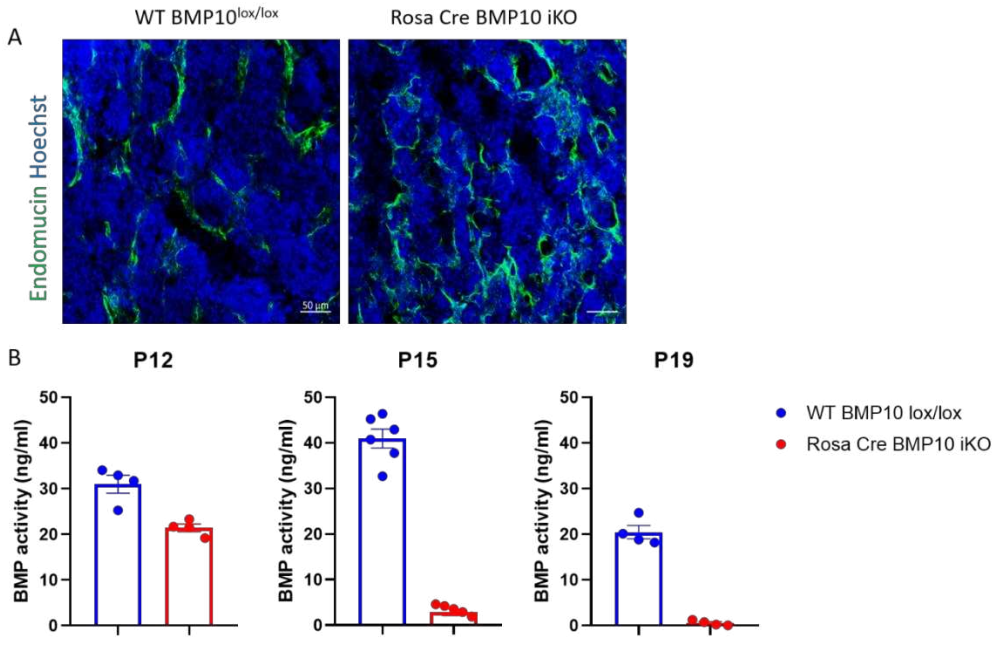


***Figure 32: Rosa Cre BMP10 iKO mice revealed the bone marrow vascular phenotype at P12 when there is still circulating BMP10 activity.***

*(A) Representative maximum-intensity confocal images of P12 bone marrow showing Emcn+ sinusoidal vessels (green) of WT* BMP10$^{lox/lox}$ *(left) vs Rosa Cre BMP10 iKO (right) of pups injected with tamoxifen from P9-P11. (B) Relative BMP activity measured in the plasma using BRE assay of WT* BMP10$^{lox/lox}$ *(blue) vs Rosa Cre BMP10 iKO (red) of P12 pups, P15 and P19. Data is expressed as mean ± SEM. Mann-Whitney tests were used to asses statistical significance (ns p-value > 0.05; * p-value ≤ 0.05; ** p-value ≤ 0.01; *** p-value ≤ 0.001; **** p-value ≤ 0.0001).*

Additionally, we performed a study where we singularly blocked ALK1 receptor and BMP10 ligand at P9 using neutralising antibodies. Unexpectedly, neither by blocking the receptor nor the ligand did the animals phenocopied the vascular and haematopoietic defect observed in R26 CreERT2 BMP10 iKO model (Figure 33).

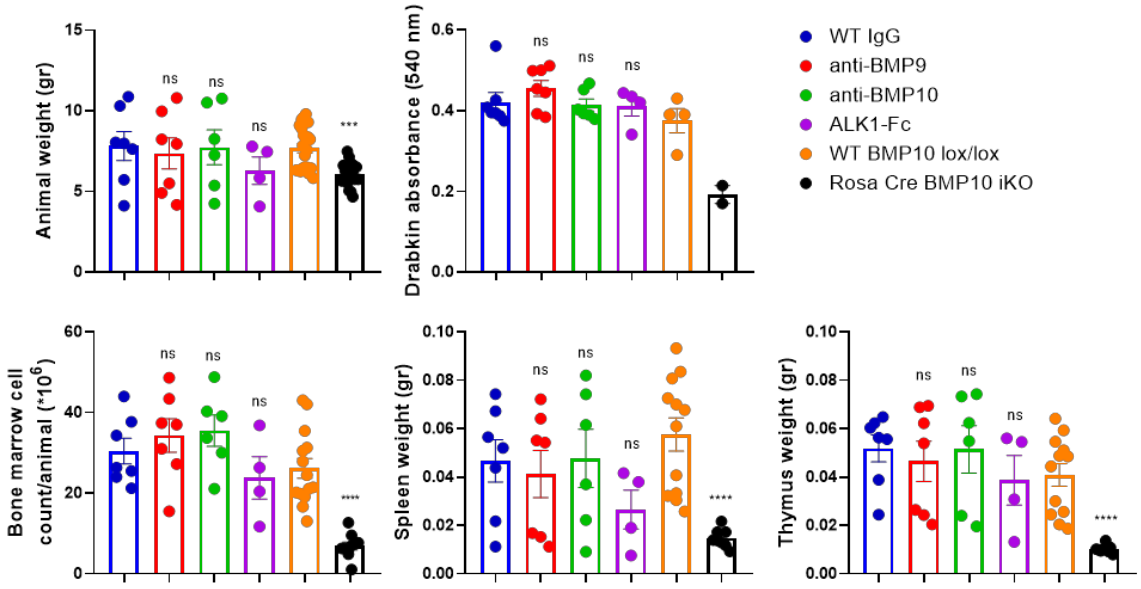


***Figure 33: Injecting neutralising antibodies against either BMP9, BMP10 or ALK1 did not phenocopied hematopoietic defect observed in Rosa Cre iKO BMP10.***

*Relative quantifications for (A) total animal weight, (B) drabkin absorbance (540 nm), (C) total count of bone marrow cells per animal (digested with collagenase), (D) spleen weight and (E) thymus weight of animals at P19-P20. Represented WT IgG injected at P9 (blue), anti-BMP9 injected at P9 (red), anti-BMP10 injected at P9 (green), ALK1-Fc injected at P9 (purple), WT* $Bmp10^{lox/lox}$ injected with tamoxifen from P9 to P11 *(orange) and Rosa Cre iKO BMP10 (black) animals* injected with tamoxifen from P9 to P11. *Injection dosages for IgG CTL dosage 10 mg/Kg, anti-BMP10 5 mg/kg, anti BMP9 10 mg/kg, ALK1-Fc 5 mg/kg. Tamoxifen injection for WT BMP10 lox/lox and Rosa Cre BMP10 iKO 75 mg/kg. Data is expressed as mean ± SEM. Mann-Whitney tests were used to asses statistical significance (ns p-value > 0.05; * p-value ≤ 0.05; ** p-value ≤ 0.01; *** p-value ≤ 0.001; **** p-value ≤ 0.0001).*

Although we tried to find reasons behind these observed results, they were somehow worrisome, especially the lack of phenotype observed by blocking ALK1. This led us to question whether the phenotype that we were studying was actually not a result from BMP10 deletion but an artefact due to Cre toxicity instead.

A PubMed search for Cre toxicity in the Rosa CreERT2 model, led us to discover a paper published from in 2009 from Journal of Immunology in which the authors described a phenotype highly similar to that one we were observing in the Rosa Cre BMP10 iKO. In particular, they revealed a direct hematological effect due to the activation of R26CreERT2 regardless of floxed gene on both adults and embryo. For that, we generated the missing

control group harboring R26CreERT2 without *Bmp10*$^{lox/lox}$ and we repeated all our analysis on control mice to assess whether or not the described phenotype was a result of BMP10 deletion or an artefact due to aberrant Cre recombination. Indeed, we could confirm that the observed phenotype was not resulting from the deletion of BMP10 as our control group R26CreERT2 without *Bmp10*$^{lox/lox}$ exhibited the same phenotype as the Rosa Cre iKO BMP10 group.

Indeed, while the issue of Cre toxicity has been documented over the years, it still seems to be generally disregarded in the field of vascular biology. For that, we proposed to publish these finding of the R26CreERT2 toxicity, which, despite being similar to the publication from 2009, it still brings new information and a fresher point of view on this overlooked matter. Nonetheless, it seems that we are not the only group that stumbled upon this problem and that other teams are starting to report it. It is strongly advisable to include CreERT2 controls injected with tamoxifen in all the experiments. Next, the manuscript submitted to Scientific Reports journal was included.

# Warning regarding toxicity of tamoxifen activated CreERT2 in young Rosa26CreERT2 mice: Cre positive controls without a floxed allele are necessary

Martina Rossi[1], Nicolas Chaumontel[1], Sabine Bailly[1], Emmanuelle Tillet[1*], Claire Bouvard[1*#]

1 Laboratory BioSanté U1292, Univ. Grenoble Alpes, INSERM, CEA, F-38000, Grenoble, France.

*equal contributions

#corresponding author

claire.bouvard@univ-grenoble-alpes.fr
U1292 Biosanté CEA/INSERM/UGA
17 rue des Martyrs - Bat C3
38054 Grenoble Cedex, FRANCE
tel: (33) 04 38 78 42 25
Fax: (33) 04 38 78 50 58

## Abstract

The Cre-lox system is a versatile and powerful tool used in mouse genetics. It allows spatial and/or temporal control of the deletion of a target gene. The Rosa26-CreERT2 (R26CreERT2) mouse model allows ubiquitous expression of CreERT2. Once activated by tamoxifen, CreERT2 will enter the nuclei and delete floxed DNA sequences. Here we show that intraperitoneal injection of tamoxifen in young R26CreERT2 mice leads to morbidity and mortality within 10 days after the first injection, in the absence of a floxed allele. Activation of CreERT2 by tamoxifen led to severe hematological defects, with anemia and a strong disorganization of the bone marrow vascular bed. Cell proliferation was significantly reduced in the bone marrow and the spleen resulting in the depletion of several hematopoietic cells. However, not all cell types or organs were affected to the same extent. We realize that many research groups are not aware of the potential toxicity of Cre recombinases, resulting in misinterpretation of the observed phenotype and in a waste of time and resources. We discuss the necessity to include tamoxifen injected CreERT2 controls lacking a floxed allele in experimental designs and to improve communication about the limitations of Cre-lox mouse models among the scientific community.

# Introduction

Genetically modified mice are commonly used in research, as animal models of human diseases or in order to elucidate the activity and function of genes *in vivo*. However, there are several hidden pitfalls one can encounter when using some of these models. This can lead to misinterpretation of the results and wrongful use of the animals. Here we report that tamoxifen injection in young Rosa26-CreERT2 (R26CreERT2) pups (P9 to P11) in the absence of a floxed allele leads to severe toxicity and mortality.

The Cre-lox system is based on the ability of the bacteriophage P1 Cre-recombinase to catalyze the cleavage of a DNA sequenced flanked by loxP sites. The expression of the CRE recombinase can be under the control of a promoter that is active in a specific cell type or tissue, allowing tissue-specific deletion of the target gene (referred to as spatial regulation), or it can be under the control of a promoter allowing ubiquitous expression of the Cre, and therefore ubiquitous deletion of the target gene. More recently, temporal regulation of the deletion of the target gene has been achieved using a Cre recombinase fused to a modified ligand binding domain of the estrogen receptor. This resulting CreERT binds to tamoxifen or 4-hydroxytamoxifen (4-OHT), but not to estradiol [1]. The CreERT is present in the cytoplasm, and bound to heat shock proteins. When synthetic steroids (such as tamoxifen or 4-OHT) are administered, binding of CreERT to HSP90 is disrupted, allowing for steroid-mediated CreERT translocation into the nucleus, where it will recognize and excise floxed DNA sequences [2]. The CreERT2 was generated after the CreERT in order to increase the efficiency of the tamoxifen or 4-OHT induction [3]. These models are useful to circumvent developmental lethality. Several transgenic mouse lines expressing CreERT2 under the control of a ubiquitous or tissue specific promoter have been generated. In our case we needed a tamoxifen-inducible deletion in the whole body to study a gene that is required during development and expressed in several tissues and cell types. This can be achieved with the R26CreERT2 model, where CreERT2 is inserted into the Rosa26 locus, which is widely used for constitutive ubiquitous expression in mice [4,5].

The potential side effects associated with tamoxifen administration are usually known and taken into account and tamoxifen-treated controls are commonly used [6]. However, it appears that the scientific community is not well aware of potential off-target effects due to Cre recombinase activity by itself, and Cre-positive controls without floxed alleles are lacking from most publications, including from our group. Mammalian genomes contain recombinase recognition sites called cryptic or pseudo loxP sites, which can be cleaved by Cre recombinase [7,8]. Cre expression in mammalian cells can cause DNA damage and reduce proliferation [9]. Steroid-inducible Cre recombinases were initially thought to be safer than constitutive Cre [10], but it has been reported that tamoxifen activation of CreERT2 in adult mice resulted in cleavage of cryptic loxP sites, chromosomal abnormalities and transient hematologic toxicity [11]. In adult mice this toxicity is tolerated and animals can quickly recover. We previously showed that complete blood counts and blood chemistry panel of adult tamoxifen injected R26CreERT2 mice were

normal [12]. However, the effects on young pups have not been reported. In the present study, WT and R26CreERT2 pups received intraperitoneal (IP) injections of tamoxifen from P9 to P11. We show that induction of CreERT2 by tamoxifen in young R26CreERT2 mice leads to severe toxicity, in the absence of a floxed target gene. We observed morbidity and mortality within ten days after the first injection. The pups stop gaining weight and present hematological defects with severe anemia and disorganization of the bone marrow vascular bed. We realized that many groups are still not aware of this problem and waste time and resources investigating a phenotype that is not due to the loss of the target gene, but that is caused by the recombinase itself. Many published studies using Cre/loxP transgenic mouse models do not include Cre-positive controls lacking the targeted floxed DNA sequence, and thus may have attributed roles to a target gene that were in fact due to Cre toxicity in part or entirely. We present here the toxic side effects observed and discuss the necessity to include appropriate controls in experimental designs and to report and communicate about the limitations related to transgenic models.

# Results

## Tamoxifen-induced CreERT2 activation in R26CreERT2 pups affects weight gain and survival with severe defects in hematopoietic organs

Without tamoxifen injection, R26CreERT2 and their WT littermates survive and grow normally and no obvious toxicity is observed (data not shown). However, when tamoxifen was injected IP (75 mg/kg) for 3 consecutive days from postnatal day 9 (P9) to P11, we could observe that R26CreERT2 animals stopped gaining weight after P15, which was not the case for their tamoxifen injected WT littermates (Fig. 1a-b). This effect did not seem to be sex-specific as male and female mice were both affected (Fig. S1a). Therefore male and female pups were pooled in all the other figures of the manuscript. Animal survival was affected in the R26CreERT2 group, as 25 percent of the mice were dead at P19 (Fig. S1b). The remaining mice were not healthy, some of them presenting diarrhea, therefore the animals had to be euthanized at the latest at P20 in accordance with ethical guidelines. Autopsy revealed that the major hematopoietic organs were strongly affected in tamoxifen injected R26CreERT2, in comparison with tamoxifen injected WT littermates: Bone marrow looked pale (Fig. 1c) with a reduced cell number although bone size was not affected (Fig. 1d). Spleen and thymus were significantly smaller (Fig. 1c-d). In addition, the color of the intestines was abnormal, with the presence of gas (Fig. S1c). Tamoxifen-injected WT mice were healthy, indicating that the observed phenotype was not induced by tamoxifen alone, but by the activation of CreERT2 by tamoxifen.

## Tamoxifen-induced CreERT2 activation in R26CreERT2 pups affects several blood cellular components and leads to severe anaemia

Analysis of the whole blood at P19 (Fig. 2 and table S1) revealed that activation of CreERT2 by tamoxifen leads to severe anemia, as red blood cell count (RBC), hemoglobin (HGB) and haematocrit (HCT) were strongly decreased. Reticulocytes (RBC precursors) were also totally depleted, indicating no compensatory blood cell production in order to reduce anemia. White blood cell count (WBC) was also significantly decreased. Within the WBC population, lymphocytes and neutrophils were depleted while monocytes were not. Platelet levels (PLT) of R26CreERT2 mice were not different from WT controls. Together, these results support that tamoxifen activation of CreERT2 strongly affects several specific blood cellular components.

## Tamoxifen-induced CreERT2 activation in pups affects several hematopoietic lineage-restricted precursors in bone marrow and spleen

Cells found in the blood result from the differentiation of precursors that are present in the bone marrow and in the spleen. We used flow cytometry to quantify several precursors: $Ter119^{+}CD71^{+}$ erythroblasts (precursors for reticulocytes and then red blood cells), $B220^{+}CD19^{+}$ B cell precursors and $CD11b^{+}Gr\text{-}1^{+}$ myeloblasts (precursors for granulocytes and monocytes). In line with the results obtained from the blood samples, we observed that erythroblasts were totally depleted in the bone marrow and spleen of tamoxifen treated R26CreERT2 mice, compared to tamoxifen treated WT littermates, both as a percentage of cells and as a number of erythroblasts per mouse (Fig. 3 and supplementary figure S2). B cell precursors were significantly reduced in both bone marrow and spleen, both as a percentage of cells and as a number of B cell precursors per animal (Fig. 3b and S2). The percentage of myeloblasts in the total cell population was decreased in the spleen but increased in the bone marrow, probably because of the loss of other cell types in the bone marrow (Fig. 3c and S2). The number of myeloblasts per animal was significantly reduced in the spleen, but the reduction was not statistically significant in the bone marrow (Fig. 3c and S2).

## Tamoxifen-induced CreERT2 activation in R26CReERT2 pups results in a strong disorganization of BM sinusoidal vessels

Haematopoietic and endothelial cells of the bone marrow are tightly linked from early development through the adulthood. The vascular niche supports hematopoiesis in the bone marrow [13,14]. In order to assess the state of the bone marrow vasculature, P19 femur sections were stained with an antibody against endomucin (Emcn), a marker expressed by venous and capillary endothelial cells. The vascular network of the diaphysis of the bone marrow of tamoxifen-treated R26CreERT2 mice was dramatically disorganized, while no obvious defects were observed in the column-like vessels of the metaphysis (Fig. 4a). In the diaphysis, several areas of the bone marrow were devoid of hematopoietic cells, appearing as black holes in the

images (Fig. 4a-b), while the vascular area in the bone marrow was strongly increased, with dilated sinusoids forming an abnormal network (Fig. 4b-c).

### Tamoxifen-induced CreERT2 activation decreases proliferation in the bone marrow and spleen of R26CreERT2 pups

It has been shown previously that Cre can reduce proliferation [9]. To assess proliferation in our pups, we performed an Edu incorporation assay at P17. We observed a strong reduction of proliferation in hematopoietic organs such as the spleen and the bone marrow of tamoxifen-treated R26CreERT2 mice, compared to tamoxifen-treated WT controls (Fig. 5). This decreased cell proliferation in hematopoietic organs could explain why several precursors and cell types are depleted in these organs and in the blood. We also analyzed other tissues, such as intestine liver or lung, but we found no obvious differences in cell proliferation between R26CreERT2 and WT mice in these organs (Fig. S3).

### Tamoxifen-induced CreERT2 activation increases the number of CD41+ megakaryocytes in the bone marrow of R26CreERT2 pups

Interestingly, CreERT2 activation did not affect platelet counts in blood, whereas WBC and RBC counts were strongly reduced. We thus wanted to study megakaryocytes (MK), which are responsible for producing platelets. Immunostaining of the bone marrow using an anti CD41 antibody to identify cells from the megakaryocytic lineage revealed an increase in the number of CD41+ cells in R26CreERT2 tamoxifen treated mice, compared to WT tamoxifen treated controls (Fig. 6).

## Discussion

The Cre/lox recombinase system has several advantages, including the ability to control Cre expression spatiotemporally through the use of mouse models whose genome can be constitutively or inducibly altered (temporal control) either ubiquitously or in a specific subset of cells (spatial control). It is thus a highly versatile tool for studying gene function. Nonetheless, this system has some limitations. In particular, the potential risks of Cre recombinase toxicity, which appears to be widely ignored. Our results show that administration of tamoxifen to R26CreERT2 pups, in absence of a targeted floxed allele, is toxic. Within few days after tamoxifen injection, these pups stop gaining weight and present severe anemia and diarrhea, with a significant reduction in spleen and thymus weight and hypocellular bone marrow. Some mortality is observed and the remaining mice have to be euthanized for ethical reasons ten to twelve days after the first tamoxifen injection. This toxicity is not due to tamoxifen, as it is not observed in tamoxifen treated WT mice, and it is not due to the presence of CreERT2 alone, as it is not observed in non-injected R26CreERT2 mice. In fact, it is due to

the induction of CreERT2 by tamoxifen. Our results in pups are in accordance with previous reports showing anemia in adult mice or embryos [11,15]. However, we show here that the phenotype is more severe in pups than in adults as it leads to premature mortality. Analysis of these animals revealed that several lineage-restricted precursors in bone marrow and spleen were significantly depleted and proliferation in these organs was strongly reduced. Interestingly, not all precursors were affected to the same extent. Erythroblasts seemed to be more affected than B cell precursors and myeloblasts. In blood, the numbers of red blood cells and white blood cells were strongly reduced, while platelet counts were unchanged compared to WT littermates. Cell proliferation was dramatically reduced in bone marrow and spleen, but not in other tissues such as intestines, lung or liver. Overall, it seems that although CreERT2 is ubiquitously expressed in the R26-CreERT2 model, some tissues and cell types are more sensitive than others. In particular, the bone marrow is extremely sensitive. During the first three to four weeks after birth, long bones expand rapidly, blood vessels start to form morphologically distinct capillary networks, and hematopoietic cells proliferate to cope with growth in blood and marrow volume. In the metaphysis, the capillaries form column-like structures that support bone growth and in the diaphysis a dense vascular network of sinusoids is formed, surrounded by proliferating hematopoietic cells. At 3-4 weeks, bone growth decelerates, the main structures are established and hematopoietic stem cells transition into a hibernating state [14,16–19]. In tamoxifen-injected R26CreERT2 pups, no obvious defect was observed in bone growth and columnar capillaries of the metaphysis seemed normal. However, in the bone marrow, in addition to a reduction in overall proliferation and number of hematopoietic cells, the sinusoids were completely disorganized, with an increased vascular area and enlarged lumens. The observed vascular defect could be a consequence of the depletion of hematopoietic cells in the bone marrow, or could be directly caused by recombinase toxicity. This disorganization of the vascular bed can in turn have effects on the surrounding cells in the bone marrow. Interestingly, the number of megakaryocytes, which produce platelets, was increased. It has been shown that the majority of the MK reside directly at the sinusoid BM, and it was proposed that the vasculature could dictate the distribution of MK in the BM [20]. The hypervascularization observed upon CreERT2 activation could therefore support MK stability, explaining why we find more MK in the BM of tamoxifen injected R26-CreERT2 mice. It is also possible that levels of activated CreERT2 are lower in MK or that they are more resistant to DNA damage caused by recombinase than other hematopoietic cell types. The effect on the blood vessels of the BM and on MK has not been reported in previous studies on R26CreERT2 mice.

Other models with ubiquitous expression of CreERT or CreERT2 are available. Tamoxifen administration to Ubc-CreERT and CAG-CreERT2 mice led to anemia and reduction of cellularity of bone marrow and spleen. This was attributed to the deletion of the floxed target gene, but it could in fact be due to recombinase toxicity [21,22]. The results of these studies should be reanalyzed with tamoxifen treated Cre positive controls lacking floxed genes. Cre toxicity has also been reported in tissue specific models. Cre expression in postmeiotic spermatids, under the control of protamine 1 *Ptm1* promoter, results in sterility due to illegitimate

chromosome rearrangement [23]. DNA damage and tetraploidy was observed in the epidermis of keratin5 and keratin14 promoter –driven Cre expressing mice [24]. Cre recombinase cardiotoxicity has also been reported in constitutive or inducible models using the α-myosin heavy chain (αMHC) promoter [25,26]. Glucose intolerance has been reported in pancreatic beta cell specific RIP-Cre mice, which raised concerns in the field of diabetes and suggested to revisit the conclusions of many studies that did not include Cre controls [10]. Toxicity has also been described in T cell specific models [27,28]. However, the discovery of Cre toxicity in one field does not necessarily come to the attention of researchers from other fields. In the field of angiogenesis, a recent letter from 2020 showed that tamoxifen-activated CreERT impairs retinal angiogenesis in neonates, independently of gene deletion [29]. This publication should entice researchers to start including Cre positive controls, which is not the current practice at least in the field of vascular development.

One way of avoiding misinterpretation is to be aware of the limitations of the model used. The risk of Cre toxicity having an impact on the study can depend on the recombinase and promoter used, genetic background, developmental stage, cell type or organ of interest, and on the protocol for tamoxifen administration (route, dose, frequency). Indeed, young mice seem more sensitive than adults. Differences in Cre toxicity among different cell types or organs can depend on the expression level of the recombinase, but also on tamoxifen biodistribution and concentration in the cell or organ of interest (for inducible models) [26,28,30]. It is necessary to report these off-target effects for each strain and each protocol and to communicate among researchers. These studies should be referenced in the mouse genome informatics database. Although some companies give general guidelines about the Cre/lox system, they should also directly warn customers that are purchasing a specific mouse strain in which Cre toxicity has been reported.

Different ways to reduce toxicity have been proposed, such as the use of self-deleting Cre expression vectors [31] or optimization of the protocol to find the lower possible dose of tamoxifen that allows efficient target gene deletion. But more importantly, appropriate Cre positive controls should be used, especially with young mice. With Cre/lox transgenic models, a very common breeding scheme is to cross mice homozygous for the loxP-flanked allele and heterozygous for the Cre transgene with mice homozygous for the loxP-flanked allele but lacking the Cre transgene. Half of the progeny will be Cre positive, the other half will be Cre negative and all will be homozygous for the loxP-flanked allele. It is especially convenient when working with pups, as controls and mutants come from the same parents and can be analyzed simultaneously. Adding a Cre positive control lacking a floxed allele can be complicated, and increases the overall number of mice used, however it has to be tested in order to avoid misinterpretation. Our work support that it is essential for young R26-CreERT2. Firstly because of the hematopoietic toxicity. Secondly because even if the cell type of interest does not show DNA damage, anemia and poor overall health could have an effect on the biological system of interest.

The use of animals in research is tightly regulated and the 3Rs rule (Replacement, Reduction, and Refinement) is one of the most important ethical principles. Although adding a Cre control group can increase the number of animals in a specific experiment, we believe that it can be necessary to answer the research question accurately. Moreover, reporting Cre toxicity issues and improving communication should reduce the overall number of animals used by preventing repetition and misleading interpretation.

# Methods

## Mice

Rosa26-CreERT2 mice (Gt(ROSA)26Sor$^{tm2(cre/ERT2)Brn}$ ; MGI:3764519; provided by Pr P. Chambon, IGBMC, Illkirch, France) were maintained in a C57BL/6 background. The R26 locus was kept at heterozygosity for the CreERT2 knock-in in all experiments. The offspring genotypes were determined by PCR as previously reported [32], Cre positive (R26CreERT2) and Cre negative (WT) mice were obtained in Mendelian proportions (1:1). Without tamoxifen injection, these mice were viable and fertile. To induce CreERT2 activation, pups received daily intraperitoneal (IP) injections of tamoxifen (T5648, Sigma) diluted in corn oil for 3 consecutive days from postnatal day 9 to postnatal day 11 at a dosage of 75 mg/kg, as recommended by the Jackson laboratory. R26creERT2 and WT control littermates were injected with tamoxifen and monitored simultaneously. Body weight was recorded every day during the injection period and then on alternate days until the day of euthanasia. Euthanasia was performed using an intraperitoneal injection of pentobarbital 180 mg/kg. Upon sacrifice, bones, spleen, and thymus were dissected and weights of spleen and thymus were recorded. Mice were housed in a pathogen-free barrier facility, under 14-hour light / 10-hour dark cycle and temperature-controlled environment with access to a standard diet and water ad libitum. All animal experiments were performed in accordance with the relevant guidelines and regulations of Directive 2010/63/EU of the European Parliament on the protection of animals used for scientific purposes and the protocols were approved by an institutional ethics committee (CEtEA, CEEA44) and the study is reported in accordance with ARRIVE guidelines.

## Complete blood count analysis

Mice received an IP injection of pentobarbital 180 mg/kg and blood was collected by cardiac puncture in an EDTA-coated tube and analyzed on a Procyte Dx hematological analyzer (Idexx) within 2h after sampling.

## Flow cytometric analysis

Bone Marrow (BM) single cell suspensions were obtained as described by Amend et al33. Briefly, bones (femur and tibiae) were isolated, the metaphysis were cut and pooled bones of each mice were centrifuged at 5000 rpm for 30 sec in a 0.5 mL tube with a perforated bottom placed into 1.5 mL tube. Collected cell pellets were resuspended in 1 ml ice-cold HBSS. Spleens were mechanically dissociated using a sterile plunger in 1mL of ice-cold HBSS. BM and spleen cell suspensions were filtered through a 70 µm strainer. Red blood cells were lysed by the addition of RBC lysis buffer (Biolegend) and incubated on ice for 10 min. Cells were washed and resuspended in HBSS supplemented with 5 mM EDTA, 1% Fetal calf serum at 20 million cells/ml. Fc receptors were blocked by incubation with TruStain FcX PLUS (Biolegend) and 50 µl of cells were stained at 4°C with the following conjugated antibodies CD71-PE (clone RI7217), Ter119-FITC (clone TER-119); Gr-1-PE (clone RB6-8C5), CD11b-FITC (clone M1/70); CD19-PE (clone 6D5), B220-FITC (clone RA3-6B2). All antibodies were from Biolegend and used at the recommended concentrations. Cells were stained with DAPI for dead cell exclusion. Cells were analyzed on a FACSMelody flow cytometer and data was analyzed with the FlowJo software.

## Bone sample preparation

Mice were sacrificed either at postnatal day 17 for proliferation assay or at postnatal day 19 for bone vasculature structure assessment and prepared for immunofluorescence analysis as described by Kusumbe et al [34]. Freshly dissected long bones were fixed in 10% formalin solution (HT5011, Sigma) for 4 hours followed by decalcification in 0.5M EDTA for 24 hours under gentle agitation at 4°C. Bones were then washed in PBS and incubated in 20% sucrose and 2% PVP in PBS for 24h at 4°C. Bones were embedded in 8% gelatin, 20% sucrose 2% PVP in PBS and stored at -80°C for at least 24 hours prior to sectioning.

## Imunostaining and confocal imaging

Embedded bones were sectioned at 100 µm thickness using microtome cryostat from Leica (CM3050 S). Sections were hydrated using PBS and permeabilized using 0.5% Triton-X100 in PBS for 15 minutes at room temperature (RT). Samples were then incubated in blocking solution (0.3% Triton, 1% BSA, 2% donkey serum in PBS) for 30 min at RT prior to primary antibody staining. Primary antibodies were diluted in blocking solution, incubated O/N at 4 °C. Species-specific secondary antibodies (Jackson) diluted in blocking buffer were added and incubated for 2-3 hours at RT. Nuclei were stained with Hoechst (1/1000 in PBS) and mounted using FluorSave mounting media. The following primary antibodies were used: rat monoclonal anti-Endomucin (sc-65495, Santa Cruz, diluted 1/200), goat polyclonal anti-CD31 (AF3628,

R&D, diluted 1/100), rat monoclonal CD41 FITC-conjugated (MWReg30, Biolegend, diluted 1/50). All secondary antibodies were from Jackson ImmunoResearch and diluted 1/200. Images were acquired using a LSM 880 Airyscan Confocal microscope (Zeiss), and processed and analyzed using Zen (Zeiss) and Fiji softwares.

## Proliferation assay *in vivo*

EdU from Click-iT EdU Alexa-555 imaging Kit (C10638, Thermofisher Scientific) was prepared at 2.5 mg/ml in PBS. Seventeen-day old mice received an intraperitoneal injection of of EdU (0.3 mg per mouse). Mice were euthanized 3 hours later and femurs, spleen, intestine, lung and liver were harvested for immunofluorescence analysis. Bone samples were processed as described above. Spleen samples were fixed in 10% formalin solution (HT5011, Sigma) for 4 hours followed by overnight (O/N) at 4ºC in a 15% sucrose in PBS. The following day spleen samples were placed into a 30% sucrose in PBS O/N at 4ºC and subsequently mounted in OCT embedding compound and stored at -80 °C. Intestines, lung and liver were fixed in 4% paraformaldehyde O/N at 4ºC and were dehydrated and embedded in paraffin. Sections were prepared at 10 µm thickness. Click-iT EdU Alexa-555 imaging kit was used as recommended by the manufacturer (C10638, Thermofisher Scientific ). Nuclei were stained with Hoechst 33342 (1/1000). Anti-endomucin antibody (sc-65495, Santa Cruz, diluted 1/200) was used to stain vessels in bone marrow and spleen. WGA-FITC lectin (W834 Invitrogen, 5 µg/mL) was used to stain glycoconjugates in intestines, lung and liver. Images were acquired using a LSM 880 Airyscan Confocal microscope (Zeiss), and processed and analyzed with Zen (Zeiss) and Fiji softwares. The number of Edu positive nuclei and the number of total nuclei stained with Hoechst were analyzed using Fiji. For each mouse, three images per organ were analyzed and the average of the three different measurements was used for statistical analysis.

## Statistical analysis

Statistical analysis was performed using GraphPad Prism software to assess differences between WT and R26CreERT2 mice. Two-way analysis of variance (ANOVA) was used for weight curve analysis, Log-rank Mantel cox test was used to analyze survival curves and Mann Whitney test was used for all other graphs. Differences were considered statistically significant for $p<0.05$. All data is presented in mean ± SEM unless indicated.

# References


1. Feil, R., Wagner, J., Metzger, D. & Chambon, P. Regulation of Cre Recombinase Activity by Mutated Estrogen Receptor Ligand-Binding Domains. *Biochem. Biophys. Res. Commun.* **237**, 752–757 (1997).
2. Feil, R. *et al.* Ligand-activated site-specific recombination in mice. *Proc. Natl. Acad. Sci. U. S. A.* **93**, 10887–10890 (1996).
3. Indra, A. K. *et al.* Temporally-controlled site-specific mutagenesis in the basal layer of the epidermis: comparison of the recombinase activity of the tamoxifen-inducible Cre-ERT and Cre-ERT2 recombinases. *Nucleic Acids Res.* **27**, 4324–4327 (1999).
4. Soriano, P. Generalized lacZ expression with the ROSA26 Cre reporter strain. *Nat. Genet.* **21**, 70–71 (1999).
5. Hameyer, D. *et al.* Toxicity of ligand-dependent Cre recombinases and generation of a conditional Cre deleter mouse allowing mosaic recombination in peripheral tissues. *Physiol. Genomics* **31**, 32–41 (2007).
6. Zhong, Z. A. *et al.* Optimizing tamoxifen-inducible Cre/loxp system to reduce tamoxifen effect on bone turnover in long bones of young mice. *Bone* **81**, 614–619 (2015).
7. Thyagarajan, B., Guimarães, M. J., Groth, A. C. & Calos, M. P. Mammalian genomes contain active recombinase recognition sites. *Gene* **244**, 47–54 (2000).
8. Semprini, S. *et al.* Cryptic loxP sites in mammalian genomes: genome-wide distribution and relevance for the efficiency of BAC/PAC recombineering techniques. *Nucleic Acids Res.* **35**, 1402–1410 (2007).
9. Loonstra, A. *et al.* Growth inhibition and DNA damage induced by Cre recombinase in mammalian cells. *Proc. Natl. Acad. Sci.* **98**, 9209–9214 (2001).
10. Lee, J.-Y. *et al.* RIP-Cre revisited, evidence for impairments of pancreatic beta-cell function. *J. Biol. Chem.* **281**, 2649–2653 (2006).

11. Higashi, A. Y. *et al.* Direct Hematological Toxicity and Illegitimate Chromosomal Recombination Caused by the Systemic Activation of CreER $^{T2}$. *J. Immunol.* **182**, 5633–5640 (2009).
12. Bouvard, C. *et al.* Different cardiovascular and pulmonary phenotypes for single- and double-knock-out mice deficient in BMP9 and BMP10. *Cardiovasc. Res.* **118**, 1805–1820 (2022).
13. Morrison, S. J. & Scadden, D. T. The bone marrow niche for haematopoietic stem cells. *Nature* **505**, 327–334 (2014).
14. Sivaraj, K. K. & Adams, R. H. Blood vessel formation and function in bone. *Development* **143**, 2706–2715 (2016).
15. Naiche, L. A. & Papaioannou, V. E. Cre activity causes widespread apoptosis and lethal anemia during embryonic development. *Genes. N. Y. N 2000* **45**, 768–775 (2007).
16. Takizawa, H., Boettcher, S. & Manz, M. G. Demand-adapted regulation of early hematopoiesis in infection and inflammation. *Blood* **119**, 2991–3002 (2012).
17. Benz, C. *et al.* Hematopoietic Stem Cell Subtypes Expand Differentially during Development and Display Distinct Lymphopoietic Programs. *Cell Stem Cell* **10**, 273–283 (2012).
18. Bowie, M. B. *et al.* Hematopoietic stem cells proliferate until after birth and show a reversible phase-specific engraftment defect. *J. Clin. Invest.* **116**, 2808–2816 (2006).
19. Langen, U. H. *et al.* Cell–matrix signals specify bone endothelial cells during developmental osteogenesis. *Nat. Cell Biol.* **19**, 189–201 (2017).
20. Stegner, D. *et al.* Thrombopoiesis is spatially regulated by the bone marrow vasculature. *Nat. Commun.* **8**, 127 (2017).
21. Ding, L., Saunders, T. L., Enikolopov, G. & Morrison, S. J. Endothelial and perivascular cells maintain haematopoietic stem cells. *Nature* **481**, 457–462 (2012).

22. Wang, T. *et al.* Smc3 is required for mouse embryonic and adult hematopoiesis. *Exp. Hematol.* **70**, 70-84.e6 (2019).
23. Schmidt, E. E., Taylor, D. S., Prigge, J. R., Barnett, S. & Capecchi, M. R. Illegitimate Cre-dependent chromosome rearrangements in transgenic mouse spermatids. *Proc. Natl. Acad. Sci. U. S. A.* **97**, 13702–13707 (2000).
24. Janbandhu, V. C., Moik, D. & Fässler, R. Cre recombinase induces DNA damage and tetraploidy in the absence of loxP sites. *Cell Cycle Georget. Tex* **13**, 462–470 (2014).
25. Rehmani, T., Salih, M. & Tuana, B. S. Cardiac-Specific Cre Induces Age-Dependent Dilated Cardiomyopathy (DCM) in Mice. *Molecules* **24**, 1189 (2019).
26. Bersell, K. *et al.* Moderate and high amounts of tamoxifen in αMHC-MerCreMer mice induce a DNA damage response, leading to heart failure and death. *Dis. Model. Mech.* **6**, 1459–1469 (2013).
27. Kurachi, M., Ngiow, S. F., Kurachi, J., Chen, Z. & Wherry, E. J. Hidden Caveat of Inducible Cre Recombinase. *Immunity* **51**, 591–592 (2019).
28. Zeiträg, J., Alterauge, D., Dahlström, F. & Baumjohann, D. Gene dose matters: Considerations for the use of inducible CD4-CreERT2 mouse lines. *Eur. J. Immunol.* **50**, 603–605 (2020).
29. Brash, J. T. *et al.* Tamoxifen-Activated CreERT Impairs Retinal Angiogenesis Independently of Gene Deletion. *Circ. Res.* **127**, 849–850 (2020).
30. Donocoff, R. S., Teteloshvili, N., Chung, H., Shoulson, R. & Creusot, R. J. Optimization of tamoxifen-induced Cre activity and its effect on immune cell populations. *Sci. Rep.* **10**, 15244 (2020).
31. Pfeifer, A., Brandon, E. P., Kootstra, N., Gage, F. H. & Verma, I. M. Delivery of the Cre recombinase by a self-deleting lentiviral vector: efficient gene targeting in vivo. *Proc. Natl. Acad. Sci. U. S. A.* **98**, 11450–11455 (2001).

32. Ouarné, M. *et al.* BMP9, but not BMP10, acts as a quiescence factor on tumor growth, vessel normalization and metastasis in a mouse model of breast cancer. *J. Exp. Clin. Cancer Res. CR* **37**, 209 (2018).
33. Amend, S. R., Valkenburg, K. C. & Pienta, K. J. Murine Hind Limb Long Bone Dissection and Bone Marrow Isolation. *J. Vis. Exp. JoVE* (2016) doi:10.3791/53936.
34. Kusumbe, A. P., Ramasamy, S. K., Starsichova, A. & Adams, R. H. Sample preparation for high-resolution 3D confocal imaging of mouse skeletal tissue. *Nat. Protoc.* **10**, 1904–1914 (2015).

# Acknowledgements

We thank the staff from the animal facility and the flow cytometry facility from IRIG, the microscopy facility MuLife of IRIG/DBSCI, funded by CEA Nanobio and GRAL LabEX (ANR-10-LABX-49-01) financed within the Chemistry Biology Health (CBH) Graduate School of University Grenoble Alpes (ANR-17-EURE-0003). We thank Jenny Molet (Clinatec, CEA Grenoble) for CBC analysis, Lisa Scognamillo (Laboratory BioSanté, Univ. Grenoble Alpes, INSERM, CEA) for technical help and Laurence Petit and Thierry Jaffredo (IBPS, CNRS) for scientific discussions.

The team receives funding from : Agence Nationale de la Recherche, Grant/Award Numbers: ANR-17-CE14-0006, ANR-17-EURE-0003, ANR-20-CE14-0002-02; Association Maladie deRendu-Osler (AMRO); Commissariat à l'Energie Atomique et aux Energies Alternatives; Communauté Université Grenoble Alpes; Fondation pour la Recherche Médicale, Grant/Award Number: EQU202003010188; H2020 Marie Skłodowska-Curie Actions, Grant/Award Number: V.A.Cure-814316; Institut National de la Santé et de la Recherche Médicale

# Author contributions

MR, NC, ET and CB carried out experiments; MR, ET and CB conceived and planned experiments; MR prepared figures; CB wrote the manuscript; ET, CB and SB supervised the project, contributed to the final version of the manuscript and the funding. ET and CB contributed equally. All authors reviewed the manuscript.

# Data availability statement

Data is available upon written request to the corresponding author.

## Additional information

The authors declare no conflict of interest

## Figure legends

**Figure 1. Tamoxifen-induced CreERT2 activation in pups affects gain weight and hematopoietic organs.** (a) Experimental design for Cre ERT2 activation with tamoxifen injection. Litters are composed of WT and R26CreERT2 animals. Tamoxifen was injected IP at 75 mg/kg for 3 consecutive days from P9 to P11 and animals were euthanized at P19 or P20. (b) Weight curves of WT (n=17) and R26CreERT2 (n=27). Values are expressed as a percentage of weight gain compared to the weight at P9 (first tamoxifen injection). Two-way ANOVA with multiple comparisons was carried out to analyze differences in weight gain. (c) Representative images of femurs, spleens and thymus. 3 animals for each group are represented. Scale bar 1 cm. (d) Measurements of bone marrow cell count from two tibias and 2 femurs per animal, femur length, thymus weight, spleen weight, and number of cells per spleen (n=4-11 mice per group). Mann-Whitney tests were used to assess statistical significance between two groups in these bar graphs. * p-value ≤ 0.05; ** p-value ≤ 0.01; *** p-value ≤ 0.001; **** p-value ≤ 0.0001. Data are expressed as mean ± SEM of WT (●) and R26CreERT2 (▼) pups.

**Figure 2. Tamoxifen-induced CreERT2 activation in pups affects several blood cellular components.** Tamoxifen was injected IP at 75 mg/kg for 3 consecutive days from P9 to P11 and animals were euthanized at P19. Complete blood count analysis of WT (●) and R26CreERT2 (▼). RBC = Red Blood Cells, HGB = Hemoglobin, HCT = Hematocrit, RET = Reticulocytes, WBC = White Blood Cells, PLT = Platelets. Data are expressed as mean ± SEM of n=8-11 mice per group. Mann-Whitney tests were used to assess statistical significance ( **** p-value ≤ 0.0001)

**Figure 3. Tamoxifen-induced CreERT2 activation in pups affects lineage-restricted precursors in the bone marrow.** Tamoxifen was injected IP at 75 mg/kg for 3 consecutive days from P9 to P11 and animals were euthanized at P19. Bone marrow from femurs and tibias from WT (●) and R26CreERT2 (▼) were analyzed by flow cytometry. Representative dot plots and quantitative analysis of Ter119+ CD71+ erythroblasts (a), B220+ CD19+ B cell precursors (b), and CD11b+ Gr-1+ myeloblasts (c). Data are expressed as a percentage of the total live cells analyzed as a number of cells per animal and are represented as mean ± SEM of n=8-11 animals per group. Mann-Whitney tests were used to assess statistical significance (* p-value ≤ 0.05; ** p-value ≤ 0.01; *** p-value ≤ 0.001; **** p-value ≤ 0.0001).

**Figure 4. Tamoxifen-induced CreERT2 activation in pups results in a strong disorganization of sinusoidal vessels within the diaphysis of the bone marrow.** Tamoxifen was injected IP at 75 mg/kg for 3 consecutive days from P9 to P11 and animals were euthanized

at P19. Representative tile-scan images of femurs displaying both metaphysis and diaphysis (a, scale bars 500 µm), and representative single field confocal images of the bone marrow in the diaphysis (b, scale bars 50 µm) showing endomucin (Emcn, green) stained sinusoid vessels and cell nuclei stained in blue with Hoechst. White arrows are showing areas lacking hematopoietic cells. Quantitative analysis of the Emcn positive area, as a percentage of the total area of the field (c). Each data point represents the average of three different measurements per animal. Data are expressed as mean ± SEM of n=6-9 mice per group. Mann-Whitney tests were used to assess statistical significance of differences between WT (●) and R26CreERT2 (▼) tamoxifen injected pups (*** p-value ≤ 0.001).

**Figure 5. Tamoxifen-induced CreERT2 activation in pups results in loss of EdU+ proliferative cells in bone marrow and spleen.** Tamoxifen was injected IP at 75 mg/kg for 3 consecutive days from P9 to P11 and Edu was injected IP at P17 and animals were euthanized 3 hours later. Representative images and quantitative analysis of the percentage of Edu+ proliferative cells in bone marrow (a, b) and spleen (c, d) of WT (●) and R26CreERT2 (▼) pups. Endomucin (Emcn) staining (vessels) is represented in green, Edu+ proliferative cells are represented in red, and nuclei in blue. Data are expressed as mean ± SEM of n=3-4 per group. Mann-Whitney tests were used to assess statistical significance (* p-value ≤ 0.05). scale bars 50 µm.

**Figure 6. Tamoxifen-induced CreERT2 activation in pups results in an increase in CD41+ megakaryocytes in the bone marrow.** Tamoxifen was injected IP at 75 mg/kg for 3 consecutive days from P9 to P11 and animals were euthanized at P19. (a) Representative images of bone marrow sections of WT (●) and R26CreERT2 (▼) pups. CD41+ megakaryocytes are stained in green, CD31+ vessels in red and nuclei in blue. (b) Quantitative analysis of the number of CD41+ megakaryocytes per square millimeter. Data are expressed as mean ± SEM of n=5-8 mice per group. Mann-Whitney tests were used to assess statistical significance (** p-value ≤ 0.01). scale bars 100 µm.

# DATA SUPPLEMENT

**Supplementary figure legends**

**Figure S1.** WT (●) and R26CreERT2 (▼) mice received intraperitoneal injections of tamoxifen at 75 mg/kg for 3 consecutive days from P9 to P11. (a) Body weight was recorded from P9 to P20 for males and females. Data are expressed as body weight or as a percentage of gain in body weight compared to the body weight at P9. Data are represented as mean ± SEM of n=7-15 mice per group. (b) Survival curves of n=18 WT and n=45 R26CreERT2. (c) Representative photograph of the intestines of WT and R26CreERT2 mice at P19. The arrow shows accumulation of gas in the intestines of R26CreERT2 mice. We used two- way analysis of variance to analyze differences in weight or gain weight and log-rank Mantel cox test to analyze survival curves. * p-value ≤ 0.05; ** p-value ≤ 0.01; *** p-value ≤ 0.001; **** p-value ≤ 0.0001.

**Figure S2.** WT (●) and R26CreERT2 (▼) mice received intraperitoneal injections of tamoxifen at 75 mg/kg for 3 consecutive days from P9 to P11 and were euthanized at P19. Cell suspensions obtained from the spleen were analyzed by flow cytometry. Representative dot plots (left) and quantitative analysis (right) of Ter119+ CD71+ erythroblasts, B220+ CD19+ B cell precursors, and CD11b+ Gr-1+ myeloblasts. Data are expressed as a percentage of the total live cells analyzed or as a number of cells per animal and are represented as mean ± SEM of n=6-11 animals per group. Mann-Whitney tests were used to assess statistical significance (** p-value ≤ 0.01; *** p-value ≤ 0.001; **** p-value ≤ 0.0001).

**Figure S3.** WT (●) and R26CreERT2 (▼) mice received intraperitoneal injections of tamoxifen at 75 mg/kg for 3 consecutive days from P9 to P11. At P17 they received an intraperitoneal injection of Edu and were euthanized 3 hours later. Representative confocal microscopy images of intestine, liver and lung sections. Nuclei were stained with hoechst (blue), glycoconjugates were stained with WGA-FITC lectin (green), and proliferative cells with Edu Click-it A555 kit (red). Scale bar = 50 µm.

**Supplementary table: Tamoxifen-induced CreERT2 activation in pups affects several blood cellular components.** Complete blood count analysis of WT and R26CreERT2 pups. RBC = Red Blood Cells, HGB = Hemoglobin, HCT = Hematocrit, MCV = Mean Corpuscular Volume, MCH = Mean Corpuscular Hemoglobin, MCHC = Mean Corpuscular Hemoglobin Concentration, RET = Reticulocytes, PLT = Platelets, PCT = Plateletcrit, WBC = White Blood Cells, NEUT = Neutrophils, LYMPH = Lymphocytes, MONO = Monocytes, EO = Eosinophils. Values are mean ± standard deviation.

| | WT (Mean ± SD) | R26CreERT2 (Mean ± SD) |
|---|---|---|
| RBC (10^6/µL) | 5.53 ± 0.23 | 2.55 ± 0.2 |
| HGB (g/dL) | 9.17 ± 0.45 | 4.23 ± 0.2 |
| HCT (%) | 30.45 ± 1.75 | 12.39 ± 0.93 |
| MCV (fL) | 54.85 ± 1.38 | 48.96 ± 1.24 |
| MCH (pg) | 16.45 ± 0.33 | 16.39 ± 0.74 |
| MCHC (g/dL) | 30.75 ± 0.99 | 33.66 ± 1.14 |
| RET (10^3/µL) | 1161.85 ± 326.05 | 15.07 ± 4.3 |
| RET (%) | 23.78 ± 1.48 | 0.59 ± 0.19 |
| PLT (10^3/µL) | 631.5 ± 138.5 | 657.22 ± 79.73 |
| PCT (%) | 0.5 ± 0.07 | 0.59 ± 0.07 |
| WBC (10^3/µL) | 1.72 ± 0.61 | 0.32 ± 0.12 |
| NEUT (10^3/µL) | 0.33 ± 0.13 | 0.09 ± 0.03 |
| LYMPH (10^3/µL) | 1.27 ± 0.53 | 0.16 ± 0.06 |
| MONO (10^3/µL) | 0.04 ± 0.03 | 0.04 ± 0.08 |
| EO (10^3/µL) | 0.08 ± 0.03 | 0 ± 0 |

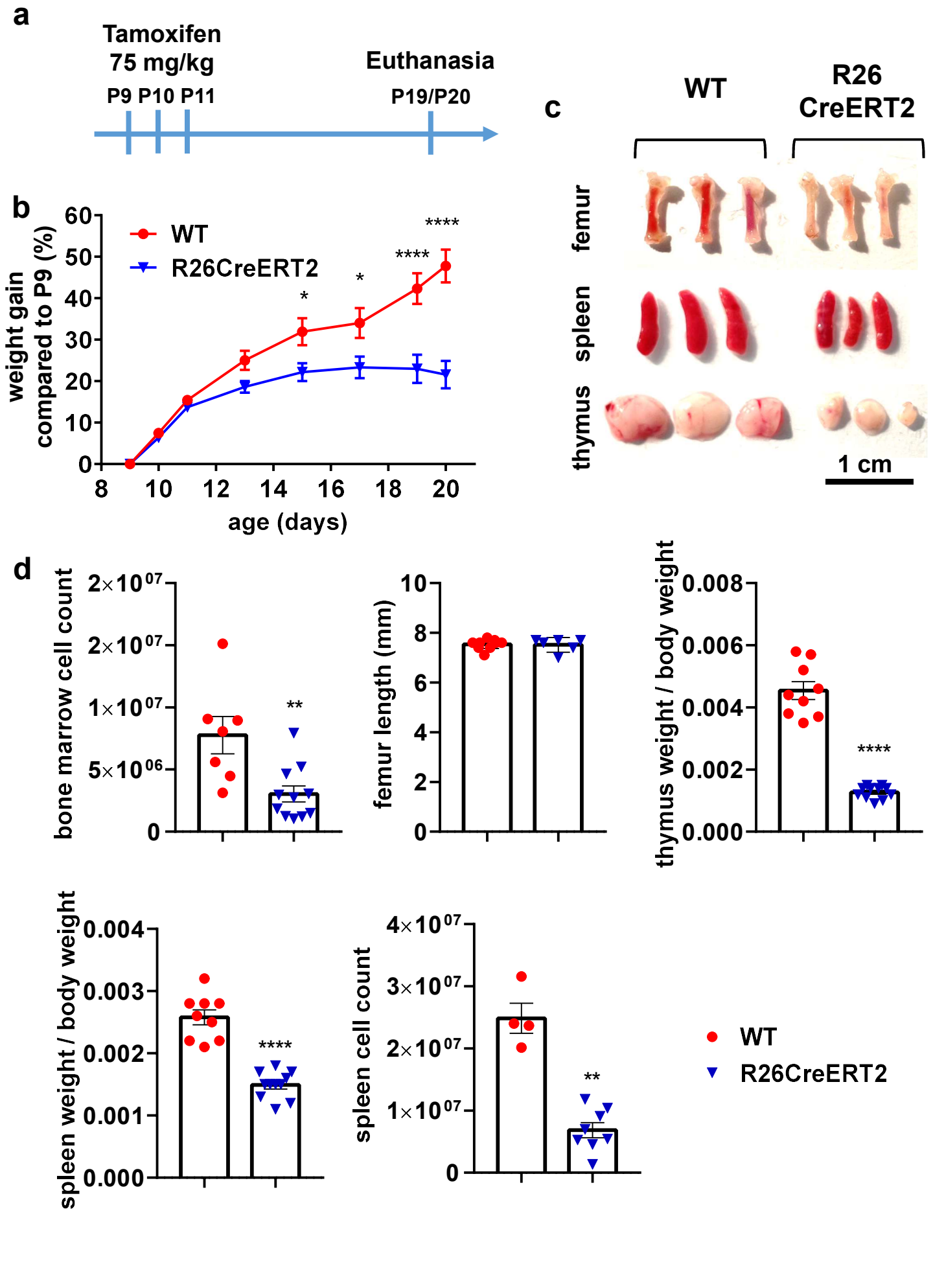
a
Tamoxifen
75 mg/kg
P9 P10 P11
Euthanasia
P19/P20
b
weight gain compared to P9 (%)
WT
R26CreERT2
age (days)
c
WT
R26 CreERT2
femur
spleen
thymus
1 cm
d
bone marrow cell count
femur length (mm)
thymus weight / body weight
spleen weight / body weight
spleen cell count
WT
R26CreERT2

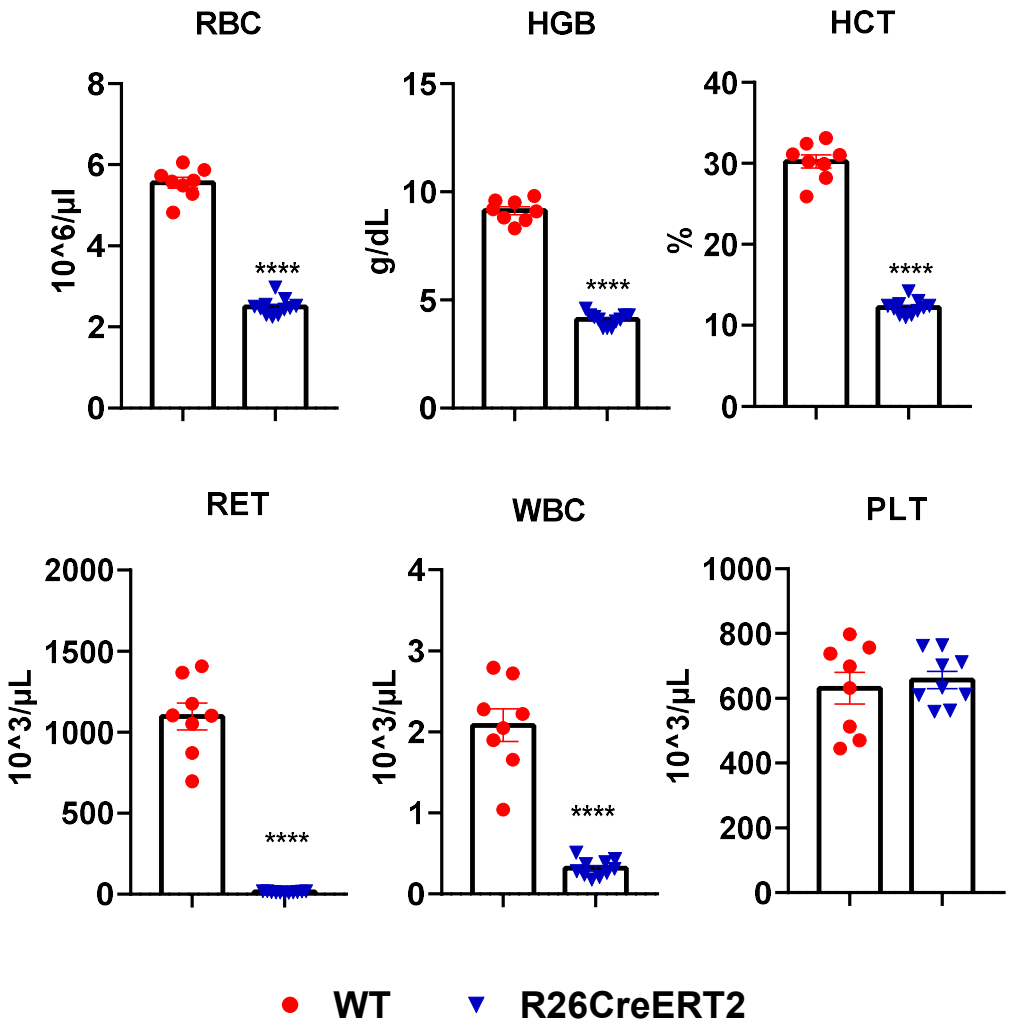
RBC
HGB
HCT
10^6/µl
g/dL
%
****
RET
WBC
PLT
10^3/µL
WT
R26CreERT2

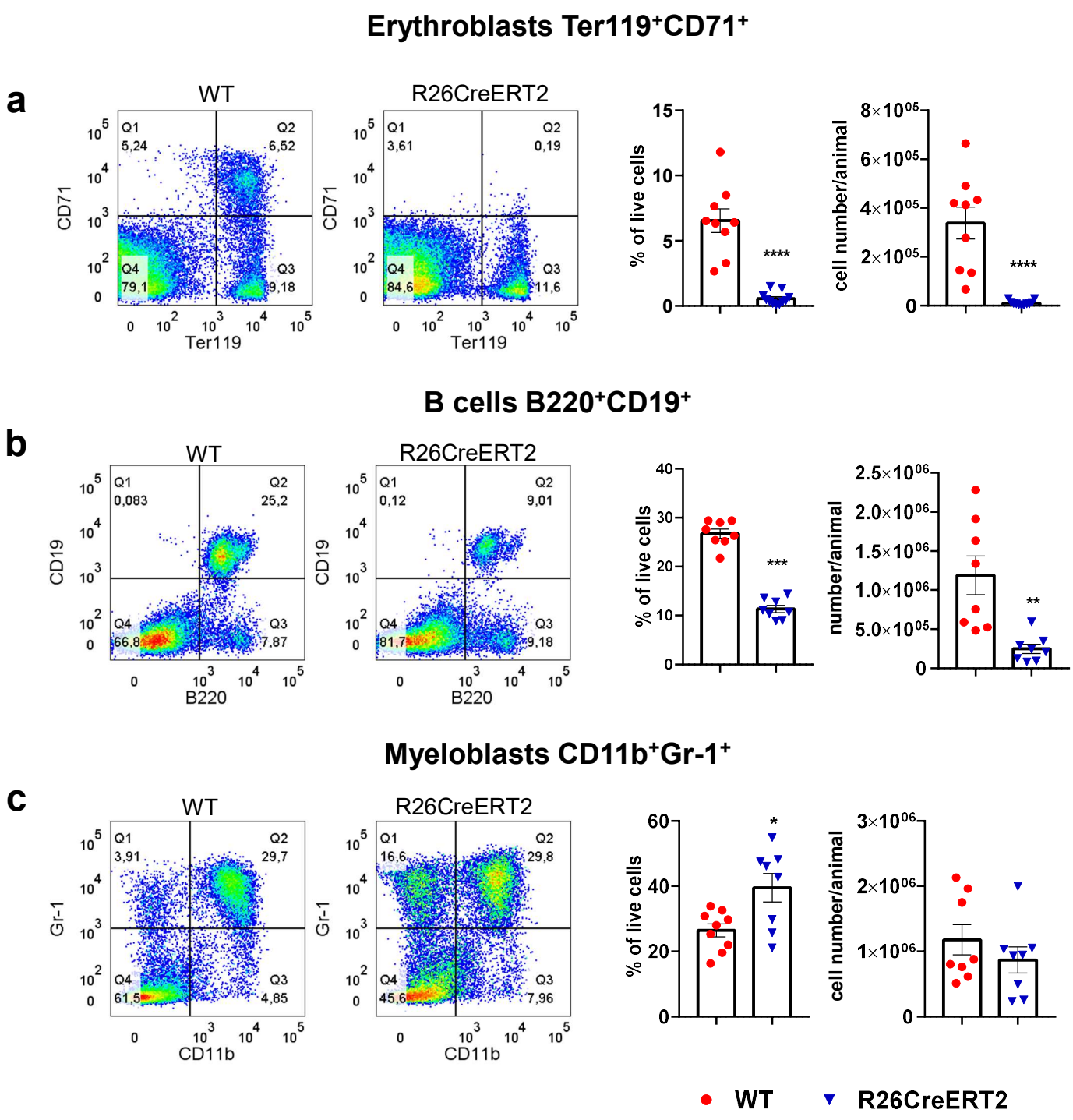
Erythroblasts Ter119+CD71+
a
WT
R26CreERT2
CD71
Ter119
Q1 5,24
Q2 6,52
Q4 79,1
Q3 9,18
Q1 3,61
Q2 0,19
Q4 84,6
Q3 11,6
% of live cells
cell number/animal
****
B cells B220+CD19+
b
CD19
B220
Q1 0,083
Q2 25,2
Q4 66,8
Q3 7,87
Q1 0,12
Q2 9,01
Q4 81,7
Q3 9,18
number/animal
***
**
Myeloblasts CD11b+Gr-1+
c
Gr-1
CD11b
Q1 3,91
Q2 29,7
Q4 61,5
Q3 4,85
Q1 16,6
Q2 29,8
Q4 45,6
Q3 7,96
*
WT
R26CreERT2

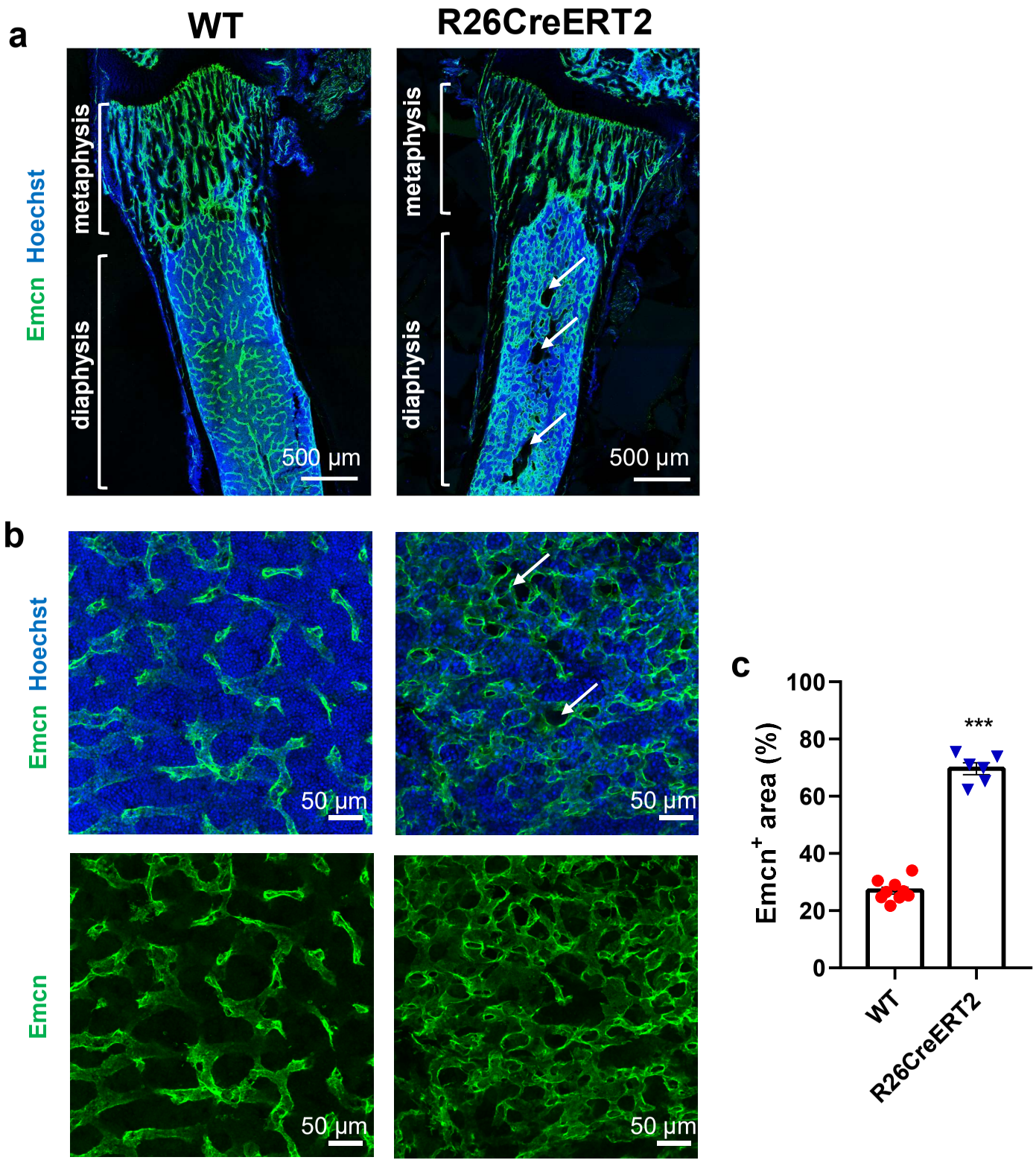
a
WT
R26CreERT2
Emcn Hoechst
metaphysis
diaphysis
500 μm
500 μm
b
Emcn Hoechst
Emcn
50 μm
50 μm
50 μm
50 μm
c
Emcn+ area (%)
100
80
60
40
20
0
***
WT
R26CreERT2

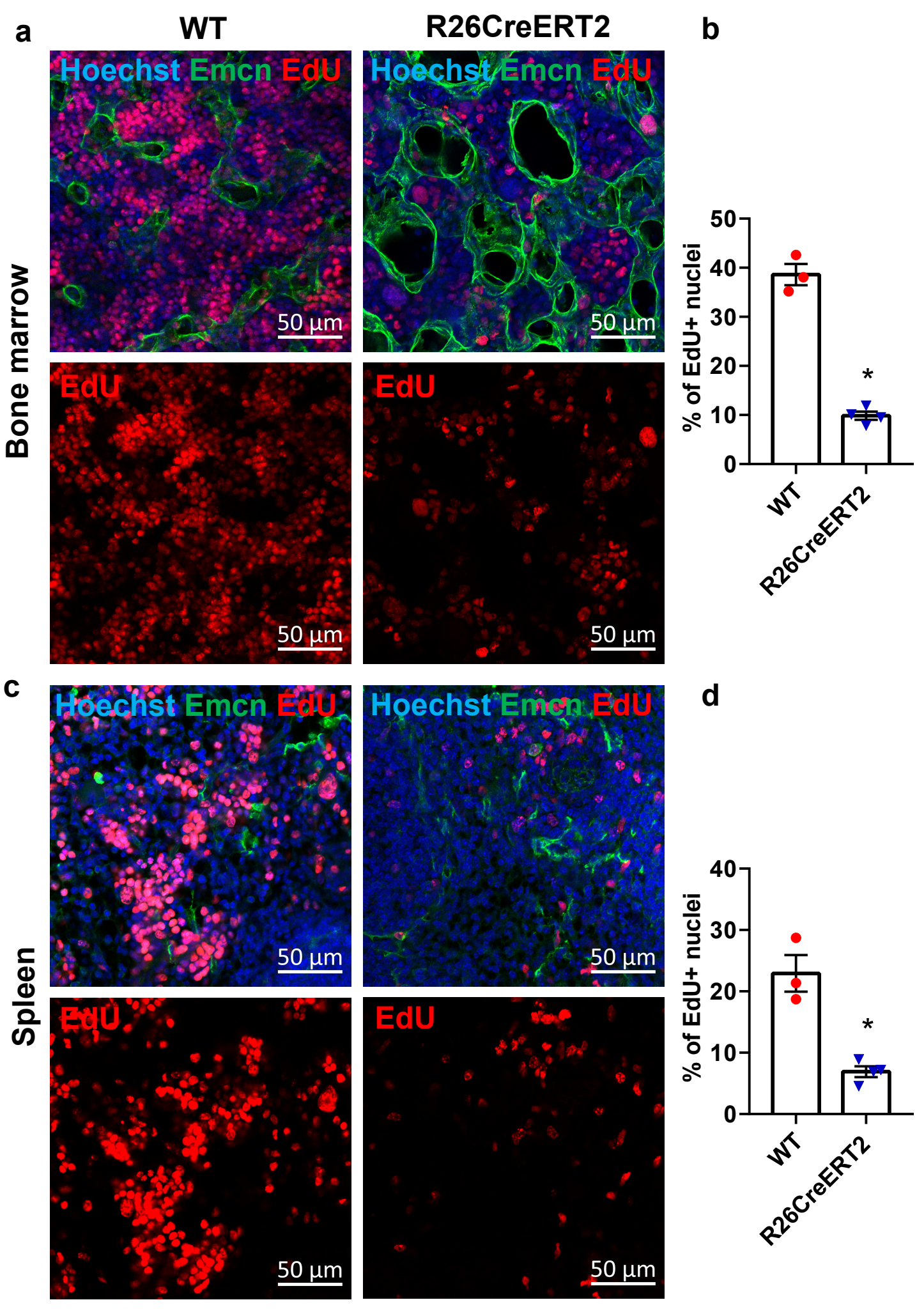
a
WT
R26CreERT2
b
Bone marrow
Hoechst Emcn EdU
EdU
50 µm
% of EdU+ nuclei
50
40
30
20
10
0
*
WT
R26CreERT2
c
d
Spleen

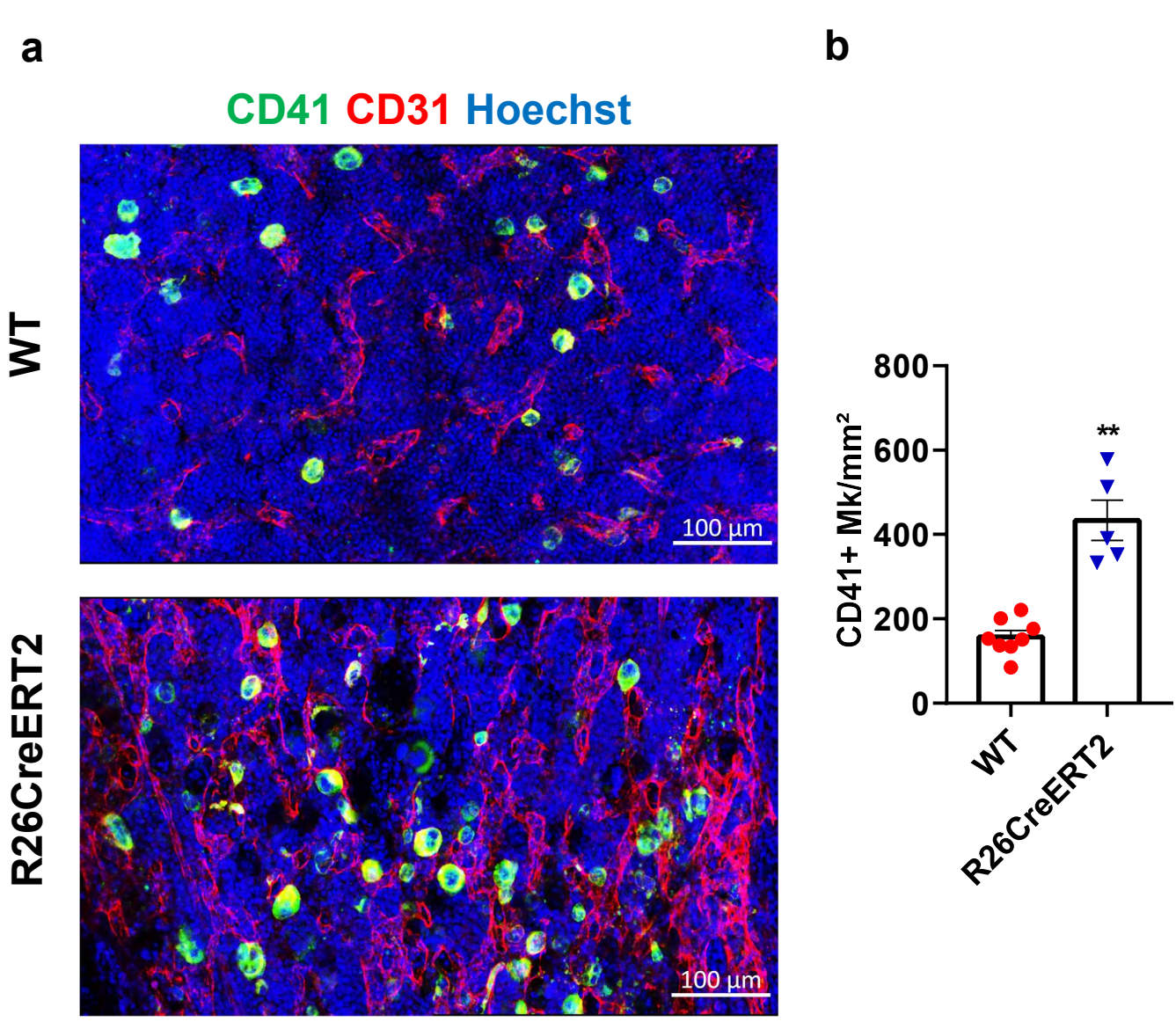
a
b
CD41 CD31 Hoechst
WT
R26CreERT2
100 µm
100 µm
CD41+ Mk/mm²
800
600
400
200
0
**
WT
R26CreERT2

# Figure S1

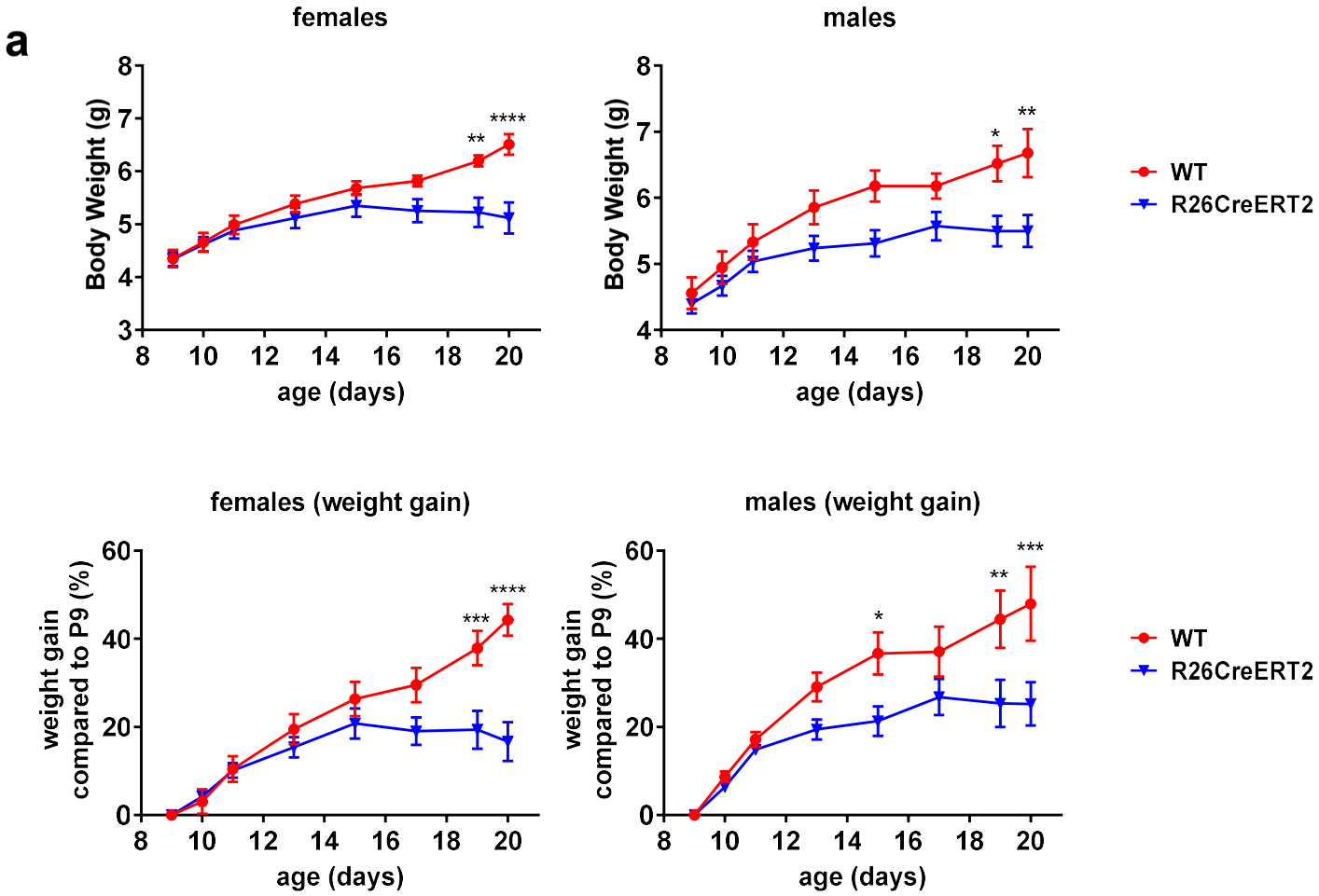
a
females
males
Body Weight (g)
age (days)
**
****
*
**
females (weight gain)
males (weight gain)
weight gain compared to P9 (%)
***
****
*
**
***
WT
R26CreERT2
b
Percent survival
tamoxifen
age (days)
*
WT
R26CreERT2
c
WT
R26CreERT2
gas
1 cm

# Figure S2

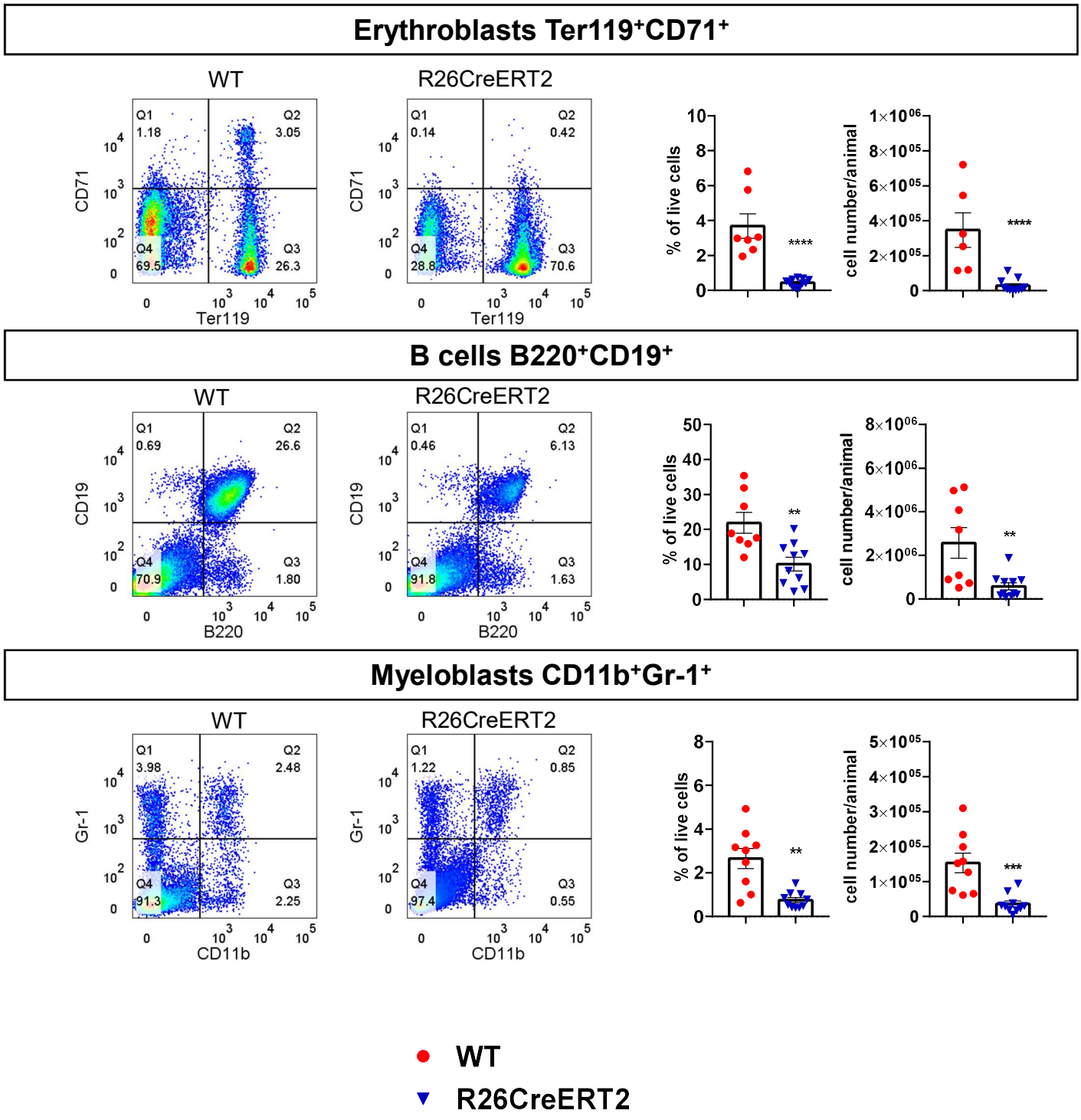
Erythroblasts Ter119+CD71+
WT
R26CreERT2
CD71
Ter119
Q1 1.18
Q2 3.05
Q4 69.5
Q3 26.3
Q1 0.14
Q2 0.42
Q4 28.8
Q3 70.6
% of live cells
cell number/animal
****
B cells B220+CD19+
CD19
B220
Q1 0.69
Q2 26.6
Q4 70.9
Q3 1.80
Q1 0.46
Q2 6.13
Q4 91.8
Q3 1.63
**
Myeloblasts CD11b+Gr-1+
Gr-1
CD11b
Q1 3.98
Q2 2.48
Q4 91.3
Q3 2.25
Q1 1.22
Q2 0.85
Q4 97.4
Q3 0.55
***
WT
R26CreERT2

**Figure S3**

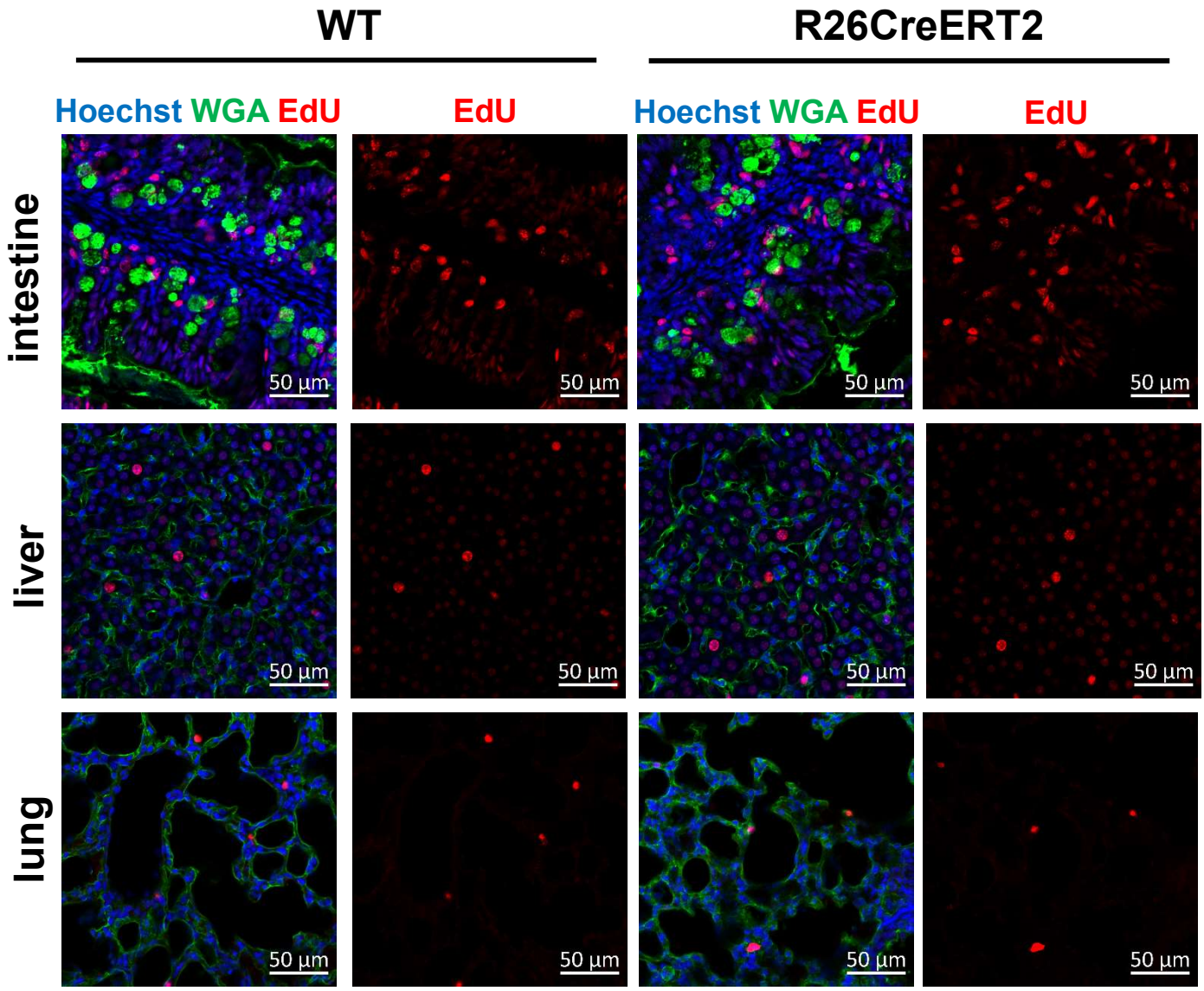
WT
R26CreERT2
Hoechst WGA EdU
EdU
Hoechst WGA EdU
EdU
intestine
liver
lung
50 µm

# Part III – Deciphering the function of cardiac versus liver BMP10

Due to the Cre toxicity found in the Rosa Cre BMP10 iKO pups, we could not study the postnatal function of BMP10 using this model and we had to re-orient the thesis project. In "Part I - Introduction to 1st article (contribution as 3rd author)" I explained that double KO adults are viable although they present significant cardiovascular defects (279). In addition, the critical function of both BMP9 an BMP10 in the context of postnatal vascular development characterised by reduced retinal vascular expansion and increased vascular density, had been proven using neutralising antibodies against BMP10 in BMP9 KO mice (191). Nonetheless, the usage of antibodies could result in cross-reactivity or side effects thus compromising the results. The generation of the Rosa Cre BMP10 iKO pups allowed the team to study the function of BMP9 and BMP10 in postnatal angiogenesis using transgenic mice models. Prior to the beginning of my PhD project, some preliminary results gathered from my team using the Rosa Cre double-KO revealed a vascular phenotype similar to that found using neutralising antibodies against BMP10 in BMP9 KO mice.

We first set up to confirm these preliminary findings in the Rosa Cre cDKO model and to better characterise them. The results obtained are described in Part 1 "Combined loss of BMP9 and BMP10 leads to severe vascular defects during active angiogenesis". Once these findings had been confirmed, we generated tissue-specific BMP10 KO models as is was explained in the "Aims" section (Table 4) with the purpose of deciphering the function of cardiac versus hepatic BMP10 in the context of vascular development. Indeed, the finding of BMP10 being expressed in adults by both the right atria and the liver (136), opened up for the question as for whether BMP10 coming from different sources could have different functions. In particular, we generated transgenic mice for tissue-specific deletion of BMP10 by crossing *Bmp10*$^{lox/lox}$ mice with:

- αMHC-MerCreMer transgenic mice: expressing an inducible cardiac-specific alpha-myosin heavy chain promoter (αMHC) directing expression of a tamoxifen-inducible Cre recombinase fused to two mutant estrogen-receptor ligand-binding domains (MerCreMer) to cardiac myocytes (277) – from hereafter referred to as MerCreMer BMP10 iKO;
- Lrat Cre: transgenic mice: constitutively expressing a Cre recombinase directed by mouse Lrat Cre (lecithin-retinol acyltransferase) promoter specific to hepatic stellate cells (278)– from hereafter referred to as Lrat Cre BMP10 KO.

The generation of Lrat Cre BMP10 KO model had been started by M2 Elisa Redman in 2020 whom took care of the mice crossing and gathered some preliminary qPCR data in which she

showed loss of hepatic BMP10 loss in the liver but not in the heart in these models. Prior to any experiments, the generated mice models had to be validated to confirm tissue-specific loss of BMP10. Next, we plan to find the source of BMP10 circulating homodimer and BMP9/BMP10 circulating heterodimer, as well as their activity in blood. Detected circulating homodimer BMP9 probably comes from the liver where is mainly produced by the hepatic stellate cells. However, concerning the circulating BMP10 homodimer, it is still unclear whether it comes from the right atria or the liver as both have been found to be sources of the BMP10 ligand. Moreover, the discovery of the BMP9/BMP10 circulating active heterodimer and the finding of the liver as a common source of BMP9 and BMP10 secretion led to hypothesised that, this organ could be the source of the heterodimer, which is active in the circulation. The generation of tissue-specific BMP10 KO models allowed us to answer these questions. The results obtained are described in Part 2 "Validation of generated mice models and characterisation of circulating BMP10 homodimer and BMP9/BMP10 heterodimer".

After characterising the origin of the circulating homodimer BMP10 and heterodimer BMP9/BMP10 using tissue specific KO models, we sought out to find out what are their respective function *in vivo* in the context of postnatal angiogenesis and lymphatic maturation and maintenance. It is important to note that the function of BMP10 had only been addressed using neutralising antibodies and that these questions had not been yet addressed using transgenic mice models for the deletion of BMP10. As a readout for postnatal angiogenesis we utilised the retina model, while for the analysis of the lymphatic vessel formation/maturation we started by analysing the lymphatic capillaries in the dorsal ear of the pups. The results obtained are described in Part 3 "Deletion of cardiac BMP10 in parallel with BMP9 did not reveal aberrant postnatal angiogenesis".

## 1. Combined loss of BMP9 and BMP10 leads to severe vascular defects during active angiogenesis

In this part of the work we first set up to confirm the role of BMP9 and BMP10 in vascular development using the double-KO *Bmp9*$^{-/-}$; R26CreERT2 *Bmp10*$^{lox/lox}$ (Rosa Cre cDKO). Animals were injected with tamoxifen at P2-P3 and the development of the retinal vasculature was analysed by whole mount immunofluorescence at P6 **(Figure 34 A)**. As discussed in the introductory chapter "3.2.1 Mouse retina as a model to study postnatal angiogenesis" the retina of the mice develops during the first three weeks after birth. Analysis at P6 allows for the study of the vasculature of the superficial plexus forming during the first week after birth. We analysed the four groups including WT BMP10$^{lox/lox}$, BMP9 KO, Rosa Cre BMP10 iKO and Rosa Cre cDKO by staining the dissected retina using isolectin B4 (IB4) which is a lectin highly specificity for endothelial cell **(Figure 34 B).** As it can be observed, single deletion of either BMP9 (BMP9 KO) or BMP10 (Rosa Cre BMP10 iKO) do not affect the development of the vascular bed. In contrast, concomitant deletion of both ligands, reveal and vascular hyperplasia at the sprouting front.

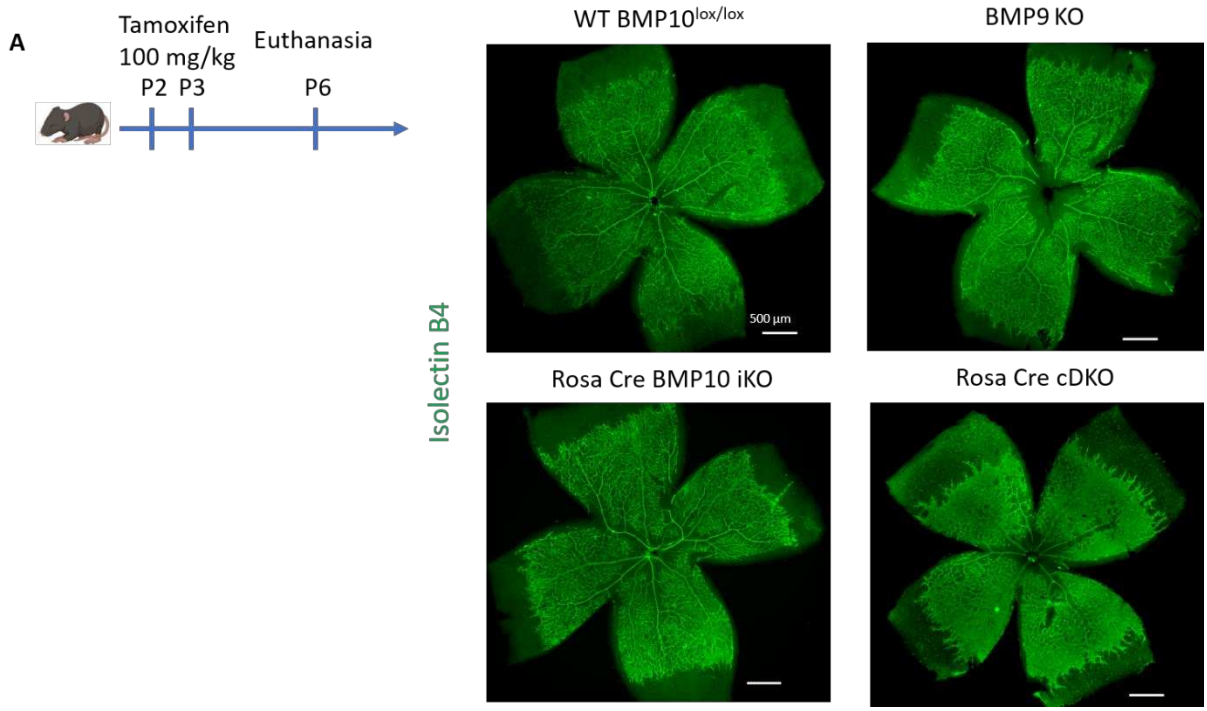


**Figure 34: Concomitant deletion of Bmp9 and Bmp10 increases retina vascularisation**.

*(A) Experimental plan to study post-natal angiogenesis. Litters were injected with tamoxifen on post-natal day 2 and 3 (100 mg/kg dosage) and euthanised at P6. (B) Representative immunofluorescence images showing retina-developing blood vessels stained with isolectin B4. Four different groups analysed WT BMP10$^{lox/lox}$, BMP9 KO , Rosa Cre BMP10 iKO and Rosa Cre cDKO. Data is expressed as mean ± SEM. Mann-Whitney tests were used to asses statistical significance (ns p-value > 0.05; * p-value ≤ 0.05; ** p-value ≤ 0.01; *** p-value ≤ 0.001; **** p-value ≤ 0.0001).*

These finding were in accordance to previously published data using neutralising antibodies against BMP10 into BMP9 KO (191), as well as preliminary data from the team using the Rosa cDKO model. Next, we took a closer look at the retina of these mice to better characterise the observed phenotype. In particular, we observed that Rosa Cre cDKO mice reveal a significant decrease of the radial extension, which is quantified as the vessel growth from the central optic nerve to the vascular front (Figure 35 A and E). Moreover, at the vascular front, we observed a strong increase capillaries density (Figure 35 B and F). To determine whether this was attributable to an increased endothelial cell number we stained the endothelial cells using ETS-related gene (ERG), a nuclear transcription factor expressed by endothelial cells. We could confirm that the increase in vascular density was accompanied by an increase of ETS-related gene (ERG)+ endothelial cells number, while their size remained unchanged (Figure 35 B, G and H). Moreover, we observed a dilation of the veins but not the arteries, which can be differentiated from veins as they retain αSMA coverage and their diameter is more narrow (Figure 35 C and I). Finally, we identified an arterial loss of αSMA coverage, which was quantified as mean fluorescence intensity (Figure 35 D and J).

Taken together, we could confirm that BMP9 and BMP10 are both involved in the control of retina angiogenesis. This described phenotype resembles that observed in inducible homozygous deletion of either ALK1 or ENG in postnatal or adult mice although, in our hands, no retina AVMs were detected. The fact that the phenotypes obtained by the deletion of either receptor ALK1 or co-receptor ENG are stronger compared to that of the ligands BMP9/BMP10, could be reasoned by the activation of ALK1-SMAD1/5/8 pathway via another ligand or a constitutive receptor-ligand signalling independent of BMP9-10/ALK1.

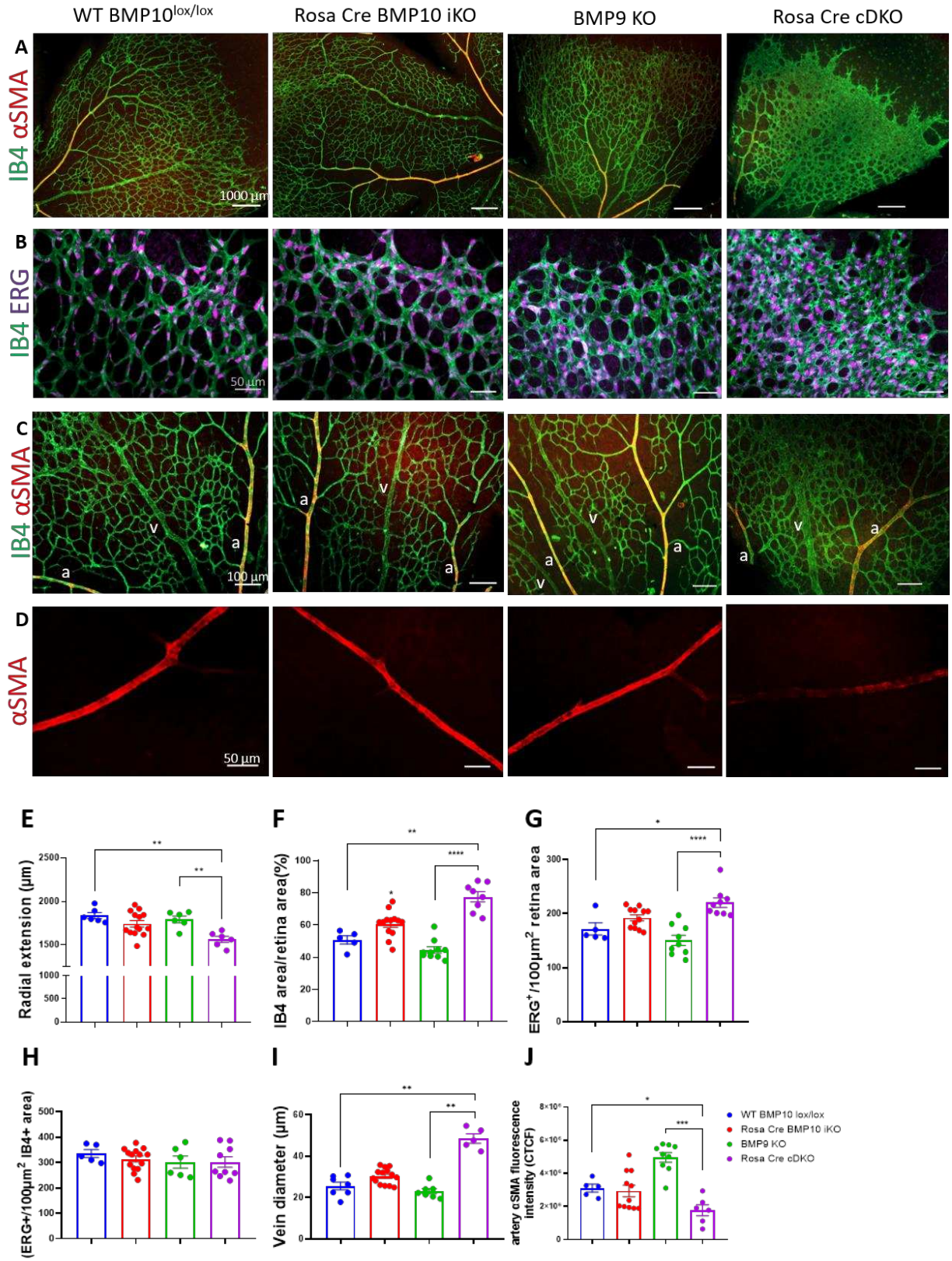


*Figure 35:Concomitant deletion of BMP9 and BMP10 results in increase vasculature in the capillaries front, EC hyperplasia and veins enlargement.*

*Representative immunofluorescence images of P6 retina vessels of WT BMP10$^{lox/lox}$, Rosa Cre BMP10 iKO BMP9 KO and Rosa Cre cDKO showing (A) IB4(green)/αSMA(red), (B) IB4(green)/ERG(purple) EC, (C) IB4(green)/αSMA(red) veins (v) and arteries (a) and, (D) αSMA (red) arterial coverage. Relative quantifications of (E) radial expansion (µm),*

*(F) IB4 stained vascular area at the front, (G) total ERG+ ECs per retina area, (H) total ERG+ ECs per 100 µm² of IB4⁺ vascular area, (I) vein diameter and (J) αSMA arterial fluorescence intensity. Each data point represents the average of four separate quantifications per animal. Data is expressed as mean ± SEM. Mann-Whitney tests were used to asses statistical significance (ns p-value > 0.05; * p-value ≤ 0.05; ** p-value ≤ 0.01; *** p-value ≤ 0.001; **** p-value ≤ 0.0001).*

## Postnatal angiogenesis observation made with Rosa Cre BMP10 iKO

The Rosa CreERT2 toxicity, makes is more complicated to study the function of BMP10 in this context as all the experiments should include a CreERT2 control in which the mouse lacks loxP sites. Bearing this in mind, we performed an experiment on the Rosa Cre BMP10 iKO mice to analyse the effect of BMP10 deletion on developing retina at P6 using the same invalidation scheme, however, we are still missing the Rosa Cre control. Retina vasculature stained with isolectin B4, did not reveal any overt defect in the vascularisation of the retina (Figure 36 A), which can let us to safely conclude that the phenotype observed in the Rosa Cre cDKO does not result from Cre toxicity. Nonetheless, we noticed that, in P6 retina of Rosa Cre BMP10 iKO, veins sometimes take up αSMA coverage. In particular, not only the main ensheathing arterioles but also branching thinner ones appeared to be covered by αSMA in the Rosa Cre BMP10 iKO (Figure 36 B - C). Although few hypothesis could be ventured to explain this phenotype, at this point, without the right CreERT2 control, we cannot make any further assumptions.

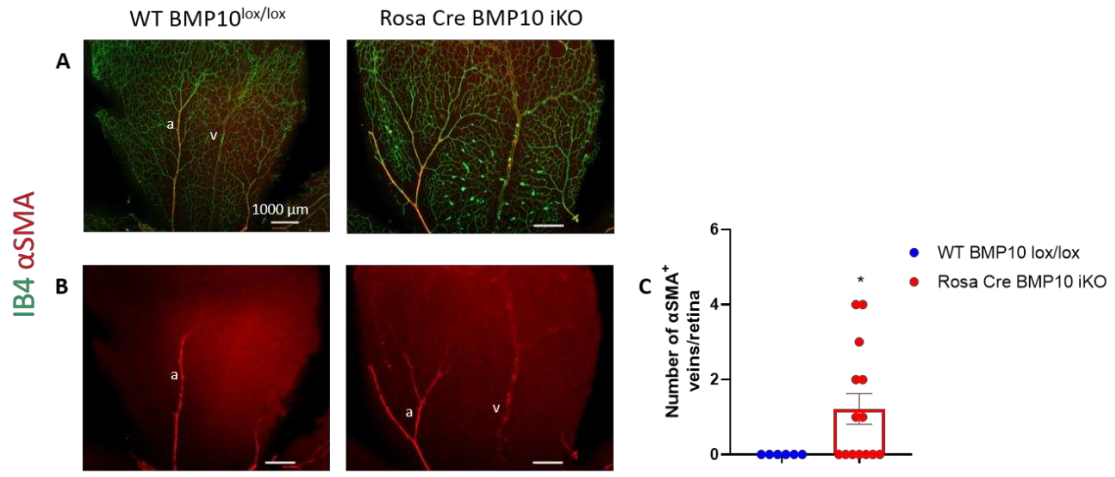


***Figure 36: Rosa Cre BMP10 iKO show abnormal veins smooth muscle coverage in postnatal angiogenic retina.***
*(A) Representative immunofluorescence images taken at 5X magnification of whole mount P6 retina showing IB4(green)/αSMA(red) vessels and (B) αSMA (red) only to reveal muscle coverage of vasculature of WT BMP10lox/lox vs Rosa Cre BMP10 iKO. (C) Relative quantification of total number of αSMA⁺ veins/retina. Each data point represents the total number of αSMA⁺ veins per animal. Data is expressed as mean ± SEM. Mann-Whitney tests were used to asses statistical significance (ns p-value > 0.05; * p-value ≤ 0.05; ** p-value ≤ 0.01; *** p-value ≤ 0.001; **** p-value ≤ 0.0001).*

At this point, considering that BMP10 is expressed in both liver and right atria we sought out to study which BMP10, cardiac vs hepatic, holds a role in postnatal angiogenesis. To study that we implemented MerCreMer cDKO and Lrat Cre DKO as previously mentioned.

## 2. Validation of generated mice models and characterisation of circulating BMP10 homodimer and BMP9/BMP10 heterodimer

As mentioned, after generating tissue specific BMP10 KO models we had to first validate that the gene deletion was targeting the organ of interest. For that, we performed qPCR of BMP10 and BMP9 expressed in the liver as well as BMP10 expressed in the right atria **(Figure 37)**. As it can be observed in the figure, we could confirm loss of BMP10 in the liver of Lrat Cre BMP10 KO **(Figure 37 A)** and loss of BMP10 in the right atria of the MerCreMer BMP10 iKO **(Figure 37 C).** Levels of BMP9 in the liver of both KO models remain unchanged **(Figure 37 B).**The efficiency of BMP10 loss in Rosa Cre BMP10 iKO model in both liver and right atria was previously demonstrated in adults (136,195), however it still needs to be carried out in pups.

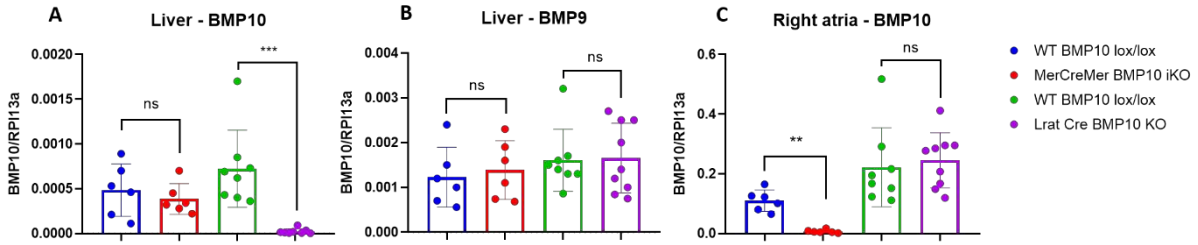


***Figure 37: qPCR of liver BMP10 and BMP9 and liver and right atria of P9 pups.***
*(A) mRNA relative expression of BMP10 in liver from WT BMP10$^{lox/lox}$, MerCreMer BMP10 iKO, WT Bmp10$^{lox/lox}$ and Lrat Cre BMP10 KO. (B) mRNA relative expression of BMP9 in liver from WT BMP10$^{lox/lox}$, MerCreMer BMP10 iKO, WT Bmp10$^{lox/lox}$ and Lrat Cre BMP10 KO. (C) mRNA relative expression of BMP10 in right atria from WT BMP10$^{lox/lox}$, MerCreMer BMP10 iKO, WT BMP10$^{lox/lox}$ and Lrat Cre BMP10 KO. When needed animals were injected with tamoxifen at P3 and P4 (75 mg/kg) and euthanised at P9. Data is expressed as mean ± SEM. Mann-Whitney tests were used to asses statistical significance (ns p-value > 0.05; * p-value ≤ 0.05; ** p-value ≤ 0.01; *** p-value ≤ 0.001; **** p-value ≤ 0.0001).*

Next, we sought out to measure the circulating activity of BMP9 and BMP10 using plasma obtained from single Rosa CreBMP10 iKO, Lrat Cre BMP10 KO and MerCreMer BMP10 iKO. For that, the most commonly used method is to assess ALK1-induced activity using BMP responsive element (BRE) luminescent cell-based assay. The BRE was identified in the promoter region of the ID1 gene, 1 kb upstream of the transcription start site, and was found to be 100% identical in human and mouse genes. As BMP9 and BMP10 have very high affinity to ALK1, stimulating cells with low concentrated plasma (0.5% to 1%) will result in ALK1 activation by only BMP9 and BMP10. Presence of circulating BMP9 and BMP10 activates ALK1-SMAD1/5/8 dependent pathways triggering BRE-controlled expression of firefly luciferase that can be then quantified.

Analysis of tissue specific BMP10 deletion would ultimately allow to confirm the source responsible for the detected circulating activity. The plasma obtained was used to stimulate mouse 3T3 fibroblast cells that were previously transfected with three plasmids encoding for:

- ALK1 receptor (as these cells do not naturally express it);
- pGL3(BRE)2-luc (encoding firefly luciferase downstream of ID1 promoter–derived BMP responsive element promoter (BRE));
- PRL-TKluc (control encoding renilla luciferase downstream of the thymidine kinase promoter).

Upon transfection, the cells will express firefly luciferase when the SMAD1/5/8 pathway is activated (53). The activation of the SMAD pathway by BMP9 and BMP10 via the ALK1 receptor is then quantifiable by calculating the total BRE firefly luciferase signal normalised to the renilla luciferase **(Figure 38 A)**. The results obtained from this test confirmed that the measured circulating activity comes from the liver as only Lrat Cre BMP10 KO loses the BMP activity but not the MerCreMer BMP10 iKO **(Figure 38 B)**. This finding is a further prove to our hypothesis that the heterodimer, which is responsible for circulating activity, comes from the liver. In addition, in its absence, circulating BMP9 alone at such lower concentrations is not able to signal via ALK1.

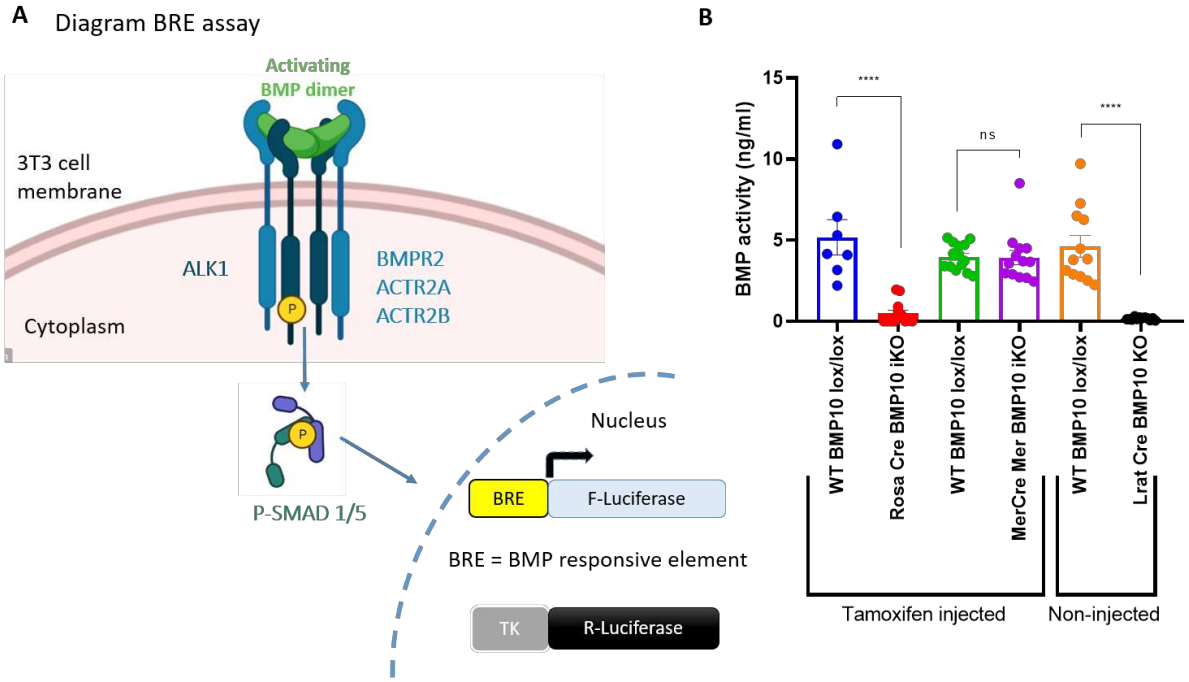


***Figure 38: BMP10 secreted from the liver, but not the heart, is responsible for activity detected in the plasma.***

*(A) Diagram showing the principle of BRE assay: 3T3 cells are transfected with 3 plasmids: ALK1, pGL3(BRE)2-luc (encoding firefly luciferase downstream of BMP responsive element promoter) and pRL-TKluc (control encoding renilla luciferase downstream of the thymidine kinase promoter). Transfection will result in cells expressing firefly luciferase when the SMAD1/5/8 pathway is activated. The activation of the SMAD pathway by BMP9 and BMP10 via the ALK1 receptor is then quantifiable. (B) Relative quantification expressed in ng/ml of BMP activity in 3T3 cells*

*transfected with ALK1, pGL3(BRE)2-luc and pRL-TKluc and stimulated with 0.5 or 1% of plasma obtained from P18-P21 CTL BMP10$^{lox/lox}$ mice, Rosa Cre BMP10 iKO, αMHC-MerCreMer BMP10 iKO and LRatCre BMP10 KO. Statistical analysis were made from plasma of controls vs KO animals coming from the same litters: from left to right: WT BMP10$^{lox/lox}$ vs Rosa Cre BMP10 iKO, WT BMP10$^{lox/lox}$ vs αMHC-MerCreMer BMP10 iKO, WT BMP10$^{lox/lox}$ mice vs LRatCre BMP10 KO. Samples were obtained from 3-weeks old animals apart from the WT BMP10$^{lox/lox}$ vs αMHC-MerCreMer BMP10 iKO where age ranges from 3-5 weeks. Data is expressed as mean ± SEM. Mann-Whitney tests were used to asses statistical significance (ns p-value > 0.05; * p-value ≤ 0.05; ** p-value ≤ 0.01; *** p-value ≤ 0.001; **** p-value ≤ 0.0001).*

## Detected measured circulating homodimer BMP10 and heterodimer BMP9/BMP10 comes from the liver

In this next part, we aimed to characterise circulating BMP10 using tissue specific BMP10 KO models to find out where does circulating measured BMP10 form comes from. For that, Rosa Cre BMP10 litters were injected with tamoxifen from P9-P11 (75 mg/kg), while for αMHC-MerCreMer BMP10 ranging from 2 to 4 weeks were injected with tamoxifen for two consecutive days (100 mg/kg) and euthanised 10 days after the last injection. Plasma obtained from 3-5 weeks old Rosa CreBMP10, Lrat Cre BMP10 KO and MerCreMer BMP10 iKO was tested using Pro-BMP10 ELISA. The Pro-BMP10 ELISA detects circulating precursor form of BMP10 using anti-BMP10 as the capture antibody, and biotinylated anti-propeptide BMP10 as the detecting antibody. Obtained results from the Pro-BMP10 ELISA on plasma from the different groups are summarised in Figure 39.

The values obtained from the different BMP10 KO groups have been compared to those of the control littermates bearing *Bmp10$^{lox/lox}$* gene but not the Cre recombinase. From the figure, it can be observed that ubiquitous deletion of BMP10 results in a significant depletion of measured circulating BMP10 (Rosa Cre BMP10 iKO), as expected. Moreover, only when hepatic BMP10 is deleted (Lrat Cre BMP10 KO), there is a loss of measured circulating BMP10, but not when cardiac BMP10 is deleted (MerCreMer BMP10 iKO). This indicates that the circulating measured BMP10 does in fact come from the liver. As we do not have a purified quantified Pro-BMP10, we could not use a standard curve to detect the levels of circulating BMP10. For that, the obtained results are expressed in absorbance levels. Of note, Pro-BMP10 ELISA has been used as it detects higher levels of BMP10 compared to the BMP10 ELISA recognising the processed form (279,289). Still, we need to perform this experiment using BMP10 ELISA and corroborate these findings. Considering that BMP10 ELISA detect very low levels of processed BMP10, the experiment should be carried on younger animals since the levels of BMP9 and BMP10 peak during three weeks after birth, and gradually decrease as blood vessels mature (134,191).

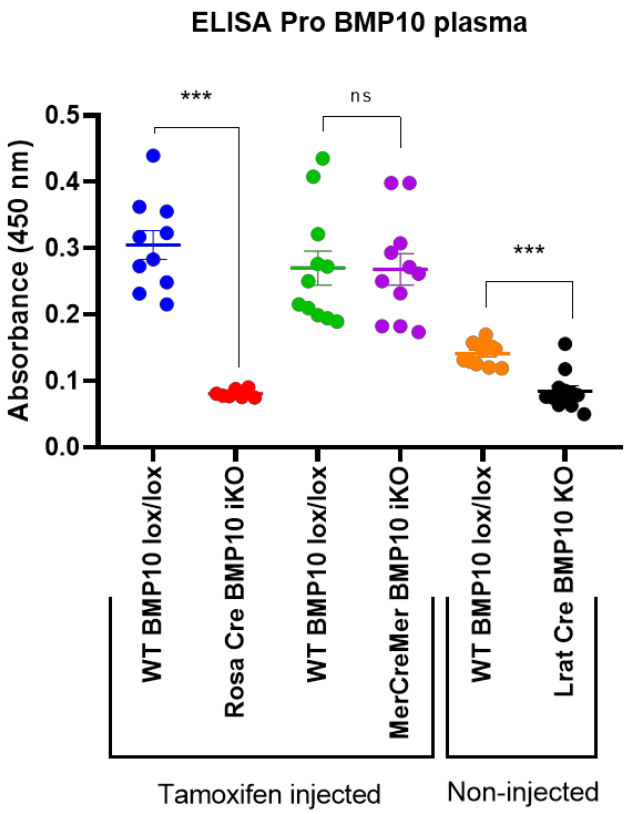


***Figure 39: Circulating measured BMP10 comes from the liver.***

*ELISA measurements of circulating BMP10 in plasma. Capture antibody anti-BMP10, and detecting antibody biotinylated anti-propeptide were utilised. Statistical analysis were made from plasma of controls vs KO animals coming from the same litters. From left to right: WT BMP10$^{lox/lox}$ vs Rosa Cre BMP10 iKO, WT BMP10$^{lox/lox}$ vs αMHC-MerCreMer BMP10 iKO, WT BMP10$^{lox/lox}$ mice vs LRatCre BMP10 KO. Samples were obtained from 3-weeks old animals apart from the WT BMP10$^{lox/lox}$ vs αMHC-MerCreMer BMP10 iKO where age ranges from 3-5 weeks. Rosa Cre BMP10 litters were injected with tamoxifen from P9-P11 (75 mg/kg), while for αMHC-MerCreMer, BMP10 animals from 2 to 4 weeks were injected for two consecutive days (100 mg/kg) and euthanised 10 days after the last injection. Data is expressed as mean ± SEM. Mann-Whitney tests were used to asses statistical significance (ns p-value > 0.05; * p-value ≤ 0.05; ** p-value ≤ 0.01; *** p-value ≤ 0.001; **** p-value ≤ 0.0001).*

The next part of this work was aimed to prove the origin of BMP10 contributing in the formation of the heterodimer. We hypothesised that BMP9 and BMP10 heterodimer is formed in the hepatic stellate cells in the liver as it is the only known common source of the ligands. To test this hypothesis we implemented a sandwich cross ELISA developed by our group to detect the heterodimer in plasma devoid of BMP10 in a tissue specific manner (αMHC-MerCreMer BMP10 iKO vs Lrat Cre BMP10 KO). This cross-ELISA, relies on the usage of capture anti-mature BMP9 antibody and a detection anti-mature biotinylated BMP10 antibody. (Figure 40 A). Figure 40 B summarises the obtained results obtain from the cross ELISA on plasma from animals ranging from 3-5 weeks old.

The values obtained from the different BMP10 KO groups have been compared to those of the control littermates bearing *Bmp10$^{lox/lox}$* gene but no Cre enzyme. The test allowed us to confirm our hypothesis about the hepatic origin of BMP10 contributing in the formation of the heterodimer responsible for the circulating activity in the plasma. First, we confirmed that ubiquitous deletion of BMP10 results in a depletion of circulating BMP9-BMP10 heterodimer (Rosa Cre BMP10 iKO), as expected. In addition, in agreement with our assumption, only when hepatic BMP10 is deleted (Lrat Cre BMP10 KO), there is a loss of circulating BMP9-BMP10 heterodimer, but not when cardiac BMP10 is deleted (MerCreMer BMP10 iKO). This confirms

that the circulating BMP9-BMP10 heterodimer does in fact come from the BMP10 secreted by the liver.

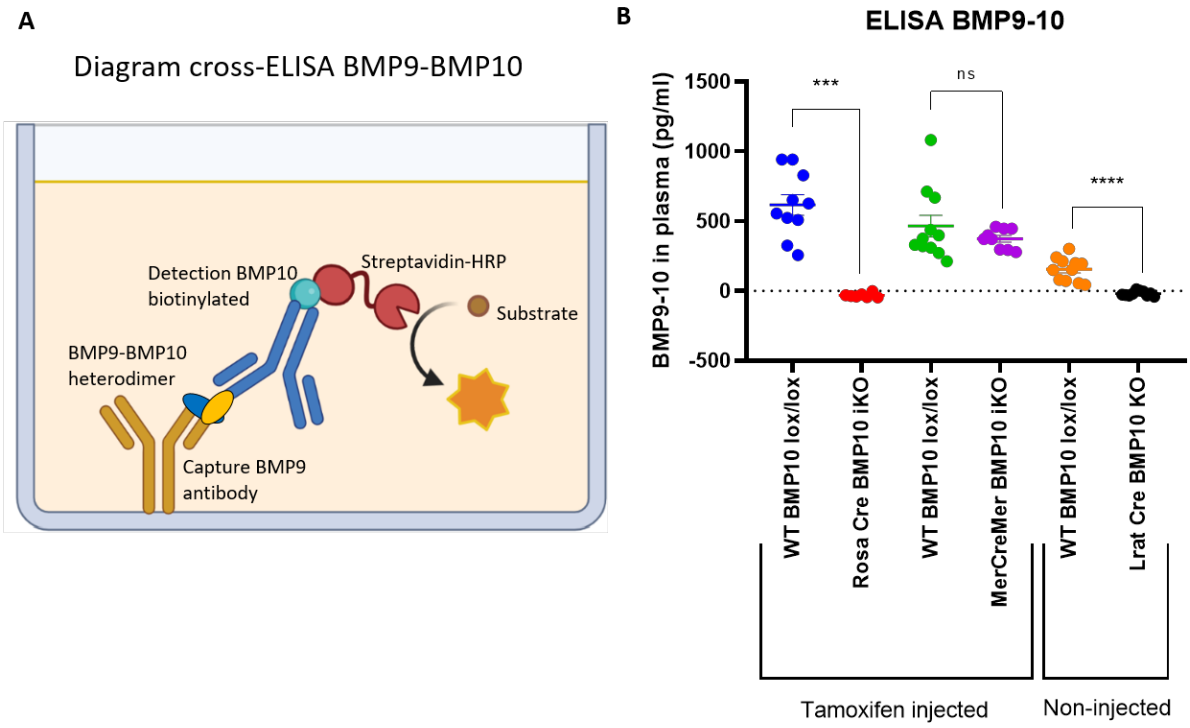


*Figure 40: BMP9-BMP10 heterodimer comes from the liver.*

*(A) Diagram representing BMP9-BMP10 cross-ELISA using capture anti-mature BMP9 antibody and a detection biotinylated anti-mature BMP10 antibody. Streptavidin binds to biotin and the conjugated HRP catalyses the conversion of chromogenic to chemiluminescent substrate. (B) ELISA measurements of circulating BMP9-BMP10 heterodimer in mouse plasma. Statistical analysis were made from plasma of controls vs KO animals coming from the same litters. From left to right: WT BMP10$^{lox/lox}$ vs Rosa Cre BMP10 iKO, WT BMP10$^{lox/lox}$ vs αMHC-MerCreMer BMP10 iKO, WT BMP10$^{lox/lox}$ mice vs Lrat Cre BMP10 KO. Samples were obtained from 3-weeks old animals apart from the WT BMP10$^{lox/lox}$ vs αMHC-MerCreMer BMP10 iKO where age ranges from 3-5 weeks. Rosa Cre BMP10 litters were injected with tamoxifen from P9-P11 (75 mg/kg), while for αMHC-MerCreMer BMP10 animals from 2 to 4 weeks were injected for two consecutive days (100 mg/kg) and euthanised 10 days after the last injection. Data is expressed as mean ± SEM. Mann-Whitney tests were used to asses statistical significance (ns p-value > 0.05; * p-value ≤ 0.05; ** p-value ≤ 0.01; *** p-value ≤ 0.001; **** p-value ≤ 0.0001).*

An observation that we made from both Pro-BMP10 ELISA and BMP9/BMP10 heterodimer ELISA results is that there is a difference in measured levels of BMP10 in the different WT groups. In particular, the levels of circulating BMP10 in the Lrat WT group are lower compared to the other two WT groups. Lrat Cre BMP10 is constitutively active and does not need tamoxifen activation, which is not the same for the R26CreERT2 and the αMHC-MerCreMer. BMP10 levels are higher in WT groups that were injected with tamoxifen (WT BMP10$^{lox/lox}$ in blue and green in the figures), which is not the case for the WT BMP10 group that was not injected with tamoxifen (WT BMP10$^{lox/lox}$ in orange in the figure). As the background strain and the age of the animals were approximately the same for all groups, one explanation to this

phenomenon could be that, tamoxifen injection somehow results in increase of circulating BMP10 homodimer and BMP9/BMP10 heterodimer. It is widely known that tamoxifen administration may have some adverse side effects that could lead to incorrect interpretation of results (290). Therefore, Lrat Cre animals should be injected with tamoxifen to check whether the detected levels of homodimer BMP10 and heterodimer BMP9/BMP10 are higher compared to the non-injected WT group.

## 3. Deletion of cardiac BMP10 in parallel with BMP9 did not reveal aberrant postnatal angiogenesis

To study the function of tissue specific BMP10 in the context of postnatal angiogenesis we crossed the two tissue specific BMP10 lines (MerCreMer BMP10 iKO; Lrat Cre BMP10 KO) with BMP9 KO to obtain *Bmp9*$^{-/-}$;αMHC-MerCreMer *Bmp10*$^{lox/lox}$ conditional KO (from hereafter called MerCreMer cDKO) and *Bmp9*$^{-/-}$;Lrat Cre *Bmp10*$^{lox/lox}$ constitutive KO (from hereafter called Lrat Cre DKO). Postnatal retinal development of MerCreMer cDKO and Lrat Cre DKO vs BMP9 KO littermate controls were analysed at P6. As it can been observed in **Figure 41 A-G**, we observed that specific deletion of cardiac BMP10 in concomitant with BMP9 germline deletion (MerCreMer cDKO), did not lead to any obvious alterations in postnatal angiogenesis resembling the Rosa Cre cDKO. This result was surprising since, considering the main source of BMP10 is the right atria, one would expect that the ligand coming from this source holds the vascular function. Nonetheless, as we proved that the detected circulating BMP10 and the heterodimer BMP9/BMP10 come from the liver, it could be reasoned that the liver BMP10 has an important function that has been neglected up until now. Nonetheless, there are yet no studies addressing the functional role of liver BMP10.

As for the Lrat Cre dKO, it could seem that the also these dKO mice do not display overt phenotype **(Figure 41 H-N)**. However, we still cannot make any conclusion from these two DKO mice, as they were obtained from crossing heterozygous *Bmp9*$^{+/-}$; Lrat Cre *Bmp10*$^{lox/lox}$ parents and we did not validated loss of BMP9 and BMP10 in the liver therefore, we cannot be certain whether they are actual double knock-out. Crossing BMP9 KO with Lrat Cre *Bmp10*$^{lox/lox}$ leads to severe fertility problems. Indeed, we have generated 54 crossing and, despite it is recommended to use Lrat Cre+ females, we only managed to get 4 Lrat Cre dKO from male Lrat Cre + parents. These animals are still alive and we are not certain if they are true dKO. It could be that hepatic BMP10 has an important function during embryonic development and that, concomitant deletion of BMP9 and hepatic BMP10 results in embryonic lethality. Indeed, we managed to prove that hepatic BMP10 is responsible for the detected circulating active BMP10 and the formation of the active heterodimer, yet the role remains to be determined. Indeed, further analysis are needed in order to explain this observed phenomenon.

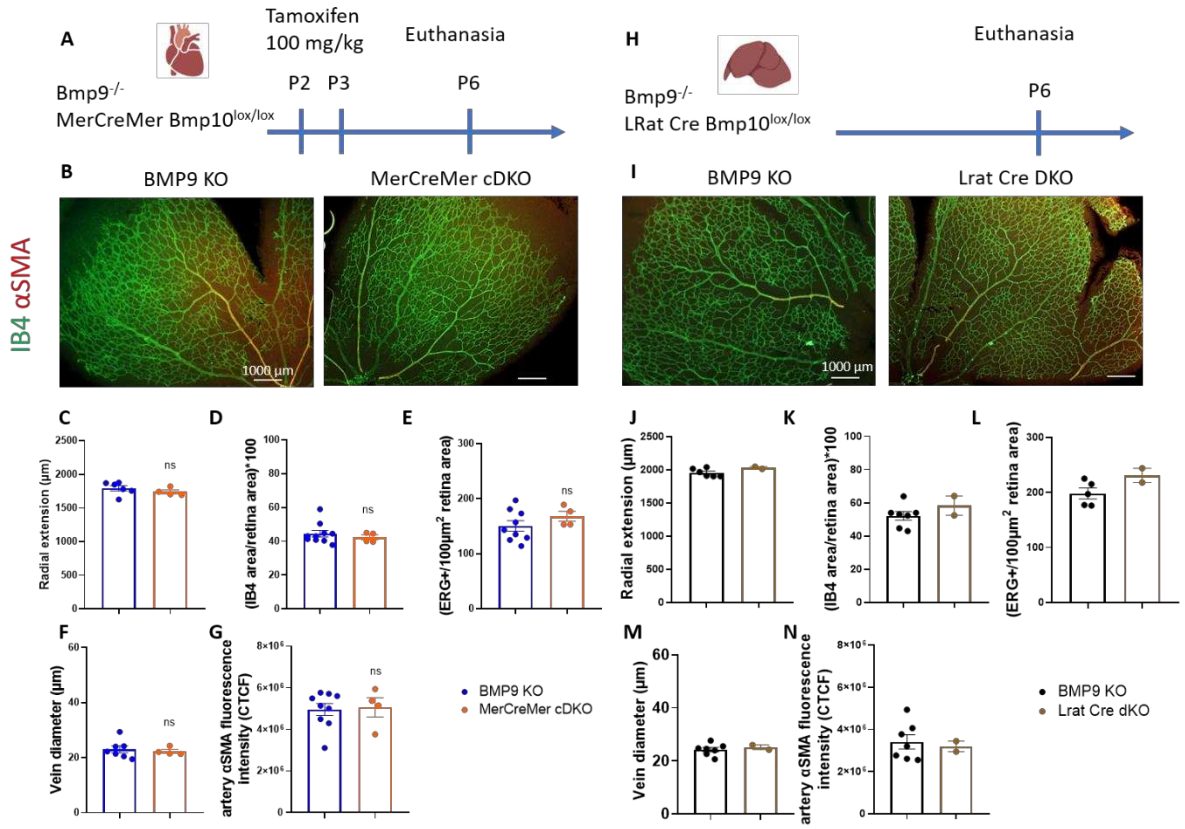


*Figure 41: BMP10 from the right atria is not critical for postnatal retinal development.*

*(A) Experimental plan to study cardiac BMP10 post-natal angiogenetic role. Litters were injected with tamoxifen on post-natal day 2 and 3 (100 mg/kg dosage) and euthanised at P6 (B). Representative immunofluorescence images of P6 retina showing IB4(green)/αSMA(red) vessels of BMP9 KO vs MerCreMer cDKO and (C-G) relative quantifications of radial expansion (µm), IB4 stained vascular area, total ERG+ ECs per retina area, vein diameter. (µm) and αSMA arterial fluorescence intensity. (H) Experimental plan to study hepatic BMP10 post-natal angiogenetic role. Litters were euthanised at P6. (I) Representative immunofluorescence images of P6 retina showing IB4(green)/αSMA(red) vessels of BMP9 KO vs LRat DKO and (J-N) relative quantifications of radial expansion (µm), IB4 stained vascular area, total ERG+ ECs per retina area, vein diameter. (µm) and αSMA arterial fluorescence intensity. Each data point represents the average of four separate quantifications per animal. Data is expressed as mean ± SEM. Mann-Whitney tests were used to asses statistical significance (ns p-value > 0.05; * p-value ≤ 0.05; ** p-value ≤ 0.01; *** p-value ≤ 0.001; **** p-value ≤ 0.0001).*

Overall, our attempt to find which BMP10, either the one coming from the heart or the liver, holds a role in retinal postnatal angiogenesis, did not lead us to any conclusion for the moment. Indeed, it seems that deletion of BMP10 from the right atria in parallel with BMP9 is not sufficient to disrupt postnatal vascular development, suggesting that the remaining factors are able to maintain ALK1 induced vascular quiescence. Yet, it remains to be confirmed what is the role of the hepatic BMP10.

The next part will focus on the analysis of the specific role of BMP10 postnatal lymphatic vessels remodelling and maintenance using ubiquitous and tissue-specific BMP10 KO models.

## 4. BMP10 seems to hold a function in postnatal lymphatic vessels remodelling and maintenance

BMP9 has been shown to be an important factor for lymphatic vessel maturation and homeostasis during embryonic development, postnatal and adult homeostasis (176). In particular, BMP9 KO mice revealed lymphatic vessels hyperplasia and significant reduction and maturation of valves at both embryonic and neonatal stages as well as decreased draining efficiency in adults (176). We questioned whether, like BMP9, BMP10 as well retains a specific function in lymphatic vessel maturation/maintenance. However, to study the function of BMP10 in embryonic lymphatic development and valves formation is not possible as BMP10 is essential for embryo cardiac development (254). The only model to us available at this stage was the Rosa Cre iKO BMP10, which we found out to be subjected to Cre ERT2 toxicity independent of BMP10 deletion. Considering this, we chose to study the postnatal lymphatic development by inducing BMP10 deletion as early as P3 and analysing the ears lymphatics at P9, using as control both *Bmp10*$^{lox/lox}$ as well as Rosa CreERT2 control. As the ears grow after birth, be believed that it could make an interesting model to study the lymphatic formation.

We analysed the ears of single BMP9 KO, Rosa Cre BMP10 iKO and Rosa Cre cDKO at P9. Indeed, we could show that deletion of BMP10 alone is sufficient to reveal a lymphatic defect, similar to that observed in the BMP9 KO (Figure 42 D). In particular, the area occupied by the lymphatic vessels stained with LYVE-1$^{+}$ marker, as well as their diameter, is significantly increased in the Rosa Cre BMP10 iKO mice compared to the WT littermates.

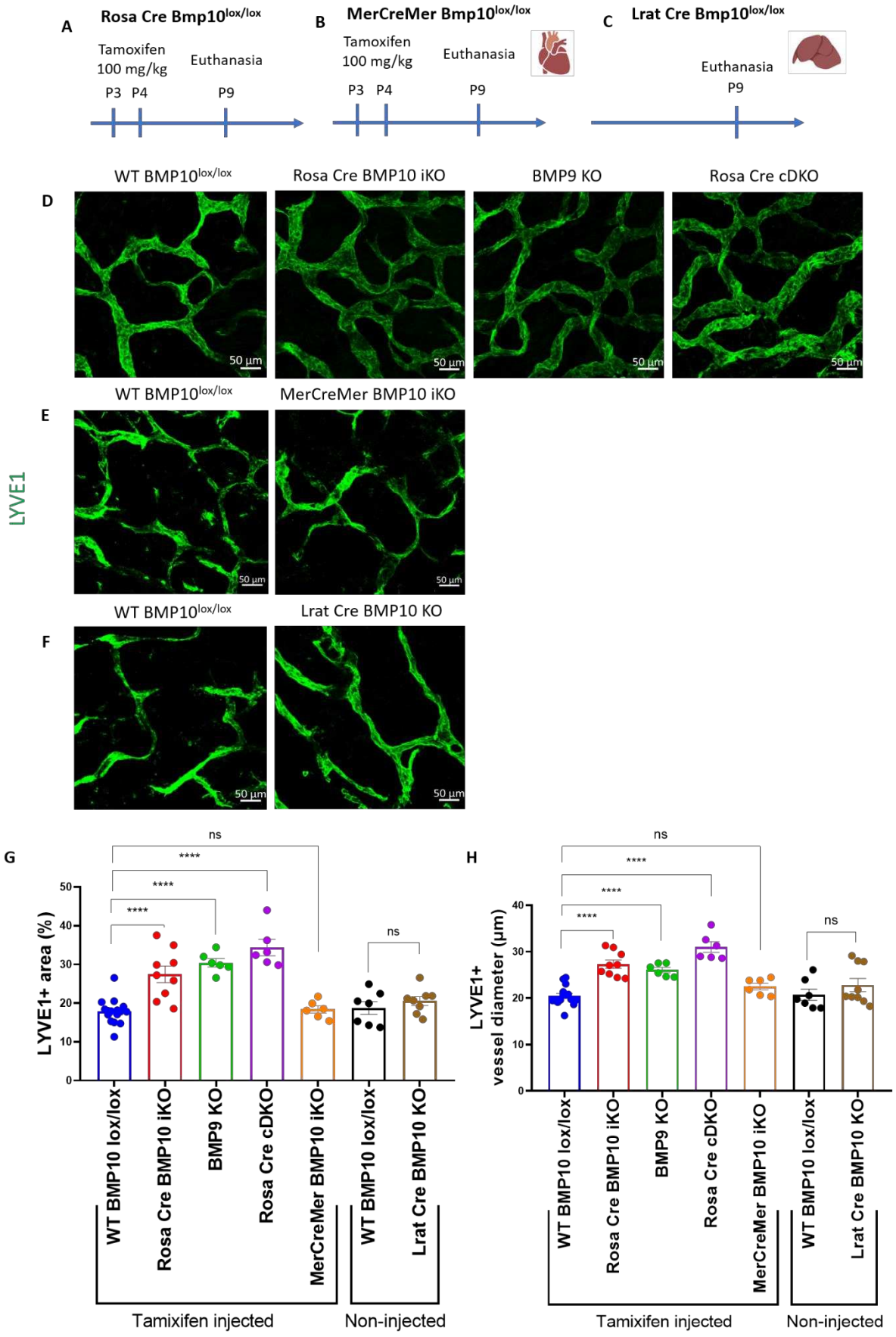


*Figure 42: BMP9 and BMP10 single KO present capillaries lymphatics vessels enlargement.*

*(A-C) Experimental plan to study Bmp10 role in post-natal lymphangiogenesis using Rosa Cre BMP10 iKO,*

*MerCreMer BMP10 iKO and Lrat Cre BMP10 KO. When needed litters were injected with tamoxifen on post-natal day 3 and 4 (100 mg/kg dosage) and euthanised at P9. (D) Representative immunofluorescence images of P9 dorsal ear showing LYVE-1+ lymphatic vessels WT BMP10$^{lox/lox}$, Rosa Cre Bmp10 iKO,* Bmp9$^{-/-}$ *and Rosa Cre cDKO.(E) Representative immunofluorescence images of P9 dorsal ear showing LYVE-1+ lymphatic vessels WT* BMP10$^{lox/lox}$ *vs MerCreMer Bmp10 iKO. (F) Representative immunofluorescence images of P9 dorsal ear showing LYVE-1+ lymphatic vessels WT* BMP10$^{lox/lox}$ *vs L-Rat Bmp10 iKO. (G-H) Relative quantifications of LYVE-1+ area (G) and lymphatic vessels diameter (H) for all groups. To quantify ear skin capillary mean lymphatic size, six horizontal lines were evenly laid on the images, and the diameters of lymphatic vessels that crossed these lines with an angle above 45° were measured using Image J. Each data point represents the average of three separate quantifications per animal. Data is expressed as mean ± SEM. Mann-Whitney tests were used to asses statistical significance (ns p-value > 0.05; * p-value ≤ 0.05; ** p-value ≤ 0.01; *** p-value ≤ 0.001; **** p-value ≤ 0.0001).*

To make sure that the phenotype was not a Cre toxicity artefact, we performed the same experiment on Cre ERT2$^{+/-}$ control without lox/P sites, and we injected the animals with tamoxifen using the same induction scheme (injection P3-P4) and dorsal ears were analysed at P9 **(Figure 43)**. As it can be observed, no obvious lymphatic capillaries defect were detected upon Cre ERT2 activation in the absence of floxed *Bmp10.* This experiment led us to confirm that the phenotype observed is indeed resulting from ubiquitous deletion of BMP10 and not from a CreERT2-induced artefact.

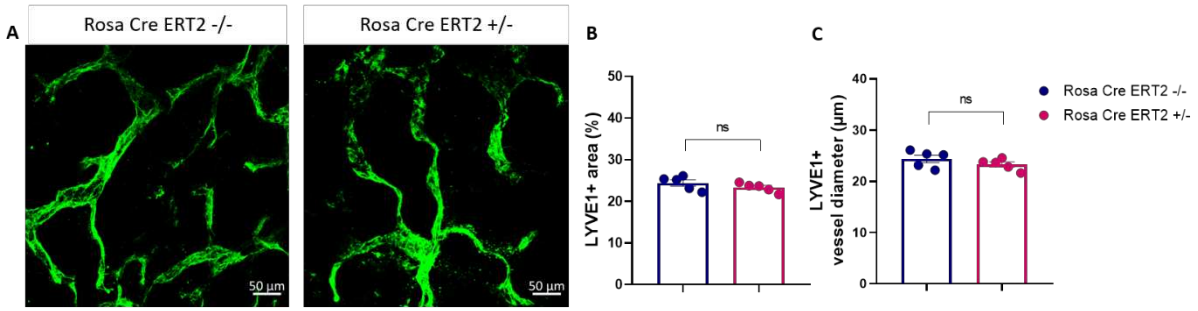


***Figure 43: Rosa Cre ERT2 activation does not influence lymphatic maintenance in postnatal pups.***
*(A) Representative immunofluorescence images of P9 dorsal ear showing LYVE-1+ lymphatic vessels of Rosa Cre ERT2-/- vs Rosa Cre ERT2+/-. (B) Relative quantifications of LYVE-1+ area and (C) lymphatic vessels diameter. To quantify ear skin capillary mean lymphatic size, six horizontal lines were evenly laid on the images, and the diameters of lymphatic vessels that crossed these lines with an angle above 45° were measured using Image J. Each data point represents the average of three separate quantifications per animal. Data is expressed as mean ± SEM. Mann-Whitney tests were used to asses statistical significance (ns p-value > 0.05; * p-value ≤ 0.05; ** p-value ≤ 0.01; *** p-value ≤ 0.001; **** p-value ≤ 0.0001).*

At this point, having shown that BMP10 seems to have a role during early postnatal development of lymphatic capillaries, we wanted to study whether this function came from BMP10 coming from the heart or the liver. We hypothesised that the heterodimer BMP9/BMP10 could have a function in this context. Indeed, the heterodimer has been found to be active in the circulating plasma. Considering that lymphatic capillaries act as filters for the plasma coming from the blood, we hypothesised that the circulating heterodimer had a function in the maintenance of this system by signalling via ALK1 receptor found in LECs. To

study that we used our models for tissue specific deletion of BMP10: MerCreMer BMP10 iKO, and Lrat Cre BMP10 KO. Whereas needed, pups were injected with tamoxifen at P3 and P4 and the condition of the lymphatic capillaries network from the dorsal ears were analysed at P9 using an antibody against LYVE-1 marker (Figure 42 A). However, immunofluorescence analysis did not reveal any obvious defect in MerCreMer BMP10 iKO and Lrat Cre BMP10 KO compared to their WT littermates (Figure 42 E-H).

Differently from the Rosa Cre BMP10 iKO in which, upon early tamoxifen injection, the mice die early due to Cre toxicity, MerCreMer BMP10 iKO and Lrat Cre BMP10 KO can survive after deletion of tissue-specific BMP10. For that, we also analysed the matured lymphatics of the ears of MerCreMer BMP10 iKO at three weeks and that of Lrat Cre BMP10 KO at 6-8 months old. Again, no differences were observed between WT and tissue specific BMP10 KO (Figure 44 and Figure 45).

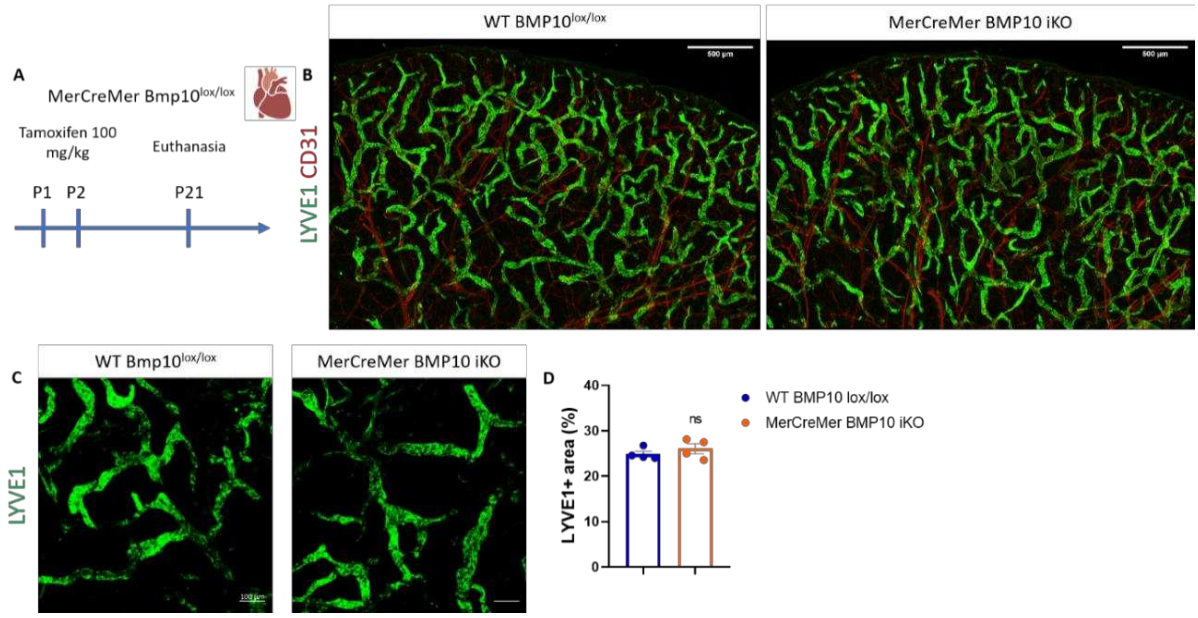


*Figure 44: Early deletion of cardiac BMP10 does not affect lymphatic capillaries in young mouse models.*
*(A) Experimental plan to study cardiac BMP10 role in post-natal lymphangiogenesis . Litters were injected with tamoxifen on post-natal day 1 and 2 (100 mg/kg dosage) and euthanised at P21. (B) Representative tile scan maximum-intensity confocal images of P21 dorsal ear showing LYVE1+ lymphatic vessels and CD31 blood vessels of WT* $BMP10^{lox/lox}$ *(left) vs MerCreMer Bmp10 iKO (right). (C) Representative maximum-intensity confocal images of P21 dorsal ear showing LYVE1+ lymphatic vessels of WT* $BMP10^{lox/lox}$ *(left) vs MerCreMer Bmp10 iKO (right) and (D) relative quantifications of LYVE1+ area for both groups. Each data point represents the average of three separate quantifications per animal. Data is expressed as mean ± SEM. Mann-Whitney tests were used to asses statistical significance (ns p-value > 0.05; * p-value ≤ 0.05; ** p-value ≤ 0.01; *** p-value ≤ 0.001; **** p-value ≤ 0.0001).*

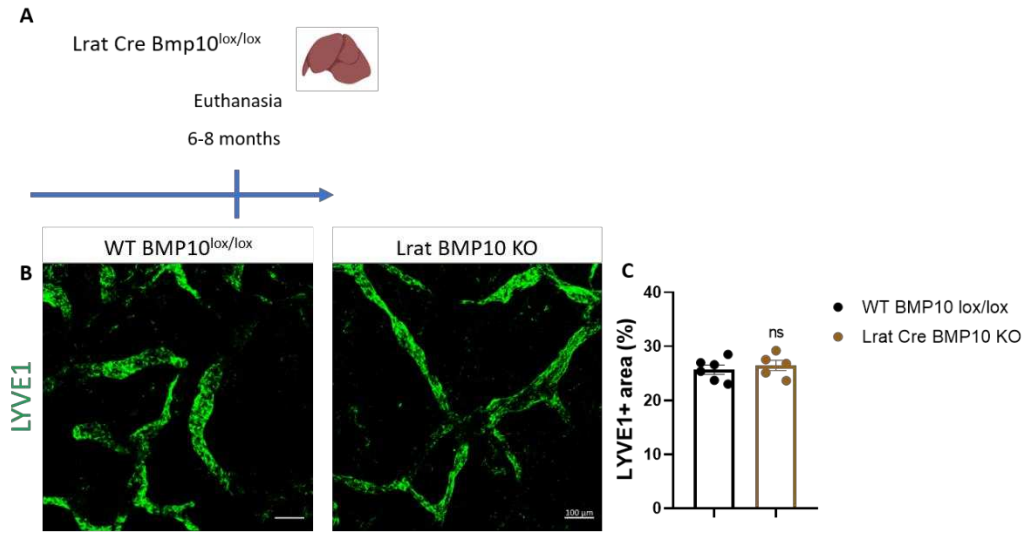


*Figure 45: Deletion of hepatic BMP10 does not affect lymphatic capillaries in adult mouse models.*
*(A) Experimental plan to study hepatic Bmp10 role in post-natal lymphangiogenesis . Litters were euthanised at 6 to 8 months of age. (B) Representative maximum-intensity confocal images of adult dorsal ear showing LYVE1+ lymphatic vessels of WT BMP10$^{lox/lox}$ vs LRat Bmp10 KO and (C) relative quantifications of LYVE1+ area for all groups. Each data point represents the average of three separate quantifications per animal. Data is expressed as mean ± SEM. Mann-Whitney tests were used to asses statistical significance (ns p-value > 0.05; * p-value ≤ 0.05; ** p-value ≤ 0.01; *** p-value ≤ 0.001; **** p-value ≤ 0.0001).*

The lack of phenotype observed in the Lrat Cre BMP10 KO model collides against the hypothesis of the heterodimer BMP-BMP10 having a specific lymphatic role. If it was the case, deletion of hepatic BMP10 (Lrat Cre BMP10 KO) would reveal a phenotype like the one observed in BMP9 KO and Rosa Cre BMP10 iKO, which is not the case.

Studying the dermal lymphatic vasculature in postnatal mice model is quite tricky as the whole ear is more a jelly-like protrusion and separating the two skin layers to visualize the lymphatic vessels is difficult to achieve. During my secondment organized in the framework of the V.A. cure program, I stayed in Uppsala in the Vascular Development Unit headed by Taija Mäkinen in the Rudbeck Laboratory. Here, with the help of PhD student Hans Schoofs, we managed to remove the epidermis of fixed ears at P9 to allow for antibody penetrance, and we performed a tissue clearing protocol, followed by staining with a combination of lymphatics/blood vessels markers. To study the process of lymphangiogenesis and maintenance of lymphatic vessels, several lymphatic endothelial markers can be used namely VEGFR-3, LYVE-1, Prox-1 and PDPN (291). Among the different antibodies tested, the one that gave the best staining result was VEGFR3. During the one-week stay in Uppsala, I learned to image whole mount cleared ears using tissue-deep 2-photon microscopy technique. The obtained 3D image was then processed using Imaris program and VEGFR3 occupied volume in the total ear was quantified **(Figure 46)**. This protocol could be applied in the future to have a better overview of the ear lymphatics upon BMP10 deletion.

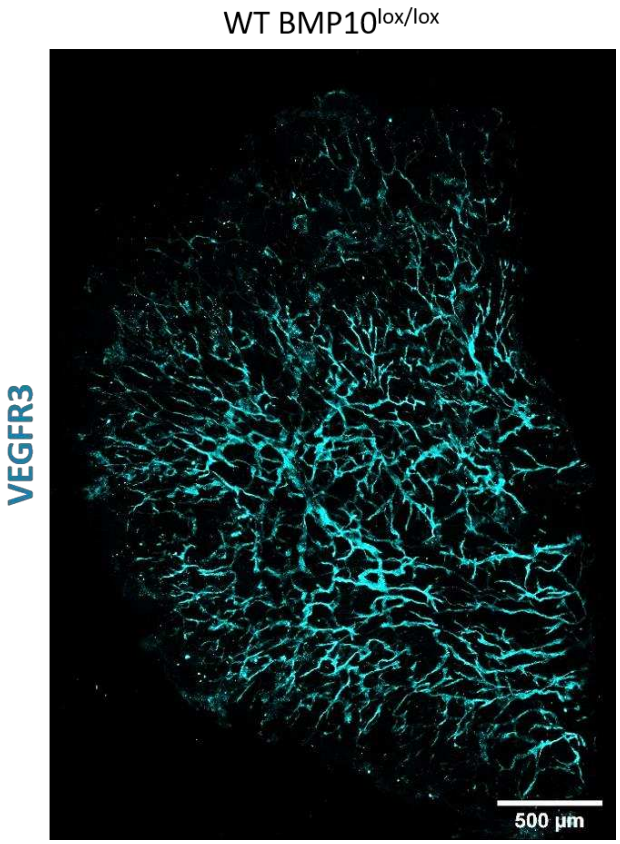


*Figure 46: Whole ear staining of VEGFR3+ lymphatic vessels in WT BMP10 lox/lox at P9.*

Usually, lymphatic vessels are analysed ideally at P21, when the dorsal and ventral ear skin can be easily peeled away from the intervening cartilage (292). Unfortunately, due early death caused by Rosa CreERT2 toxicity, we could not study the role of BMP10 in dorsal ear lymphatic vessels at that stage, nor in the context of lymphatic drainage in adult to see whether, like in BMP9 KO, also BMP10 deficiency impair this process. Nonetheless, it is also possible to study the lymphatic vasculature on other organs such as the trachea or ventral skin (for lymphatic capillaries) and the mesentery (for collecting and pre-collecting lymphatic vessels).

To that aim, we set an experimental plan to induce earlier deletion of BMP10 by injecting tamoxifen at P1 and P2 and analyse the lymphatic vessels of the trachea. In Figure 47 are represented confocal images obtain from LYVE-1+ lymphatic capillaries of the trachea at P6 where it can be appreciated a slight enlargement of the capillaries diameters. If confirmed, this finding would be in accordance to what is observed in the ear lymphatics at P9. Nevertheless, this observation needs to be validated in a higher number of animals in order to be able to assess its statistical significance and the Cre ERT2 control needs to be included.

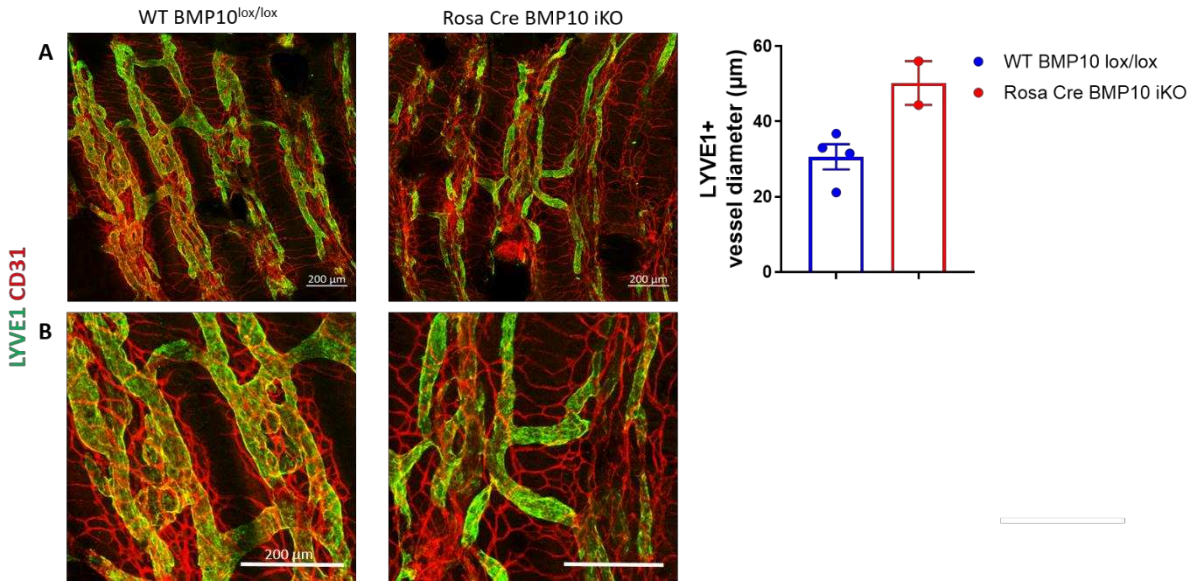


***Figure 47: Deletion of BMP10 results in in slight increase in diameter of total lymphatic vessels in trachea of postnatal mice.***

*(A) Representative confocal immunofluorescence images of P5 trachea showing LYVE-1 lymphatic vessels (green) and CD31 blood vessels (red) of WT BMP10$^{lox/lox}$ (left), vs Rosa Cre BMP10 iKO (right) and (B) relative quantification of vessel diameter (µm). One image per animal was taken and each data point represent an average of 20 measurements per image. Data is expressed as mean ± SEM.*

Overall Rosa Cre BMP10 iKO pups revealed a phenotype that resembles the defects shown in BMP9 KO model in that mice display lymphatic vessels hyperplasia (156,175). This finding introduces, for the first time the function of BMP10 in the context of lymphatic maturation during early postnatal stages. Indeed, further analysis are needed to better characterise the function of BMP10 in lymphatic vessels maturation and maintenance.

# Methodology

## Transgenic mice generation

The generation of BMP9-KO mice was previously described (191) Briefly, exon 2 encoding the entire mature C-terminal region of BMP10 was replaced by a neomycin resistance cassette by homologous recombination of embryonic stem cells. Heterozygous offspring crossed out for 9 generations to obtained *Bmp9*$^{-/-}$ mice in a C57BL/6 background.

To circumvent the early embryonic lethality of BMP10-KO mice (137), the Institut Clinique de la Souris (Illkirch, France) generated a *Bmp10*$^{lox/lox}$ mouse by flanking *lox*P sites around exon 2 which could be then crossed with mice carrying Cre recombinase under the control of different promoters; Rosa26 Cre (Rosa Cre), Lrat Cre and αMHC-MerCreMer (MerCreMer) respectively. The Cre knock-in loci were kept at heterozygosity in all experiments. All mice were maintained in a C57BL/6 background in the animal facility of the CEA Grenoble.

Rosa26-CreER$^{T2}$ mice were generously provided by Prof. P. Chambon (293). αMHC-MerCreMer was generated as previously described (277) and purchased by JAX (stock #00565). Briefly, cDNA encoding the mutant estrogen receptor ligand-binding domain (Mer) flanking Cre recombinase (Cre) was subcloned downstream of the α-MHC 5.5-kb cardiac-specific promoter, which was used to generate transgenic mice. Lrat Cre was generated as previously described (278) and generously provided Dr. Schwabe. Briefly, a bacterial artificial chromosomes (BAC) containing the Lrat gene was modified by recombineering to insert a Cre recombinase: polyA:FRT (flippase recognition target) flanked neomycin cassette (with 60 bp overhangs) into the ATG site of the Lrat gene sequence. The neomycin cassette was removed by arabinose-induced flippase. The BAC was microinjected into the pronuclei of fertilized CBA x C57BL/6J oocytes. Founder line 1 exhibited the highest level of expression in the liver and hepatic stellate cells. This founder was bred to C57BL/6J mice. Mice were backcrossed to C57BL/6J for at least 7 generations.

To generate double-KO mice for BMP9 and BMP10 (ubiquitous or tissue-specific), BMP9 KO mice were crossed either with Rosa26-CreER$^{T2}$, Lrat Cre or αMHC-MerCreMer; *Bmp10$^{lox/lox}$*

The offspring genotypes were determined by PCR as previously reported (195). To induce Cre activation from Rosa Cre and MerCreMer, pups received daily intraperitoneal injections with tamoxifen (Sigma) either for two consecutive days (dosage of 100 mg/kg) or for three consecutive days (dosage 75 mg/kg) depending upon the experiment. Lrat Cre were constitutively active. Mice were housed in a pathogen-free barrier facility, under 14-hour light / 10-hour dark cycle and temperature-controlled environment with access to a standard diet water. All animal experiments were performed in agreement with the Institutional Guidelines, and were in accordance with National Institutes of Health guidelines.

## Enzyme-linked immunosorbent assay (ELISA)

Pro-BMP10 ELISA was performed using an anti-BMP10 capture antibody (clone 13C11) and a biotinylated anti-Pro-BMP10 antibody (BAF3956) detection antibody that recognises both human and mouse Pro-BMP10. For heterodimer BMP9-BMP10 ELISA measurements were performed as previously described (136). Briefly, 96-well plates were coated with the capture antibody: anti-BMP9 (MAB3209, R&D Systems), and incubated O/N at RT. The following day plates were blocked with 5% BSA in PBS, and incubated with plasma diluted in PBS, 0.05% Tween 20, 0.5% Triton X-100 for 2h at RT. Biotinylated detection antibody against BMP10 (anti-mature BMP10: DuoSet R&D Systems, DY2926) was then added and incubated for 2h at RT. Absorbance were read at 450 nm. For Pro-BMP10 ELISA, results are expressed in absorbance measurements, while for BMP9/BMP10 heterodimer detection, available purified heterodimer that had been quantified by Western blotting was used for standard curve.

## Cell culture, transfection, and dual luciferase activity assay

Mouse fibroblasts 3T3 cells were transfected for 4h with a mixture of the reporter plasmid pGL3(BRE)2-luc encoding firefly luciferase downstream of ID1 promoter–derived BMP responsive element promoter (BRE), pRL-TKluc encoding for renilla luciferase downstream of the thymidine kinase promoter (control) and a plasmid encoding human ALK1, as previously described (136). Cells were stimulated with 0.5% plasma O/N. The morning after cells were lysed for luciferase assay measurement.

## Retina preparation and immunofluorescence

Eyeballs were isolated from euthanised pups at P6, then fixed in 4% PFA for 30 minutes at RT, and subsequently dissected under a binocular microscopy. Isolated retina were then blocked in 1% BSA, 0.3% Triton-X100 for 10 min and then incubated with primary antibodies under gentle shaking O/N at 4 °C. The morning after were washed in PBS-Tween 0.1% 3 times for 10 minutes and then incubated in secondary antibodies diluted in blocking buffer for 2h at RT. After washing, stained retina were re-fixed for 10 min in PFA- glutaraldehyde 1% prior to mounting. Antibody used: Isolectin B4 AF488 (Thermofisher, I21411), 1/100 diluted in PBLEC buffer, mouse αSMA coupled with Cy3 (Sigma, C6198), 1/200 diluted in blocking buffer, ERG (Cell Signalling, 97249) 1/200, coupled with Donkey anti rabbit cy5 1/200 (Jackson, 711-175-152). PBLEC buffer composition: 50 µl $MgCl_2$ 1M; 50 µl $CaCl_2$ 1M; 5 µl $MnCl_2$ 1M; 5 ml Triton X-100 10% in 50 ml of PBS. All images were obtained with either a Zeiss Axio Imager M2 fluorescence microscope equipped with an Apotome and ZEN software or a Zeiss Axio Observer Z1 inverted fluorescence microscope and Axiovision 4.8 software. All images were processed with Fiji software.

## Organs preparation for lymphatic vessel immunofluorescence

Either dorsal ear and P9, or ventral skin or trachea at P5 were freshly dissected and fixed O/N at 4°C to be prepared for lymphatic vessels immunofluorescence. Fixed tissues were incubated in PBS, BSA 2%, Triton 0.3% blocking buffer for 6h at 4°C, after primary antibodies appropriately diluted in blocking buffer were added and incubate O/N at 4°C. The following morning samples were thoroughly washed 5 times for 1 hour at 4°C using PBS Triton 0.3%. After, samples were incubated with secondary antibodies appropriately diluted in blocking buffer and incubated O/N at 4°C. Next, samples were washed: 6 times for 1 hour with PBS Triton 0.3% for 30 min at 4°C. At this point, stained samples were re-fix stained with 4% PFA in PBS at 4° O/N, re-washed and mounted/ antibody used: LYVE1 (R&D Systems, AF2125), 1/100 coupled with Alexa488 Donkey anti-Goat (Jackson,705.546.147); CD31 (homemade, MEC 13), 1/5 coupled with Cy3 Donkey anti-Rat (Jackson, 712-165-153).

## Ear preparation for 2-photon confocal

Dissected whole ears at P9 were fixed O/N in 4% PFA and soaked in PBS for a minimum of 48h. The epidermis was manually peeled off under a binocular microscopy and then incubated in CUBIC-L solution O/N at 37 °C. The following morning ears were washed in PBST for 1h under rotation at RT, then blocked in PBST 5% BSA for 2h RT. Next, primary antibodies appropriately diluted in PBS BSA 3% were added for O/N incubation at 4 °C. The following day, samples were

washed 3 times for 1h under rotation and after incubated with secondary antibodies appropriately diluted in PBS BSA 3% O/N at 4 °C. After incubation, ears were washed in PBS 2 times for 1h, and after incubated in CUBIC-R solution for 30 min at 37 °C under rotation.

*Figure 48: Final result for P9 ear mounting for 2-photon microscopy.*

Samples were then mounted on superfrost slides using 300µm spacers (dorsal side facing down) using a µDish 50mm (that functions as a coverslip). At moment of imaging, the dish will be filled of water to avoid vaporisation of the drop in contact with microscopic lens (See  for final result). Antibody used: VEGFR3 (R&D Systems, AF743) 1/100 coupled with Anti-Goat AF647 (Jackson, 705-605-147) 1/500.

# Discussion

BMP9 and BMP10 are two ligands belonging to the TGF- β superfamily, which controls and modulates a wide range of important biological processes. Our groups discovered 15 years ago that both BMP9 and BMP10 hold a high specificity for ALK1 receptor mainly expressed in endothelial cells (ECs), until then considered an orphan receptor (53). Mutations in the BMP9/BMP10/ALK1/ENG signalling pathway are linked to vascular diseases including hereditary hemorrhagic telangiectasia (HHT) and pulmonary arterial hypertension (PAH). In particular, a major threat of HHT is the development of AVM in vital organs such as the lungs, liver, or brain, which can rupture at any moment potentially leading to ischemic injury and stroke. Therefore, it is crucial to understand how AVM forms in order to provide therapeutic treatment for these vascular lesions.

BMP9-BMP10/ALK1/ENG signalling axis is very important in the context of vascular development. Constitutive ALK1 and ENG in mice leads to early embryonic death resulting from severe vascular defects and AVM development (130–133). Moreover, homozygous ALK1 iKO mice (either newborns or adults) die few days after tamoxifen induced invalidation and show strong vessel development defects characterised by vessels hyperplasia, AVMs in retinas as well as other internal organs such as brain and guts, poor smooth muscle coverage and lung haemorrhage (239,192,133). On the other hand, homozygous ENG iKO phenotype is not as striking as ALK1 iKO. In these models, retinas exhibits delayed remodelling of the capillary plexus, with increased veins diameter and proliferation of endothelial cells and localized AVMs as well as abnormal smooth muscle coverage of the veins, although animals survive for longer compared to ALK1 iKO (242). *In vivo* BMP9 and BMP10 have been shown to hold both redundant and specific functions. This duality is believed to depend on their site of expression, kinetics, as well as the different availability of target cells surface receptors expression. As they have been shown to be the functional ligands of ALK1/ENG signalling, a thorough understanding of their roles *in vivo* is clinically relevant to understand vascular diseases like HHT and PAH and, to date, the mechanisms and functions of these factors are still not completely clear. It has been documented that using neutralising antibodies against both BMP9 and BMP10 leads to AVMs formation in the retinal developing vasculature and in intestines (192,193). However,

genetic deletion of BMP9 combined with either postnatal blockade of BMP10 (191) or tamoxifen-mediated CreERT2 BMP10 deletion (discussed in the part III of results section), did not reveal AVM formation.

Regarding BMP9, it has been shown to be mostly redundant in postnatal angiogenesis, although it partially holds a function in the closure of the ductus arteriosus (DA) and in the maintenance and formation of in lymphatic vessels (157,176). Also, different genetic backgrounds and pathogenic environment revealed different sensitivities to the deletion of BMP9. In particular, in the 129/Ola background, BMP9 has been shown to be important for liver endothelial cell fenestration and prevention of fibrosis and BMP9 deletion in the context of hypoxia induced PAH seems to partially protects from the adaptive muscularisation of the pulmonary arterial vascular tree (279,294).

Since the generation of the iKO BMP10 model allowing to overcome embryonic lethality, the function of BMP10 *in vivo* has received increased attention. Prior to the beginning of my project, the team had shown that BMP10 iKO adults from the C57BL/6 background do not display any overt vascular phenotype (279). On the other hand, we showed that in an hypoxia induced environment, mice devoid of BMP10 developed significant cardiac enlargement. This finding indicates that BMP10 does indeed play an important role in cardiac remodelling that could not be revealed under normal physiological conditions, most likely because the heart does not undergo further remodelling at that point (discussed in the Part I of results section). Moreover, like for BMP9, BMP10 has been shown to play a role in the DA closure as, when blocked using neutralising antibodies, the DA reopens after birth due to an EndMT defect (157). Besides, as the concept of genetic modifiers is gaining ground in the study of BMP9 function, as different strains of BMP9 KO revealed different sensitivities, it would be interesting to study whether it is the same for BMP10.

On the other hand, if from one side it is possible now to use iKO to induce BMP10 deletion, we have shown that the use of tamoxifen-inducible BMP10 KO in the whole body using R26CreERT2 model in pups results in Cre toxicity. In particular, we proved that Cre ERT2 animals, in the absence of floxed BMP10, display impaired haematopoiesis and bone marrow vasculature defects making the study of BMP10, using this CreERT2 line, more difficult (as the right controls need to be included in all experiments) and, in some instances, even impracticable. We noticed that although Rosa Cre BMP10 iKO did not reveal any overt vascularisation defect, sometimes in the developing retinal vasculature, veins uptake αSMA coverage. Importantly, it still needs to be validated whether this observation is a consequence of BMP10 deletion or an artefact due to Cre toxicity. If we can show that BMP10 deletion results in αSMA vein coverage, it could hypothesised that it results from a failure of arteriovenous identity or a partial activation of the EndMT program. Indeed, in EC-specific SMAD4 iKO mice, SMA coverage in the vasculature of the retina is decreased in arteries and increased in veins,

implying either a loss of arteriovenous identity or an increase in venous muscularisation in response to higher blood flow (153,243). To this regards, it has been shown that muscularisation of arteriovenous malformations results from increased blood flow (242), which could partially explanation the observed phenotype. It has been proposed that BMP2/BMP4 signalling via vein-specific ALK3 type I receptor activates SMAD1/5 signalling resulting in transcriptional activation of EphB4 and COUP genes specifying venous identity (65). It could be plausible that BMP10, having some affinity for ALK3 ligand, could also have a role in vein identity via this signalling pathway. Nonetheless, more in depth analysis should be carried out to confirm this observed phenotype and including the Cre ERT2 control lacking floxed *Bmp10* gene. Another hypothesis that could be ventured on the uptake of αSMA by the veins could be that lack of BMP10 could lead to a partial activation of the EndMT program. To that account, a partial EndMT activation can results in the appearance of cells with endothelial and mesenchymal characteristics including αSMA uptake to the expenses of the endothelial markers. BMP9 and BMP10 have been described to up-regulate the expression of transcription factors involved in EndMT, including SNAI (157). It could be proposed that, as a response to loss of BMP10, BMP9 activates a compensatory mechanism resulting in overexpressing markers such as SNAI1/2 initiating a partial EndMT, resulting in veins up taking αSMA coverage. Indeed, at this stage, these are only conjectures and there is a need for further analysis including the right controls before being able to make any conclusion.

More recently, an ANF-Cre *Bmp10*$^{lox/lox}$ mouse model for tissue-specific deletion of BMP10 in the right atrium was developed, with the Cre being active from E10.5 onwards (280). These animals were viable throughout adulthood, which was unexpected considering the well-characterised role of BMP10 during cardiac development. Moreover, in this work, the potential function of BMP10 coming from the liver was not mentioned. As the main source of BMP10 is the right atria, the scientific community tends to consider the ligand coming from this organ to be the most important, thus neglecting the hepatic BMP10.

On a different note, an alternative route to avoid the Cre toxicity issue observed using the R26 CreERT2, and being able to study the postnatal function of BMP10, could be to cross ANF-Cre BMP10 with Lrat Cre BMP10. However, we are not certain that these are the two only sources of BMP10 expression, and generating such a model could not be as efficient as using an ubiquitous promoter such as Rosa Cre.

Next we confirmed that concomitant deletion of BMP9 and BMP10 leads to strong vascular defect in postnatal retinal angiogenesis characterised by a decrease in radial extension, significant enlargement of the veins, and increase in vascularisation in the front accompanied by a raise of ERG+ endothelial cells number. This phenotype is similar to the one described using neutralising antibodies against BMP10 in BMP9 KO (191). In addition, we could confirm

that the phenotype is not linked to a Cre toxicity as the Rosa Cre BMP10 iKO did not reveal any overt vascular phenotype.

The increase of vein diameter is consistent with vessels enlargement observed in adults (279). Blood flows from central retina artery to the capillaries to be then drained out to the central vein. For that, the central area of the retina is characterised by a thicker vasculature compared to that of the peripheral retina (295). Hyperplasia has been shown to results from increase in blood flow, which could explain the veins enlargement in the central retina and increase in total ECs. Analysis of mice models deficient for ALK1 or ENG allowed their functional identification in the context of development and maintenance of arteriovenous identity. Mutations in genes associated with HHT have been shown to disrupt vascular remodelling and the maintenance of vessel wall integrity (296).
Moreover, we observed a loss of arterial αSMA coverage, which could result from vSMCs loss, or phenotype switching from a contractile (quiescent) to a synthetic (proliferative) state. This finding is also in agreement with a recent publication in which it was shown that double-KO *Bmp9* $^{-/-}$; ANF-Cre *Bmp10*$^{lox/lox}$ (ANF-Cre dKO), in which BMP10 was deleted specifically from the heart, resulted dramatic changes in vascular tone and diminution of the vSMC layer, as well as reduced systemic and right ventricular systolic pressure (280). This would support the active role of BMP9 and BMP10 in the maintenance of EC quiescence, allowing for either direct or indirect recruitment of smooth muscle cells that, in turn, would establish a quiescent mature vasculature. Indeed, the absence of these ligands disrupts the quiescent state, resulting in vessel dilation and loss of SMC coverage. The next step should involve examining different markers of pericytes/smooth muscle cells surrounding the retinal vasculature as well as markers of contractility in order to get a better understanding about the mechanisms underlying this observed phenotype.
Still, the vasculature defects observed in the double-KOs (either in the ANF-Cre *Bmp10*$^{lox/lox}$ or the Rosa CreERT2 *Bmp10*$^{lox/lox}$) are not as strong as the ones described when their receptors are deleted. In particular, concomitant deletion of the two ligands did not reveal AVM formations, supporting the theory that other ligands can bind ALK1. Interestingly, a recent study found that insulin, which has been known to promotes angiogenesis and maintains vascular homeostasis via the canonical PI3K and MAPK signalling pathways, could induce a cross-reaction between its insulin receptor (IR) and the ENG/ALK1 complex to control gene expression via the SMAD1/5 signalling pathway (297). It would be interesting to see if blocking insulin in our Rosa dKO model would result in the development of retina AVMs similar to those seen in ALK1 and ENG KOs.
Another question that remains to be answered is whether this observed increase of endothelial cells at the vascular front, is associated with an increase in proliferation resulting from an angiogenic stimuli such as VEGF. For that a quantification of circulating VEGF and EdU test to check for eventual increase in proliferation should be also carried out in the future.

BMP10 has been shown to be expressed in the right atria of the adults and, although not to the same extent, by the liver (136). However, up to date, to our knowledge, there are no studies addressing the function of the hepatic BMP10. In 2018 Tillet *et al*., showed that BMP9 and BMP10 can form an heterodimer found in the circulation that is responsible for activating ALK1 receptor (136). Moreover, the heterodimerisation of BMP9/10 via disulphide bridge suggests a common production site of both BMPs, which we hypothesised to be the liver. To prove this hypothesis, we generated mice models for tissue specific BMP10 KO by crossing out *BMP10*$^{lox/lox}$ model with either (i) αMHC-MerCreMer mice (MerCreMer BMP10 iKO – inducible cardiac specific deletion) or (ii) Lrat Cre mice (Lrat Cre BMP10 KO – constitutive liver specific deletion). We managed to validate that the Cre drivers correctly invalidate BMP10 specifically at its expression site. Results obtained from ELISA for the detection of both Pro-BMP10 and BMP9/BMP10 revealed that ubiquitous deletion of BMP10 results in a loss of measured circulating Pro-BMP10 and heterodimer BMP9/BMP10, as expected. Moreover, only when hepatic BMP10 was deleted (Lrat Cre BMP10 KO), we could observe a loss of measured circulating Pro-BMP10 and BMP9/BMP10, but not when cardiac BMP10 was deleted (MerCreMer BMP10 iKO). This confirms that the circulating measured BMP10 as well as the heterodimer does in fact come from the liver. To our knowledge, this is the first time that the hepatic BMP10 is being studied after the discovery of the heterodimer. Moreover, using the BRE assay we were able to prove that indeed, the heterodimer coming from the liver is responsible for ALK1-induced activity.

It is important to keep in mind that with the Pro-BMP10 ELISA we managed to measure levels of circulating unprocessed BMP10, however we still need to quantify the levels of mature circulating BMP10. Nonetheless, using ELISA to measure Pro-BMP10 has been shown to detect higher levels of BMP10 compared to the BMP10 ELISA detecting the mature form which has been shown to detect very low levels of mature BMP10 (279,289). Also, the levels detected with the ELISA test do not necessarily correspond to the true *in vivo* levels. In particular, our group has demonstrated that purifying mice plasma with an anti-BMP10 column leads to a higher yield of detected BMP10 than raw plasma, implying the presence of a dormant BMP10 reservoir that is unmasked by the purification step process (136). It is tempting to speculate that this dormant reservoir comes from the right atria. Indeed, this hypothesis should be tested in the future, by using plasma from the three groups and perform the ELISA before and after the purification step using an anti-BMP10 column to confirm (i) whether the levels of detected BMP10 are increase and (ii) to check whether BMP10 coming from the heart is detectable in Lrat BMP10 KO.

Another remark from the Pro-BMP10 and BMP9/BMP10 ELISA that we made was that BMP10 levels are higher in WT groups that were injected with tamoxifen, which is not the case for the WT BMP10 group that was not injected with tamoxifen **(Figure 38 and Figure 39)**. As the background strain and the age of the animals were approximately the same for all groups, one

explanation to this phenomenon could be that, tamoxifen injection somehow results in increase of circulating BMP10. It is widely known that tamoxifen administration may have some adverse side effects that could lead to misleading interpretation of results (290). A previous report shows tamoxifen induced triacylglycerol accumulation due to fatty acid synthesis activation (298). One explanation of increase BMP10 levels in injected animals could be a higher demand in fat metabolism due to tamoxifen injection. To this account, ALK1 has been reported as to mediate low-density lipoprotein (LDL) uptake (299), and BMP9 has been recently described as a mediator of this transcytosis (300) as well as being reported as fat metabolism regulator (301). A recent study demonstrates the role of BMP10 in regulation of lipid metabolisms in mouse-derived muscle cells (302). To verify for a potential tamoxifen -induced artefact, WT *Bmp10*$^{lox/lox}$ and Lrat Cre BMP10 should be injected with tamoxifen, to see if the detected BMP10 levels are increased in the WT group compared to the non-injected ones. Moreover, one should bear in mind that a potential cofounding effect might be also due to the delivery vehicle for tamoxifen. Previous reports revealed fatty livers in mice administered with corn oil (303). Therefore, potential toxicity due to delivery of corn oil alone should be also addressed in future studies. Still, whether or not we can confirm an increase of BMP10 circulating due to tamoxifen or corn oil administration, it would not answer whether these substances somehow unmasks undetectable circulating BMP10 or do in fact stimulates its production or release into the bloodstream from the tissue where its produced.

At this point we know that the BMP9/BMP10 heterodimer is responsible for the detected activity in the peripheral blood (136), and we could confirm that the source of the BMP10 contributing in its formation is the liver, yet its biological role is still to be determined. Conditional gene knock-down at the transcription level is a widely used method to study gene function; however, this system relies in the deletion of a targeted gene at the DNA level and do not affect directly the protein product of the gene. To study the biological function of the BMP9/BMP10 heterodimer, one should consider that this protein is the result of BMP9 and BMP10 ligands fusing into a heterodimer. Genetic deletion of homodimeric BMP9 or BMP10 at the DNA level would not be the best option to study the function of the heterodimer as it will not only knock-down its expression, but that of the BMP9 and BMP10 homodimers too. To be able to study specific function of the heterodimer, alternate routes shall be considered in the future. For instance, much interest has been directed toward targeting protein degradation to study its biological function (304–306). Theoretically, to block the heterodimer, target peptides against unique regions of the individual substrates could be used. Nonetheless, before accomplish this, a characterisation of the BMP9/BMP10 structure is needed.

Having confirmed the roles of BMP9 and BMP10 in postnatal retinal angiogenesis, we aimed to study cardiac vs hepatic BMP10 role in this context. For that, we generated double-KO models for cardiac and hepatic BMP10 deletion in parallel with BMP9: MerCreMer cDKO and Lrat Cre DKO respectively. To our surprise, we did not see any overt vascular defect in the MerCreMer

cDKO. As for the Lrat Cre dKO, we still cannot make any conclusion. From the two Lrat Cre DKO mice that we analysed (obtained from crossing heterozygous *Bmp9*$^{+/-}$*; Bmp10*$^{lox/lox}$ parents), we did not validated loss of BMP9 and BMP10 in the liver therefore, we cannot conclude that these are actually double knock-out. We noticed that crossing BMP9 KO with Lrat Cre *Bmp10*$^{lox/lox}$ leads to severe fertility problems. Since this experiment, we have made 54 crossings and only managed to get four Lrat Cre dKO which are still alive. However, we are unsure whether or not a successful BMP10 recombination occurred in the liver of these animals. To our opinion these findings bring hepatic BMP10 into play and it would be of interest to further analyse its function. Reasonably, one could assume that the hepatic BMP10 has an important function during embryonic development and that, concomitant deletion of BMP9 and hepatic BMP10 results in embryonic lethality. Moreover, we do not know at which stage during gestation is the Lrat Cre activated, and this calls for future validation.

Another opened question that we had was whether, like BMP9, BMP10 has a specific function in lymphatic vessels formation/maintenance. We could confirm that deletion of BMP10 alone is sufficient to reveal a defect in the lymphatic capillaries phenotype, which is not due to Cre toxicity. The lymphatic vessels hyperplasia detected resembles those observed in the BMP9 KO model (156,175). Indeed, further analysis are needed to better characterise the function of BMP10 in lymphatic vessels maturation and maintenance. Preliminary findings revealed that the phenotype is also observable in the capillaries of the trachea, although this needs further confirmation.

Having observed from these preliminary data that deletion of BMP10 seems to have similar repercussion as BMP9 KO in the context of postnatal lymphatic development, we hypothesised that the BMP9/BMP10 heterodimer could have a function on lymphatic vessels maintenance/formation. We aimed to unveil its potential function using the Lrat BMP10 KO model to specifically delete BMP10 from the liver. Given that lymphatic capillaries act as filters for blood plasma, we hypothesised that the circulating heterodimer present in plasma could have a specific function via the ALK1 receptor signalling (which is known to be expressed in LECs). However, immunofluorescence analysis of LYVE-1 stained lymphatic vessels of the dorsal ear of MerCreMer BMP10 iKO and Lrat Cre BMP10 KO revealed no obvious defect when compared to WT littermates in both postnatal and adult mice. A plausible explanation for the lack of phenotype for tissue-specific BMP10 KO is that BMP10 from the unaffected source can compensate for each other. To test this, mice could be crossed to produce newborns with both tissue specific Cre: Lrat Cre and MerCreMer *Bmp10*$^{lox/lox}$ and see if the phenotype seen in the Rosa Cre BMP10 iKO is reproducible.

Overall, we still have no cue as for the functional role of cardiac and hepatic BMP10. From one side we have shown that hepatic BMP10 is the source of the detected circulating forms BMP10 and BMP9/BMP10 heterodimer, yet is function is unknown. On the other side, the function of

the cardiac BMP10 during postnatal development is at the moment unknown. As BMP10 has been shown to be an important regulator of cardiovascular development, growth, and maturation, it would be interesting to investigate whether postnatal deletion of the ligand coming from the heart (MerCreMer iKO) affects cardiac lymphatics. Indeed, the cardiac lymphatic developmental process endures throughout postnatal stages and it seems to reach its completion 2-3 weeks after birth (307). Also, the first cardiac lymphatics sprouts appear at the base of the heart just after the appearance of the first coronary vessels on E12 (307,308), before the onset of coronary blood circulation at E14 , so they could be also be studied using the ANF Cre *Bmp10*$^{lox/lox}$ model in which the Cre is active after E10.5.

Overall, my thesis work has led to several advances in the understanding of the *in vivo* function of BMP10 in both active angiogenesis and homeostasis and lymphatic vessels maturation/maintenance. Moreover, the generation of tissue specific models for BMP10 deletion allowed us confirm that the liver is the secretion source of both homodimeric BMP10 and heterodimeric BMP9/BMP10 opening up for new biological questions.

# Perspectives

Overall, I trust that my thesis project brought to some advancement in the understanding of the specific and redundant function of BMP10 in different contexts. To this, I wish to stress some point that I personally believe to be important as well to propose new ideas that, to my consideration should be further investigated in the future.

## BMP10 – specific function in the context of blood and lymphatic vascular bed formation and homeostasis

The R26Cre ERT2; *Bmp10*$^{lox/lox}$, despite its proved Cre toxicity, still makes a good model to study the function of BMP10. Nonetheless, it is important to keep in mind to use the right controls for any eventual planned experiments. We showed that in the retina of Rosa Cre BMP10 iKO sometimes vein uptake of αSMA coverage. In the future, it should be analysed whether this is a true consequence of BMP10 deletion of an artefact due to Cre toxicity. If confirmed that the phenotype results from loss of BMP10, it would be interesting to further investigate whether it results from a failure of arteriovenous identity, or a partial activation of EndMT.

Moreover, as discussed, the idea that genetic modifiers is taking hold within the context of pathologies related to vascular development/homeostasis. In particular, a strain-dependent effect for either deletion of BMP9 or ENG has been identified with the 129/Ola background being more sensitive to deletion of BMP9 compared to other mice strain. It should be analysed whether this is the case for BMP10 as well. In rare cases, mutations in genes encoding for BMP9 and BMP10 have been found to be associated with patients affected by HHT and PAH. Analysis of vascular-sensitive background strain, upon an external insult, could shed a light into the mechanistics behind these diseases. Nonetheless, it needs to be taken into account that backcross breeding to obtain a new genetic found could take a long time.

Among other findings, this project allowed to introduce the idea that not only BMP9, but also BMP10 has a role in lymphatic vasculature formation/maintenance. Apart from the need to better characterise its function by analysing mesenteric collecting vessels, the lymphatic valves

and the drainage efficiency, it may be interesting in the future to investigate the role of BMP10 during lymphatics development. To study this aspect, in my opinion, a good model would be achieved by crossing mice harbouring ANF Cre specific to the right atria where the Cre recombinase becomes activated after E10.5, together with LratCre *BMP10$^{lox/lox}$*. Considering the BMP10 function in cardiac development, it could also be interesting to utilise this model to study BMP10 function during the development of cardiac lymphatics as it develops after the activation of the ANF Cre mediating BMP10 deletion in the heart.

Moreover, the use of tissue specific models allowed us to prove the origin of BMP10 homodimer and BMP9/BMP10 heterodimer circulating in plasma is the liver. However, it seems that there is some "masked" BMP10 in the circulation and it should be analysed whether it comes from the right atria BMP10. Indeed, it could be that cardiac BMP10, besides its autocrine function, also bear an endocrine role allowing to compensate for the eventual lack of circulating BMP10 coming from the liver and that it could, from there, reach the location where its function is needed. This would allow us to explain the lack of phenotype observed in the lymphatic capillaries of cardiac and hepatic tissue-specific BMP10 deletion.
Another hypothesis could be that there is another source of BMP10 that is activated under stressed conditions which, alone, is able to maintain vascular homeostasis via ALK1 axis. I believe it could be worth to further investigate this theory, which would allow to better understand the mechanisms behind the sources of biosynthesis and expression of this ligand and therefore, its functional role in physiological as well as pathological conditions. Indeed, BMP10 expression in the rat central nervous system (CNS) has been described to be up-regulated as a response to brain lesion and repair and its expression has been shown to be controlled by astrocyte activation (309). It could be envisioned that a similar mechanisms could happen when BMP9 is absent in parallel with induced loss of BMP10 from its two main secretory organs known.

### Lrat Cre dKO - a mouse model to be further characterised

With regards to the generation of the *Bmp9$^{-/-}$* Lrat Cre *Bmp$^{lox/lox}$ Cre dKO*, we observed that crossing these two lines leads to severe fertility problems. Indeed, we do not know when the Lrat Cre promoter gets activated during gestation and whether, embryonic deletion of hepatic BMP9 and BMP10 leads to lethality. I believe that these observations calls for further analysis.

### BMP9 and BMP10 function via ALK1-signalling in vascular context – are we missing other ligands?

BMP9 and BMP10 play a clear role in maintaining vascular quiescence. Under physiological conditions, the concomitant deletion of both BMP9 and BMP10 disrupts the quiescent state, resulting in vessel dilation and reduction of SMC coverage in both postnatal and adult stages. The ubiquitous Rosa dKO model did not develop AVMs like the ones observed in the ALK1 or

ENG KO models. It would be interesting investigate for other potential ligands able to prevent formation of AVMs by maintaining the signalling via ALK1/ENG receptors. For instance, as it was recently shown that insulin induces a cross-reaction between its IR receptor and ENG/ALK1 complex to control gene expression via SMAD1/5 (297), it could be analysed if, using anti-insulin neutralising antibodies in the Rosa dKO, would result in the development of AVMs similar to those seen in ALK1 and ENG KOs. If this could be confirmed it would prove that insulin, and probably other ligands, are able to prevent the formation of AVMs in the absence of BMP9 and BMP10. This type of investigation would allow for a better understanding behind the mechanisms leading to the formations of arteriovenous malformation thus paving the way toward new therapeutic strategies for diseases in which this signalling axis in involved such as HHT and PAH.

Over the past few decades, much effort has been put toward the understanding of BMP9/10/ALK1/ENG signalling pathway. It is critical to continue toward this direction in order to gain a better understanding of the physiological and pathological role of this pathway in the context of vascular development to be able to propose new therapeutic strategies as well as to explore the function of the ligands in other contexts.

### BMP9 and BMP10 as therapeutic targets

The generation of tissue specific models for BMP10 described in this manuscript could be applied in the future to study their specific function under pathological conditions. We have successfully shown that in response to hypoxia, BMP10 deficient mice have a defect in cardiac remodelling. It could be interesting to analyse the two tissue specific models after PAH-inducement. It could be hypothesised that this defect in cardiac remodelling results from loss of cardiac BMP10 and that, in the absence of liver BMP10 this phenotype does not develop. Indeed this hypothesis needs further validation.
Hopefully, my thesis project brought to the community new information about BMP9 and BMP10 in the context of vascular homeostasis and vascular diseases. Ultimately, the aim of understanding their function is directed toward the need of developing new therapies in the context of vascular pathologies as well as other conditions, which sees them involved. While the role of these growth factors in the maintenance of vascular quiescence is now relatively well accepted, their use in the clinic, particularly in the context of PAH, is still under debate. This further stresses the importance of better understanding the fine regulation of BMP9 and BMP10.

BMP9 treatment has been proposed for bone regeneration as well as in preclinical models of oxygen-induced retinal neovascularization and left ventricular heart failure (310,311). Given its specificity toward different receptors, attention has been directed toward the generation of modified BMPs that only bind to a specific receptor, for example, a BMP9 mutant (D366E) was

engineered that does not bind to ALK2 and can thus be used as a specific activator of ALK1 (146). Indeed, a thorough understanding of these ligand/receptor complexes in different contexts will benefit toward the development of new therapeutic strategies. A recent study showed that ALK1 is not the only type I receptor involved in BMP-induced vascular regulation: loss of function of ALK2 and ALK3 as well as BMPRII revealed vascular defects upon angiogenesis (312). Drug candidates targeting this pathway are being developed in the context of vascular diseases. Certainly, a better understanding of the molecular insights of this signalling pathway could ultimately allow for the development of small peptides derived from these BMPs, which could selectively and specifically enhance/suppress receptor-mediated signalling.

# Bibliography


1. Taylor AM, Bordoni B. Histology, Blood Vascular System. In: StatPearls [Internet]. Treasure Island (FL): StatPearls Publishing; 2022 [cited 2022 Jul 19]. Available from: http://www.ncbi.nlm.nih.gov/books/NBK553217/

2. Tucker WD, Arora Y, Mahajan K. Anatomy, Blood Vessels. In: StatPearls [Internet]. Treasure Island (FL): StatPearls Publishing; 2022 [cited 2022 Jul 19]. Available from: http://www.ncbi.nlm.nih.gov/books/NBK470401/

3. Jouda H, Larrea Murillo L, Wang T. Current Progress in Vascular Engineering and Its Clinical Applications. Cells. 2022 Jan 31;11(3):493.

4. Breslin JW, Yang Y, Scallan JP, Sweat RS, Adderley SP, Murfee WL. Lymphatic Vessel Network Structure and Physiology. Compr Physiol. 2018 Dec 13;9(1):207–99.

5. Dejana E, Hirschi KK, Simons M. The molecular basis of endothelial cell plasticity. Nat Commun. 2017 Feb 9;8(1):14361.

6. Risau W. Mechanisms of angiogenesis. Nature. 1997 Apr 17;386(6626):671–4.

7. Carmeliet P. Mechanisms of angiogenesis and arteriogenesis. Nat Med. 2000 Apr;6(4):389–95.

8. Ribatti D, Vacca A, Nico B, Roncali L, Dammacco F. Postnatal vasculogenesis. Mech Dev. 2001 Feb;100(2):157–63.

9. Ribatti D, Pezzella F. Overview on the Different Patterns of Tumor Vascularization. Cells. 2021 Mar 13;10(3):639.

10. Drake CJ. Embryonic and adult vasculogenesis. Birth Defects Res Part C Embryo Today Rev. 2003;69(1):73–82.

11. Goldie LC, Nix MK, Hirschi KK. Embryonic vasculogenesis and hematopoietic specification. Organogenesis. 2008;4(4):257–63.

12. Poole TJ, Finkelstein EB, Cox CM. The role of FGF and VEGF in angioblast induction and migration during vascular development. Dev Dyn Off Publ Am Assoc Anat. 2001 Jan;220(1):1–17.

13. Kelly MA, Hirschi KK. Signaling hierarchy regulating human endothelial cell development. Arterioscler Thromb Vasc Biol. 2009 May;29(5):718–24.

14. Marcelo KL, Goldie LC, Hirschi KK. Regulation of endothelial cell differentiation and specification. Circ Res. 2013 Apr 26;112(9):1272–87.

15. De Val S, Black BL. Transcriptional control of endothelial cell development. Dev Cell. 2009 Feb;16(2):180–95.

16. Oh SY, Kim JY, Park C. The ETS Factor, ETV2: a Master Regulator for Vascular Endothelial Cell Development. Mol Cells. 2015 Dec 31;38(12):1029–36.

17. Schuh AC, Faloon P, Hu QL, Bhimani M, Choi K. In vitro hematopoietic and endothelial potential of flk-1−/− embryonic stem cells and embryos. Proc Natl Acad Sci U S A. 1999 Mar 2;96(5):2159–64.

18. Xu K, Cleaver O. Tubulogenesis during blood vessel formation. Semin Cell Dev Biol. 2011 Dec;22(9):993–1004.

19. Caduff JH, Fischer LC, Burri PH. Scanning electron microscope study of the developing microvasculature in the postnatal rat lung. Anat Rec. 1986 Oct;216(2):154–64.

20. Burri PH, Djonov V. Intussusceptive angiogenesis--the alternative to capillary sprouting. Mol Aspects Med. 2002 Dec;23(6S):S1-27.

21. Nitzsche B, Rong WW, Goede A, Hoffmann B, Scarpa F, Kuebler WM, et al. Coalescent angiogenesis—evidence for a novel concept of vascular network maturation. Angiogenesis. 2022;25(1):35–45.

22. Mentzer SJ, Konerding MA. Intussusceptive Angiogenesis: Expansion and Remodeling of Microvascular Networks. Angiogenesis. 2014 Jul;17(3):499–509.

23. Djonov VG, Kurz H, Burri PH. Optimality in the developing vascular system: branching remodeling by means of intussusception as an efficient adaptation mechanism. Dev Dyn Off Publ Am Assoc Anat. 2002 Aug;224(4):391–402.

24. Djonov V, Baum O, Burri PH. Vascular remodeling by intussusceptive angiogenesis. Cell Tissue Res. 2003 Oct 1;314(1):107–17.

25. Logothetidou A, De Spiegelaere W, Vandecasteele T, Tschulenk W, Walter I, Van den Broeck W, et al. Intussusceptive Pillar Formation in Developing Porcine Glomeruli. J Vasc Res. 2018;55(5):278–86.

26. Uccelli A, Wolff T, Valente P, Maggio ND, Pellegrino M, Gürke L, et al. Vascular endothelial growth factor biology for regenerative angiogenesis. Swiss Med Wkly [Internet]. 2019 Jan 27 [cited 2022 Jul 21];(3). Available from: https://smw.ch/article/doi/smw.2019.20011

27. Carmeliet P. Angiogenesis in life, disease and medicine. Nature. 2005 Dec 15;438(7070):932–6.

28. Carmeliet P, Jain RK. Molecular mechanisms and clinical applications of angiogenesis. Nature. 2011 May 19;473(7347):298–307.

29. Bouïs D, Kusumanto Y, Meijer C, Mulder NH, Hospers GAP. A review on pro- and anti-angiogenic factors as targets of clinical intervention. Pharmacol Res. 2006 Feb;53(2):89–103.

30. Armulik A, Genové G, Betsholtz C. Pericytes: developmental, physiological, and pathological perspectives, problems, and promises. Dev Cell. 2011 Aug 16;21(2):193–215.

31. De Smet F, Segura I, De Bock K, Hohensinner PJ, Carmeliet P. Mechanisms of vessel branching: filopodia on endothelial tip cells lead the way. Arterioscler Thromb Vasc Biol. 2009 May;29(5):639–49.

32. Adams RH, Eichmann A. Axon guidance molecules in vascular patterning. Cold Spring Harb Perspect Biol. 2010 May;2(5):a001875.

33. Benedito R, Rocha SF, Woeste M, Zamykal M, Radtke F, Casanovas O, et al. Notch-dependent VEGFR3 upregulation allows angiogenesis without VEGF-VEGFR2 signalling. Nature. 2012 Mar 18;484(7392):110–4.

34. Geudens I, Gerhardt H. Coordinating cell behaviour during blood vessel formation. Development. 2011 Nov 1;138(21):4569–83.

35. Carlier A, Geris L, Bentley K, Carmeliet G, Carmeliet P, Van Oosterwyck H. MOSAIC: a multiscale model of osteogenesis and sprouting angiogenesis with lateral inhibition of endothelial cells. PLoS Comput Biol. 2012;8(10):e1002724.

36. Betsholtz C. Cell–cell signaling in blood vessel development and function. EMBO Mol Med. 2018 Mar;10(3):e8610.

37. Lindahl P, Johansson BR, Levéen P, Betsholtz C. Pericyte loss and microaneurysm formation in PDGF-B-deficient mice. Science. 1997 Jul 11;277(5323):242–5.

38. Betsholtz C. Insight into the physiological functions of PDGF through genetic studies in mice. Cytokine Growth Factor Rev. 2004 Aug;15(4):215–28.

39. Fantin A, Vieira JM, Gestri G, Denti L, Schwarz Q, Prykhozhij S, et al. Tissue macrophages act as cellular chaperones for vascular anastomosis downstream of VEGF-mediated endothelial tip cell induction. Blood. 2010 Aug 5;116(5):829–40.

40. Benedito R, Roca C, Sörensen I, Adams S, Gossler A, Fruttiger M, et al. The notch ligands Dll4 and Jagged1 have opposing effects on angiogenesis. Cell. 2009 Jun 12;137(6):1124–35.

41. Spatial and temporal role of the apelin/APJ system in the caliber size regulation of blood vessels during angiogenesis. EMBO J. 2008 Feb 6;27(3):522–34.

42. del Toro R, Prahst C, Mathivet T, Siegfried G, Kaminker JS, Larrivee B, et al. Identification and functional analysis of endothelial tip cell-enriched genes. Blood. 2010 Nov 11;116(19):4025–33.

43. Saharinen P, Bry M, Alitalo K. How do angiopoietins Tie in with vascular endothelial growth factors? Curr Opin Hematol. 2010 May;17(3):198–205.

44. Fukuhara S, Sako K, Noda K, Zhang J, Minami M, Mochizuki N. Angiopoietin-1/Tie2 receptor signaling in vascular quiescence and angiogenesis. Histol Histopathol. 2010 Mar;25(3):387–96.

45. Gaengel K, Niaudet C, Hagikura K, Laviña B, Muhl L, Hofmann JJ, et al. The Sphingosine-1-Phosphate Receptor S1PR1 Restricts Sprouting Angiogenesis by Regulating the Interplay between VE-Cadherin and VEGFR2. Dev Cell. 2012 Sep 11;23(3):587–99.

46. Benn A, Hiepen C, Osterland M, Schütte C, Zwijsen A, Knaus P. Role of bone morphogenetic proteins in sprouting angiogenesis: differential BMP receptor-dependent signaling pathways balance stalk vs. tip cell competence. FASEB J. 2017 Nov;31(11):4720–33.

47. Akla N, Viallard C, Popovic N, Lora Gil C, Sapieha P, Larrivée B. BMP9 (Bone Morphogenetic Protein-9)/Alk1 (Activin-Like Kinase Receptor Type I) Signaling Prevents Hyperglycemia-Induced Vascular Permeability. Arterioscler Thromb Vasc Biol. 2018 Aug;38(8):1821–36.

48. Jain RK. Molecular regulation of vessel maturation. Nat Med. 2003 Jun 1;9(6):685–93.

49. Potente M, Gerhardt H, Carmeliet P. Basic and therapeutic aspects of angiogenesis. Cell. 2011 Sep 16;146(6):873–87.

50. Dyer LA, Patterson C. Development of the endothelium: an emphasis on heterogeneity. Semin Thromb Hemost. 2010 Apr;36(3):227–35.

51. Maisonpierre PC, Suri C, Jones PF, Bartunkova S, Wiegand SJ, Radziejewski C, et al. Angiopoietin-2, a natural antagonist for Tie2 that disrupts in vivo angiogenesis. Science. 1997 Jul 4;277(5322):55–60.

52. Desroches-Castan A, Tillet E, Bouvard C, Bailly S. BMP9 and BMP10: Two close vascular quiescence partners that stand out. Dev Dyn Off Publ Am Assoc Anat. 2022 Jan;251(1):178–97.

53. David L, Mallet C, Mazerbourg S, Feige JJ, Bailly S. Identification of BMP9 and BMP10 as functional activators of the orphan activin receptor-like kinase 1 (ALK1) in endothelial cells. Blood. 2006 Oct 26;109(5):1953–61.

54. Cavallaro U, Dejana E. Adhesion molecule signalling: not always a sticky business. Nat Rev Mol Cell Biol. 2011 Mar;12(3):189–97.

55. Tillet E, Vittet D, Féraud O, Moore R, Kemler R, Huber P. N-cadherin deficiency impairs pericyte recruitment, and not endothelial differentiation or sprouting, in embryonic stem cell-derived angiogenesis. Exp Cell Res. 2005 Nov 1;310(2):392–400.

56. Hsieh HJ, Liu CA, Huang B, Tseng A, Wang L. Shear-induced endothelial mechanotransduction: The interplay between reactive oxygen species (ROS) and nitric oxide (NO) and the pathophysiological implications. J Biomed Sci. 2014 Jan 13;21:3.

57. Jones EAV, le Noble F, Eichmann A. What determines blood vessel structure? Genetic prespecification vs. hemodynamics. Physiol Bethesda Md. 2006 Dec;21:388–95.

58. Swift MR, Weinstein BM. Arterial–Venous Specification During Development. Circ Res. 2009 Mar 13;104(5):576–88.

59. Niklason L, Dai G. Arterial Venous Differentiation for Vascular Bioengineering. Annu Rev Biomed Eng. 2018 Jun 4;20:431–47.

60. Mukouyama Y suke, Shin D, Britsch S, Taniguchi M, Anderson DJ. Sensory nerves determine the pattern of arterial differentiation and blood vessel branching in the skin. Cell. 2002 Jun 14;109(6):693–705.

61. Corada M, Nyqvist D, Orsenigo F, Caprini A, Giampietro C, Taketo MM, et al. The Wnt/beta-catenin pathway modulates vascular remodeling and specification by upregulating Dll4/Notch signaling. Dev Cell. 2010 Jun 15;18(6):938–49.

62. Lawson ND, Vogel AM, Weinstein BM. sonic hedgehog and vascular endothelial growth factor act upstream of the Notch pathway during arterial endothelial differentiation. Dev Cell. 2002 Jul;3(1):127–36.

63. You LR, Lin FJ, Lee CT, DeMayo FJ, Tsai MJ, Tsai SY. Suppression of Notch signalling by the COUP-TFII transcription factor regulates vein identity. Nature. 2005 May 5;435(7038):98–104.

64. Hong CC, Peterson QP, Hong JY, Peterson RT. Artery/Vein Specification Is Governed by Opposing Phosphatidylinositol-3 Kinase and MAP Kinase/ERK Signaling. Curr Biol. 2006 Jul 11;16(13):1366–72.

65. Neal A, Nornes S, Payne S, Wallace MD, Fritzsche M, Louphrasitthiphol P, et al. Venous identity requires BMP signalling through ALK3. Nat Commun. 2019 Jan 28;10(1):453.

66. Randolph GJ, Miller NE. Lymphatic transport of high-density lipoproteins and chylomicrons. J Clin Invest. 2014 Mar;124(3):929–35.

67. Aspelund A, Robciuc MR, Karaman S, Makinen T, Alitalo K. Lymphatic System in Cardiovascular Medicine. Circ Res. 2016 Feb 5;118(3):515–30.

68. Oliver G, Kipnis J, Randolph GJ, Harvey NL. The Lymphatic Vasculature in the 21st Century: Novel Functional Roles in Homeostasis and Disease. Cell. 2020 Jul 23;182(2):270–96.

69. Alitalo K. The lymphatic vasculature in disease. Nat Med. 2011 Nov 7;17(11):1371–80.

70. Schwartz N, Chalasani MLS, Li TM, Feng Z, Shipman WD, Lu TT. Lymphatic Function in Autoimmune Diseases. Front Immunol. 2019 Mar 20;10:519.

71. Simons M, Eichmann A. Lymphatics Are in My Veins. Science. 2013 Aug 9;341(6146):622–4.

72. Hägerling R, Pollmann C, Andreas M, Schmidt C, Nurmi H, Adams RH, et al. A novel multistep mechanism for initial lymphangiogenesis in mouse embryos based on ultramicroscopy. EMBO J. 2013 Mar 6;32(5):629–44.

73. Stanczuk L, Martinez-Corral I, Ulvmar MH, Zhang Y, Laviña B, Fruttiger M, et al. cKit Lineage Hemogenic Endothelium-Derived Cells Contribute to Mesenteric Lymphatic Vessels. Cell Rep. 2015 Mar 17;10(10):1708–21.

74. Pichol-Thievend C, Betterman KL, Liu X, Ma W, Skoczylas R, Lesieur E, et al. A blood capillary plexus-derived population of progenitor cells contributes to genesis of the dermal lymphatic vasculature during embryonic development. Dev Camb Engl. 2018 May 17;145(10):dev160184.

75. Martinez-Corral I, Ulvmar MH, Stanczuk L, Tatin F, Kizhatil K, John SWM, et al. Nonvenous origin of dermal lymphatic vasculature. Circ Res. 2015 May 8;116(10):1649–54.

76. Lioux G, Liu X, Temiño S, Oxendine M, Ayala E, Ortega S, et al. A Second Heart Field-Derived Vasculogenic Niche Contributes to Cardiac Lymphatics. Dev Cell. 2020 Feb 10;52(3):350-363.e6.

77. Maruyama K, Miyagawa-Tomita S, Mizukami K, Matsuzaki F, Kurihara H. Isl1-expressing non-venous cell lineage contributes to cardiac lymphatic vessel development. Dev Biol. 2019 Aug 15;452(2):134–43.

78. Stone OA, Stainier DYR. Paraxial Mesoderm Is the Major Source of Lymphatic Endothelium. Dev Cell. 2019 Jul 22;50(2):247-255.e3.

79. Secker GA, Harvey NL. VEGFR signaling during lymphatic vascular development: From progenitor cells to functional vessels. Dev Dyn. 2015;244(3):323–31.

80. Uhrin P, Zaujec J, Breuss JM, Olcaydu D, Chrenek P, Stockinger H, et al. Novel function for blood platelets and podoplanin in developmental separation of blood and lymphatic circulation. Blood. 2010 May 13;115(19):3997–4005.

81. Sabine A, Davis MJ, Bovay E, Petrova TV. Characterization of Mouse Mesenteric Lymphatic Valve Structure and Function. Methods Mol Biol Clifton NJ. 2018;1846:97–129.

82. Klaourakis K, Vieira JM, Riley PR. The evolving cardiac lymphatic vasculature in development, repair and regeneration. Nat Rev Cardiol. 2021 May;18(5):368–79.

83. Margaris KN, Black RA. Modelling the lymphatic system: challenges and opportunities. J R Soc Interface. 2012 Apr 7;9(69):601–12.

84. Lund AW, Medler TR, Leachman SA, Coussens LM. Lymphatic Vessels, Inflammation, and Immunity in Skin Cancer. Cancer Discov. 2016 Jan;6(1):22–35.

85. Bekisz S, Baudin L, Buntinx F, Noël A, Geris L. In Vitro, In Vivo, and In Silico Models of Lymphangiogenesis in Solid Malignancies. Cancers. 2022 Mar 16;14(6):1525.

86. Doh SJ, Yamakawa M, Santosa SM, Montana M, Guo K, Sauer JR, et al. Fluorescent reporter transgenic mice for in vivo live imaging of angiogenesis and lymphangiogenesis. Angiogenesis. 2018 Nov 1;21(4):677–98.

87. Gritz E, Hirschi KK. Specification and function of hemogenic endothelium during embryogenesis. Cell Mol Life Sci. 2016;73:1547–67.

88. Mikkola HKA, Orkin SH. The journey of developing hematopoietic stem cells. Dev Camb Engl. 2006 Oct;133(19):3733–44.

89. Jagannathan-Bogdan M, Zon LI. Hematopoiesis. Dev Camb Engl. 2013 Jun;140(12):2463–7.

90. Mangel M, Bonsall MB. Stem cell biology is population biology: differentiation of hematopoietic multipotent progenitors to common lymphoid and myeloid progenitors. Theor Biol Med Model. 2013 Jan 17;10:5.

91. Seita J, Weissman IL. Hematopoietic Stem Cell: Self-renewal versus Differentiation. Wiley Interdiscip Rev Syst Biol Med. 2010;2(6):640–53.

92. Barone C, Orsenigo R, Meneveri R, Brunelli S, Azzoni E. One Size Does Not Fit All: Heterogeneity in Developmental Hematopoiesis. Cells. 2022 Jan;11(6):1061.

93. Palis J, Robertson S, Kennedy M, Wall C, Keller G. Development of erythroid and myeloid progenitors in the yolk sac and embryo proper of the mouse. Dev Camb Engl. 1999 Nov;126(22):5073–84.

94. Vanuytsel K, Steinberg M, Murphy G. Recapitulating Hematopoietic Development in a Dish. In 2019. p. 45–71.

95. Morrison SJ, Weissman IL. The long-term repopulating subset of hematopoietic stem cells is deterministic and isolatable by phenotype. Immunity. 1994 Nov;1(8):661–73.

96. Dzierzak E, Bigas A. Blood Development: Hematopoietic Stem Cell Dependence and Independence. Cell Stem Cell. 2018 May 3;22(5):639–51.

97. Yvernogeau L, Gautier R, Petit L, Khoury H, Relaix F, Ribes V, et al. In vivo generation of haematopoietic stem/progenitor cells from bone marrow-derived haemogenic endothelium. Nat Cell Biol. 2019 Nov;21(11):1334–45.

98. Ottersbach K. Endothelial-to-haematopoietic transition: an update on the process of making blood. Biochem Soc Trans. 2019 Apr 30;47(2):591–601.

99. Zovein A, Hofmann J, Lynch M, French W, Turlo K, Yang Y, et al. Fate Tracing Reveals the Endothelial Origin of Hematopoietic Stem Cells. Cell Stem Cell. 2009 Jan 1;3:625–36.

100. Goldie LC, Lucitti JL, Dickinson ME, Hirschi KK. Cell signaling directing the formation and function of hemogenic endothelium during murine embryogenesis. Blood. 2008 Oct 15;112(8):3194–204.

101. Wang Q, Stacy T, Miller JD, Lewis AF, Gu TL, Huang X, et al. The CBFbeta subunit is essential for CBFalpha2 (AML1) function in vivo. Cell. 1996 Nov 15;87(4):697–708.

102. Growney JD, Shigematsu H, Li Z, Lee BH, Adelsperger J, Rowan R, et al. Loss of Runx1 perturbs adult hematopoiesis and is associated with a myeloproliferative phenotype. Blood. 2005 Jul 15;106(2):494–504.

103. Lange L, Morgan M, Schambach A. The hemogenic endothelium: a critical source for the generation of PSC-derived hematopoietic stem and progenitor cells. Cell Mol Life Sci. 2021;78(9):4143–60.

104. Koyano-Nakagawa N, Kweon J, Iacovino M, Shi X, Rasmussen TL, Borges L, et al. Etv2 Is Expressed in the Yolk Sac Hematopoietic and Endothelial Progenitors and Regulates Lmo2 Gene Expression. STEM CELLS. 2012;30(8):1611–23.

105. Piera-Velazquez S, Jimenez SA. Endothelial to Mesenchymal Transition: Role in Physiology and in the Pathogenesis of Human Diseases. Physiol Rev. 2019 Apr;99(2):1281–324.

106. Hong L, Du X, Li W, Mao Y, Sun L, Li X. EndMT: A promising and controversial field. Eur J Cell Biol. 2018 Sep 1;97(7):493–500.

107. Welch-Reardon KM, Wu N, Hughes CCW. A role for partial endothelial-mesenchymal transitions in angiogenesis? Arterioscler Thromb Vasc Biol. 2015 Feb;35(2):303–8.

108. Weiss A, Attisano L. The TGFbeta superfamily signaling pathway. Wiley Interdiscip Rev Dev Biol. 2013 Feb;2(1):47–63.

109. Morikawa M, Derynck R, Miyazono K. TGF-β and the TGF-β Family: Context-Dependent Roles in Cell and Tissue Physiology. Cold Spring Harb Perspect Biol. 2016 May 2;8(5):a021873.

110. Hanna A, Frangogiannis NG. The Role of the TGF-β Superfamily in Myocardial Infarction. Front Cardiovasc Med [Internet]. 2019 [cited 2022 Jul 1];6. Available from: https://www.frontiersin.org/article/10.3389/fcvm.2019.00140

111. Derynck R, Budi EH. Specificity, versatility, and control of TGF-β family signaling. Sci Signal. 2019 Feb 26;12(570):eaav5183.

112. Katagiri T, Watabe T. Bone Morphogenetic Proteins. Cold Spring Harb Perspect Biol. 2016 Jun;8(6):a021899.

113. Miyazawa K, Miyazono K. Regulation of TGF-β Family Signaling by Inhibitory Smads. Cold Spring Harb Perspect Biol. 2017 Mar;9(3):a022095.

114. Martinez-Hackert E, Sundan A, Holien T. Receptor binding competition: A paradigm for regulating TGF-β family action. Cytokine Growth Factor Rev. 2020 Oct;S1359610120302069.

115. Nickel J, Mueller TD. Specification of BMP Signaling. Cells. 2019 Dec 5;8(12):1579.

116. Gámez B, Rodriguez-Carballo E, Ventura F. BMP signaling in telencephalic neural cell specification and maturation. Front Cell Neurosci [Internet]. 2013 [cited 2022 Jul 27];7. Available from: https://www.frontiersin.org/articles/10.3389/fncel.2013.00087

117. Zhang YE. Non-Smad Signaling Pathways of the TGF-β Family. Cold Spring Harb Perspect Biol [Internet]. 2017 Feb [cited 2021 Feb 9];9(2). Available from: https://www.ncbi.nlm.nih.gov/pmc/articles/PMC5287080/

118. Bragdon B, Moseychuk O, Saldanha S, King D, Julian J, Nohe A. Bone Morphogenetic Proteins: A critical review. Cell Signal. 2011 Apr 1;23(4):609–20.

119. Urist MR. Bone: formation by autoinduction. Science. 1965 Nov 12;150(3698):893–9.

120. Urist MR, Strates BS. Bone Morphogenetic Protein. J Dent Res. 1971 Nov 1;50(6):1392–406.

121. Hopkins DR, Keles S, Greenspan DS. The Bone Morphogenetic Protein 1/Tolloid-like Metalloproteinases. Matrix Biol J Int Soc Matrix Biol. 2007 Sep;26(7):508.

122. Daluiski A, Engstrand T, Bahamonde ME, Gamer LW, Agius E, Stevenson SL, et al. Bone morphogenetic protein-3 is a negative regulator of bone density. Nat Genet. 2001 Jan;27(1):84–8.

123. Kokabu S, Gamer L, Cox K, Lowery J, Tsuji K, Raz R, et al. BMP3 suppresses osteoblast differentiation of bone marrow stromal cells via interaction with Acvr2b. Mol Endocrinol Baltim Md. 2012 Jan;26(1):87–94.

124. Susan-Resiga D, Essalmani R, Hamelin J, Asselin MC, Benjannet S, Chamberland A, et al. Furin Is the Major Processing Enzyme of the Cardiac-specific Growth Factor Bone Morphogenetic Protein 10. J Biol Chem. 2011 Jul;286(26):22785–94.

125. Tillet E, Bailly S. Emerging roles of BMP9 and BMP10 in hereditary hemorrhagic telangiectasia. Front Genet. 2015 Jan 8;5:456.

126. Jiang H, Salmon RM, Upton PD, Wei Z, Lawera A, Davenport AP, et al. The Prodomain-bound Form of Bone Morphogenetic Protein 10 Is Biologically Active on Endothelial Cells. J Biol Chem. 2016 Feb;291(6):2954–66.

127. Sengle G, Ono RN, Lyons KM, Bächinger HP, Sakai LY. A New Model for Growth Factor Activation: Type II Receptors Compete with the Prodomain for BMP-7. J Mol Biol. 2008 Sep 12;381(4):1025–39.

128. Heinke J, Wehofsits L, Zhou Q, Zoeller C, Baar KM, Helbing T, et al. BMPER is an endothelial cell regulator and controls bone morphogenetic protein-4-dependent angiogenesis. Circ Res. 2008 Oct 10;103(8):804–12.

129. Miyazono K, Maeda S, Imamura T. BMP receptor signaling: Transcriptional targets, regulation of signals, and signaling cross-talk. Cytokine Growth Factor Rev. 2005 Jun 1;16(3):251–63.

130. Urness LD, Sorensen LK, Li DY. Arteriovenous malformations in mice lacking activin receptor-like kinase-1. Nat Genet. 2000 Nov;26(3):328–31.

131. Oh SP, Seki T, Goss KA, Imamura T, Yi Y, Donahoe PK, et al. Activin receptor-like kinase 1 modulates transforming growth factor-β1 signaling in the regulation of angiogenesis. Proc Natl Acad Sci. 2000 Mar 14;97(6):2626–31.

132. Duff SE, Li C, Garland JM, Kumar S. CD105 is important for angiogenesis: evidence and potential applications. FASEB J Off Publ Fed Am Soc Exp Biol. 2003 Jun;17(9):984–92.

133. Tual-Chalot S, Oh P, Arthur H. Mouse Models of Hereditary Haemorrhagic Telangiectasia: Recent Advances and Future Challenges. Front Genet [Internet]. 2015 [cited 2022 Jul 11];6. Available from: https://www.frontiersin.org/articles/10.3389/fgene.2015.00025

134. Bidart M, Ricard N, Levet S, Samson M, Mallet C, David L, et al. BMP9 is produced by hepatocytes and circulates mainly in an active mature form complexed to its prodomain. Cell Mol Life Sci CMLS. 2011 Jun 28;69:313–24.

135. Bonnardel J, T'Jonck W, Gaublomme D, Browaeys R, Scott CL, Martens L, et al. Stellate Cells, Hepatocytes, and Endothelial Cells Imprint the Kupffer Cell Identity on Monocytes Colonizing the Liver Macrophage Niche. Immunity. 2019 Oct 15;51(4):638-654.e9.

136. Tillet E, Ouarné M, Desroches-Castan A, Mallet C, Subileau M, Didier R, et al. A heterodimer formed by bone morphogenetic protein 9 (BMP9) and BMP10 provides most BMP biological activity in plasma. J Biol Chem. 2018 Jul 13;293(28):10963–74.

137. Chen H. BMP10 is essential for maintaining cardiac growth during murine cardiogenesis. Development. 2004 Mar 31;131(9):2219–31.

138. Chen H, Brady Ridgway J, Sai T, Lai J, Warming S, Chen H, et al. Context-dependent signaling defines roles of BMP9 and BMP10 in embryonic and postnatal development. Proc Natl Acad Sci. 2013 Jul 16;110(29):11887–92.

139. Capasso TL, Li B, Volek HJ, Khalid W, Rochon ER, Anbalagan A, et al. BMP10-mediated ALK1 signaling is continuously required for vascular development and maintenance. Angiogenesis. 2020 May;23(2):203–20.

140. Mi LZ, Brown CT, Gao Y, Tian Y, Le VQ, Walz T, et al. Structure of bone morphogenetic protein 9 procomplex. Proc Natl Acad Sci. 2015 Mar 24;112(12):3710–5.

141. Wohl AP, Troilo H, Collins RF, Baldock C, Sengle G. Extracellular Regulation of Bone Morphogenetic Protein Activity by the Microfibril Component Fibrillin-1. J Biol Chem. 2016 Jun 10;291(24):12732–46.

142. Sengle G, Charbonneau NL, Ono RN, Sasaki T, Alvarez J, Keene DR, et al. Targeting of Bone Morphogenetic Protein Growth Factor Complexes to Fibrillin. J Biol Chem. 2008 May 16;283(20):13874–88.

143. Ali IHA, Brazil DP. Bone morphogenetic proteins and their antagonists: current and emerging clinical uses. Br J Pharmacol. 2014 Aug;171(15):3620–32.

144. Yao Y, Jumabay M, Ly A, Radparvar M, Wang AH, Abdmaulen R, et al. Crossveinless 2 regulates bone morphogenetic protein 9 in human and mouse vascular endothelium. Blood. 2012 May 24;119(21):5037–47.

145. Jumabay M, Zhumabai J, Mansurov N, Niklason KC, Guihard PJ, Cubberly MR, et al. Combined effects of bone morphogenetic protein 10 and crossveinless-2 on cardiomyocyte differentiation in mouse adipocyte-derived stem cells. J Cell Physiol. 2018 Mar;233(3):1812–22.

146. Salmon RM, Guo J, Wood JH, Tong Z, Beech JS, Lawera A, et al. Molecular basis of ALK1-mediated signalling by BMP9/BMP10 and their prodomain-bound forms. Nat Commun. 2020 Dec;11(1):1621.

147. Luo J, Tang M, Huang J, He BC, Gao JL, Chen L, et al. TGFbeta/BMP type I receptors ALK1 and ALK2 are essential for BMP9-induced osteogenic signaling in mesenchymal stem cells. J Biol Chem. 2010 Sep 17;285(38):29588–98.

148. Mazerbourg S, Sangkuhl K, Luo CW, Sudo S, Klein C, Hsueh AJW. Identification of Receptors and Signaling Pathways for Orphan Bone Morphogenetic Protein/Growth Differentiation Factor Ligands Based on Genomic Analyses. J Biol Chem. 2005 Sep;280(37):32122–32.

149. Townson SA, Martinez-Hackert E, Greppi C, Lowden P, Sako D, Liu J, et al. Specificity and Structure of a High Affinity Activin Receptor-like Kinase 1 (ALK1) Signaling Complex. J Biol Chem. 2012 Aug;287(33):27313–25.

150. Aykul S, Martinez-Hackert E. Transforming Growth Factor-β Family Ligands Can Function as Antagonists by Competing for Type II Receptor Binding*. J Biol Chem. 2016 May;291(20):10792–804.

151. Goumans MJ, Zwijsen A, ten Dijke P, Bailly S. Bone Morphogenetic Proteins in Vascular Homeostasis and Disease. Cold Spring Harb Perspect Biol [Internet]. 2018 Feb [cited 2021 Feb 9];10(2). Available from: https://www.ncbi.nlm.nih.gov/pmc/articles/PMC5793761/

152. Baeyens N, Larrivée B, Ola R, Hayward-Piatkowskyi B, Dubrac A, Huang B, et al. Defective fluid shear stress mechanotransduction mediates hereditary hemorrhagic telangiectasia. J Cell Biol. 2016 Sep 26;214(7):807–16.

153. Ola R, Künzel SH, Zhang F, Genet G, Chakraborty R, Pibouin-Fragner L, et al. SMAD4 Prevents Flow Induced Arteriovenous Malformations by Inhibiting Casein Kinase 2. Circulation. 2018 Nov 20;138(21):2379–94.

154. Morikawa M, Koinuma D, Tsutsumi S, Vasilaki E, Kanki Y, Heldin CH, et al. ChIP-seq reveals cell type-specific binding patterns of BMP-specific Smads and a novel binding motif. Nucleic Acids Res. 2011 Nov;39(20):8712–27.

155. Long L, Ormiston ML, Yang X, Southwood M, Gräf S, Machado RD, et al. Selective enhancement of endothelial BMPR-II with BMP9 reverses pulmonary arterial hypertension. Nat Med. 2015 Jul;21(7):777–85.

156. Levet S, Ciais D, Merdzhanova G, Mallet C, Zimmers TA, Lee SJ, et al. Bone morphogenetic protein 9 (BMP9) controls lymphatic vessel maturation and valve formation. Blood. 2013 Jul 25;122(4):598–607.

157. Levet S, Ouarné M, Ciais D, Coutton C, Subileau M, Mallet C, et al. BMP9 and BMP10 are necessary for proper closure of the ductus arteriosus. Proc Natl Acad Sci. 2015 Jun 23;112(25):E3207–15.

158. Szulcek R, Sanchez-Duffhues G, Rol N, Pan X, Tsonaka R, Dickhoff C, et al. Exacerbated inflammatory signaling underlies aberrant response to BMP9 in pulmonary arterial hypertension lung endothelial cells. Angiogenesis. 2020 Nov;23(4):699–714.

159. Park JES, Shao D, Upton PD, Morrell NW, Griffiths MJD, Wort SJ. BMP-9 Induced Endothelial Cell Tubule Formation and Inhibition of Migration Involves Smad1 Driven Endothelin-1 Production. PLoS ONE. 2012;7(1):13.

160. Poirier O, Ciumas M, Eyries M, Montagne K, Nadaud S, Soubrier F. Inhibition of apelin expression by BMP signaling in endothelial cells. Am J Physiol-Cell Physiol. 2012 Aug 15;303(11):C1139–45.

161. Tu L, Desroches-Castan A, Mallet C, Guyon L, Cumont A, Phan C, et al. Selective BMP-9 Inhibition Partially Protects Against Experimental Pulmonary Hypertension. Circ Res. 2019 Mar 15;124(6):846–55.

162. Park JES, Shao D, Upton PD, Morrell NW, Griffiths MJD, Wort SJ. BMP-9 Induced Endothelial Cell Tubule Formation and Inhibition of Migration Involves Smad1 Driven Endothelin-1 Production. PLoS ONE. 2012;7(1):13.

163. Upton PD, Park JES, De Souza PM, Davies RJ, Griffiths MJD, Wort SJ, et al. Endothelial protective factors BMP9 and BMP10 inhibit CCL2 release by human vascular endothelial cells. J Cell Sci. 2020 Jul 15;133(14):jcs239715.

164. Mitrofan CG, Appleby SL, Nash GB, Mallat Z, Chilvers ER, Upton PD, et al. Bone morphogenetic protein 9 (BMP9) and BMP10 enhance tumor necrosis factor-α-induced monocyte recruitment to the vascular endothelium mainly via activin receptor-like kinase 2. J Biol Chem. 2017 Aug 18;292(33):13714–26.

165. D'Amato G, Luxán G, de la Pompa JL. Notch signalling in ventricular chamber development and cardiomyopathy. FEBS J. 2016 Dec;283(23):4223–37.

166. Srivastava D, Olson EN. A genetic blueprint for cardiac development. Nature. 2000 Sep 14;407(6801):221–6.

167. Savolainen SM, Foley JF, Elmore SA. Histology Atlas of the Developing Mouse Heart with Emphasis on E11.5 to E18.5. Toxicol Pathol. 2009;37(4):395–414.

168. Meyer D, Birchmeier C. Multiple essential functions of neuregulin in development. Nature. 1995 Nov 23;378(6555):386–90.

169. Gassmann M, Casagranda F, Orioli D, Simon H, Lai C, Klein R, et al. Aberrant neural and cardiac development in mice lacking the ErbB4 neuregulin receptor. Nature. 1995 Nov 23;378(6555):390–4.

170. Lee KF, Simon H, Chen H, Bates B, Hung MC, Hauser C. Requirement for neuregulin receptor erbB2 in neural and cardiac development. Nature. 1995 Nov;378(6555):394–8.

171. Ferrara N, Carver-Moore K, Chen H, Dowd M, Lu L, O'Shea KS, et al. Heterozygous embryonic lethality induced by targeted inactivation of the VEGF gene. Nature. 1996 Apr 4;380(6573):439–42.

172. Suri C, Jones PF, Patan S, Bartunkova S, Maisonpierre PC, Davis S, et al. Requisite role of angiopoietin-1, a ligand for the TIE2 receptor, during embryonic angiogenesis. Cell. 1996 Dec 27;87(7):1171–80.

173. Qu X, Liu Y, Cao D, Chen J, Liu Z, Ji H, et al. BMP10 preserves cardiac function through its dual activation of SMAD-mediated and STAT3-mediated pathways. J Biol Chem. 2019 Dec 27;294(52):19877–88.

174. Niessen K, Zhang G, Ridgway JB, Chen H, Yan M. ALK1 signaling regulates early postnatal lymphatic vessel development. Blood. 2010 Feb 25;115(8):1654–61.

175. Yoshimatsu Y, Lee YG, Akatsu Y, Taguchi L, Suzuki HI, Cunha SI, et al. Bone morphogenetic protein-9 inhibits lymphatic vessel formation via activin receptor-like kinase 1 during development and cancer progression. Proc Natl Acad Sci. 2013 Nov 19;110(47):18940–5.

176. Levet S, Ciais D, Merdzhanova G, Mallet C, Zimmers TA, Lee SJ, et al. Bone morphogenetic protein 9 (BMP9) controls lymphatic vessel maturation and valve formation. Blood. 2013 Jul 25;122(4):598–607.

177. Derynck R, Akhurst RJ. BMP-9 balances endothelial cell fate. Proc Natl Acad Sci U S A. 2013 Nov 19;110(47):18746–7.

178. David L, Mallet C, Mazerbourg S, Feige JJ, Bailly S. Identification of BMP9 and BMP10 as functional activators of the orphan activin receptor-like kinase 1 (ALK1) in endothelial cells. Blood. 2007 Mar 1;109(5):1953–61.

179. Scharpfenecker M, van Dinther M, Liu Z, van Bezooijen RL, Zhao Q, Pukac L, et al. BMP-9 signals via ALK1 and inhibits bFGF-induced endothelial cell proliferation and VEGF-stimulated angiogenesis. J Cell Sci. 2007 Feb 27;120(6):964–72.

180. van Meeteren LA, Thorikay M, Bergqvist S, Pardali E, Stampino CG, Hu-Lowe D, et al. Anti-human activin receptor-like kinase 1 (ALK1) antibody attenuates bone morphogenetic protein 9 (BMP9)-induced ALK1 signaling and interferes with endothelial cell sprouting. J Biol Chem. 2012 May 25;287(22):18551–61.

181. Larrivée B, Prahst C, Gordon E, del Toro R, Mathivet T, Duarte A, et al. ALK1 signaling inhibits angiogenesis by cooperating with the Notch pathway. Dev Cell. 2012 Mar 13;22(3):489–500.

182. Suzuki Y, Ohga N, Morishita Y, Hida K, Miyazono K, Watabe T. BMP-9 induces proliferation of multiple types of endothelial cells in vitro and in vivo. J Cell Sci. 2010 May 15;123(10):1684–92.

183. Richter A, Alexdottir MS, Magnus SH, Richter TR, Morikawa M, Zwijsen A, et al. EGFL7 Mediates BMP9-Induced Sprouting Angiogenesis of Endothelial Cells Derived from Human Embryonic Stem Cells. Stem Cell Rep. 2019 Jun 11;12(6):1250–9.

184. Li Y, Shang Q, Li P, Yang Z, Yang J, Shi J, et al. BMP9 attenuates occurrence of venous malformation by maintaining endothelial quiescence and strengthening vessel walls via SMAD1/5/ID1/α-SMA pathway. J Mol Cell Cardiol. 2020 Oct;147:92–107.

185. Yang Z, Li P, Shang Q, Wang Y, He J, Ge S, et al. CRISPR-mediated BMP9 ablation promotes liver steatosis via the down-regulation of PPARα expression. Sci Adv. 2020 Nov;6(48):eabc5022.

186. Rahit KMTH, Tarailo-Graovac M. Genetic Modifiers and Rare Mendelian Disease. Genes. 2020 Feb 25;11(3):239.

187. Desroches-Castan A, Tillet E, Ricard N, Ouarné M, Mallet C, Feige JJ, et al. Differential Consequences of Bmp9 Deletion on Sinusoidal Endothelial Cell Differentiation and Liver Fibrosis in 129/Ola and C57BL/6 Mice. Cells. 2019 Sep 13;8(9):E1079.

188. Breitkopf-Heinlein K, Meyer C, König C, Gaitantzi H, Addante A, Thomas M, et al. BMP-9 interferes with liver regeneration and promotes liver fibrosis. Gut. 2017 May;66(5):939–54.

189. Li P, Li Y, Zhu L, Yang Z, He J, Wang L, et al. Targeting secreted cytokine BMP9 gates the attenuation of hepatic fibrosis. Biochim Biophys Acta BBA - Mol Basis Dis. 2018 Mar 1;1864(3):709–20.

190. Bourdeau A, Faughnan ME, McDonald ML, Paterson AD, Wanless IR, Letarte M. Potential Role of Modifier Genes Influencing Transforming Growth Factor-β1 Levels in the Development of Vascular Defects in Endoglin Heterozygous Mice with Hereditary Hemorrhagic Telangiectasia. Am J Pathol. 2001 Jun;158(6):2011–20.

191. Ricard N, Ciais D, Levet S, Subileau M, Mallet C, Zimmers TA, et al. BMP9 and BMP10 are critical for postnatal retinal vascular remodeling. Blood. 2012 Jun 21;119(25):6162–71.

192. Ola R, Dubrac A, Han J, Zhang F, Fang JS, Larrivée B, et al. PI3 kinase inhibition improves vascular malformations in mouse models of hereditary haemorrhagic telangiectasia. Nat Commun. 2016 Dec;7(1):13650.

193. Ruiz S, Zhao H, Chandakkar P, Chatterjee PK, Papoin J, Blanc L, et al. A mouse model of hereditary hemorrhagic telangiectasia generated by transmammary-delivered immunoblocking of BMP9 and BMP10. Sci Rep. 2016 Dec;6(1):37366.

194. Laux DW, Young S, Donovan JP, Mansfield CJ, Upton PD, Roman BL. Circulating Bmp10 acts through endothelial Alk1 to mediate flow-dependent arterial quiescence. Development. 2013 Aug 15;140(16):3403–12.

195. Ouarné M, Bouvard C, Boneva G, Mallet C, Ribeiro J, Desroches-Castan A, et al. BMP9, but not BMP10, acts as a quiescence factor on tumor growth, vessel normalization and metastasis in a mouse model of breast cancer. J Exp Clin Cancer Res CR. 2018 Aug 30;37(1):209.

196. Little SC, Mullins MC. BMP heterodimers assemble hetero-type I receptor complexes that pattern the DV axis. Nat Cell Biol. 2009 May;11(5):637–43.

197. Neugebauer JM, Kwon S, Kim HS, Donley N, Tilak A, Sopory S, et al. The prodomain of BMP4 is necessary and sufficient to generate stable BMP4/7 heterodimers with enhanced bioactivity in vivo. Proc Natl Acad Sci. 2015 May 5;112(18):E2307–16.

198. Kim HS, Neugebauer J, McKnite A, Tilak A, Christian JL. BMP7 functions predominantly as a heterodimer with BMP2 or BMP4 during mammalian embryogenesis. Bronner ME, editor. eLife. 2019 Sep 30;8:e48872.

199. Valera E, Isaacs MJ, Kawakami Y, Belmonte JCI, Choe S. BMP-2/6 Heterodimer Is More Effective than BMP-2 or BMP-6 Homodimers as Inductor of Differentiation of Human Embryonic Stem Cells. PLOS ONE. 2010 Jun 17;5(6):e11167.

200. Shovlin CL, Buscarini E, Sabbà C, Mager HJ, Kjeldsen AD, Pagella F, et al. The European Rare Disease Network for HHT Frameworks for management of hereditary haemorrhagic telangiectasia in general and speciality care. Eur J Med Genet. 2022 Jan;65(1):104370.

201. McDonald J, Wooderchak-Donahue W, VanSant Webb C, Whitehead K, Stevenson DA, Bayrak-Toydemir P. Hereditary hemorrhagic telangiectasia: genetics and molecular diagnostics in a new era. Front Genet [Internet]. 2015 [cited 2022 Jul 30];6. Available from: https://www.frontiersin.org/articles/10.3389/fgene.2015.00001

202. Wooderchak-Donahue WL, McDonald J, O'Fallon B, Upton PD, Li W, Roman BL, et al. BMP9 Mutations Cause a Vascular-Anomaly Syndrome with Phenotypic Overlap with Hereditary Hemorrhagic Telangiectasia. Am J Hum Genet. 2013 Sep;93(3):530–7.

203. Hodgson J, Ruiz-Llorente L, McDonald J, Quarrell O, Ugonna K, Bentham J, et al. Homozygous GDF2 nonsense mutations result in a loss of circulating BMP9 and BMP10 and are associated with either PAH or an "HHT-like" syndrome in children. Mol Genet Genomic Med. 2021;9(12):e1685.

204. Shovlin CL, Guttmacher AE, Buscarini E, Faughnan ME, Hyland RH, Westermann CJ, et al. Diagnostic criteria for hereditary hemorrhagic telangiectasia (Rendu-Osler-Weber syndrome). Am J Med Genet. 2000 Mar 6;91(1):66–7.

205. Benzinou M, Clermont FF, Letteboer TGW, Kim J hyun, Espejel S, Harradine KA, et al. Mouse and human strategies identify PTPN14 as a modifier of angiogenesis and hereditary haemorrhagic telangiectasia. Nat Commun. 2012 Jan 10;3(1):616.

206. Kawasaki K, Freimuth J, Meyer DS, Lee MM, Tochimoto-Okamoto A, Benzinou M, et al. Genetic variants of Adam17 differentially regulate TGFβ signaling to modify vascular pathology in mice and humans. Proc Natl Acad Sci U S A. 2014 May 27;111(21):7723–8.

207. Robert F, Desroches-Castan A, Bailly S, Dupuis-Girod S, Feige JJ. Future treatments for hereditary hemorrhagic telangiectasia. Orphanet J Rare Dis. 2020 Jan 7;15(1):4.

208. Lai YC, Potoka KC, Champion HC, Mora AL, Gladwin MT. Pulmonary Arterial Hypertension. Circ Res. 2014 Jun 20;115(1):115–30.

209. Ruopp NF, Cockrill BA. Diagnosis and Treatment of Pulmonary Arterial Hypertension: A Review. JAMA. 2022 Apr 12;327(14):1379–91.

210. Lai YC, Potoka KC, Champion HC, Mora AL, Gladwin MT. Pulmonary arterial hypertension: the clinical syndrome. Circ Res. 2014 Jun 20;115(1):115–30.

211. Evans JDW, Girerd B, Montani D, Wang XJ, Galiè N, Austin ED, et al. BMPR2 mutations and survival in pulmonary arterial hypertension: an individual participant data meta-analysis. Lancet Respir Med. 2016 Feb 1;4(2):129–37.

212. Nasim MdT, Ogo T, Ahmed M, Randall R, Chowdhury HM, Snape KM, et al. Molecular genetic characterization of SMAD signaling molecules in pulmonary arterial hypertension. Hum Mutat. 2011;32(12):1385–9.

213. Austin ED, Ma L, LeDuc C, Berman Rosenzweig E, Borczuk A, Phillips JA, et al. Whole exome sequencing to identify a novel gene (caveolin-1) associated with human pulmonary arterial hypertension. Circ Cardiovasc Genet. 2012 Jun;5(3):336–43.

214. Ma L, Roman-Campos D, Austin ED, Eyries M, Sampson KS, Soubrier F, et al. A novel channelopathy in pulmonary arterial hypertension. N Engl J Med. 2013 Jul 25;369(4):351–61.

215. Kerstjens-Frederikse WS, Bongers EMHF, Roofthooft MTR, Leter EM, Douwes JM, Dijk AV, et al. TBX4 mutations (small patella syndrome) are associated with childhood-onset pulmonary arterial hypertension. J Med Genet. 2013 Aug 1;50(8):500–6.

216. Trembath RC, Thomson JR, Machado RD, Morgan NV, Atkinson C, Winship I, et al. Clinical and molecular genetic features of pulmonary hypertension in patients with hereditary hemorrhagic telangiectasia. N Engl J Med. 2001 Aug 2;345(5):325–34.

217. Chaouat A, Coulet F, Favre C, Simonneau G, Weitzenblum E, Soubrier F, et al. Endoglin germline mutation in a patient with hereditary haemorrhagic telangiectasia and

dexfenfluramine associated pulmonary arterial hypertension. Thorax. 2004 May;59(5):446–8.

218. Hadinnapola C, Bleda M, Haimel M, Screaton N, Swift A, Dorfmüller P, et al. Phenotypic Characterization of EIF2AK4 Mutation Carriers in a Large Cohort of Patients Diagnosed Clinically With Pulmonary Arterial Hypertension. Circulation. 2017 Nov 21;136(21):2022–33.

219. Wang G, Fan R, Ji R, Zou W, Penny DJ, Varghese NP, et al. Novel homozygous BMP9 nonsense mutation causes pulmonary arterial hypertension: a case report. BMC Pulm Med. 2016 Jan 22;16(1):17.

220. Wang XJ, Lian TY, Jiang X, Liu SF, Li SQ, Jiang R, et al. Germline *BMP9* mutation causes idiopathic pulmonary arterial hypertension. Eur Respir J. 2019 Mar;53(3):1801609.

221. Eyries M, Montani D, Nadaud S, Girerd B, Levy M, Bourdin A, et al. Widening the landscape of heritable pulmonary hypertension mutations in paediatric and adult cases. Eur Respir J. 2019 Mar;53(3):1801371.

222. Gurumurthy CB, Lloyd KCK. Generating mouse models for biomedical research: technological advances. Dis Model Mech. 2019 Jan 1;12(1):dmm029462.

223. Tian X, Zhou B. Strategies for site-specific recombination with high efficiency and precise spatiotemporal resolution. J Biol Chem. 2021 Jan 1;296:100509.

224. Schulze S, Lammers M. The development of genome editing tools as powerful techniques with versatile applications in biotechnology and medicine: CRISPR/Cas9, ZnF and TALE nucleases, RNA interference, and Cre/loxP. ChemTexts. 2020 Nov 24;7(1):3.

225. Kim H, Kim M, Im SK, Fang S. Mouse Cre-LoxP system: general principles to determine tissue-specific roles of target genes. Lab Anim Res. 2018 Dec;34(4):147–59.

226. Goodwin AM. In vitro assays of angiogenesis for assessment of angiogenic and anti-angiogenic agents. Microvasc Res. 2007;74(2–3):172–83.

227. Rezzola S, Belleri M, Gariano G, Ribatti D, Costagliola C, Semeraro F, et al. In vitro and ex vivo retina angiogenesis assays. Angiogenesis. 2014 Jul;17(3):429–42.

228. Chávez MN, Aedo G, Fierro FA, Allende ML, Egaña JT. Zebrafish as an Emerging Model Organism to Study Angiogenesis in Development and Regeneration. Front Physiol [Internet]. 2016 [cited 2022 Aug 26];7. Available from: https://www.frontiersin.org/articles/10.3389/fphys.2016.00056

229. Stahl A, Connor KM, Sapieha P, Chen J, Dennison RJ, Krah NM, et al. The Mouse Retina as an Angiogenesis Model. Invest Ophthalmol Vis Sci. 2010 Jun;51(6):2813–26.

230. Cleaver O. Mouse models of vascular development and disease. Curr Opin Hematol. 2021 May 1;28(3):179–88.

231. Gerhardt H. VEGF and Endothelial Guidance in Angiogenic Sprouting. In: Ruhrberg C, editor. VEGF in Development [Internet]. New York, NY: Springer; 2008 [cited 2022 Jul 22]. p. 68–78. (Molecular Biology Intelligence Unit). Available from: https://doi.org/10.1007/978-0-387-78632-2_6

232. Chen D, Schwartz MA, Simons M. Developmental Perspectives on Arterial Fate Specification. Front Cell Dev Biol. 2021 Jun 25;9:691335.

233. Xu C, Hasan SS, Schmidt I, Rocha SF, Pitulescu ME, Bussmann J, et al. Arteries are formed by vein-derived endothelial tip cells. Nat Commun. 2014 Dec 15;5(1):5758.

234. Pitulescu ME, Schmidt I, Giaimo BD, Antoine T, Berkenfeld F, Ferrante F, et al. Dll4 and Notch signalling couples sprouting angiogenesis and artery formation. Nat Cell Biol. 2017 Aug;19(8):915–27.

235. Lee HW, Shin JH, Simons M. Flow goes forward and cells step backward: endothelial migration. Exp Mol Med. 2022 Jun;54(6):711–9.

236. Lee HW, Xu Y, He L, Choi W, Gonzalez D, Jin SW, et al. Role of Venous Endothelial Cells in Developmental and Pathologic Angiogenesis. Circulation. 2021 Oct 19;144(16):1308–22.

237. Park H, Furtado J, Poulet M, Chung M, Yun S, Lee S, et al. Defective Flow-Migration Coupling Causes Arteriovenous Malformations in Hereditary Hemorrhagic Telangiectasia. Circulation. 2021 Sep 7;144(10):805–22.

238. Queisser A, Seront E, Boon LM, Vikkula M. Genetic Basis and Therapies for Vascular Anomalies. Circ Res. 2021 Jun 25;129(1):155–73.

239. Park SO, Wankhede M, Lee YJ, Choi EJ, Fliess N, Choe SW, et al. Real-time imaging of de novo arteriovenous malformation in a mouse model of hereditary hemorrhagic telangiectasia. J Clin Invest. 2009 Nov 2;119(11):3487–96.

240. Tual-Chalot S, Mahmoud M, Allinson KR, Redgrave RE, Zhai Z, Oh SP, et al. Endothelial depletion of Acvrl1 in mice leads to arteriovenous malformations associated with reduced endoglin expression. PloS One. 2014;9(6):e98646.

241. Garrido-Martin EM, Nguyen HL, Cunningham TA, Choe S woon, Jiang Z, Arthur HM, et al. Common and Distinctive Pathogenetic Features of Arteriovenous Malformations in Hereditary Hemorrhagic Telangiectasia 1 and Hereditary Hemorrhagic Telangiectasia 2 Animal Models—Brief Report. Arterioscler Thromb Vasc Biol. 2014 Oct;34(10):2232–6.

242. Mahmoud M, Allinson KR, Zhai Z, Oakenfull R, Ghandi P, Adams RH, et al. Pathogenesis of Arteriovenous Malformations in the Absence of Endoglin. Circ Res. 2010 Apr 30;106(8):1425–33.

243. Crist AM, Lee AR, Patel NR, Westhoff DE, Meadows SM. Vascular deficiency of Smad4 causes arteriovenous malformations: a mouse model of Hereditary Hemorrhagic Telangiectasia. Angiogenesis. 2018;21(2):363–80.

244. Srinivasan S, Hanes MA, Dickens T, Porteous MEM, Oh SP, Hale LP, et al. A mouse model for hereditary hemorrhagic telangiectasia (HHT) type 2. Hum Mol Genet. 2003 Mar 1;12(5):473–82.

245. Han C, Choe SW, Kim YH, Acharya AP, Keselowsky BG, Sorg BS, et al. VEGF neutralization can prevent and normalize arteriovenous malformations in an animal model for hereditary hemorrhagic telangiectasia 2. Angiogenesis. 2014 Oct;17(4):823–30.

246. Park SO, Lee YJ, Seki T, Hong KH, Fliess N, Jiang Z, et al. ALK5- and TGFBR2-independent role of ALK1 in the pathogenesis of hereditary hemorrhagic telangiectasia type 2. Blood. 2008 Jan 15;111(2):633–42.

247. Chen W, Sun Z, Han Z, Jun K, Camus M, Wankhede M, et al. De novo cerebrovascular malformation in the adult mouse after endothelial Alk1 deletion and angiogenic stimulation. Stroke J Cereb Circ. 2014 Mar;45(3):900–2.

248. Milton I, Ouyang D, Allen CJ, Yanasak NE, Gossage JR, Alleyne CH, et al. Age-dependent lethality in novel transgenic mouse models of central nervous system arteriovenous malformations. Stroke. 2012 May;43(5):1432–5.

249. Li DY, Sorensen LK, Brooke BS, Urness LD, Davis EC, Taylor DG, et al. Defective angiogenesis in mice lacking endoglin. Science. 1999 May 28;284(5419):1534–7.

250. Bourdeau A, Dumont DJ, Letarte M. A murine model of hereditary hemorrhagic telangiectasia. J Clin Invest. 1999 Nov 15;104(10):1343–51.

251. Choi EJ, Chen W, Jun K, Arthur HM, Young WL, Su H. Novel Brain Arteriovenous Malformation Mouse Models for Type 1 Hereditary Hemorrhagic Telangiectasia. PLoS ONE. 2014 Feb 10;9(2):e88511.

252. Chu GC, Dunn NR, Anderson DC, Oxburgh L, Robertson EJ. Differential requirements for Smad4 in TGFbeta-dependent patterning of the early mouse embryo. Dev Camb Engl. 2004 Aug;131(15):3501–12.

253. Lan Y, Liu B, Yao H, Li F, Weng T, Yang G, et al. Essential Role of Endothelial Smad4 in Vascular Remodeling and Integrity. Mol Cell Biol. 2007 Nov;27(21):7683–92.

254. Chen H. BMP10 is essential for maintaining cardiac growth during murine cardiogenesis. Development. 2004 Mar 31;131(9):2219–31.

255. Gomez-Arroyo JG, Farkas L, Alhussaini AA, Farkas D, Kraskauskas D, Voelkel NF, et al. The monocrotaline model of pulmonary hypertension in perspective. Am J Physiol Lung Cell Mol Physiol. 2012 Feb 15;302(4):L363-369.

256. Kay JM, Smith P, Heath D, Will JA. Effects of phenobarbitone, cinnarizine, and zoxazolamine on the development of right ventricular hypertrophy and hypertensive pulmonary vascular disease in rats treated with monocrotaline. Cardiovasc Res. 1976 Mar;10(2):200–5.

257. Buermans HPJ, Redout EM, Schiel AE, Musters RJP, Zuidwijk M, Eijk PP, et al. Microarray analysis reveals pivotal divergent mRNA expression profiles early in the development of either compensated ventricular hypertrophy or heart failure. Physiol Genomics. 2005 May 11;21(3):314–23.

258. Ruiter G, de Man FS, Schalij I, Sairras S, Grünberg K, Westerhof N, et al. Reversibility of the monocrotaline pulmonary hypertension rat model. Eur Respir J. 2013 Aug;42(2):553–6.

259. Meyrick B, Reid L. Hypoxia-induced structural changes in the media and adventitia of the rat hilar pulmonary artery and their regression. Am J Pathol. 1980 Jul;100(1):151–78.

260. Sato K, Webb S, Tucker A, Rabinovitch M, O'Brien RF, McMurtry IF, et al. Factors influencing the idiopathic development of pulmonary hypertension in the fawn hooded rat. Am Rev Respir Dis. 1992 Apr;145(4 Pt 1):793–7.

261. Hoshikawa Y, Nana-Sinkam P, Moore MD, Sotto-Santiago S, Phang T, Keith RL, et al. Hypoxia induces different genes in the lungs of rats compared with mice. Physiol Genomics. 2003 Feb 6;12(3):209–19.

262. Voelkel NF, Tuder RM, Wade K, Höper M, Lepley RA, Goulet JL, et al. Inhibition of 5-lipoxygenase-activating protein (FLAP) reduces pulmonary vascular reactivity and pulmonary hypertension in hypoxic rats. J Clin Invest. 1996 Jun 1;97(11):2491–8.

263. Nicolls MR, Mizuno S, Taraseviciene-Stewart L, Farkas L, Drake JI, Al Husseini A, et al. New models of pulmonary hypertension based on VEGF receptor blockade-induced endothelial cell apoptosis. Pulm Circ. 2012 Oct;2(4):434–42.

264. Taraseviciene-Stewart L, Kasahara Y, Alger L, Hirth P, Mc Mahon G, Waltenberger J, et al. Inhibition of the VEGF receptor 2 combined with chronic hypoxia causes cell death-dependent pulmonary endothelial cell proliferation and severe pulmonary hypertension. FASEB J Off Publ Fed Am Soc Exp Biol. 2001 Feb;15(2):427–38.

265. Ciuclan L, Bonneau O, Hussey M, Duggan N, Holmes AM, Good R, et al. A novel murine model of severe pulmonary arterial hypertension. Am J Respir Crit Care Med. 2011 Nov 15;184(10):1171–82.

266. Vitali SH, Hansmann G, Rose C, Fernandez-Gonzalez A, Scheid A, Mitsialis SA, et al. The Sugen 5416/hypoxia mouse model of pulmonary hypertension revisited: long-term follow-up. Pulm Circ. 2014 Dec;4(4):619–29.

267. Bogaard HJ, Natarajan R, Henderson SC, Long CS, Kraskauskas D, Smithson L, et al. Chronic pulmonary artery pressure elevation is insufficient to explain right heart failure. Circulation. 2009 Nov 17;120(20):1951–60.

268. Wang Z, Patel JR, Schreier DA, Hacker TA, Moss RL, Chesler NC. Organ-level right ventricular dysfunction with preserved Frank-Starling mechanism in a mouse model of pulmonary arterial hypertension. J Appl Physiol Bethesda Md 1985. 2018 May 1;124(5):1244–53.

269. Akazawa Y, Okumura K, Ishii R, Slorach C, Hui W, Ide H, et al. Pulmonary artery banding is a relevant model to study the right ventricular remodeling and dysfunction that occurs in pulmonary arterial hypertension. J Appl Physiol Bethesda Md 1985. 2020 Aug 1;129(2):238–46.

270. Boehm M, Tian X, Mao Y, Ichimura K, Dufva MJ, Ali K, et al. Delineating the molecular and histological events that govern right ventricular recovery using a novel mouse model of pulmonary artery de-banding. Cardiovasc Res. 2020 Aug 1;116(10):1700–9.

271. Borgdorff MAJ, Koop AMC, Bloks VW, Dickinson MG, Steendijk P, Sillje HHW, et al. Clinical symptoms of right ventricular failure in experimental chronic pressure load are associated with progressive diastolic dysfunction. J Mol Cell Cardiol. 2015 Feb;79:244–53.

272. Reynolds AM, Xia W, Holmes MD, Hodge SJ, Danilov S, Curiel DT, et al. Bone morphogenetic protein type 2 receptor gene therapy attenuates hypoxic pulmonary hypertension. Am J Physiol-Lung Cell Mol Physiol. 2007 May;292(5):L1182–92.

273. Dignam JP, Scott TE, Kemp-Harper BK, Hobbs AJ. Animal models of pulmonary hypertension: Getting to the heart of the problem. Br J Pharmacol. 2022;179(5):811–37.

274. Theilmann AL, Hawke LG, Hilton LR, Whitford MKM, Cole DV, Mackeil JL, et al. Endothelial *BMPR2* Loss Drives a Proliferative Response to BMP (Bone Morphogenetic Protein) 9 via Prolonged Canonical Signaling. Arterioscler Thromb Vasc Biol. 2020 Nov;40(11):2605–18.

275. Hautefort A, Mendes-Ferreira P, Sabourin J, Manaud G, Bertero T, Rucker-Martin C, et al. Bmpr2 Mutant Rats Develop Pulmonary and Cardiac Characteristics of Pulmonary Arterial Hypertension. Circulation. 2019 Feb 12;139(7):932–48.

276. Lambert M, Capuano V, Boet A, Tesson L, Bertero T, Nakhleh MK, et al. Characterization of Kcnk3-Mutated Rat, a Novel Model of Pulmonary Hypertension. Circ Res. 2019 Sep 13;125(7):678–95.

277. Sohal DS, Nghiem M, Crackower MA, Witt SA, Kimball TR, Tymitz KM, et al. Temporally regulated and tissue-specific gene manipulations in the adult and embryonic heart using a tamoxifen-inducible Cre protein. Circ Res. 2001 Jul 6;89(1):20–5.

278. Mederacke I, Hsu CC, Troeger JS, Huebener P, Mu X, Dapito DH, et al. Fate tracing reveals hepatic stellate cells as dominant contributors to liver fibrosis independent of its aetiology. Nat Commun. 2013 Dec;4(1):2823.

279. Bouvard C, Tu L, Rossi M, Desroches-Castan A, Berrebeh N, Helfer E, et al. Different cardiovascular and pulmonary phenotypes for single- and double-knock-out mice deficient in BMP9 and BMP10. Cardiovasc Res. 2021 Jun 4;cvab187.

280. Wang L, Rice M, Swist S, Kubin T, Wu F, Wang S, et al. BMP9 and BMP10 Act Directly on Vascular Smooth Muscle Cells for Generation and Maintenance of the Contractile State. Circulation. 2020 Dec 18;CIRCULATIONAHA.120.047375.

281. Veillette A. SLAM-Family Receptors: Immune Regulators with or without SAP-Family Adaptors. Cold Spring Harb Perspect Biol. 2010 Mar;2(3):a002469.

282. Oguro H, Ding L, Morrison SJ. SLAM family markers resolve functionally distinct subpopulations of hematopoietic stem cells and multipotent progenitors. Cell Stem Cell. 2013 Jul 3;13(1):102–16.

283. Xu C, Gao X, Wei Q, Nakahara F, Zimmerman SE, Mar J, et al. Stem cell factor is selectively secreted by arterial endothelial cells in bone marrow. Nat Commun. 2018 Jun 22;9(1):2449.

284. Sivaraj KK, Adams RH. Blood vessel formation and function in bone. Dev Camb Engl. 2016 Aug 1;143(15):2706–15.

285. Chen Q, Liu Y, Jeong HW, Stehling M, Dinh VV, Zhou B, et al. Apelin+ Endothelial Niche Cells Control Hematopoiesis and Mediate Vascular Regeneration after Myeloablative Injury. Cell Stem Cell. 2019 Dec 5;25(6):768-783.e6.

286. Ramasamy SK. Structure and Functions of Blood Vessels and Vascular Niches in Bone. Stem Cells Int. 2017;2017:5046953.

287. Kusumbe AP, Ramasamy SK, Adams RH. Coupling of angiogenesis and osteogenesis by a specific vessel subtype in bone. Nature. 2014 Mar 20;507(7492):323–8.

288. Comazzetto S, Murphy MM, Berto S, Jeffery E, Zhao Z, Morrison SJ. Restricted Hematopoietic Progenitors and Erythropoiesis Require SCF from Leptin Receptor+ Niche Cells in the Bone Marrow. Cell Stem Cell. 2019 Mar 7;24(3):477-486.e6.

289. Hodgson J, Swietlik EM, Salmon RM, Hadinnapola C, Nikolic I, Wharton J, et al. Characterization of *GDF2* Mutations and Levels of BMP9 and BMP10 in Pulmonary Arterial Hypertension. Am J Respir Crit Care Med. 2020 Mar 1;201(5):575–85.

290. Wüst RCI, Houtkooper RH, Auwerx J. Confounding factors from inducible systems for spatiotemporal gene expression regulation. J Cell Biol. 2020 May 19;219(7):e202003031.

291. Stacker SA, Achen MG, Jussila L, Baldwin ME, Alitalo K. Lymphangiogenesis and cancer metastasis. Nat Rev Cancer. 2002 Aug;2(8):573–83.

292. Yamazaki T, Li W, Yang L, Li P, Cao H, Motegi S ichiro, et al. Whole-Mount Adult Ear Skin Imaging Reveals Defective Neuro-Vascular Branching Morphogenesis in Obese and Type 2 Diabetic Mouse Models. Sci Rep. 2018 Jan 11;8(1):430.

293. Imayoshi I, Ohtsuka T, Metzger D, Chambon P, Kageyama R. Temporal regulation of Cre recombinase activity in neural stem cells. Genes N Y N 2000. 2006 May;44(5):233–8.

294. Desroches-Castan A, Tillet E, Ricard N, Ouarné M, Mallet C, Belmudes L, et al. Bone Morphogenetic Protein 9 Is a Paracrine Factor Controlling Liver Sinusoidal Endothelial Cell Fenestration and Protecting Against Hepatic Fibrosis. Hepatol Baltim Md. 2019 Oct;70(4):1392–408.

295. Forrester JV, Dick AD, McMenamin PG, Lee WR. The Eye: Basic Sciences in Practice 2nd Edition [Internet]. W.B. Saunders Ltd; 2002 [cited 2022 Jul 11]. Available from: https://abdn.pure.elsevier.com/en/publications/the-eye-basic-sciences-in-practice-2nd-edition

296. Sabbà C, Cirulli A, Rizzi R, Pasculli G, Gallitelli M, Specchia G, et al. Angiogenesis and hereditary hemorrhagic telangiectasia. Rendu-Osler-Weber disease. Acta Haematol. 2001;106(4):214–9.

297. Ahmed T, Flores PC, Pan CC, Ortiz HR, Lee YS, Langlais PR, et al. EPDR1 is a Non-canonical Effector of Insulin-mediated Angiogenesis Regulated by an Endothelial-specific TGF-β Receptor Complex. J Biol Chem [Internet]. 2022 Jul 21 [cited 2022 Aug 11];0(0). Available from: https://www.jbc.org/article/S0021-9258(22)00739-6/abstract

298. Cole LK, Jacobs RL, Vance DE. Tamoxifen induces triacylglycerol accumulation in the mouse liver by activation of fatty acid synthesis. Hepatology. 2010;52(4):1258–65.

299. Kraehling JR, Chidlow JH, Rajagopal C, Sugiyama MG, Fowler JW, Lee MY, et al. Genome-wide RNAi screen reveals ALK1 mediates LDL uptake and transcytosis in endothelial cells. Nat Commun. 2016 Nov 21;7:13516.

300. Tao B, Kraehling JR, Ghaffari S, Ramirez CM, Lee S, Fowler JW, et al. BMP-9 and LDL crosstalk regulates ALK-1 endocytosis and LDL transcytosis in endothelial cells. J Biol Chem. 2020 Dec;295(52):18179–88.

301. Um JH, Park SY, Hur JH, Lee HY, Jeong KH, Cho Y, et al. Bone morphogenic protein 9 is a novel thermogenic hepatokine secreted in response to cold exposure. Metabolism. 2022 Apr 1;129:155139.

302. Dang TTH, Yun JW. BMP10 positively regulates myogenic differentiation in C2C12 myoblasts via the Smad 1/5/8 signaling pathway. Mol Cell Biochem. 2021 May;476(5):2085–97.

303. Takeda M, Imaizumi M, Sawano S, Manabe Y, Fushiki T. Long-term optional ingestion of corn oil induces excessive caloric intake and obesity in mice. Nutrition. 2001 Feb 1;17(2):117–20.

304. Watt GF, Scott-Stevens P, Gaohua L. Targeted protein degradation in vivo with Proteolysis Targeting Chimeras: Current status and future considerations. Drug Discov Today Technol. 2019 Apr 1;31:69–80.

305. Ibrahim AFM, Shen L, Tatham MH, Dickerson D, Prescott AR, Abidi N, et al. Antibody RING-Mediated Destruction of Endogenous Proteins. Mol Cell. 2020 Jul 2;79(1):155-166.e9.

306. Békés M, Langley DR, Crews CM. PROTAC targeted protein degraders: the past is prologue. Nat Rev Drug Discov. 2022 Mar;21(3):181–200.

307. Brakenhielm E, Alitalo K. Cardiac lymphatics in health and disease. Nat Rev Cardiol. 2019 Jan;16(1):56–68.

308. Gancz D, Perlmoter G, Yaniv K. Formation and Growth of Cardiac Lymphatics during Embryonic Development, Heart Regeneration, and Disease. Cold Spring Harb Perspect Biol. 2020 Jun;12(6):a037176.

309. Yan Y, Gong P, Jin W, Xu J, Wu X, Xu T, et al. The cell-specific upregulation of bone morphogenetic protein-10 (BMP-10) in a model of rat cortical brain injury. J Mol Histol. 2012 Oct;43(5):543–52.

310. Ntumba K, Akla N, Oh SP, Eichmann A, Larrivée B. BMP9/ALK1 inhibits neovascularization in mouse models of age-related macular degeneration. Oncotarget. 2016 Aug 10;7(35):55957–69.

311. Morine KJ, Qiao X, York S, Natov PS, Paruchuri V, Zhang Y, et al. Bone Morphogenetic Protein 9 Reduces Cardiac Fibrosis and Improves Cardiac Function in Heart Failure. Circulation. 2018 Jul 31;138(5):513–26.

312. Lee HW, Chong DC, Ola R, Dunworth WP, Meadows S, Ka J, et al. Alk2/ACVR1 and Alk3/BMPR1A Provide Essential Function for Bone Morphogenetic Protein–Induced Retinal Angiogenesis. Arterioscler Thromb Vasc Biol. 2017 Apr;37(4):657–63.